Study of the Effects of Key Processing Parameters on the Cost and Quality of Ti-Al Powders Produced Using the TiPro Process

A thesis submitted in fulfilment

of the requirements for the degree

of

Doctor of Philosophy

in Materials and Processing

at

The University of Waikato

by

Kenneth Sichone

The University of Waikato

2015

THE UNIVERSITY OF
WAIKATO
Te Whare Wānanga o Waikato

Abstract

The high cost of titanium has motivated a global drive to research and develop low-cost titanium production technologies. In New Zealand, the TiPro process has been invented at the University of Waikato. The process starts with a combustion reaction between TiO_2 and Al powders, followed by: solid/liquid separation by extrusion which separates the metal rich liquid from the Al_2O_3 solid. The metal-rich phase is subsequently purified to reduce its oxygen content to acceptable level (e.g. <0.3 wt%).

The aim of this study was to establish such key relationships required to maximise the yield of Ti-Al and quality of the Ti-Al powder product. An in-depth understanding of the effects of key process parameters (e.g. heating rate, temperature, time and pressure) and starting TiO_2/Al composite powder characteristics (e.g. microstructure and compressibility) on the quality, production rate and cost of Ti-Al based powders was achieved. The solid/liquid separation step was identified to be most critical in determining the quality and cost of Ti-Al powders produced using the TiPro process. The results indicated that the microstructure of reactant powders, wetting properties of TiAl alloy on the Al_2O_3 particles, the viscosity of the liquid TiAl and the degree of saturation of the combustion product with liquid TiAl are some of the major factors in the extraction of TiAl from the combustion product using extrusion as the solid/liquid separation technique. In the current state of the invention, where the alloy is extracted by extruding the combustion product, the TiPro process is not viable due to poor yields. The throughput, alloy product purity and yield of the TiPro process are constrained by the solid/ liquid separation unit operation. When extrusion is the sole separation technique, the alloy yields are limited to only 10% of total input. This falls far below the minimum yield, (60%) that is required to make the process economically viable. Therefore, unless the solid/ liquid separation is supplemented by other separation techniques, such as froth flotation and leaching, the cost of producing titanium alloy powders by the TiPro process will be high and the quality of the alloy poor, consequently making the process uneconomical.

This study has demonstrated that froth flotation can recover 65.7 wt% of TiAl content of the extrusion by-product into a 71.0 wt% TiAl grade product. This corresponds to removing 20 wt% of the total Al_2O_3 contained in the extrusion by-

product (flotation feed). The potential exists to increase the TiAl grade further by multiple flotation stages. However, further work is required to investigate more suitable reagents than the HF acid that was used to activate Al_2O_3 in this study.

List of Publications

Journals

Factors affecting the separation of Ti-Al alloy in the TiPro process

Author/s: K. Sichone, D. Zhang, S. Raynova

Key Engineering Materials, v 551, p 44-54, 2013, *Cost-Affordable Titanium IV*

Conference Proceedings /Presentations

1 Oxygen Reduction in TiAl Produced by the TiPro Process

TMS2014 143rd Annual Meeting & Exhibition, February 16-20, 2014, San Diego, California, USA.

2 Recovery of TiAl from the TiPro Process By-product by Froth Flotation

Author/s: K. Sichone, B. Gabbitas, D. Zhang

International Workshop on Gamma Alloy Technology GAT 2013 Toulouse, France, June 11-14,

3 Factors Affecting the Separation of Ti-Al alloy in the TiPro process

Author/s: K. Sichone, D. Zhang, S. Raynova

TMS2014 142nd Annual Meeting & Exhibition, March 16-20, 2013, San Antonio, Texas, USA.

4 TiAl Production by the TiPro process: *Solid/Liquid Separation*

Author/s: K. Sichone, D. Zhang, B. Gabbitas

Powder Processing, Consolidation and Metallurgy of Titanium Conference, December 02-07, 2011, Brisbane, Queensland, Australia.

Acknowledgements

This study was carried out with financial support from The University of Waikato Doctoral Scholarship and the Claude McCarthy Fellowship. I gratefully acknowledge the unflinching support of my Chief Supervisor, Prof. Brian Gabbitas, his predecessor Prof. Deliang Zhang and the Second Supervisor Prof. Janis Swan. I could not have asked for a better team.

Many thanks to the Science Librarian Cheryl Ward, the administrative staff and technicians in the School of Engineering and the Department of Earth & Ocean Sciences; particularly Mary Dalbeth, Janine Williams, Helen Turner, Annette Rodgers, Stella Raynova, Chris Wang, Steve Hardy, Steve Newcombe, Martin Gore, Indar Singh, Yuanji Zhang, Steve Cameron, Brett Nichol, to name a few, who made my whole study experience at the University of Waikato something I will continue to cherish. Thanks to Gwenda Pennington and Carol Robinson for the timely support and guidance when I needed it.

Finally, I would like to thank my wife Bessie and family (Joshua, Kavwa, Vwanganji and Salifya) for being supportive and picking up the slack when I was away from home.

Table of Contents

List of Figures

List of Tables

Glossary

Symbol	Meaning	Units
A	Cross-sectional area	m^2
C	Total flotation feed weight reporting to the TiAl concentrate	g
c_{Ti}	Ti content of the TiAl-rich concentrate	wt%
C_p	Molar heat capacity	cal $mol^{-1}K^{-1}$
d_{10}	Diameter of ten-percentile particles	µm
d_{50}	Diameter of fifty-percentile particles	µm
d_{90}	Diameter of ninety-percentile particles	µm
D_H	Hydraulic diameter	m
f_{Ti}	Ti content of the flotation feed	wt%
f_s	Volume fraction of solid particles in the liquid	Fraction
G	Gibbs free energy	kcal mol^{-1}
ΔG	Gibbs free energy change of formation or reaction	kcal mol^{-1}
γ	Surface tension	Kg sec^{-2}
θ	Contact angle	degrees (^{o})
η	Viscosity	Pa sec
H	Heat content, Enthalpy	kcal mol^{-1}
ΔH°	Enthalpy change of formation or reaction	kcal mol^{-1}
$\Delta H°_T$	Enthalpy change of formation or reaction at T degrees K	kcal mol^{-1}
ΔH^f	Enthalpy change of fusion or melting	kcal mol^{-1}
K_p	Permeability constant	m^2
L	Thickness	m
m_{Ti}	Stoichiometric Ti content of the compound TiAl	wt%
P	Pressure	kPa, atm, mbar
ΔP	Pressure drop	kPa, atm, mbar
P_c	Capillary pressure	kPa, atm, mbar
P_{nw}, P_w	Pressure of non-wetting & wetting phases	kPa, atm, mbar
Q	Volumetric flow rate	m^3sec^{-1}
R_1	Minimum principal radius of curvature of the interface	m
R_2	Maximum principal radius of curvature of the interface	m
$R_{Al_2O_3}$	Recovery of Al_2O_3 to the TiAl-rich concentrate	%
R_{TiAl}	Recovery of TiAl to the TiAl-rich concentrate	%
T	Absolute temperature	degrees Kelvin, K
T_{ad}	Adiabatic temperature	degree Celsius, ^{o}C
T_c	Combustion temperature	degree Celsius, ^{o}C
T_{ig}	Ignition temperature	degree Celsius, ^{o}C

Chapter 1

Introduction

1.1 Background

Titanium alloys have many favourable properties such as high strength to weight ratio, good ductility and fracture toughness, high corrosion resistance, high melting point and good biocompatibility with human tissue, making them very important engineering materials for many applications in aerospace, chemical engineering, automotive, biomedical and other industries.

Despite having desirable properties and being highly abundant in the earth's crust (0.63 percent by weight), the annual world production of titanium and its alloys is limited to only about 230,000 tonnes, due to the high cost of production. On the other hand, the strong demand for titanium alloys driven by fast economic development of countries such as China and India and the strong interest in using titanium alloys for making different products causes a shortage of the titanium alloy products and dramatic price increases. This opens many opportunities for new titanium alloy product manufacturers. For example between 2002 and 2011, China increased its Ti production capacity from 3,800 tonnes to 103,500 tonnes (Qian *et al.*, 2012). Russia also increased its titanium output by 23.7 percent in 2012 (Kenerly, 2012; Qian, *et al.*, 2012).

In New Zealand, the TiPro process which is a low cost titanium alternative that can be used to produce titanium alloy powders from titanium dioxide (TiO_2) and aluminium (Al) powders, has been developed at the University of Waikato through research projects funded by the Foundation for Research, Science and Technology (FRST), Titanox Development Ltd (TDL) and WaikatoLink Ltd. The TiPro process comprises two stages. In the first stage a composite powder is produced by high energy mechanical milling of a TiO_2/Al powder mixture. The composite powder is preheated to initiate the combustion synthesis reaction in the subsequent stage of solid/liquid separation. The combustion synthesis product, which is a mixture of liquid TiAl and solid Al_2O_3 (corundum) is extruded by applying light pressure in order to recover TiAl. The TiPro process has the potential to lower the production cost of Ti-Al alloy powders and make them more affordable for non-aerospace applications. The by-product of the process is

an Al_2O_3/Ti_xAl_y composite that can either be used as an engineering material for various applications or processed to recover the residual TiAl and Al_2O_3 as separate products. The TiPro process has passed the proof of concept stage, but needs systematic research to establish the key relationships underlying the process before it is ready to be scaled up to pilot plant level. This research aims to establish such key process parameters affecting the cost and quality of Ti-Al alloy powders produced by the TiPro process.

Titanium extraction technology and output have lagged behind other metallurgical processes. For instance after its discovery in Cornwall, UK by William Gregor round about 1790 it was only purified in the early 1900s (Donachie, 2000). The first commercial process, the Hunter Process, was not developed until 1910. Extraction of titanium from its ores and its subsequent processing presents special problems because of its immense reactivity. Titanium readily reacts with oxygen, carbon, hydrogen and nitrogen. The resulting contamination is detrimental in processing and application (Donachie, 2000; Schwandt *et al.*, 2010). To minimize contamination, titanium processing is carried out using high purity precursors and in carefully controlled environments. Therefore the existing titanium production processes are characterized by a need for high purity precursors, low energy efficiency, long complex and slow sequence of batch steps which result into low world annual output and a relatively high cost of the metal. The 2011 market price of titanium powder varied between about US$15/kg and US$1000/kg depending on grade (Qian, *et al.*, 2012). Table 1.1 compares the cost of producing a 25 mm plate from titanium, steel and aluminium. Titanium metal costs five times aluminium and about fifty times that of steel (Imam & Froes, 2010).

Table 1.1: Cost of titanium and alternative materials (Imam & Froes, 2010)

	Material ($/lb)		
Item	Titanium	Steel	Aluminium
Ore	0.22(rutile)	0.02	0.01
Metal	5.44	0.10	1.10
Ingot	9.07	0.15	1.15
25-mmSheet	15.00-50.00	0.30-0.60	1.00-5.00

The cost sensitive applications often opt for less costly alternatives such as steel.

The production cost reduction strategies by the titanium industry have included modifying conventional technologies and developing alternative technologies. In 2007, more than twenty companies around the world were reported to be researching and developing low cost titanium production processes (Hogan *et al.*, 2008). Notable modifications of conventional technologies include the Kroll process-based TiRO process and the Armstrong process which is based on the Hunter process chemistry. Both processes have been modified to run in continuous mode in order to increase throughput, energy efficiency and consequently reduce the cost of production. In addition to modification, research and development efforts have focussed on direct titanium production from titanium dioxide TiO_2, which is unlike the modified technologies that first convert TiO_2 into $TiCl_4$. It is anticipated that significant cost reduction can be achieved by replacing the more costly $TiCl_4$ (Table 1.2) which accounts for 52 percent of the total cost in the extraction of titanium from its ores (Hartman *et al.*, 1998; Lütjering & Williams, 2010; Turner *et al.*, 2001). Under the direct titanium production technologies category are the FFC electrolytic process and TiPro process. The TiPro process has a greater potential to lower the cost of titanium because the pertinent chemical reactions are faster and the process does not need complex or costly equipment.

Table 1.2: Cost of titanium precursor materials (Imam & Froes, 2010)

	Cost	
Precursor	$/lb Material	$/lb Contained Ti
TiO_2 (Metal Grade)	1.75	2.94
$TiCl_4$	1.00	4.00
Ti Sponge	5.44	5.44

1.2 Significance of the Current Study

The TiPro process has gone through the conceptual stage, but needs systematic research to establish the key relationships underlying the process. The results from the current study will be utilised in optimising the processing conditions and scale up for commercialisation of the low cost production of titanium alloys by the TiPro process. Lowering the production cost of titanium has the potential to expand the use of titanium for those cost-sensitive applications, such as the

automobile industry, that continue to shun titanium for alternative materials on account of cost. Using the TiPro process, the potential to lower the cost of titanium production exists due to the use of locally available low cost inputs and the simplicity of the technology. The vast ironsand deposits of New Zealand, such as the Taharoa deposit mined for iron by the now Blue Scope steel on the west coast of North Island, contain significant amounts of by-product titanium and are some of the well-established TiO_2 resources (Barakat & Drain, 2006). Shallow drilling cores off the southern Taranaki Coast validated by aeromagnetic surveys in 2010 and 2011 have estimated ironsand deposits equivalent to 200 million tonnes of concentrate at 60 percent iron (Scoop Independent News, 2011). Other areas off the west coast of the North Island have potential deposits. The other process input used in the alloy refining step $CaCl_2$ is a low cost material too.

The viability of low cost titanium production innovations like the TiPro process facilitates the growth of the New Zealand titanium industry into an employment and revenue creation alternative.

1.3 Problem Statement and Objectives of this Study

In the TiPro process, TiO_2 is reacted with Al to cost effectively produce TiAl(O) and Al_2O_3. However to produce an acceptable grade of TiAl, the TiAl has to be free of Al_2O_3 and dissolved oxygen. The separation of TiAl from Al_2O_3 poses a challenge. Similarities in specific gravity (4.25 for TiAl and about 3.98 for Al_2O_3), implies that traditional techniques such as gravity separation are not effective.

The cost of titanium alloys can be reduced by replacing the conventional Kroll process based technologies with combustion synthesis reactions of low cost materials such as TiO_2 and Al. The powders produced can be used in near-net shapes thereby cutting the costs associated with fabrication, $TiCl_4$, magnesium reduction and repeated melts (Figure 1.1).

Table 1.3: R & D projects on titanium production processes in 2007 (Hogan, *et al.*, 2008)

Organisation/Process Name	Country	Process Type	Product
CSIRO/ Tiro	Australia	Chemical	Powder
ITP/ Armstrong	USA	Other	Powder
MSE University of Tokyo/ EMR	Japan	Electrolysis	Powder
Cambridge University/ FCC Cambridge	UK and USA	Electrolysis	Powder
Idaho Research Foundation	USA	Chemical	Powder
Idaho Titanium Technologies	USA	Chemical	Powder
MER Corporation	USA	Electrolysis	Powder
Kyoto University/ OS	Japan	Other	Powder
Peruke (Pty) Ltd	RSA	Chemical	Powder
University of Tokyo/ Preform Reduction	Japan	Chemical	Powder
SRI International	USA	Other	Powder
Vartech	USA	Chemical	Powder
BHP Billiton Polar™ Titanium	Australia	Electrolysis	Liquid
CSIR	RSA	Other	Liquid
GTT S.R.L.	Italy	Electrolysis	Liquid
Rio Tinto QIT	Canada	Electrolysis	Liquid
Tresis International	USA	Chemical	Liquid
Mir-Chem	Germany	Chemical	Other
MIT Two- Year Initiative	USA	Electrolysis	Other
South African Titanium (Peruke)	RSA	Other	Other

Roskill Information Services

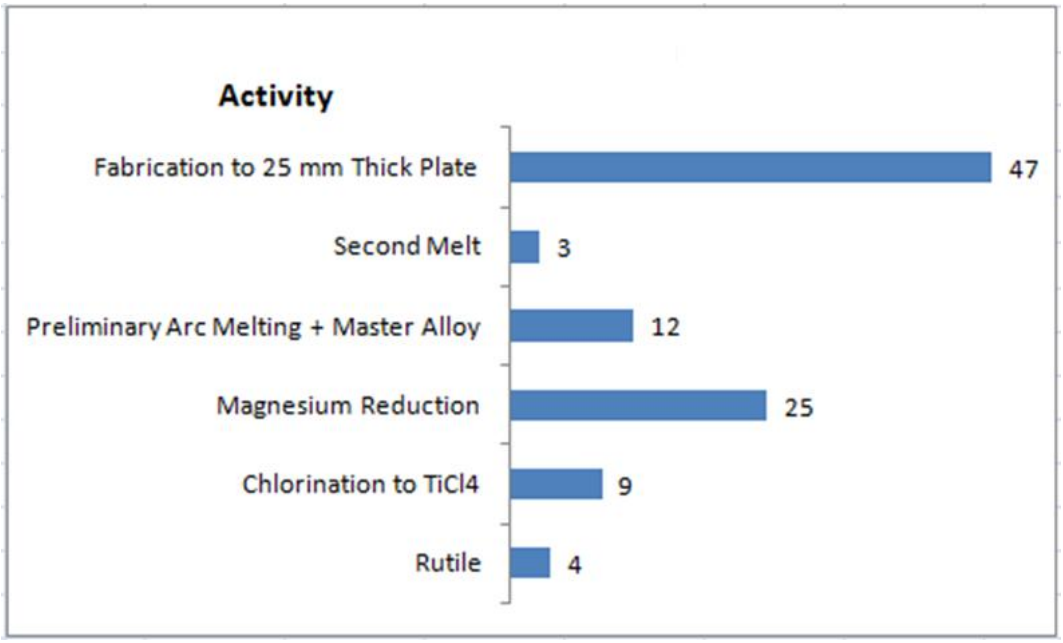

Figure 1.1: Cost by process activity based on producing a 25-mm plate from the Kroll process titanium sponge.

1.4 Theoretical Basis

High energy mechanical milling enhances the kinetics of the chemical reaction between Al and TiO_2 by creating new atomically clean reactive particle surfaces and the reduction of inter-particle diffusion distances by intimate mixing to nanometre level. The reaction temperature of mechanically milled TiO_2/Al powders is much lower than in conventional thermochemical processing (Fecht, 1995; Welham, 1998; Zhang, 2004). Therefore, the use of mechanically activated TiO_2/Al powders as feedstock for metallurgical processes can enhance process economics.

1.5 Status of TiPro Project at Commencement of this Study

By the start of this project previous studies had been attempting to attain a 50% TiAl yield since 2006. However despite adjusting the experimental conditions by varying the feed composition and increasing the extrusion pressure alloy yields at 4% remained well below the desired target. The project had opted for extrusion as the sole TiAl extraction technique and much effort had been directed at increasing alloy yields by varying parameters expected to affect the process; however the fundamentals such as characterising the type of flow and thermodynamics of the solid/liquid stage had not been explored. These made the TiPro process a potentially high technology risk.

An unpublished research update on this project (Raynova, 2007) reported only extremely low alloy yields had been achieved as at 2007. Before commencement of this study, an attempt to increase alloy yields had also been made through an undergraduate final year project but results had not improved. The main focus had up to then remained on increasing the heat content of products as it was hypothesised that doing so might increase alloy yields. The mechanism underlying the TiPro process had not been understood making scale-up difficult and unachievable as earlier studies had not provided a justifiable and robust basis for process equipment selection and sizing.

This study has provided an economic sensitivity analysis and a preliminary costing estimate (±20% accuracy) of the TiPro process. The cost of production at US$ 250 per kg (at 10% yield) falls within the range of current prices titanium powders, however; the excessive recycle stream resulting from poor yields at the solid/liquid separation stage is a major technological risk that no process plant could adequately mitigate without a further substantive capital project investment that might adversely impact the overall process economics.

Even though the project had settled on extrusion as the sole TiAl extraction technique, the physical phenomena associated with fluid flow solid/liquid separation had not been explored. The thermodynamics aspects of the process were also not elucidated. It was then clear that to achieve any significant increase in TiAl yields it was necessary to characterise the type of flow occurring and the thermodynamics during solid/liquid separation. Without an appreciation of such fundamentals, the TiPro process would be a high technological risk. This study has achieved that understanding by identifying the similarities between solid/liquid separation and liquid-phase sintering and also by characterising the extraction of liquid TiAl as flow through porous media.

Based on the Classic and Pore-filling models (Kang, 2005) of liquid-phase sintering and also considering the characteristics of flow of liquid through porous media, this study has demonstrated that solid/liquid separation by extrusion is fundamentally not an efficient separation technique. It is instead a densification technique. This study has recommended a more feasible alternative that involves dissolution of Al_2O_3 using cryolite which is a well-established operating practice in aluminium smelting.

The contribution this study has made to the project is:

1. As the research update on this project reported extremely low (only 4%) alloy yield had been achieved as at 2007 and that efforts to increase alloy yields had focussed mainly on increasing the heat content of products and extrusion pressure; this study embarked on understanding the mechanisms driving the extraction of the alloy from the combustion product. This study has achieved up to 12.23% TiAl alloy yield (three times previous research results).
2. The hypothesis that holding the combustion products above 1460^{o}C the alloy melting point might increase alloy yields was disapproved when holding for 40 min failed to achieve the anticipated benefit. Investigation into the mechanisms behind the solid/ liquid separation has shown that temperature alone cannot increase alloy yields.
3. This study has identified that mechanisms of the solid/ liquid separation in TiPro process can best understood by considering the mechanisms of liquid-phase sintering. Since there is no appreciable chemical reaction between the combustion products liquid TiAl and solid Al_2O_3, the interfacial energies have a dominant effect on microstructure evolution. Also due to a low contact angle (38^{o}) of liquid TiAl, there is good wetting between the liquid TiAl and the Al_2O_3 solid particles. The conditions prevailing during solid/liquid separation are similar to those found in liquid-phase sintering. A wetting liquid layer generates a compressive capillary force, which is equivalent to subjecting the system to a large external hydrostatic compression given by the Young and Laplace (Equation (5-1)). The large capillary pressures cause rapid particle rearrangement while the viscosity of the system is still low. Capillary pressure gradients will also cause liquid to flow from regions with large pores to regions with smaller pores thereby redistributing the liquid. This phenomenon accounts for why densification achieved with liquid-phase sintering is significantly higher than in solid-state sintering. Also since the liquid wets and spreads over the solid particles, the solid-vapour interface of the particulate system is eliminated and pores form in the liquid. The reduction of the liquid-vapour interfacial area provides a driving force for shrinkage and consequently densification of the system.

   Following particle rearrangement, densification might occur by the solution-precipitation mechanism, and the liquid layer separating the

grains progressively becomes thinner with time until the liquid capillary becomes too narrow for the liquid to flow, making the extraction of TiAl from the combustion product difficult. Therefore, extrusion cannot be used to efficiently recover TiAl from the combustion product.

4. The study has also characterised solid/ liquid separation as a porous media-flow type of problem. Therefore, physical properties of the reactants and products such as porosity, capillarity, viscosity and surface tension do limit flow of the alloy out of the combustion product consequently leading to the poor TiAl yields that have characterised TiPro process.
5. This study has successfully applied single stage froth flotation to upgrade the TiAl content of the extrusion by-product to concentrate containing 71 wt% TiAl and 30% Al_2O_3 at a recovery of about 65%. As it is apparent that the original intention of producing titanium alloys by a single stage TiPro process is not practical given the current status of the technology, froth flotation might enhance TiAl yields.
6. Less than 1 volume percent liquid phase is sufficient to coat the grains when the liquid is distributed uniformly in a material with 1-µm grain size. The liquid draws the particles together and angular particles may rotate, enabling sliding and rearrangement into a denser configuration. In systems where the liquid phase is inhomogeneously distributed (like powders milled for 1 h), differential rates of densification and grain growth produce an inhomogeneous (coarse) microstructure and a more porous texture (Reed, 1995) that could facilitate easier flow channels for TiAl.
7. This study has therefore provided a framework for further research and development of the TiPro process such as applying more effective alternatives like using cryolite to dissolve away Al_2O_3. The cryolite – alumina system is well-established in aluminium smelting because of the high solubility of Al_2O_3 in cryolite.

1.6 Research Objectives

To achieve an in-depth understanding of the effects of key process parameters (e.g. heating rate, temperature and starting TiO_2/Al composite powder characteristics on the quality, production rate and cost of Ti-Al based powders produced by using the TiPro process.

1.7 Scope

The study involved:

- preparing TiO_2/Al composite powders with different powder particle microstructures by high energy mechanical milling of TiO_2/Al mixtures with a TiO_2:Al ratio of 3:7
- conducting combustion synthesis experiments and solid/liquid separation by extrusion;
- froth flotation experiments for recovery of TiAl from the extrusion by-product
- powder purification experiments;
- characterising the products by particle size analysis, optical microscopy, x-ray diffractometry (XRD), scanning electron microscopy (SEM) and x-ray fluorescence (XRF) analysis

1.8 Thesis Outline

The thesis is divided into eight chapters as follows:

- The introduction, giving the background and motivation of the research.
- Literature review describing the existing and emerging titanium production technologies.
- Characterization of the experimental materials.
- Application of High Energy Mechanical Milling (HEMM) as a feedstock preparation unit operation for the thermic reaction between TiO_2 and Al.
- Solid/Liquid separation presenting experimental results of the separation of liquid TiAl from solid Al_2O_3 by extrusion.
- The results of the flotation experiments conducted to separate TiAl from the Al_2O_3 contained in the extrusion by-product.
- Alloy purification and process costing
- Conclusions and recommendations.

1.9 References

Adam, G., Zhang, D. L., Liang, J., & Macrae, I. (2007). A novel process for lowering the cost of titanium. *Advanced Materials Research, 29-30*, 147-152.

Barakat, M., & Drain, L. (2006). The development of Waikato North Head ironsand deposit, South Auckland. In A. B. Christie & R. L. Brathwaite (Eds.), *Geology and Exploration of New Zealand Mineral Deposits: Monograph 25* (pp. 219-224). Carlton, Vic., Australia: Australasian Institute of Mining and Metallurgy.

Barakat, M., & Ruddock, R. (2006). Taharoa ironsand mining operation, Waikato. In A. B. Christie & R. L. Brathwaite (Eds.), *Geology and Exploration of New Zealand Mineral Deposits: Monograph 25* (pp. 225-230). Carlton, Vic., Australia: Australasian Institute of Mining and Metallurgy.

Donachie, M. J., Jr,. (2000). *Titanium: A Technical Guide* (2nd ed.). Materials Park, OH: ASM International.

Fecht, H. J. (1995). Nanostructure formation by mechanical attrition. *Nanostructured Materials, 6*(1-4), 33-42.

Hartman, A. D., Gerdermann, S. J., & Hansen, J. S. (1998). Producing lower-cost titanium for automotive applications. *JOM - Journal of the Minerals Metals & Materials Society, 50*(9), 16-19.

Hogan, L., Mcginn, E., & Kendall, R. (2008). *Research and Development in Titanium: Implications for a Titanium Metal Industry in Australia.* Research Report 08.2. Canberra, Australia, Commonwealth of Australia. 59p.

Imam, M. S., & Froes, F. H. (2010). Low cost titanium and developing applications. *JOM - Journal of the Minerals Metals & Materials Society, 62*(5), 17-20.

Kenerly, S. (2012). *Russia Boosted Titanium, Magnesium Output on 11M 2012*. Retrieved 10 March, 2013, from http://www.mining.com/web/russia-boosted-titanium-magnesium-output-on-11m-2012/

Lütjering, G., & Williams, J. C. (2010). *Titanium*. Berlin, Germany: Springer.

Qian, M., Yang, Y. F., Yan, M., & Luo, S. D. (2012). Design of low cost high performance powder metallurgy titanium alloys: Some basic considerations. *Key Engineering Materials, 520*, 24-29.

Schwandt, C., Doughty, G. R., & Fray, D. J. (2010). The FFC-Cambridge process for titanium metal winning. *Key Engineering Materials, 436*, 13-25.

Scoop Independent News. (2011). *TTR New Zealand Iron Sands Resource Estimate Nearly Doubled*. Retrieved 20 January, 2012, from http://www.scoop.co.nz/stories/BU1108/S00471/ttr-new-zealand-iron-sands-resource-estimate-nearly-doubled.htm

Turner, P. C., Hartman, A., Hansen, J. S., & Gerdemann, S. J. (2001). Low cost titanium - Myth or reality. In P. R. Taylor (Ed.), *Proceedings of Sessions and Symposia sponsored by EPD, 2001 TMS Annual Meeting, New Orleans, LA, Feb. 11-15, 2001* (pp. 43-66). Warrendale, PA: Minerals, Metals and Materials Society.

Welham, N. J. (1998). Mechanical activation of the solid-state reaction between Al and TiO_2. *Materials Science and Engineering A, 255*(1-2), 81-89.

Zhang, D., & Raynova, S. R. (2009). Patent No. US 2009/0311123 A1. Method for Producing Metal Alloy and Intermediate Products.

Zhang, D. L. (2004). Processing of advanced materials using high-energy mechanical milling. *Progress in Materials Science, 49*(3-4), 537-560.

Chapter 2

Literature Review

This chapter presents an overview of the various existing and emerging titanium technologies found in the literature. The technologies are classified under conventional, modified and direct titanium categories. The latter is discussed in more detail because it is the subject of the thesis. The chapter finishes with the aims of the research and the methods that will be used to obtain the required data.

2.1 Conventional Titanium Production Technologies

2.1.1 Background

Conventional commercial titanium production technologies use the Hunter and the Kroll processes, which were developed in the 1900s. Both processes are based on reduction-oxidation reactions between the titanium tetrachloride ($TiCl_4$) precursor and alkali (Kroll) or alkali earth (Hunter) metals. The $TiCl_4$, which is produced by a multi-step, batch carbothermic-chlorination of natural or synthetic rutile (TiO_2) and subsequent repetitive distillation at elevated temperatures is the preferred precursor because it is not associated with oxygen, which is detrimental in titanium processing and applications. The Kroll process has become the standard for process evaluation (EHK Technologies, 2004; Imam *et al.*, 2000; Thompson, 2002).

2.1.2 Overview of the Process Chemistry

The conventional titanium production processes start with carbothermic chlorination of high purity natural or synthetic rutile (TiO_2) at 1000^{o}C to produce titanium tetrachloride ($TiCl_4$) in a fluid-bed reactor (Turner *et al.*, 2001):

$$TiO_2(s) + 2Cl_2(g) + C(s) = TiCl_4(g) + CO_2(g) \quad (2\text{-}1)$$

$$TiCl_4(g) = TiCl_{4(l)} \quad (2\text{-}2)$$

As the world's natural high-grade rutile deposits are diminishing, synthetic rutile is being produced from ilmenite and slags (Imam, *et al.*, 2000; Thompson, 2002). The initial product, crude $TiCl_4$, is purified further by fractional distillation. The first distillation stage removes lower boiling point impurities such as CO and CO_2

and the second stage removes higher boiling point impurities including $SiCl_4$ and $SnCl_4$. The $TiCl_4$ obtained has high purity because the titanium in this compound is not associated with oxygen (for which titanium has an enormous affinity). To obtain titanium metal, $TiCl_4$ is reduced with magnesium, sodium or calcium in an inert atmosphere.

2.1.3 Hunter Process

The Hunter process, which involves reducing $TiCl_4$ using sodium (Equation(2-3)), was the first commercial titanium production process.

$$TiCl_{4(l)} + 4Na_{(molten)} = Ti + 4NaCl_{(molten)} \quad (2\text{-}3)$$

It is not as widely applied as the Kroll process because magnesium is a more economic reductant than sodium. The process is however still used to produce extra-pure titanium for electronic applications.

2.1.4 Kroll Process

The Kroll process (Figure 2.1), which was developed by William Kroll in the 1930s and commercialised by DuPont in 1948 (Barakat & Ruddock, 2006) is the primary commercial titanium production process and the standard used to evaluate new technologies. Processing is conducted in a stainless steel retort. To start the process, 15 – 30% stoichiometric excess of molten magnesium is run into an argon–filled retort to enhance reaction kinetics (Equation (2-4)). The retort is heated and maintained between 850 and 950^oC (i.e. above the solidification point of magnesium chloride of 715^oC) but below 1025 ^oC to avoid titanium attacking the iron retort. Then, high purity $TiCl_4$ is gradually added over several days. The basic reaction is:

$$TiCl_{4(l)} + 2Mg_{(molten)} = Ti + 2MgCl_{2(molten)} \quad (2\text{-}4)$$

After several days, a spongy mass of titanium forms at the bottom of the retort and magnesium chloride ($MgCl_2$) floats as a molten top layer. The $MgCl_2$ is drained and recycled to recover the magnesium and chlorine by electrolysis. After cooling, the titanium is dug out of the retort with jackhammers, crushed in a jaw crusher and purified by vacuum distillation or helium sweep between 1000 and 1060^oC to remove entrapped residual magnesium salts. About 25 percent of the sponge is low quality due to iron and nickel contamination picked-up from the retort wall (Hartman et al., 1998; Kroll, 1940; Turner, et al., 2001). The purer portion is

mixed with scrap and pressed into a consumable vacuum arc furnace electrode, which is then remelted three times to remove inclusions and obtain a homogenous ingot for use in manufacturing (Brooks *et al.*, 2007).

2.1.5 Sponge Purification

Sponge titanium is purified by volatilising impurities such as chlorides of magnesium and other metals under vacuum. The sponge is heated to 1000°C then condensed in a cold trap. Distillation takes over 85 h (Hogan *et al.*, 2008) while the whole processing takes 21 days.

In the helium sweep purification technique, helium gas is forced through the 1000°C sponge titanium. The helium scavenges unreacted magnesium and the $MgCl_2$ reaction product, which are recovered by cooling the helium to condense magnesium and $MgCl_2$ (Hartman, *et al.*, 1998; Kroll, 1940; Turner, *et al.*, 2001).

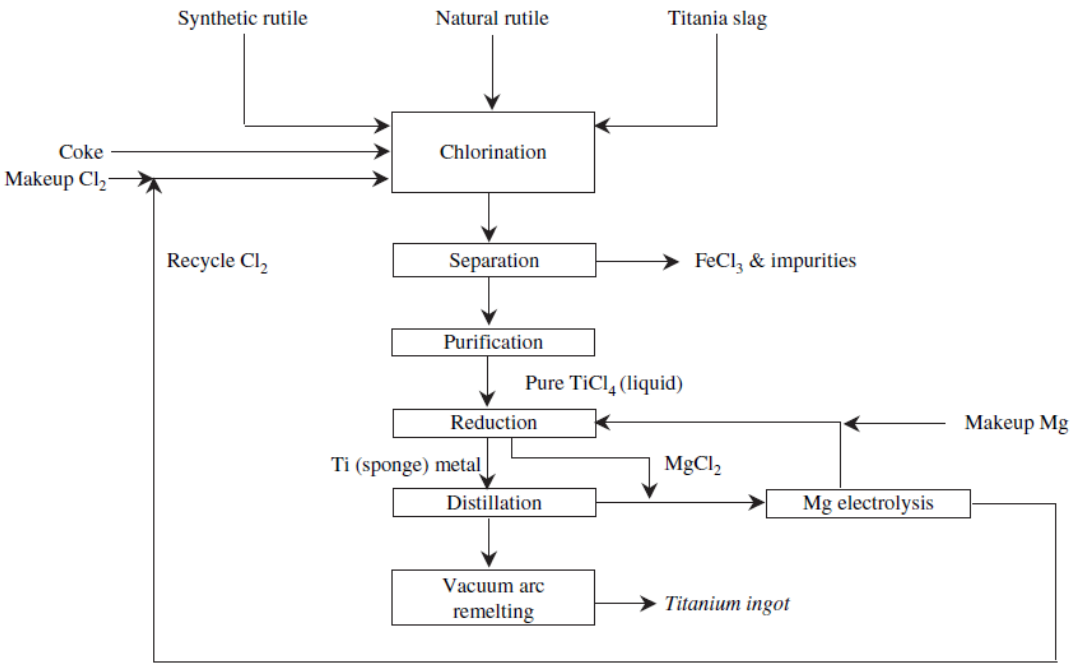

Figure 2.1: Kroll process flowsheet (Mauk et al., 2006)

2.2 Modified Technologies

Conventional commercial titanium production processes have high capital and operating costs because they require high purity feed stock and are batch processes. They are less efficient in terms of energy and yield than other metallurgical processes e.g. copper and aluminium. To ameliorate the constraints

of conventional titanium processing, modified technologies such as the Armstrong (ITP) (EHK Technologies, 2004) and TiRO™ (Doblin *et al.*, 2012) processes have been developed to respectively convert the Hunter and Kroll processes to a continuous operation.

2.2.1 Armstrong (ITP) Process

International Titanium Powder Inc. (ITP) in the USA, now Cristal Global, developed the Armstrong Process. By 2006, this continuous process had demonstrated that it could produce 16 tonnes per year of titanium metal with less than 0.05 percent (500 ppm) oxygen. Schematics of the process flowchart and the reactor are shown in Figure 2.2 and Figure 2.3, respectively.

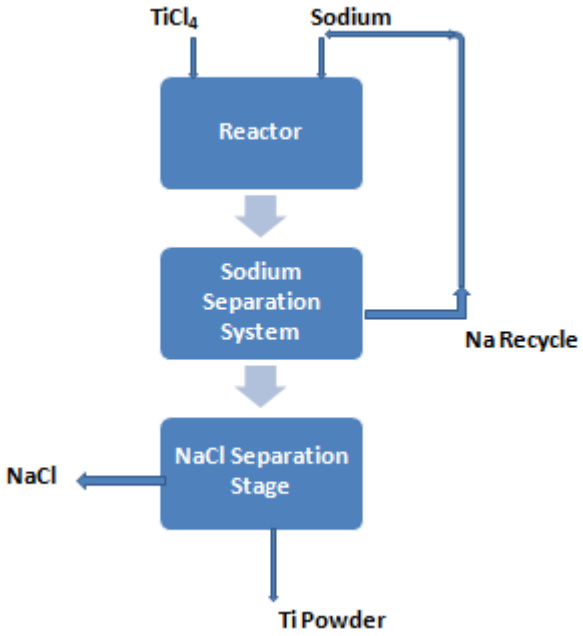

Figure 2.2: Armstrong process flow diagram (Crowley, 2003)

Like the Hunter Process, the Armstrong process is based on sodium reducing $TiCl_4$ to Ti metal using a special reactor (Figure 2.3). A flowing loop of liquid Na is reacted with $TiCl_4$ vapour that is continuously injected at a single point. The reaction goes to completion at a low temperature, producing small Ti-metal particles and a NaCl by-product that are removed from the reaction zone by the flowing Na. Control of the particle shape and size distribution is achieved by varying the relative flow rates and geometry of the reaction zone.

Further downstream the Na flowing loop, the liquid is filtered to separate the solid Ti and NaCl. Once sufficient material accumulates on the filter, the flow is

directed to another filter to maintain a continuous flow of Na. Residual Na is distilled from the filtrate. The Ti powder is washed to remove the NaCl. The washed Ti powder meets the specification of commercially pure Ti. The NaCl by-product is recycled electrolytically recover Na and Cl (Crowley, 2003).

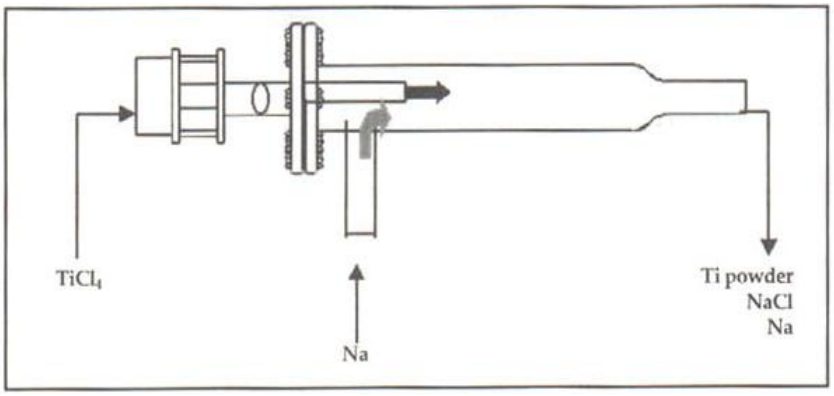

Figure 2.3: Schematic of the Armstrong process reactor (Crowley, 2003)

2.2.2 TiRO™ Process

CSIRO in Australia modified the Kroll process by replacing batch reduction of titanium tetrachloride ($TiCl_4$) with a continuous fluidised bed reactor (Doblin, *et al.*, 2012). The gas-solid reaction equation (2-5) between magnesium and $TiCl_4$ is done in the 62^oC window between the melting point of Mg (650^oC) and the melting temperature of $MgCl_2$ 712^oC (Figure 2.4).

$$2\ Mg_{(s)} + TiCl_{4(g)} = Ti_{(s)} + 2\ MgCl_{2(s)} \qquad (2\text{-}5)$$

Argon is the fluidisation medium. The intermediate product, which is a fine dispersion of Ti particles (d_{50} ≈1.7μm) in an $MgCl_2$ matrix (d_{50} ≈ 350 μm) averaging 80 wt% $MgCl_2$ and 20 wt% Ti, is vacuum distilled to separate Ti from $MgCl_2$ in a retort at 750 to 850^oC. The vacuum distilled Ti sinters to form "biscuits" that have to be lightly milled to break the agglomerates. The purity of the final TiRO™ powder is very sensitive to purity of the feed materials and the operating practice. To date, TIRO™ powder with the lowest O content of 0.3 wt% and 300 ppm Cl has been produced (Doblin, *et al.*, 2012).

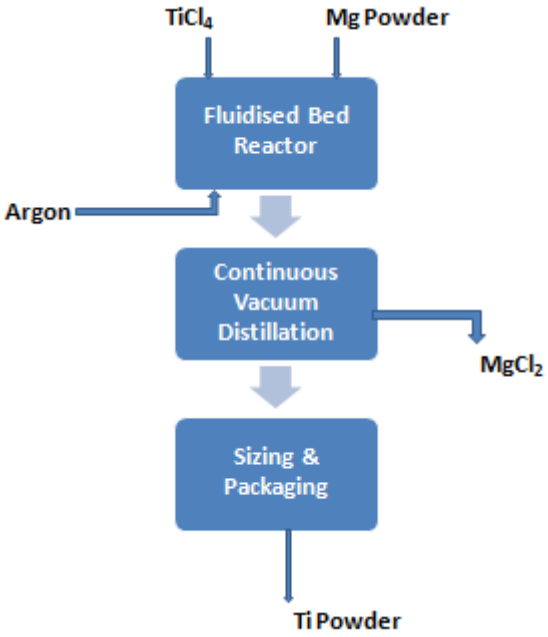

Figure 2.4: Flow diagram of the TiRO™ process (Crowley, 2003; Doblin, et al., 2012)

While the TiRO™ process has the potential to achieve a higher throughput than the traditional Kroll process because it is continuous rather than a batch $TiCl_4$ reduction step, significant reductions in production cost are still dependent on having a high purity $TiCl_4$ precursor. Also, the Grade 2 metal specification could not be obtained at the laboratory scale stage because oxygen levels exceeded the stipulated 0.25 percent.

2.2.3 Direct Titanium Production Technologies

It is evident from the breakdown of cost by process activity that modified processes may achieve only a limited improvement on conventional processes, unless fabrication and the cost of conversion of ore to metal are addressed (Imam & Froes, 2010). About 87 percent of the costs in producing titanium components from conventional titanium production processes are converting ore to metal, melting and fabrication (Table 2.1)

Direct titanium and alloy powders production from low cost materials such as TiO_2, coupled with subsequent powder metallurgy (PM) processing into near-net shape components has the greatest potential to significantly reduce titanium cost because machining and fabrication (major costs in processing) are considerably reduced (Table 2.1)

Table 2.1: Cost by process activity to fabricate a 25-mm titanium plate (Hartman, et al., 1998)

Process Activity	Cost as % of Total
Rutile	4
Chlorination to $TiCl_4$	9
Magnesium reduction	25
Preliminary arc melting + master alloy	12
Second melt	3
Fabrication to 25- mm thick plate	47

Direct titanium production technologies such as the FCC electrolytic process (EHK Technologies, 2004; Schwandt *et al.*, 2010) and the TiPro process are more attractive because they utilise TiO_2, which is cheaper than $TiCl_4$ (Table 2.2).

Table 2.2: Cost of titanium and associated inputs in 2010 (EHK Technologies, 2004; Imam & Froes, 2010)

Materials	Cost in US$/lb	
	Material	Contained Ti
Rutile (TiO_2)	1.75	2.94
$TiCl_4$	1.00	4.00
Titanium sponge (Kroll using rutile)	5.44	5.44

2.2.4 Electrolytic Processes

The four electrolytic processes for producing titanium from a TiO_2 feed are the Fray-Farthing-Chen (FFC) process, the Electro-Slag Electrolysis (ESE) and the OS Process. The FFC process (also called the Metalysis process) is reported to have higher efficiency, better operability and adaptability to continuous operation (Suzuki, 2007).

2.2.5 Electroslag Refining (ESR) Process

The Electroslag refining process (Suzuki, 2007) produces titanium by utilising an electron conductive CaF_2-CaO molten electrolyte laden with dissolved TiO_2

(Figure 2.5). The ohmic resistance provides enough heat to keep the TiO_2 and the titanium product molten.

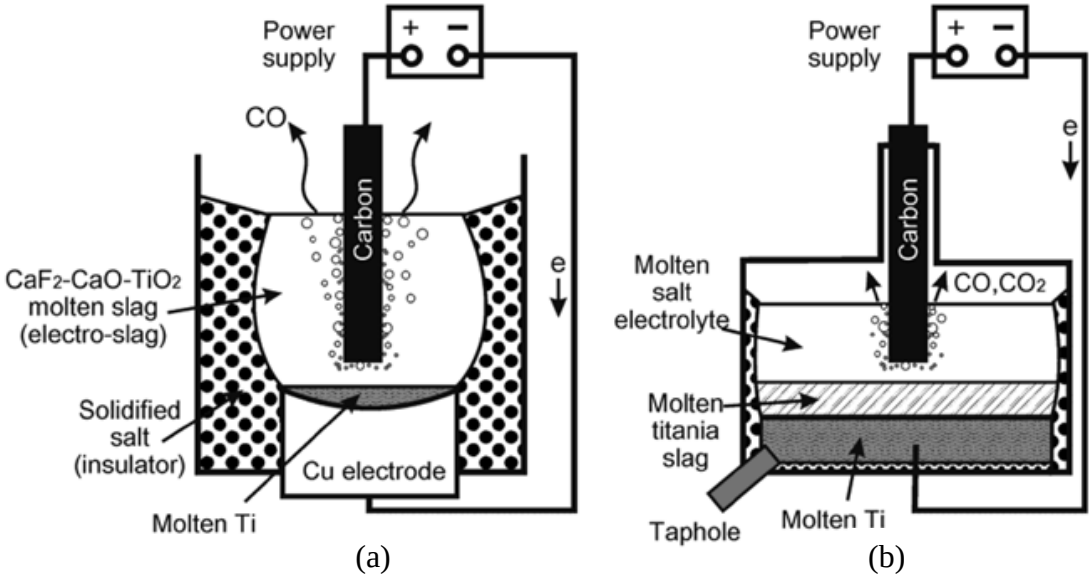

Figure 2.5: Electroslag refining by (a) Takenaka et al. and (b) Quebec Iron and Titanium Corporation (Suzuki, 2007)

The basic chemical reactions for electrolysing the TiO_2 are:

$$TiO_2 + 2Ca_{(Disolved)} = Ti + 2\ CaO_{(Disolved)} \quad (2\text{-}6)$$

$$2O^{2-} + C = xCO_{2\ (gas)} + 4e^- \quad (2\text{-}7)$$

$$O^{2-} + C = CO_{(gas)} + 2e^- \quad (2\text{-}8)$$

Contamination can occur due to formation of TiC and Ti-Fe alloy from reactions with the crucible (Suzuki, 2007). Also, the high solubility of Ca in $CaCl_2$ increases the electronic conductivity of the melt, consequently reducing the current efficiency to around 5 percent (Fray, n.d.).

2.2.6 OS Process

The OS process (Figure 2.6), which was developed by Professors Suzuki and Ono at Kyoto University, is based on the ability of $CaCl_2$ to dissolve 3.9 mol% Ca and about 20 mol% CaO at 900°C. When $CaCl_2$ is electrolysed above the decomposition voltage of CaO but below that of $CaCl_2$, the Ca^+ ions are reduced to Ca at the cathode while O_2 evolved at the anode combines with the carbon anode to produce CO and CO_2.

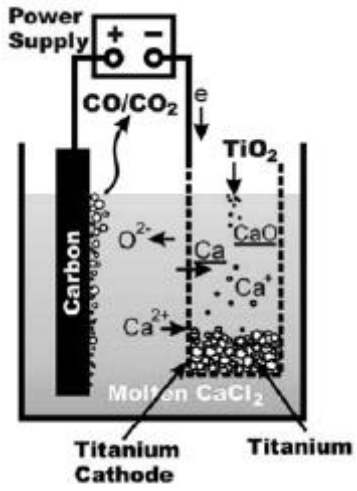

Figure 2.6: OS Process (Suzuki, 2007)

The OS process can produce low oxygen titanium in reasonable processing times. However, problems with Cl contamination and production of sub-oxides during the calciothermic reduction are yet to be resolved. Also, the titanium product is lumpy and requires further processing into a usable form (EHK Technologies, 2004).

2.2.7 FFC-Cambridge Process (Metalysis)

The Fray-Farthing-Chen (FFC) Cambridge process (Figure 2.8) was invented by D.J. Fray and co-workers at the University of Cambridge in conjunction with industry (Bertolini *et al.*, 2010; Schwandt, *et al.*, 2010). Titanium powder is produced by electrolysing a molten calcium chloride electrolyte between a sintered titanium oxide (rutile, TiO_2) preform cathode and a carbon anode at a temperature between 800ºC and 1000ºC. Synthetic rutile that is pre-treated for removing the iron is normally used to avoid contaminating the product. At an applied voltage of about 3 volts, oxygen is stripped from the TiO_2 cathode and transported through the $CaCl_2$ electrolyte to be discharged as oxygen gas at the anode made of carbon:

Cathode Reaction: $TiO_2 + 4e^- = Ti + 2\ O^{2-}{}_{(in\ CaCl2)}$ (2-9)

Anode Reaction: $2\ O^{2-}{}_{(in\ CaCl2)} + xC = xCO_{2/x} + 4e^-$ (2-10)

Net Reaction: $2\ TiO_{2(cathode)} + xC_{(gr\ anode)} = Ti + xCO_{2/x}$ (2-11)

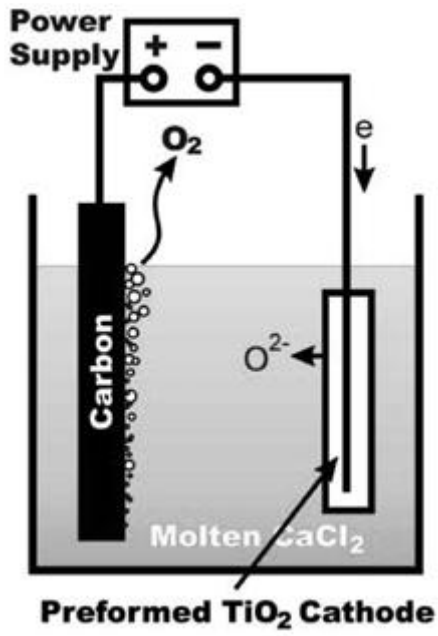

Figure 2.7: FFC process electrolysis (Suzuki, 2007)

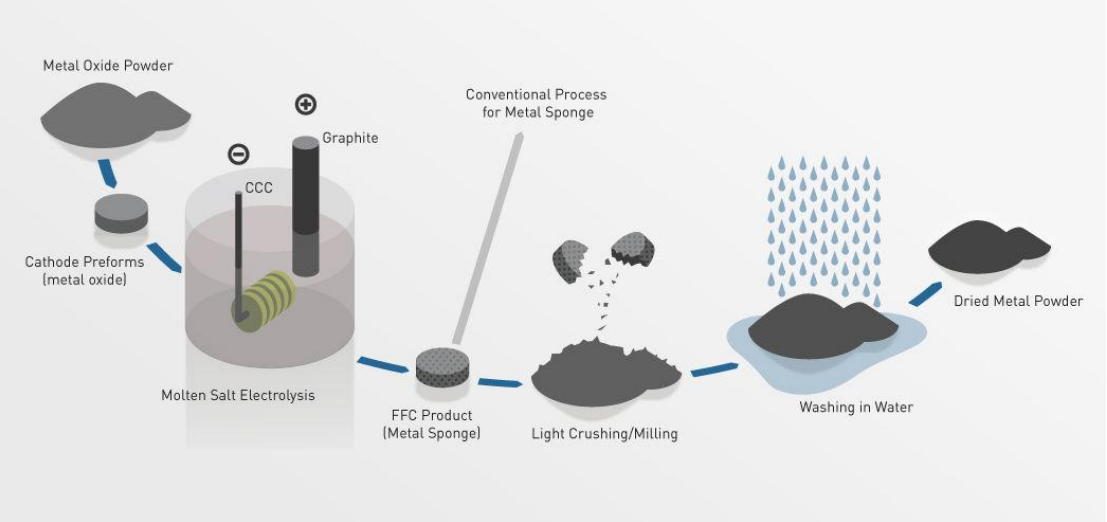

Figure 2.8: Schematic of the FFC Cambridge process (Bertolini, et al., 2010)

In 2010, the FFC process could produce ASTM Grade 4 Titanium with an oxygen content of about 2900 ppm, (Table 2.3). Further process development and optimisation work continues to increase product purity and process efficiency (Bertolini, *et al.*, 2010).

Table 2.3: Composition of titanium produced by FFC process (Bertolini, et al., 2010)

	Composition in ppm				
	O	C	Fe	Ca	Cl
FFC Ti	2900	700	140	1300	600
ASTM Gr4	4000	800	5000	1000	-

2.2.8 TiPro Process

The TiPro process (Figure 2.9) has two main stages; mechanical activation by high energy mechanical milling (HEMM), and solid/liquid separation by extrusion. A complimentary alloy purification stage may be incorporated to further reduce oxygen content. In the HEMM stage, powders blended to the desired stoichiometry are milled under an argon protective environment to prevent oxidation (Lü & Lai, 1998). To control excessive loss of powders through welding to vial walls and mill media, a process control agent isopropanol is also added. The blending ratio corresponds to the stoichiometry of the following reaction

$3TiO_2 + 7Al = 3TiAl + 2Al_2O_3 \quad \Delta H^{\circ}_{298K}$ = -178.616 kcal (2-12)

At 970°C: ΔG_{1243K} = -141.824 kcal

The Gibbs free energy of the reaction is negative in the temperature range of testing; indicating that the reaction is thermodynamically favourable. The object of high-energy mechanical milling is merely to enhance its kinetics. Since in this case high energy mechanical milling is only used as a feedstock preparation step and is not accompanied by a chemical reaction it is referred to as mechanical activation (Suryanarayana, 2004). Studies indicate that high energy mechanical milling (HEMM) of TiO_2/Al mixtures enhances kinetics and lowers the temperature of onset of the reduction reaction from about 1000°C for unmilled reactants to below 660°C depending on milling intensity. During milling there is creation of fresh surfaces, intimate mixing of reactants and consequently shortening the reactants diffusion distance. The milled composite powders produced are the feed to the solid/liquid separation stage. Integrating HEMM as a unit operation step into titanium production systems has the potential to reduce net

operating costs and the capital costs such as those for heating and refractory linings that are associated with conventional thermally activated processes (Moore & Feng, 1995; Zhang, 2004).

The subsequent solid/liquid separation stage starts by moderately preheating the TiO_2/Al composite produced by HEMM to ignite the combustion synthesis reaction.

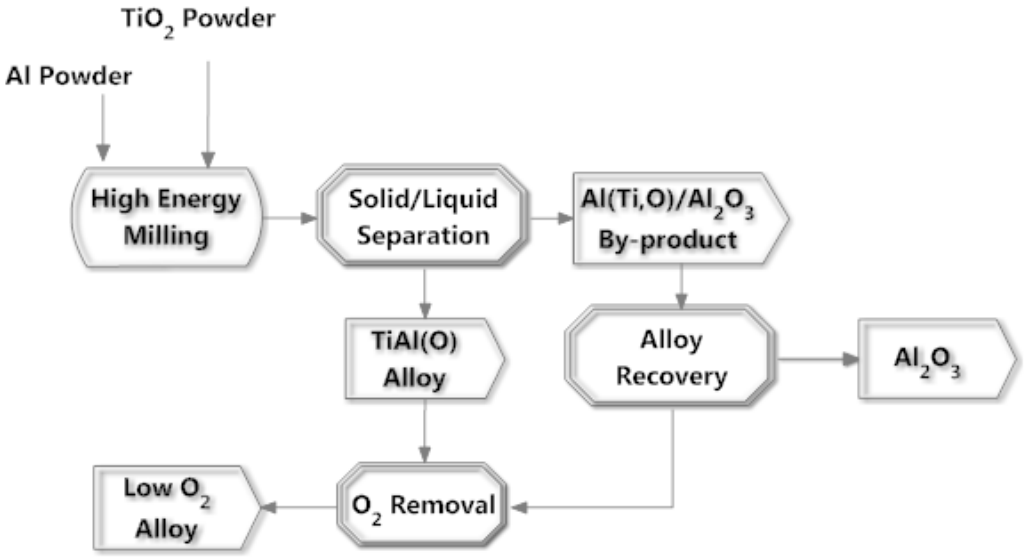

Figure 2.9: Flowsheet of the TiPro process

As milling time increases, the ignition temperature of the resultant TiO_2/Al composite powder decreases. The molten titanium-rich alloy product of combustion is separated from the alumina solid by-product by extrusion. This alloy may be purified further by calciothermic reduction to remove residual oxygen and alumina inclusions while the by-product may be processed to recover the contained titanium and alumina or used as a metal matrix composite.

2.3 Process Theory

2.3.1 High Energy Milling

High energy mechanical milling was developed at INCO's Paul D. Merica Research Laboratory about 1966 for producing oxide dispersion strengthened (ODS) nickel-based super alloys, but has since then gained recognition as a viable metallurgical processing unit operation. Before being milled, reactant powders are intimately mixed to get a homogenous composite powder. The mill is evacuated and filled with argon to avoid oxidation. When milling a ductile–brittle powder

mixture, the mixture goes through four stages of particle morphology: the initial, intermediate, final and completion stages. In the initial stage, the ductile Al powder particles go through plastic deformation and fracturing while TiO_2 particles, being brittle, are mainly fractured and incorporated into the ductile phase (Figure 2.10).

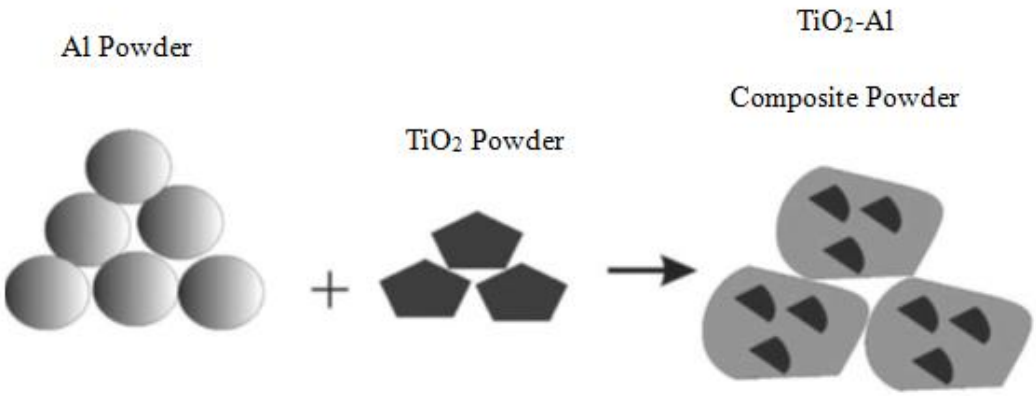

Figure 2.10: Schematic of composite powder formation through high energy mechanical milling (Zhang, 2004)

At the intermediate stage, the composite powder particles go through further refinement as fracturing and welding continues, creating lattice defects and shortening diffusion distances between particles. The particle shapes are changed into a layered structure with clear domains of component powders (Benjamin, 1990; Suryanarayana, 2004; Welham, 1998; Zhang, 2004). In the final stage, the composite powder has a fine nanostructure close to the composition of the starting powder mixture.

The particle size reduction following high energy mechanical milling of the TiO_2 and Al powder particles is accompanied by increased particle specific surface area, new atomically clean surfaces, intimate mixing to nanometre level and an increase in defect density. These factors shorten the atom diffusion path. There is also a localised temperature increase due to plastic deformation. All these effects make the milled powders so metastable they are ready to react at significantly lower temperatures than predicted by conventional process chemistry (Benjamin, 1990; Zhang, 2004).

High energy mechanical milling is a solid state powder process where powder particles are repeatedly fractured and cold-welded as the grinding media impacts the powder mixture (Zhang, 2004). During milling, the cold work energy is stored in the powder particles and then released through recovery and relaxation

processes within grain boundaries and grain growth when the powders are heated at moderate temperatures. Fecht (1995) reported that the stored enthalpy is significantly high and can be up to 40 percent of the enthalpy of fusion, depending on the intensity of high energy milling. The stored energy is mainly from reducing the grain size to nanometre level and from disordering (Zhang, 2004). This agrees with Fecht, who indicated that stored energy is in the form of grain boundaries and strain energy within the nano-particles (Fecht, 1995). Various researchers have since shown that this stored energy allows high energy milling to reduce the onset temperatures of chemical reactions and alter physical properties including melting temperature of milled powders (Adam *et al.*, 2007; Benjamin, 1990; Claussen *et al.*, 1996; Kamali & Fahim, 2009; Liu *et al.*, 2006; Welham, 1998; Zhang & Raynova, 2009; Zhang, 2004; Zhang *et al.*, 2004). Zhang *et al*. (Zhang & Raynova, 2009; Zhang, 2004; Zhang, *et al.*, 2004; Zhang *et al.*, 2009; Zhang *et al.*, 2005) demonstrated that mechanical milling can be used to initiate TiO_2-Al reactions at significantly lower temperatures than conventional thermochemical reactions. Welham (1998) also observed that the onset of the reaction between TiO_2 and Al powders decreased from 1050^{o}C in unmilled powders to 660^{o}C after 5 h of mechanical milling.

2.3.2 Solid/Liquid Separation

After the TiO_2/Al composite powder produced by high energy mechanical milling (HEMM) is preheated to the ignition temperature T_{ig}, (Figure 2.11) a combustion synthesis reaction (Takacs), also referred to as a self-propagating high temperature synthesis (SHS) reaction occurs. The heat generated raises the reaction products TiAl and Al_2O_3 to a combustion temperature T_c that is sufficiently high to volatilise impurities and produce more refined products than conventional metallurgical processing. Other advantages of high energy milling over conventional processing include simplicity; it uses cheaper equipment, and fewer processing steps, creating the potential for lower operating and capital costs.

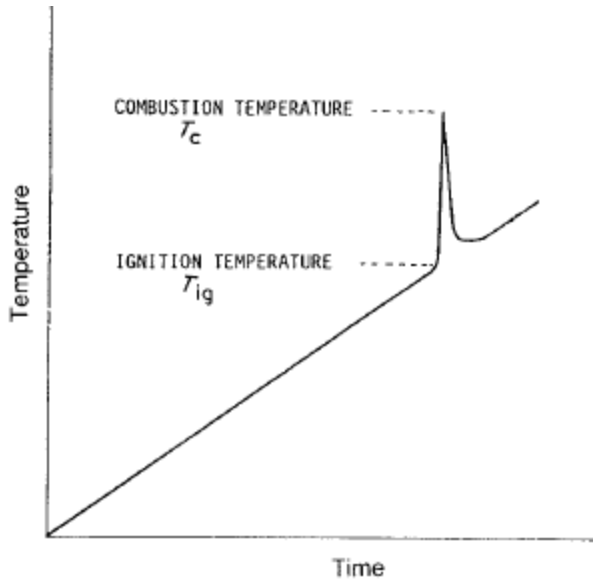

Figure 2.11: Schematic illustration of temperature profile of the thermal explosion mode combustion synthesis

The combustion synthesis reaction conditions used in the TiPro process produce solid corundum (Al_2O_3) and a liquid TiAl alloy. The density of both products is about 4 g cm^{-3} therefore they cannot be separated by gravitational methods. In previous studies, extrusion has been the main separation method.

2.3.3 Microstructural Development (Rahaman, 2003; Kang, 2005)

The solid Al_2O_3 - liquid TiAl system resulting from the combustion reaction in TiPro process is similar to conditions found in liquid-phase sintering. Liquid-phase sintering is a well-established consolidation technique in ceramic processing (Table 2.4). Unlike solid state sintering, the microstructural development during liquid-phase sintering is fast because of enhanced matter transport facilitated by the liquid. Therefore, in liquid-phase sintering where the intention is to densify the product, liquid-forming materials (additives) are deliberately added to enhance densification rates through particle rearrangement and liquid distribution. As the liquid phase forms during heating of a reactants powder compact, liquid flows into fine capillaries due to the capillary pressure difference between the fine and coarse channels of the solid particles. This liquid flow redistributes the solid particles through a phenomenon referred to as "particle rearrangement".

Two models have been formulated to explain densification during liquid-phase sintering. The model proposed by Cannon and Lenel suggests that liquid-phase sintering comprises liquid flow, solution/reprecipitation and solid-state sintering.

Based on this model, Kingery developed a densification theory for the solution/re-precipitation stage by assuming a continuous change in particle shape by flattening of the inter-particle contact area. The basic mechanisms and processes occurring in such systems and hence microstructural development have been explained in terms of three sometimes overlapping stages of liquid-phase sintering comprising:

Stage 1: Rearrangement and liquid redistribution

Stage 2: Solution-precipitation

Stage 3: Ostwald ripening

2.3.3.1 Rearrangement and Liquid Redistribution

In the presence of a wetting liquid (25 – 30 vol%), rearrangement of the solid phase particles coupled with liquid flow has been used to effect microstructural changes in materials. In traditional ceramics, the liquid phase usually a molten silicate remains as a glassy phase that gives the fabricated material a glassy appearance after cooling.

A wetting liquid phase enables the liquid phase to spread and cover the surface of the solid particles. This reduces inter-particle friction and enables particles to move more easily under the action of the compressive capillary stress exerted by the liquid. The densification attained is much higher compared to solid-state sintering.

Table 2.4: Common ceramic liquid-phase sintering systems (Rahaman, 2003)

Ceramic System	Additive content (wt %)	Application
Al_2O_3(talc)	≈5	Electrical insulators
MgO($CaO.SiO_2$)	<5	Refractories
MgO(LiF)	<3	Refractories
ZnO(Bi_2O_3)	2-3	Electrical varistors
$BaTiO_3$(TiO_2)	<1	Dielectrics
$BaTiO_3$(LiF)	<3	Dielectrics
UO_2(TiO_2)	≈1	Nuclear ceramics
ZrO_2($CaO.SiO_2$)	<1	Ionic conductors
Si_3N_4(MgO)	5-10	Structural ceramics
Si_3N_4(Y_2O_3-Al_2O_3)	5-10	Structural ceramics
SiC(Y_2O_3-Al_2O_3)	5-10	Structural ceramics
WC(Ni)	≈10	Cutting tools

The compressive capillary stress develops as the liquid wets and spreads over the solid surfaces eliminating the solid-vapour interface of the particulate system and forming pores in the liquid (Figure 2.12). The reduction of the liquid-vapour interfacial area therefore, is the driving force for shrinkage or densification of the system (Rahaman, 2003). According to Reed, less than 1 volume percent liquid phase is sufficient to coat the grains when the liquid is distributed uniformly in a material with 1-μm grain size. The liquid draws the particles together and angular particles may rotate, enabling sliding and rearrangement into a denser configuration. In systems where the liquid phase is inhomogeneously distributed (like powders milled for 1 h), differential rates of densification and grain growth produce an inhomogeneous (coarse) microstructure and a more porous texture (Reed, 1995) that could facilitate easier flow channels for TiAl.

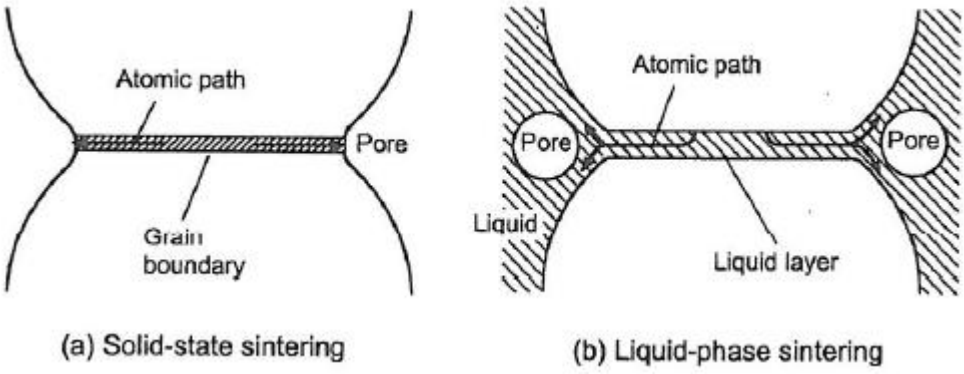

Figure 2.12: Sketch of a two-sphere model comparing microstructural development in (a) solid-state sintering with (b) liquid-phase sintering (Rahaman, 2003)

Particle rearrangement and densification in the presence of a wetting liquid is faster than in solid-state sintering because of the reduced inter-particle friction and enhanced matter transport provided by the liquid. In Figure 2.12, the pressure difference across the curved surface of the spherical pore with radius *r* in a liquid is given by the Young and Laplace equation:

$$\Delta P = -\frac{2\gamma_{lv}}{r} \qquad (2\text{-}1a)$$

γ_{lv} is the specific surface tension of the liquid-vapour interface.

The pressure in the liquid is lower than the pressure in the pore and this generates a compressive capillary stress on the particles that is equivalent to subjecting the system to an external hydrostatic pressure given by the Equation (2-1a). It is these capillary gradients that cause redistribution of the liquid and rearrangement of the particulate solid. As the capillary stresses cause the liquid to distribute itself between the particles and into small pores, further rearrangement and densification occurs, consequently limiting how much liquid alloy can be recovered by extrusion. Densification increases the viscosity of the system and drainage of the liquid alloy from small capillaries is impaired by the high capillary pressures holding the liquid. For systems with a wide particle size distribution, small particles are transported through the liquid to large particles. The net effect is coarsening of the microstructure by a process referred to as Ostwald ripening. Figure 2.13 shows a schematic of the microstructural evolution of a powder compact during liquid-phase sintering (Rahaman, 2003).

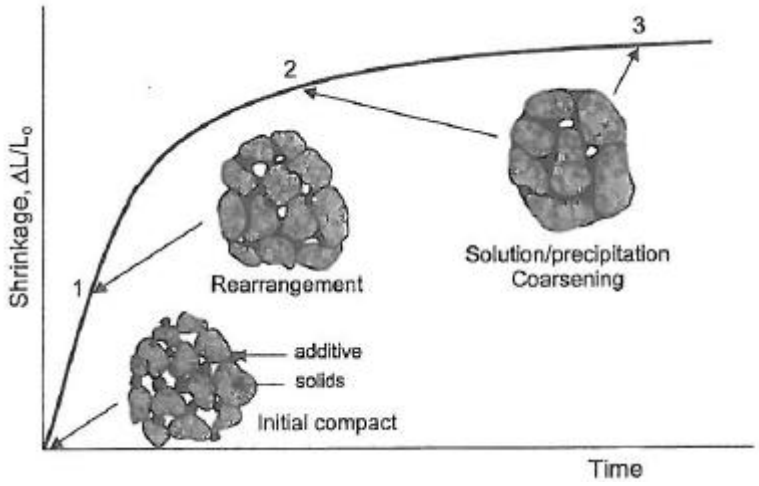

Figure 2.13: Schematic evolution of a powder compact during liquid-phase sintering showing three dominant stages (Rahaman, 2003)

2.3.4 Extrusion Mechanics

The extrusion pressure applied must overcome the crucible-wall friction and the resistive force of the solid Al_2O_3, which acts as a porous media. During extrusion, the flow of TiAl occurs as laminar flow between Al_2O_3 particles in the crucible and in the die entry-region (Reed, 1995). At the crucible wall, flow by slippage predominates. Flow of the liquid TiAl depends on die geometry, flow properties (such as viscosity) of the TiAl and permeability of the combustion synthesis product. For pressurised liquid TiAl to flow out, the permeability constant (K_p) of

the combustion synthesis product must be sufficiently high ($K_p \gg 10^{-18}\ m^2$) and the viscosity of TiAl must be low. Flow of liquid TiAl into interspaces between the corundum particles can be related to the driving force of the applied extrusion pressure drop using Darcy's law, which states that volume flow rate, Q is proportional to the differential pressure ΔP across the porous media of thickness L and cross-sectional area A. Flow rate is inversely proportional to viscosity of the fluid, η, and porous medium thickness, L.

$$Q = \frac{Kp\ A\ \Delta P}{\eta L} \tag{2-13}$$

The high porosity (around 50 percent of theoretical density) of the combustion synthesis products makes extrusion a potential alternative for recovering liquid TiAl (Moore & Feng, 1995). The molten TiAl flow direction is independent of extrusion pressure direction (Reed, 1995). The melt can preferentially flow into a pore space with a larger radius regardless of the pore orientation. Therefore, the porosity of the combustion synthesis product and the alloy phase fluidity are critical to ensuring the drainage and separation of the alloy from the solid corundum by-product. The flow of TiAl is affected by the temperature and the solids fraction of the melt. The presence of fine corundum particles in the liquid alloy phase can significantly change flow behaviour due to an under-cooling effect and increase in viscosity. This might adversely affect alloy yields during solid/liquid separation.

A high temperature during solid/liquid separation is needed to reduce viscosity and to stop the alloy from solidifying. The relationship between the viscosity of liquids and the volume fraction of solids' content can be represented by an Einstein-Roscoe type equation (Wright *et al.*, 2000):

$$\eta = \eta_o\ (1 - a f_s)^{-n} \tag{2-14}$$

where η and η_o are the viscosity of the solid-containing and solid-free liquid respectively; f_s is the volume fraction of solid particles in the liquid; *a* and *n* are constants. The reciprocal value of *a* corresponds to the maximum solids loading of the liquid before it has an infinite viscosity. The applicability of Einstein-Roscoe type equations has been confirmed empirically. The viscosity of most melts increases drastically and transitions from Newtonian to Non-Newtonian behaviour as the volume fraction of solids is increased (Figure 2.14). This phenomenon might adversely affect alloy yields during solid/liquid separation.

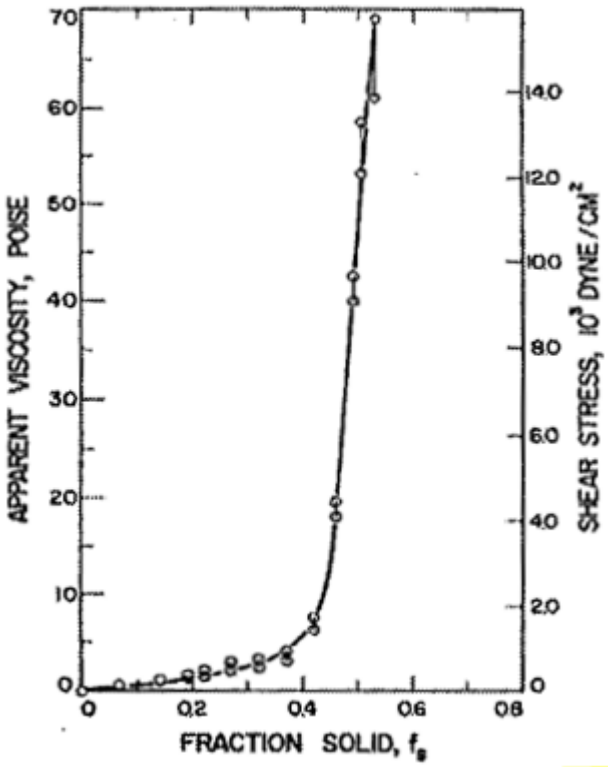

Figure 2.14: Viscosity and shear stress as functions of the solids fraction for the Sn-15%Pb alloy continuously cooled and sheared (Nafisi et al., 2004)

2.3.5 Thermodynamic Considerations

The highest temperature that can be attained by the products of the combustion synthesis reaction is estimated by the adiabatic temperature T_{ad}, calculated using the energy balance in Equation (2-15)

Energy of reaction + Energy Supplied = Energy for Heating Products (2-15)

For the TiO_2–Al powder milled for 1 h, the combustion reaction is assumed to occur at the ignition temperature 970ºC (1243K). Since the adiabatic temperature at constant pressure T_{ad} of this self-propagating high temperature synthesis system is higher than 1733 K, the TiAl melting temperature, Equation (2-15) reduces to:

$$\Delta H^{\circ}_{298} + \int_{298}^{1243} C_{p(3TiO2)}dT + \int_{298}^{934} C_{p(7Al(s))}dT + 7^{*}\Delta H^{f}_{Al} + \int_{934}^{1243} C_{p(7Al(l))}dT = \int_{298}^{1733} C_{p(3TiAl + 2Al2O3)}dT + \Delta H^{f}_{TiAl} + \int_{1733}^{Tad} C_{p(3TiAl + 2Al2O3)}dT \qquad (2-16)$$

$$178616 + \int_{298}^{1243} (53.802 - 1263900T^{-2})dT + \int_{298}^{934} (34.58 + 0.02072T)dT + 2560 + \int_{934}^{1733} 7.6dT = \int_{298}^{1733} (94.97 + 0.1038 - 2234000T^{-2})dT + \int_{1733}^{T_{ad}} (94.97 + 0.1038 - 2234000T^{-2})dT$$

$$178616 - (53.802 * (1243 - 298) + 1263900 * \left(\frac{1}{1243} - \frac{1}{298}\right) + (34.58 * (934 - 298) + 0.01036 * (934^2 - 298^2) + 2560 + 7.6 * (1733 - 934) = 94.97 * (1733 - 298) + 0.00519 * (1733^2 - 298^2) + 2234000 * \left(\frac{1}{1733} - \frac{1}{298}\right) + 94.97 * (T_{ad} - 1733) + 0.0519 * ({T_{ad}}^2 - 1733^2) + 2234000 * \left(\frac{1}{T_{ad}} - \frac{1}{1733}\right)$$

$$5.19{T_{ad}}^3 + 94970{T_{ad}}^2 - 202519643T_{ad} + 2234000 = 0$$

Solving the above polynomial yields T_{ad} = 1929.08 K (1656ºC)

Specific Heat Capacity Data

$C_{p\ (cal/K.mol)}$ = A + B*10^-3T + C*10^5T^-2 + D*10^-6T^2

Compound	A	B	C	D	Temp. Range (K)	Data Source
TiO_2 - Anatase	17.934		-4.213		298 - 2000	2
TiAl	13.37	1.42	-1.8		298 - 1733	1
$Al_{(s)}$	4.94	2.96			298 - 932	2
$Al_{(l)}$	7.6				932 -1650	2
$Al_2O_{3\alpha}$	27.43	3.06	-8.47		298 - 1373	2
$Al_2O_{3\gamma}$	25.48	4.25	-6.82			2

Enthalpy Data

Compound	MW	$\Delta H°_{298}$ (kcal/K.mol)	$L_{t,s,m,b}$ (kcal/K.mol)	Transition Temp. (K)	Data Source
$TiO_{2\ (anatase)}$	79.867	-225		1949 mp	1
$TiAl_{(s)}$	74.847	-17.4	11.4	1713	1
$Al_{(s)}$	26.98				2
$Al_{(l)}$			2.56		2
$Al_2O_{3\alpha}$		-400			2
$Al_2O_{3\gamma}$	101.96	-367.852			2

Data Sources: 1 - (Kubaschewski, *et al,*. 1993); 2 – (Barin, 1973)

The adiabatic temperature calculated using Equations (2-16) and standard enthalpy of the combustion synthesis reaction (-178.616 kcal) from Equation (2-12), is about 1656^{o}C, which is above the melting point of TiAl (1460^{o}C) but below the melting point of Al_2O_3 (2054 ^{o}C). However, to enhance liquid-solid separation, the heat content of the products has to be high enough to avoid the alloy phase fluid solidifying during extrusion. Due to heat losses, the actual combustion temperature (T_c) attained by the products is lower than the adiabatic temperature.

In combustion synthesis processing, the finer the composite powder the higher their reactivity such that it takes only moderate heating to initiate the reaction. The combustion starts at much lower temperatures compared to coarse composite powders. Consequently, the products plummet to low temperatures quicker. This is unfavourable for draining the liquid alloy out before it solidifies.

Coarse composite powders on the other hand are less reactive and have to be heated to relatively higher temperatures to initiate combustion. Since the combustion initiates at a much higher temperature, the corresponding heat content of the combustion products is higher and the alloy is maintained in molten state much longer. High ignition temperatures can potentially increase heat content of products (Figure 2.15). By the time the ignition temperature is attained, the powders would have acquired sufficient heat to maintain the alloy phase in a liquid state long enough to allow separation by extrusion. It is for this reason that coarse rather than fine microstructured composite powders are preferred.

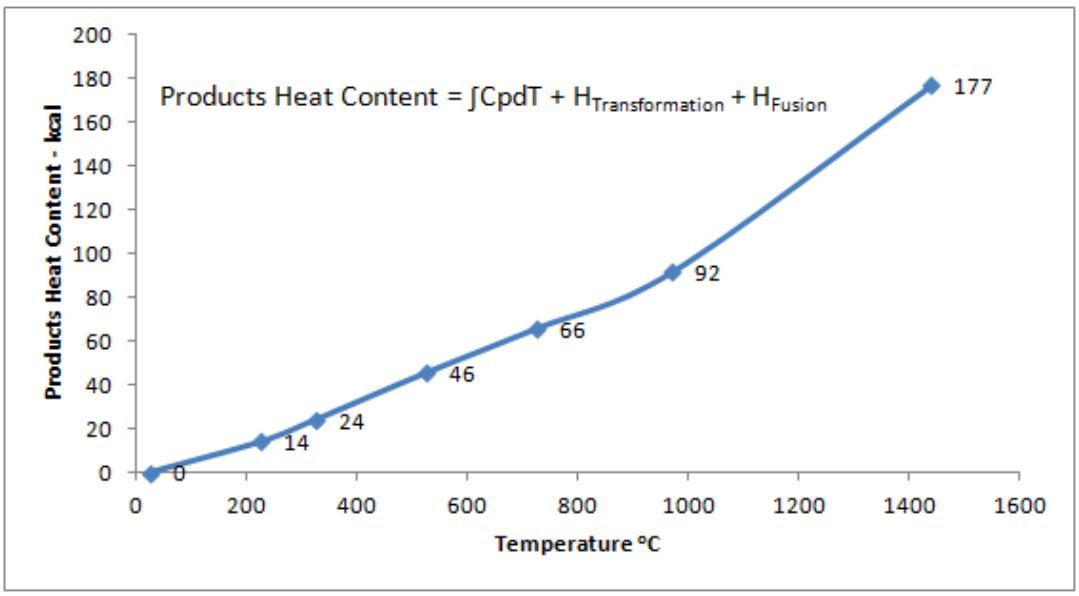

Figure 2.15: Products heat content as a function of reaction temperature

Combustion synthesis has been used to produce advanced materials ceramics, ceramic composites and intermetallic compounds since the early 1970s (Moore & Feng, 1995). Using highly reactive metals as reductants to produce metals from ores is well established in metallurgical processing. Applications include titanium production by the Kroll process and uranium reduction by calcium (Kubaschewski *et al.*, 1993). The reactions involved are called metallothermic reactions. Aluminothermic reduction uses aluminium as the reductant and calciothermic uses calcium as the reductant. Metallothermic reactions are designed so the heat generated by the reaction is sufficient to fuse one of the products of reaction and hence facilitate liquid-solid separation (Kubaschewski, *et al.*, 1993). In the TiO_2-Al system, the Ti-rich phase is melted by optimising high energy milling parameters to obtain a composite powder with a suitable microstructure. The other reaction product, Al_2O_3, remains solid. The reaction between TiO_2 and Al is sufficiently exothermic to be applied in combustion synthesis. Once heated to an ignition temperature, which depends on milling intensity, the chemical reaction is self-sustaining as it generates sufficient heat to melt the TiAl alloy but not the aluminium oxide (Al_2O_3).

Moore and Feng (1995) have reported that combustion synthesis reactions and final products are affected by the initial temperature of the reactants, the ignition temperature, the adiabatic temperature (i.e. the maximum combustion temperature under adiabatic conditions), and the actual combustion temperature (i.e. the maximum temperature under normal, non-adiabatic conditions).

When TiO_2/Al composite powders produced by high energy mechanical milling (HEMM) are heated, the combustion synthesis reaction rate is extremely high at a reaction temperature much lower than possible with unmilled reactants. Depending on milling intensity and other parameters such as TiO_2/Al mole ratio, the product contains Ti_xAl_y (O) and Al_2O_3. The CS reaction conditions that are chosen for producing TiAl by the TiPro^{TM} process result in solid corundum (Al_2O_3) and a liquid alloy that can then be separated by extruding the combustion synthesis product. The solid/ liquid separation stage in the TiPro^{TM} process for producing TiAl is based on the following nominal chemical reaction:

$$3\ TiO_2 + 7\ Al = 3\ TiAl + 2\ Al_2O_3 \qquad \Delta H^{\circ}_{298K} = -178.616\ \text{kcal} \qquad (2\text{-}17)$$

2.3.6 Physical Separation Processes

Following a chemical reaction stage of a process, a subsequent stage is often required to separate the valuable product from the by-product. Separation may be achieved by chemical or physical separation techniques. Chemical separation entails recovering valuables by altering the chemistry of one the constituents. Physical separation processes are techniques that separate components of a mixture depending on differences in their physical rather than chemical properties. However, chemicals may be added to enhance separation (Towler & Sinnott, 2012). Various physical separation processes based on different physical properties such as magnetic susceptibility, melting temperature, density, particle size, particle wetting and particle surface charge exist (Figure 2.16). For example, screening separates on the basis of size and can be used to separate materials that have different breakage characteristics. Gravity techniques such as sedimentation achieve separation due to differences in density. In previous studies (Adam, 2005), efforts to upgrade the combustion synthesis product by sedimentation (a gravity technique) yielded only little success, especially when there was little particle size difference between TiAl(O)-rich and Al_2O_3-phases. This potentially high technology risk was due to similarity in density between TiAl (4.15 g/cm^3) and Al_2O_3 (3.98 g/cm^3). In this study, an alternative physical separation process (froth flotation) has been proposed. Froth flotation is an established solid-solid separation process used to upgrade mineral processing ores. Froth flotation is often used to separate materials with similar physical properties of particles in the 1 to 800 microns size range (Figure 2.16).

In froth flotation, minerals suspended in water are separated by attaching them to air bubbles to selectively levitate the aerophilic (hydrophobic) mineral into the concentrate fraction, while leaving the other mineral in the tailings. The froth laden with hydrophobic mineral particles overflows into a launder constituting a concentrate. The hydrophilic mineral particles collect at the bottom of the tank to form tailings. In forward flotation, the more valuable mineral reports to the concentrate stream whereas in reverse flotation it reports to the tailings stream (Figure 2.17).

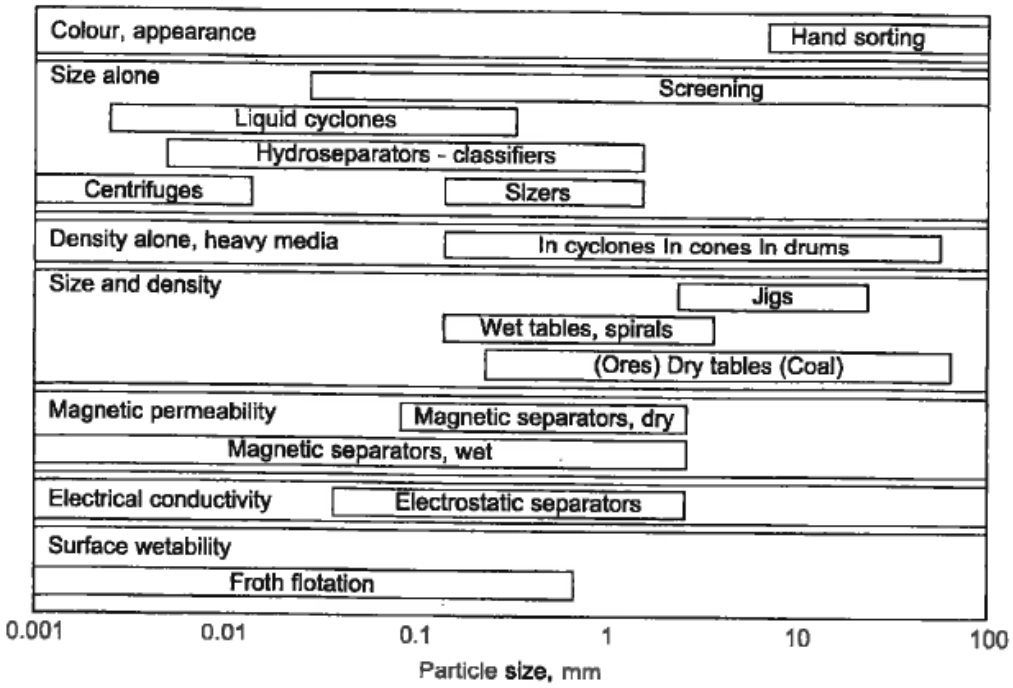

Figure 2.16: Solid to solid separation techniques and equipment (Towler & Sinnott, 2012)

To enhance attachment of mineral particles to air bubbles, a surfactant (collector) is added to the slurry. A collector acts by coating and making surfaces of mineral particles hydrophobic (aerophilic). A frother is added to make stable bubbles that can support mineral particles without collapsing. Flotation is a proven, cost-effective mineral processing technology with minimal technology risk (Crozier, 1992; Wills, 2006). Flotation separation has the extra advantage that it does not alter alloy phase chemical composition.

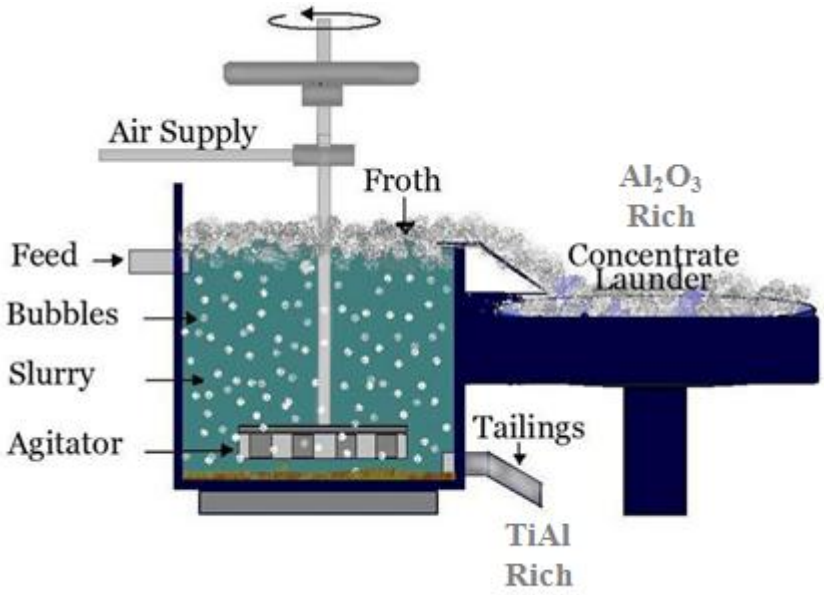

Figure 2.17: Reverse froth flotation process schematic (Aldo Miners, 2012)

2.4 Froth Flotation

Froth flotation was patented in 1906 to treat sulphide ores of copper, lead and zinc initially but due to its selectivity, applications now include processing of other low grade complex ores. The theory of froth flotation is complex and not fully understood. During flotation, the mineral being separated is selectively attached to air bubbles and lifted to the water surface from where it is skimmed off as an enriched froth. The other mineral (gangue) is left in the pulp or tailing. Air is introduced through a concentric tube surrounding the agitator shaft (Figure 2.17). As the agitator rotates, the air is broken into a dispersion of air bubbles throughout the slurry where it collides with and attaches to the particles. The rotation action of the agitator also maintains the particles in suspension. To enhance differences in physico-chemical surface properties and consequently the floatability of the particles of various minerals in the flotation pulp, a surface active reagent (collector) is added in small quantities. Excessive collector dosages tend to float other minerals and reduce their selectivity. Due to the chemical, electrical, or physical attractive forces between the polar end and mineral particles the collectors adsorb on the mineral particles with their non-polar end pointing toward the bulk solution thereby making the particles hydrophobic i.e. aerophilic (Wills, 2006). To help maintain a stable froth, a frother is also added. The particles to be separated attach themselves to the bubbles and are transported into the froth phase which overflows into a launder for recovery as a concentrate (Figure 2.17). The

froth phase enhances the overall selectivity of the flotation process by retaining the attached mineral and reducing entrainment of the tailing.

The flotation response of a mineral or compound is determined by the forces acting on its surface (Figure 2.18). The forces acting at the solid–water–air interface at equilibrium are given by Young's equation:

$$\gamma_{s/a} = \gamma_{s/w} + \gamma_{w/a}\cos\theta \qquad (2\text{-}18)$$

$\gamma_{s/a}$, $\gamma_{s/w}$ and $\gamma_{w/a}$ are the surface energies between solid and air, solid and water and water and air, respectively and θ is the contact angle between the mineral surface and the bubble.

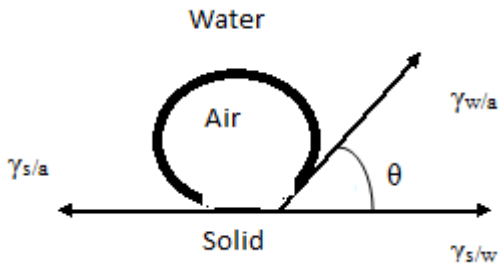

Figure 2.18 : Contact angle formed between the mineral surface and the bubble surface as a result of tensile forces

For a mineral to be recovered by flotation it must be rendered non-wettable. Wetting of a mineral particle occurs when its solid-air interface is replaced by a solid-water interface. When the contact angle θ at the water-solid interface is zero, water spreads on the solid. In such a case the solid is said to be wetted by water or hydrophilic. Air bubbles do not adhere to these hydrophilic solids when suspended in water. However, as the contact angle increases above zero, solids become hydrophobic and are not wetted by water; but air bubbles adhere to them (Yarar, 2000). This phenomenon can be represented as work of adhesion $W_{s/a}$. The work of adhesion is the force required to break the particle-bubble interface and is equivalent to the work required to separate the solid-air interface and produce separate air-water and solid-water interfaces

$$W_{s/a} = \gamma_{s/w} + \gamma_{w/a} - \gamma_{s/a} \qquad (2\text{-}19)$$

Combining Equations (2-19) and (2-20) yields

$$W_{s/a} = \gamma_{s/w} + \gamma_{w/a}(1 - \cos\theta) \qquad (2\text{-}20)$$

Equation (2.21) shows that the work of adhesion between a particle and a bubble increases with the contact angle. That is, the floatability of a mineral can be increased by increasing the contact angle. To increase the contact angle of an otherwise poorly floatable mineral, surface active reagents called collectors are added to the pulp (Wills, 2006). The flotation process can be carried out by either sending the valuable product to the froth or float fraction while maintaining the by-product or gangue in the pulp or the tailings. In direct flotation the more valuable mineral is transferred to the froth or float fraction, leaving the by-product to the tailing while in reverse flotation, the by-product in this case corundum is separated into the float fraction.

2.4.1 Collector Adhesion Mechanism

Separation of most minerals by froth flotation is based on selectively adsorbing a collector at the mineral/water interface. Since the contact angle plays an important role in froth flotation, techniques for studying factors that affect contact angles have been developed and applied in understanding the floatability of various minerals. The introduction of the concepts of the double layer and electrokinetic potentials in the interpretation of froth flotation has facilitated a physical-chemical analysis of the adsorption phenomenon as it relates to wettability and floatability of minerals (Fuerstenau & Pradip, 2005).

Through measurement of the conditions prevailing at solid/liquid/gas interfaces, a correlation among various mineral particle/water interface phenomena such as the adsorption density, contact angles, flotation response and zeta potential (Figure 2.19), has culminated into what is known as the electrostatic model of flotation.

Based on their surface bonding, minerals can be classified into non-polar and polar types. The non-polar minerals are characterized by weak molecular bonds that make them hydrophobic (i.e. difficult to wet). Mineral particles can only attach to air bubbles and subsequently be separated by flotation if they are hydrophobic. In pure state, non-polar minerals (such as sulphur, coal, diamond, talc and pure metals) are naturally floatable. In contrast, polar minerals have strong covalent or ionic surface bonding. They exhibit rapid surface wetting due to the strong reaction with water molecules that form multi-layers on the mineral surface, consequently making them hydrophilic.

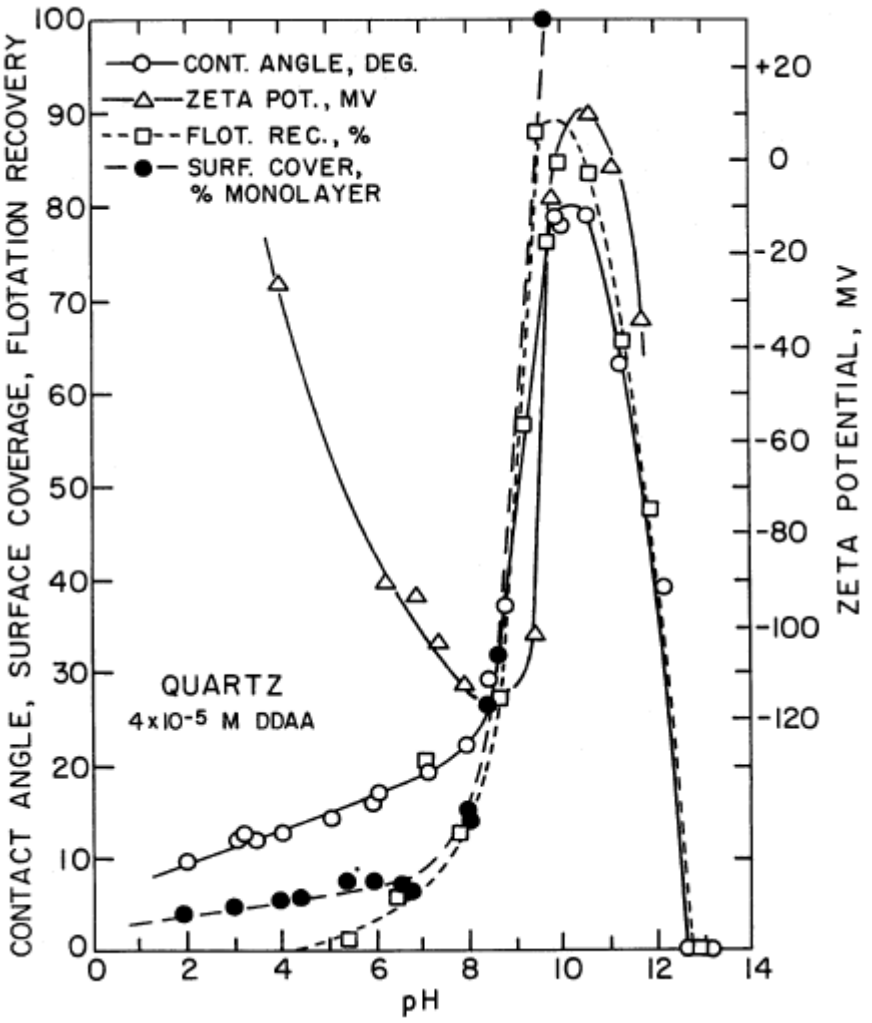

Figure 2.19: Correlation of various mineral particle/water interface phenomena

2.4.2 Electrical Double Layer

The phenomenon of the electrical double layer and electrokinetic potentials arises from the fact that when a solid is immersed into an aqueous solution a region of electrical inhomogeneity is formed at the solid-solution interface. The excess charge existing at the solid surface is balanced by a diffuse region of equal but opposite charge of the counter ions to maintain electroneutrality. Together, the surface charge and counter ions constitute the electrical double layer (Figure 2.20). The layer of counter ions adjacent to the surface (extending to the Stern plane) called Stern layer are strongly held to the surface through coulombic, chemical or Van der Waals forces. The remainder of counter ions are held by weak coulombic forces and they form a diffuse layer that extends into the liquid (Modi & Fuerstenau, 1960; Yarar, 2000).

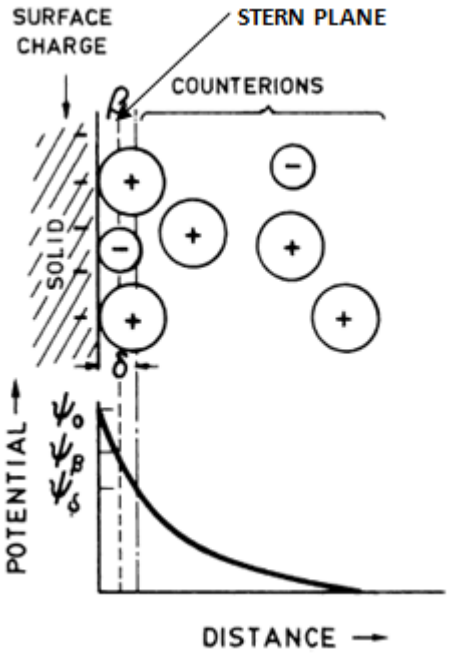

Figure 2.20: Electrical double layer phenomenon (Fuerstenau & Pradip, 2005; Yarar, 2000)

Adsorption of a collector at a mineral-water interface is in many cases controlled by the electrical double layer. Therefore, the parameters that quantify the electrical double layer such as the magnitude of the surface charge, the point of zero charge of minerals and specific adsorption of collectors have been applied in understanding selective adsorption of collectors and interpreting flotation behaviour. In the double layer, the collector ions function as counter ions therefore for the collector to be adsorbed it must carry a charge opposite to the charge of the mineral surface (Modi & Fuerstenau, 1960).

2.4.3 Electrokinetic Effect

When a phase is in relative tangential motion to an aqueous solution of an electrical double layer, an electric field is induced. The induced field results from the charge gradient at the plane of slippage (the slip plane) that is situated within the diffuse area of the electrical double layer in the bulk solution of the interface (Figure 2.20). The tangential motion along the slip plane disturbs the equilibrium of charges within the interface. The disturbance triggers a flow of charges in an attempt to restore the electrical balance across the interface on both sides of the slip plane. The interfacial flow and redistribution of charges is referred to as the electrokinetic effect. The charge gradient created at the slip plane is called the electrokinetic potential or zeta potential and is the difference in potential at the

slip plane and the potential in the bulk solution (Leja, 1982). As an indication of the particle charge surface, the zeta potential has successfully been used to delineate the favourable conditions for flotation. Extensive work carried out by Fuerstenau from 1953 to 1956 led to the electrostatic model of flotation. The model established that flotation collectors that adsorb by physical interaction with mineral particle substrates only function as counter ions in the electrical double layer. Therefore, the flotation of an oxide mineral using anionic collectors is appreciable only at pH levels below the PZC while for pH levels above the PZC, cationic collectors are required (Fuerstenau & Pradip, 2005). Electrokinetic studies have established the significance of the electrical double layer effects in the adsorption of collectors and other modifying reagents during flotation of oxide minerals.

2.4.4 Corundum Flotation Mechanism

Corundum is a polar mineral therefore recovering it by flotation requires that the particles are coated with a hydrophobic reagent called a collector (Wills, 2006). A collector may be an ionising compound which dissociates into ions in water or a non-ionising and insoluble type that renders the mineral particles hydrophobic by coating them with a thin film. Ionising collectors are widely applied in flotation. They are complex molecular compounds containing a non-polar organic group and a polar group. Due to chemical, electrical or physical attraction between the polar group and the mineral surfaces, collectors adsorb on the particles with their non-polar ends oriented towards the bulk solution thus making the particle hydrophobic (Figure 2.21).

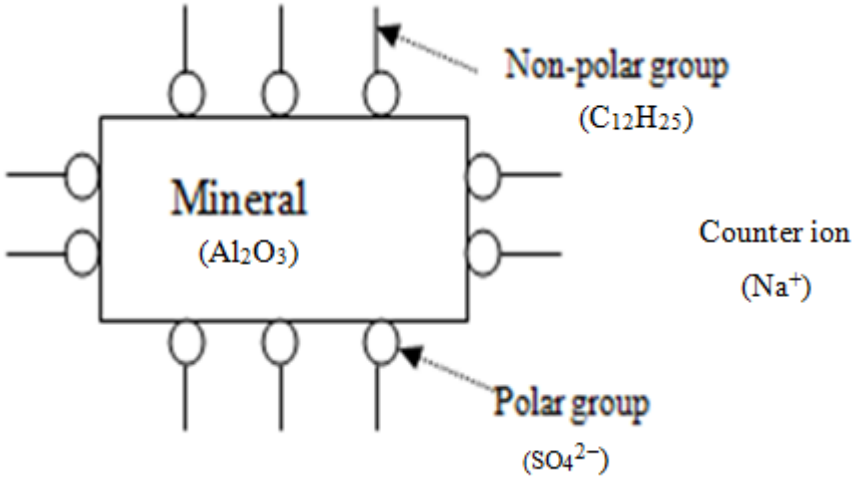

Figure 2.21: Collector adsorption on a mineral surface (Wills, 2006)

Fuerstenau and Pradip (2005) have demonstrated that in systems where the collector is physically adsorbed on the mineral surface, selective flotation depends on differences in the point for zero charge (PZC) of the minerals that are to be separated. Corundum (Al_2O_3) and TiAl can be separated by flotation in the pH window where the two minerals are oppositely charged (Modi & Fuerstenau, 1960). The PZC is determined by measuring the zeta potential as a function of pH and corresponds to the pH where the zeta potential is zero.

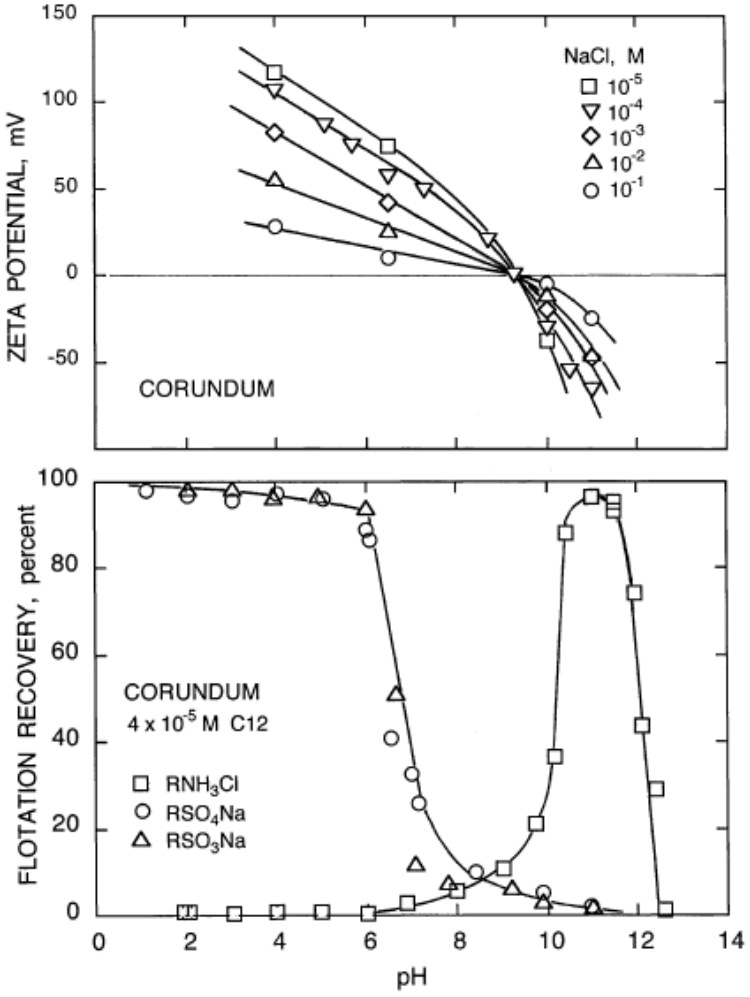

Figure 2.22: Influence of surface charge on flotation of corundum (Fuerstenau & Pradip, 2005)

The PZC of corundum is pH 9.1 while for non-oxide Ti suspensions in water the PZC lies between pH of 3 and 4 (Yeh & Hon, 1995). Above pH 4, TiAl is negatively charged while corundum remains positively charged up to pH 9.1; therefore corundum can be floated with an anionic collector by maintaining the pH as acidic as possible but above the PZC of TiAl. Within this pH window TiAl cannot be floated with an anionic collector. A cationic collector is required for pH above 9.1 (Figure 2.22 and Figure 2.23).

In their investigations on the effects of alkyl sulfonates on the wettability of Al_2O_3, Wakamatsu and Fuerstenau (1973) observed that the contact angle on Al_2O_3 was affected by the adsorption of sulfonates at the solid/water interface and was strongly controlled by the pH, the sulfonate concentration and the number of carbon atoms in the alkyl chain. As the pH was increased beyond pH 9.1 the point of zero charge (PZC), sulfonate adsorption ceased and the alumina became hydrophilic. In neutral and acidic solutions sulfonate adsorption and the contact angle increased significantly. Therefore floatability of corundum using an anionic collector increases as the slurry becomes more acidic (Figure 2.22). Since pH controls the charge at the surface of corundum particles it also controls its flotation (Modi & Fuerstenau, 1960).

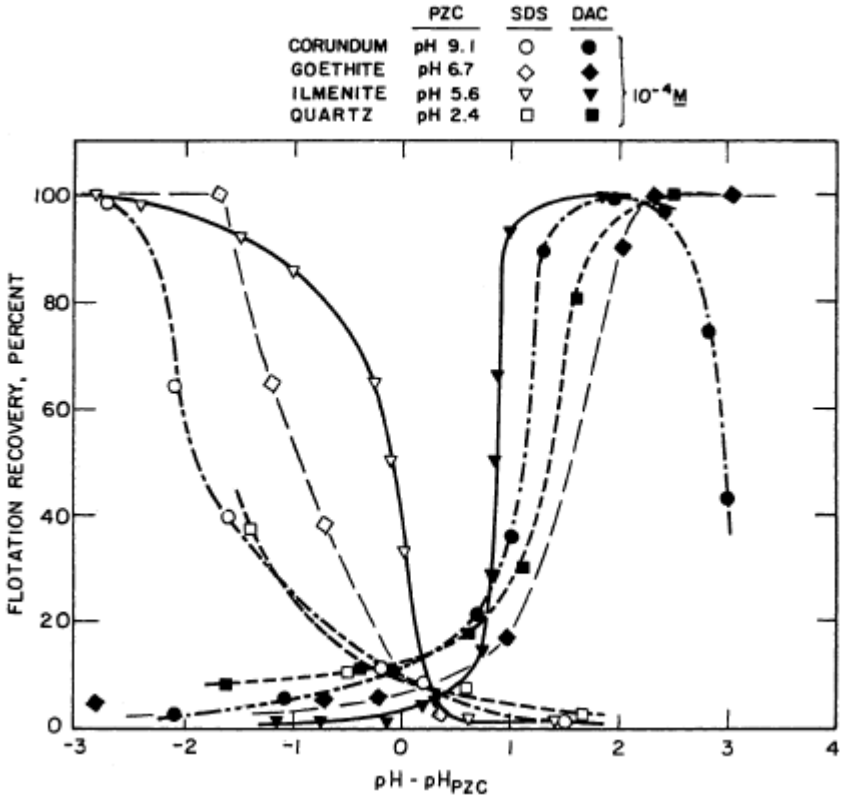

Figure 2.23: Effect of pH on flotation response of corundum with sodium dodecyl sulphate (Fuerstenau & Pradip, 2005)

2.4.5 Calciothermic Alloy Purification

The Ti-Al alloy product from the combustion synthesis (aluminothermic reduction) step contains dissolved oxygen and some Al_2O_3 inclusions that need to be removed by calciothermic or calcium hydride reduction. In calciothermic purification, the crude Ti-Al alloy powder is mixed with $CaCl_2$ and reacted with calcium vapour at about 1000^{o}C. Using calcium vapour rather than condensed

calcium is preferable because it avoids introducing contaminants. Kubaschewski and co-workers (1993) demonstrated that at 1000ºC, calcium can reduce the oxygen content in titanium down to 0.07 percent by weight by overcoming the affinity of oxygen to both the oxides of titanium and dissolving in metallic titanium phases such as α-Ti, γ-TiAl and α_2-Ti_3Al (Figure 2.24).

An unpublished previous work based on an existing patent by Zhang that describes the use of calcium vapour in a vacuum furnace failed to reproduce the results. This was attributed to poor reactor design, a feature that is also known to adversely affect scalability of the process. In this study, the vacuum furnace was replaced with an induction furnace in order to ease the control process parameters.

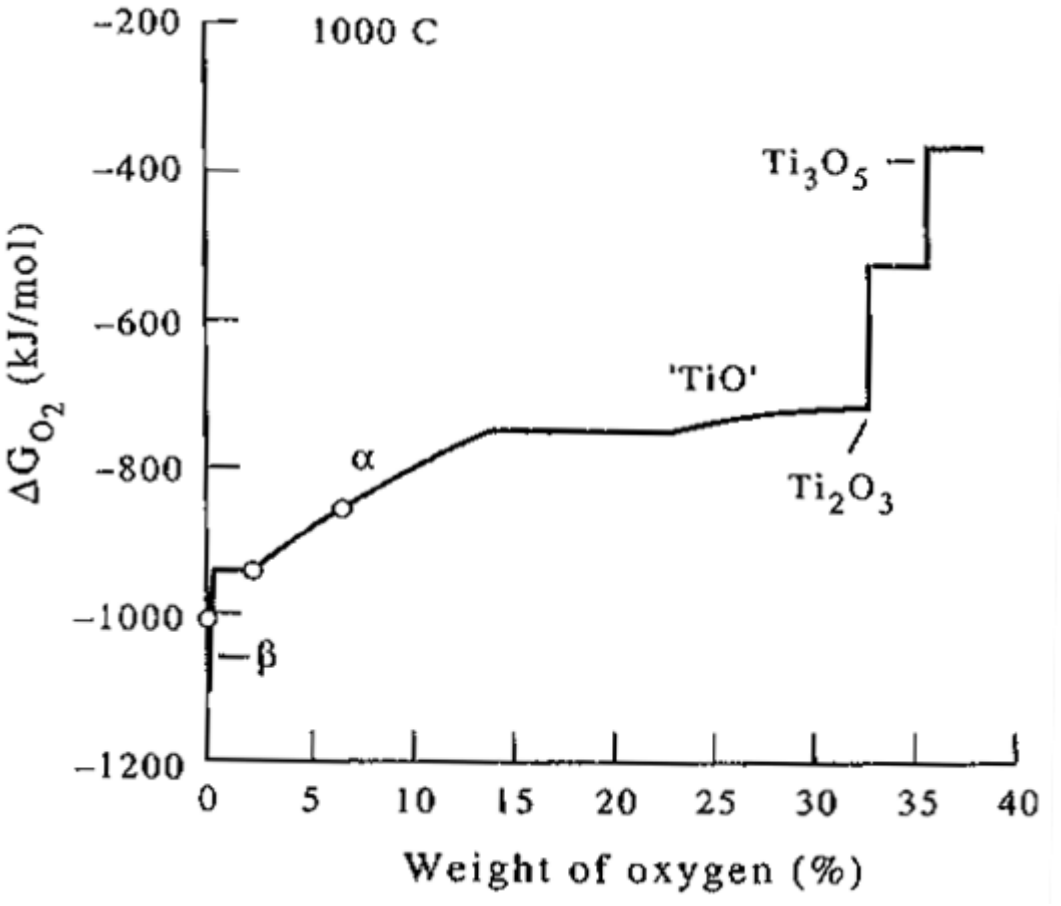

Figure 2.24. Partial Gibbs energies of dissociation of 1 mole oxygen in the titanium-oxygen system at 1000ºC (Kubaschewski, et al., 1993)

The mechanisms of the calciothermic reaction are illustrated in Figure 2.25. Calciothermic purification is based on the ability of $CaCl_2$ to dissolve up to 20 mol % CaO (the reaction product) and up to 3 mol % Ca (the reductant) at 900ºC (Suzuki, 2007; Zhang, 2010). The Gibbs energy of dissociation of CaO, MgO and BaO (i.e. assimilation of oxygen from the Ca/CaO, Mg/MgO and Ba/BaO

mixtures equilibrated with the titanium-oxygen system respectively) are represented by the three circles in Figure 2.25. The Ca/CaO reaction is the most effective in deoxidising titanium.

The inclusion/removal reaction is:

$$Al_2O_{3(solid)} + 3Ca_{(vapour)} = 2Al_{(molten)} + 3CaO_{(solid)} \quad (2\text{-}21)$$

The dissolved oxygen removal reaction is:

$$Ca_{(vapour)} + O_{(dissolved)} = CaO_{(solid)} \quad (2\text{-}22)$$

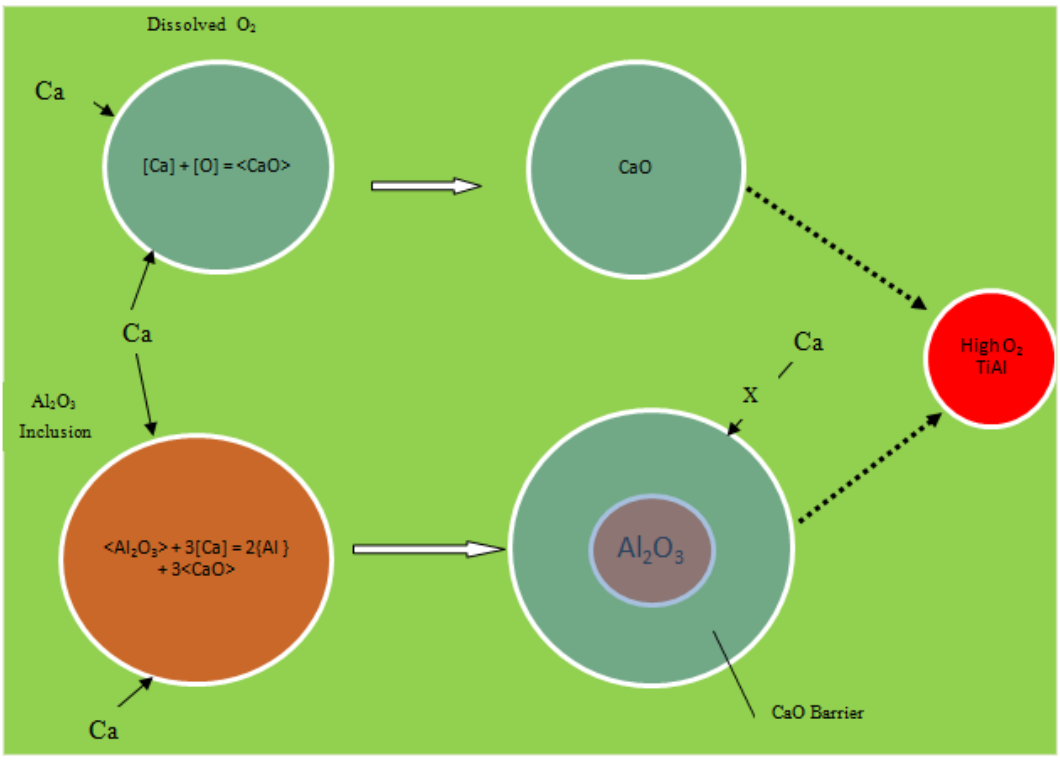

Figure 2.25: Schematic of CaO passivation in absence of $CaCl_2$ carrier

In the absence of carrier $CaCl_2$, the CaO produced in the reaction between Ca and Al_2O_3 (Figure 2.25) could inhibit further reaction and the purification process (Suzuki, 2007).

2.4.6 Calcium Hydride (CaH_2) Reduction

The dissolved oxygen and alumina inclusions (the main impurities in the alloy phase) can also be reduced using CaH_2. Compared to other reductants (Al, Mg and Si), CaH_2 reduction occurs at a lower temperature and separation of the alloy from the by-product is easily achieved by washing the product with water. CaH_2

neither forms intermediate titanium oxides such as Ti_3O_5, Ti_2O_3 (Figure 2.24) and TiO; it has very little tendency to form alloys therefore the product yield is quantitative. Also, the formation of a protective hydrogen atmosphere reduces oxygen pick-up. The reduction of Al_2O_3 with CaH_2 (Equation (2-23)) initiates at 500 ^oC and is complete by 750^oC (Wiberg & Amberger, 1971).

$$Al_2O_3 + 3CaH_2 = 2Al + CaO + H_2 \quad (2\text{-}23)$$

At 700^oC: ΔH_{973K} = +84.024 kcal ΔG_{973K} = -19.448 kcal

CaH_2 can be used to remove oxygen dissolved in combustion synthesis products by the endothermic reaction

$$CaH_2 + O_{(dissolved)} = CaO + H_2 \quad (2\text{-}24)$$

At 1000^oC: ΔH_{1273K} = +5.617 kcal ΔG_{1273K} = -33.862 kcal

The Gibbs free energy of the reaction calculated using data obtained from (Kubaschewski, 1983; Barin, 1973 and HSC Software) is negative hence thermodynamically favourable but endothermic.

2.5 Process Inputs and Raw Materials

The vast iron sand deposits of New Zealand, including the Taharoa on North Island's west coast and Waikato North Head mine deposits, which are mined for iron by New Zealand Steel, contain significant amounts of by-product titanium that can be used as a TiO_2 source (Barakat & Drain, 2006). Shallow drilling cores off the southern Taranaki coast, validated by aeromagnetic surveys in 2010 and 2011, estimate iron sand deposits equivalent to 200 million tonnes of concentrate at 60 percent iron (Scoop Independent News, 2011). There are also other potential deposits off the west coast of the North Island. The other raw material for alloy refining is $CaCl_2$, a low-cost material.

2.6 Process Parameters Optimisation

The composition and microstructure of reactant powders have a significant effect on solid state reactions. High energy mechanical milling is a well-established technique for varying microstructures of reactant powders in order to optimise reaction kinetics, energy utilisation and the separation of reaction products.

2.6.1 Effect of Mixing

High-energy mechanical milling or activation and combustion synthesis are solid state processes and homogeneity of reactant powder mixtures influence the reaction mechanism and products (Thompson, 2002). Prior to milling, the starting powders are thoroughly mixed to ensure a homogenous distribution of component powders in the desired stoichiometric ratio (Lü & Lai, 1998). Other investigations on wettability of TiO_2 by molten Al (Shen *et al.*, 2006) demonstrated that an alumina-rich phase product of the reaction can limit Al availability to TiO_2 and subsequently affect both reaction kinetics and type of aluminide formed. Therefore, the composite powder microstructure must be as uniform as possible and the alumina product of the reduction reaction needs to be optimised to achieve the desired aluminide at acceptable yields.

The composition of the titanium aluminide formed is influenced by homogeneity and TiO_2:Al ratio of the reactant composite powders in the reaction zone (Gheorghe & Rack, 2002; Shen, *et al.*, 2006; Thompson, 2002). At the microstructural level, the alumina-rich phase formed in the reaction can act as a barrier between the reactants (Figure 2.26).

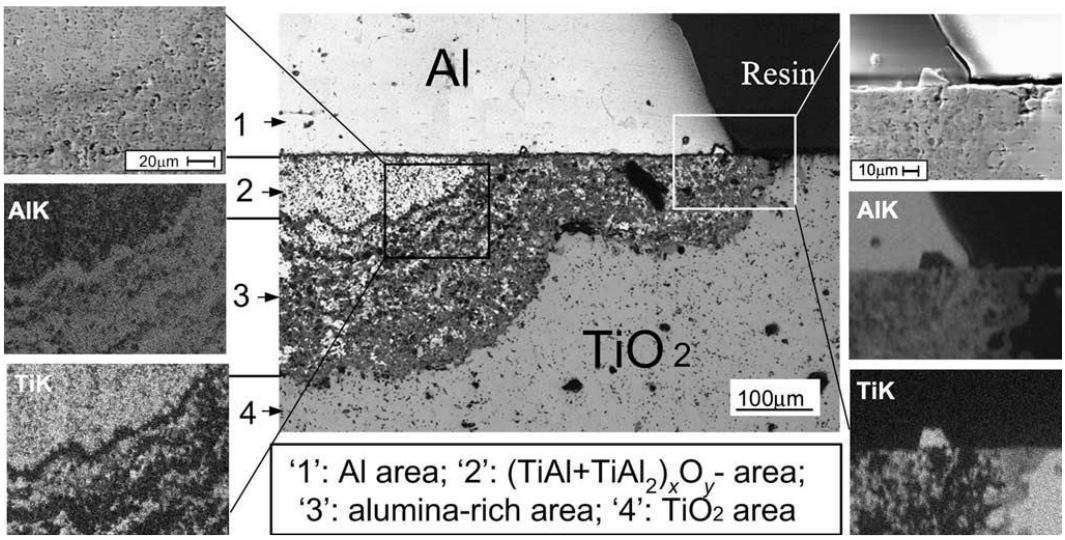

Figure 2.26: Coexisting phases and formation of an alumina-rich reaction inhibiting barrier at the TiO_2-Al interface during thermal treatment (Shen, et al., 2006)

Some researchers report that regardless of the initial composition of the reactants, $TiAl_3$ is the first intermetallic phase formed. Formation of other titanium compounds depends on the availability of TiO_2 at the reaction interface. They

proposed the following sequential reaction mechanism until all TiO_2 is consumed (Feng & Froyen, 2000; Gaus *et al.*, 2000; Welham, 1998).

$$3\ TiO_2 + 13\ Al = 3\ TiAl_3 + 2\ Al_2O_3 \qquad \Delta G_{1243K} = -172.130\ \text{kcal} \tag{2-25}$$

$$6\ TiO_2 + 7\ TiAl_3 = 13\ TiAl + 4\ Al_2O_3 \qquad \Delta G_{1243K} = -212.933\ \text{kcal} \tag{2-26}$$

$$6\ TiO_2 + 15\ TiAl = 7\ Ti_3Al + 4\ Al_2O_3 \qquad \Delta G_{1243K} = +131.146\ \text{kcal} \tag{2-27}$$

$$24\ TiO_2 + 2\ Ti_3Al = 15\ Ti_2O_3 + Al_2O_3 \qquad \Delta G_{1243K} = -430.721\ \text{kcal} \tag{2-28}$$

Gheorghe and Rack (Gheorghe & Rack, 2002) report that although the initial steps in the reaction sequence do not depend on the TiO_2:Al ratio, the final steps do. Based on the proposed reaction mechanisms, it is probably important to ensure a homogeneous distribution of reactant powders to attain the desired stoichiometry.

2.6.2 Effect of Temperature on the Enthalpy of Reaction

The reaction between TiO_2 and Al is metallothermic and should be designed so the heat generated by the chemical reaction is high enough to produce a molten TiAl product and thus facilitate separation from the solid alumina (Al_2O_3) phase (Kubaschewski, *et al.*, 1993). The widely-accepted Ti-Al phase diagram (Figure 2.27) shows the liquidus temperature of the TiAl alloy is about 1450°C. Therefore, the final temperature of the reaction products, T_{final}, needs to be above 1450°C to obtain molten TiAl.

$$T_{final} = T_{Reaction} + \Delta T \tag{2-29}$$

T_{final} is the temperature of the products; $T_{Reaction}$ is the temperature at which the reaction takes place i.e. the ignition temperature T_{ig} and ΔT is the temperature increase due to the reaction.

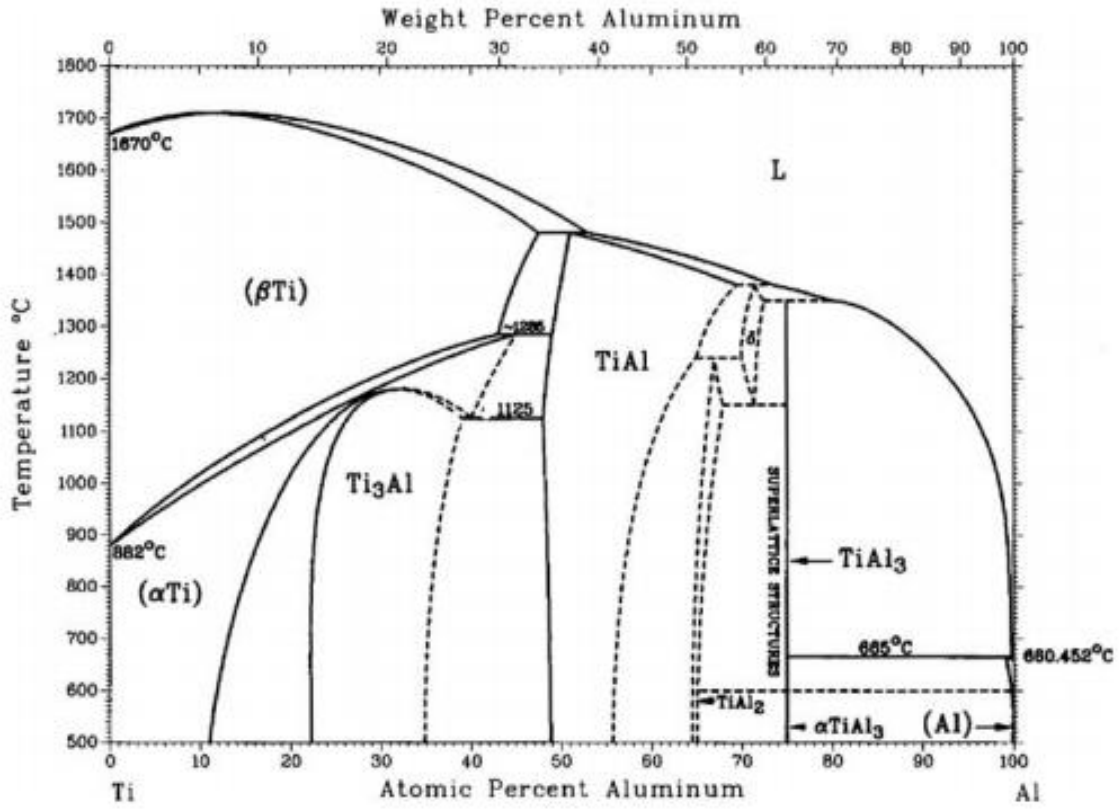

Figure 2.27: Phase diagram of the Ti - Al system (Schuster & Palm, 2006)

The temperature at which the reaction occurs, $T_{Reaction}$, and the temperature rise ΔT are influenced by composition and microstructure of the reactant mixture. Extended high energy milling lowers the ignition temperature of the powders and this makes solid state reactions possible because the onset of the reaction between TiO_2 and Al is below 660ºC, the melting temperature of aluminium (Adam, 2005). Reaction conditions need to be optimised to increase the heat content of the products of combustion. An ignition temperature that ensures sufficient heat to produce molten TiAl product without increasing heating costs and adversely affecting process economics should be used.

2.6.3 Effect of Heating Rate

Studies of a 55 vol% Al / 45% TiO_2, by differential thermal analysis (DTA), indicated that exothermic peak temperatures high enough to form a liquid alloy phase could be attained by increasing the heating rate (Gaus, *et al.*, 2000). The effect of heating on the attained exothermic peak is illustrated in Figure 2.28.

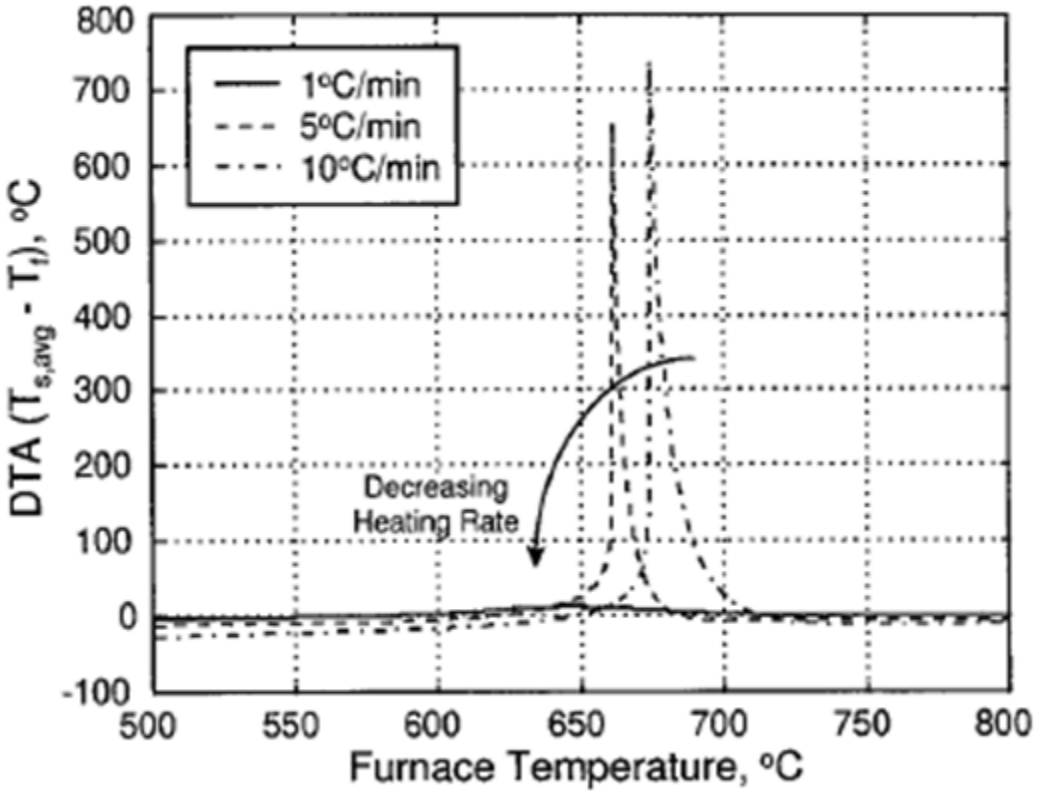

Figure 2.28: Effect of heating rate on attained exothermic peak temperature (Gaus, et al., 2000)

2.6.4 Effect of Cooling Rate on Alloy Flow and Separation

Alloy flow and yield are affected by the rate at which the combustion synthesis products are cooled. The alloy cannot flow out once solidification occurs. To maintain alloy flow and increase alloy yields, the CS products may be held at the peak temperature by continuing to heat the products for several minutes after the combustion reactions have finished using an external heat source (induction coil).

2.6.5 Effect of Milling Time

Gennari and his co-workers (Gennari *et al.*, 2006) showed that the wave velocity of the SHS process for particle sizes above 1 µm was almost linear to the inverse of the particle size and that dissolution of the transition metal ceases to be a rate controlling mechanism. Precipitation or dissolution of reaction products then becomes the rate controlling mechanism. Consequently, particle size affects composition and microstructure of reaction products. Particle size is determined by the milling time. Extending milling beyond a critical stage where fracturing exceeds welding mechanisms produces fine powders with a low onset temperature for the combustion reaction.

2.6.6 Effect of Porosity and Dilution

Gennari and his co-workers (Gennari, *et al.*, 2006) showed that porosity of reactants influences the effective thermal conductivity and energy per unit volume produced by the exothermic reaction. High porosity reduces propagation speeds in combustion synthesis reactions.

2.7 Hypothesis of the Research

The combustion reaction between TiO_2 and Al goes to completion, producing TiAl and Al_2O_3 at almost 100% conversion efficiency. However, the yield of TiAl alloy from solid/liquid separation by extrusion alone is less than 10% of the stoichiometric quantity. Mechanisms involved in solid/liquid separation of TiAl from Al_2O_3 by extrusion are not well understood. The hypothesis is that the microstructure of reactant powder mixtures will affect separation of the Ti alloy from Al_2O_3. In this research, the effects of microstructure on the solid/liquid separation process will be investigated. By controlling the milling intensity, the reactant powder microstructure can be tailored to attain sufficiently high temperatures to allow extrusion of the Ti alloy out of the combustion synthesis product. During combustion synthesis, powders with a coarse microstructure (i.e. milled for short periods) will ignite at a high temperature and increase the heat content of products. Therefore, by the time the ignition temperature is attained, the powders would have acquired sufficient heat to maintain a molten alloy phase for separation by extrusion. Coarse rather than fine microstructured composite powders are in this regard more suitable.

The yield and quality of liquid TiAl that can be extruded out of the combustion synthesis product is limited because of the wetting properties of liquid TiAl on Al_2O_3. The contact angle of liquid TiAl on Al_2O_3 is 38^o, which is low and therefore significant amounts of TiAl will be retained by Al_2O_3 particles due to wetting and solidification (Li *et al.*, 2008). Also, viscosity of most melts increases drastically and transitions from Newtonian to Non-Newtonian behaviour occur as volume fraction of solids is increased (Wright *et al.*, 2001). This phenomenon might adversely affect alloy yields during solid/liquid separation. To understand the mechanisms underlying separation of the Ti alloy from Al_2O_3 during extrusion, this research investigates the different microstructures in reactant powder mixtures produced using various milling intensities. The microstructure will be

monitored by optical and scanning electron microscopy (SEM) imaging. The composition and textural data obtained will also be used to establish the extent of combustion synthesis, delineate the extent of milling required to liberate the Ti alloy from Al_2O_3 contained in the extrusion by-product and to identify potential alternative separation methods (such as froth flotation) for increasing Ti alloy yields. The reaction temperature will be monitored with a Type B (Rhodium-Platinum) thermocouple imbedded in a 2mm hole drilled into the compact and attached to a Picolog data logger.

In previous studies (Adam, 2005), gravity separation experiments were not satisfactory because of similarities in density of TiAl and Al_2O_3. Therefore, I will evaluate the viability of using froth flotation as a complementary process to increase TiAl yields. Froth flotation is a proven cost effective mineral processing technology with minimal associated technology risk and has been applied in the separation of minerals with similar physical and chemical properties (Crozier, 1992; Wills, 2006). Froth flotation separating efficiency will be calculated from the TiAl partition between the float and the tails fractions. The TiAl content of the fractions will be determined by gravimetric methods, XRD and XRF analyses.

2.8 Aims of the Study

The aims of this study are to:

- Understand solid/liquid separation mechanism in extraction of TiAl from TiAl(O)/Al_2O_3 composite by extrusion
- Investigate effects of microstructure on TiAl yields
- Investigate froth flotation parameters to increase TiAl grade of the combustion by-product before leaching to recover the residual TiAl

2.9 References

Adam, G. (2005). *Processing of Ti(Al, O)/Al_2O_3 Powders to Produce Ti_3Al/TiAl Powders Using Novel Techniques.* PhD thesis, University of Waikato, Hamilton, New Zealand.

Adam, G., Zhang, D. L., Liang, J., & Macrae, I. (2007). A novel process for lowering the cost of titanium. *Advanced Materials Research, 29-30*, 147-152.

Agatzini-Leonardou, S., Oustadakis, P., Tsakiridis, P. H., & Markopoulos, C. (2008). Titanium leaching from red mud by diluted sulfuric acid at atmospheric pressure. *Journal of Hazardous Materials, 157*(2-3), 579-586.

Aldo Miners. (2012). *Flotation in Mining [Technology Industry Of Gold Mining Online Blog]*. Retrieved 20 December, 2012, from http://miningeducation.blogspot.com.au/2012/01/flotation-in-mining.html

Barakat, M., & Drain, L. (2006). The development of Waikato North Head ironsand deposit, South Auckland. In A. B. Christie & R. L. Brathwaite (Eds.), *Geology and Exploration of New Zealand Mineral Deposits: Monograph 25* (pp. 219-224). Carlton, Vic., Australia: Australasian Institute of Mining and Metallurgy.

Barakat, M., & Ruddock, R. (2006). Taharoa ironsand mining operation, Waikato. In A. B. Christie & R. L. Brathwaite (Eds.), *Geology and Exploration of New Zealand Mineral Deposits: Monograph 25* (pp. 225-230). Carlton, Vic., Australia: Australasian Institute of Mining and Metallurgy.

Barin, I. (1973). *Thermochemical properties of inorganic substances*. Springer-Verlag,, Berlin,New York.

Benjamin, J. D. (1990). Mechanical alloying: A perspective. *Metal Powder Report, 45*(2), 122-127.

Bertolini, M., Shaw, L., England, L., Rao, K., Deane, J., & Collins, J. (2010). The FFC Cambridge process for production of low cost titanium and titanium powders. *Key Engineering Materials, 436*, 75-83.

Brooks, G., Cooksey, M., Wellwood, G., & Goodes, C. (2007). Challenges in light metals production. *Mineral Processing & Extractive Metallurgy: Transactions of the Institution of Mining & Metallurgy, Section C, 116*(1), 25-33.

Claussen, N., Garcia, D. E., & Janssen, R. (1996). Reaction sintering of alumina-aluminide alloys (3A). *Journal of Materials Research, 11*(11), 2884-2888.

Crowley, G. (2003). How to extract low-cost titanium. *Advanced Materials & Processes, 161*(11), 25-27.

Crozier, R. D. (1992). *Flotation* (1st ed.). Oxford, U.K.: Pergamon.

Doblin, C., Chryss, A., & Monch, A. (2012). Titanium powder from the TiRO process. *Key Engineering Materials, 520*, 95-100.

EHK Technologies. (2004). *Summary of Emerging Titanium Cost Reduction Technologies*. Retrieved 15 August, 2011, from http://www.ornl.gov/sci/propulsionmaterials/pdfs/Emerging_Titanium.pdf

Fecht, H. J. (1995). Nanostructure formation by mechanical attrition. *Nanostructured Materials, 6*(1-4), 33-42.

Feng, C. F., & Froyen, L. (2000). Formation of Al_3Ti and Al_2O_3 from an Al-TiO_2 system for preparing in-situ aluminium matrix composites. *Composites Part A: Applied Science and Manufacturing, 31*(4), 385-390.

Fray, D. (n.d.). New Processes for Titanium Production – From Swarf to Moon Dust [Powerpoint]. Retrieved 22 May, 2015, from http://www.innovaltec.com/downloads/fray_iom3_presentation.pdf.

Fuerstenau, D. W., & Pradip. (2005). Zeta potentials in the flotation of oxide and silicate minerals. *Advances in Colloid and Interface Science, 114-115*, 9-26.

Gaus, S. P., Harmer, M. P., Chan, H. M., Caram, H. S., Bruhn, J., & Claussen, N. (2000). Alumina-Aluminide Alloys (3A) Technology: II, Modeling of TixAly-Al2O3 composites formation. *Journal of the American Ceramic Society, 83*(7), 1606-1612.

Gennari, S., Tamburini, U. A., Maglia, F., Spinolo, G., & Munir, Z. A. (2006). A new approach to the modeling of SHS reactions: Combustion synthesis of transition metal aluminides. *Acta Materialia, 54*(9), 2343-2351.

Gheorghe, I., & Rack, H. J. (2002). Influence of TiO_2/Al ratio on reaction path during reactive infiltration of TiO_2 by molten Al. *Materials Science and Technology, 18*(10), 1079-1084.

Hartman, A. D., Gerdermann, S. J., & Hansen, J. S. (1998). Producing lower-cost titanium for automotive applications. *JOM - Journal of the Minerals Metals & Materials Society, 50*(9), 16-19.

Hogan, L., Mcginn, E., & Kendall, R. (2008). *Research and Development in Titanium: Implications for a Titanium Metal Industry in Australia.* Research Report 08.2. Canberra, Australia, Commonwealth of Australia. 59p.

Imam, M. A., Froes, F. H., & Housley, K. L. (2000). Titanium and Titanium Alloys. In *Kirk-Othmer Encyclopedia of Chemical Technology*. Hoboken, NJ: Wiley-Interscience.

Imam, M. S., & Froes, F. H. (2010). Low cost titanium and developing applications. *JOM - Journal of the Minerals Metals & Materials Society, 62*(5), 17-20.

Kamali, A., & Fahim, J. (2009). Mechanically activated aluminothermic reduction of titanium dioxide. *International Journal of Self-propagating High-Temperature Synthesis, 18*(1), 7-10.

Kroll, W. (1940). The production of ductile titanium. *Journal of the Electrochemical Society, 78*(1), 35-47.

Kubaschewski, O., Alcock, C. B., & Spencer, P. J. (1993). *Materials Thermochemistry* (6th ed.). Oxford, U.K.: Pergamum Press.

Li, B. S., Liu, A. H., Nan, H., Bi, W. S., Guo, J. J., & Fu, H. Z. (2008). Wettability of TiAl alloy melt on ceramic moulds in electromagnetic field. *Transactions of Nonferrous Metals Society of China, 18*(3), 518-522.

Liu, Z. G., Raynova, S., & Zhang, D. L. (2006). Investigation of a Discus-Milling Process Using a Powder Mixture of Al and TiO_2. *Metallurgical and Materials Transactions A, 37A*(1), 225-233.

Lü, L., & Lai, M. O. (1998). *Mechanical Alloying*. Boston, MA: Kluwer Academic Publishers.

Mauk, J. L., Macorison, K., & Dingley, J. (2006). Geology of the Waikato North Head and Taharoa ironsand deposits. In A. B. Christie & R. L. Brathwaite (Eds.), *Geology and Exploration of New Zealand Mineral Deposits: Monograph 25* (pp. 231-234). Carlton, Vic., Australia: Australasian Institute of Mining and Metallurgy.

Moore, J. J., & Feng, H. J. (1995). Combustion synthesis of advanced materials: Part I. Reaction parameters. *Progress in Materials Science, 39*(4–5), 243-273.

Nafisi, S., Lashkari, O., Ghomashchi, M. R., & Charette, A. (2004). Effects of different fraction solids on the fluidity of rheocast 356 Al-Si alloy. *Multiphase phenomena and CFD modelling and simulation in material processes*, 119-128.

Rahaman, M. N. (2003). *Ceramic Processing and Sintering* (2nd ed.). New York: Marcel Dekker.

Reed, J. S. (1995). *Principles of Ceramics Processing* (2nd ed.). New York Wiley.

Schuster, J. C., & Palm, M. (2006). Reassessment of the binary aluminum-titanium phase diagram. *Journal of Phase Equilibria and Diffusion, 27*(3), 255-277.

Schwandt, C., Doughty, G. R., & Fray, D. J. (2010). The FFC-Cambridge process for titanium metal winning. *Key Engineering Materials, 436*, 13-25.

Scoop Independent News. (2011). *TTR New Zealand Iron Sands Resource Estimate Nearly Doubled*. Retrieved 20 January, 2012, from http://www.scoop.co.nz/stories/BU1108/S00471/ttr-new-zealand-iron-sands-resource-estimate-nearly-doubled.htm

Shen, P., Fujii, H., & Nogi, K. (2006). Wettability of polycrystalline rutile TiO_2 by molten Al in different atmospheres. *Acta Materialia, 54*(6), 1559-1569.

Suryanarayana, C. (2004). *Mechanical Alloying and Milling*. New York: Marcel Dekker.

Suzuki, R. (2007). Direct reduction processes for titanium oxide in molten salt. *JOM - Journal of the Minerals Metals & Materials Society, 59*(1), 68-71.

Takacs, L. (2002). Self-sustaining reactions induced by ball milling. *Progress in Materials Science, 47*(4), 355-414.

Thompson, P. (2002). The selection of flotation reagents via batch flotation tests. In A. L. Mular, D. N. Halbe & D. J. Barret (Eds.), *Mineral Processing Plant Design, Practice, and Control: Proceedings, Vol. 1* (pp. 136-144). Littleton, Colorado, USA: Society for Mining, Metallurgy, and Exploration.

Towler, G., & Sinnott, R. K. (2012). *Chemical Engineering Design : Principles, Practice and Economics of Plant and Process Design (2nd Edition)*. London, GBR: Butterworth-Heinemann.

Turner, P. C., Hartman, A., Hansen, J. S., & Gerdemann, S. J. (2001). Low cost titanium - Myth or reality. In P. R. Taylor (Ed.), *Proceedings of Sessions and Symposia sponsored by EPD, 2001 TMS Annual Meeting, New Orleans, LA, Feb. 11-15, 2001* (pp. 43-66). Warrendale, PA: Minerals, Metals and Materials Society.

Welham, N. J. (1998). Mechanical activation of the solid-state reaction between Al and TiO_2. *Materials Science and Engineering A, 255*(1-2), 81-89.

Wiberg, E., & Amberger, E. (1971). *Hydrides of the elements of main groups I - IV*. New York: Elsevier.

Wills, B. A. (2006). *Mineral Processing Technology : An Introduction to the Practical Aspects of Ore Treatment and Mineral Recovery* (7th ed.). Oxford, U.K.: Butterworth-Heinemann.

Wright, S., Zhang, L., Sun, S., & Jahanshahi, S. (2000). Viscosity of a CaO-MgO-Al_2O_3-SiO_2 melt containing spinel particles at 1646 K. *Metallurgical and materials transactions 31B*(1), 97-104.

Wright, S., Zhang, L., Sun, S., & Jahanshahi, S. (2001). Viscosities of calcium ferrite slags and calcium alumino-silicate slags containing spinel particles. *Journal of Non-Crystalline Solids, 282*(1), 15-23.

Ye, C, & Hon, M. (1995). Dispersion and stabilization of aqueous TiC suspension. *Ceramics International*, 21(2), 65-68.

Zhang, D. (2010). Patent No. US 2010/0064852 A1. Method for Purification of Metal Based Alloy and Intermetallic Powders.

Zhang, D., & Raynova, S. R. (2009). Patent No. US 2009/0311123 A1. Method for Producing Metal Alloy and Intermediate Products.

Zhang, D. L. (2004). Processing of advanced materials using high-energy mechanical milling. *Progress in Materials Science*, *49*(3-4), 537-560.

Zhang, D. L., Cai, Z. H., & Adam, G. (2004). The mechanical milling of Al/TiO_2 composite powders. *JOM - Journal of the Minerals Metals & Materials Society*, *56*(2), 53-56.

Zhang, D. L., Koch, C. C., & Scattergood, R. O. (2009). The role of new particle surfaces in synthesizing bulk nanostructured metallic materials by powder metallurgy. *Materials Science and Engineering A*, *516*(1-2), 270-275.

Zhang, D. L., Ying, D. Y., & Munroe, P. (2005). Formation of Al_2O_3 during heating of an Al/TiO_2 nanocomposite powder. *Journal of Materials Research*, *20*(2), 307-313.

Chapter 3

Experimental Methods

This chapter describes the materials and experimental methods used in the study. The methods are summarized in the metallurgical investigation plan (Figure 3.1). They include preparing reactants by high energy mechanical milling (HEMM), producing TiAl(O)/Al_2O_3 composites by combustion synthesis, solid/liquid separation by extrusion, froth flotation, sample characterisation by optical microscope (OM), scanning electron microscope (SEM), x-ray diffraction (XRD), differential thermal analysis (DTA), porosity by pycnometer, particle size analysis by laser particle analyser (LPSA) and particle surface charge measurement to determine the point of zero charge of TiAl.

The results from each experimental method are reported separately in Chapters 4, 5 and 6.

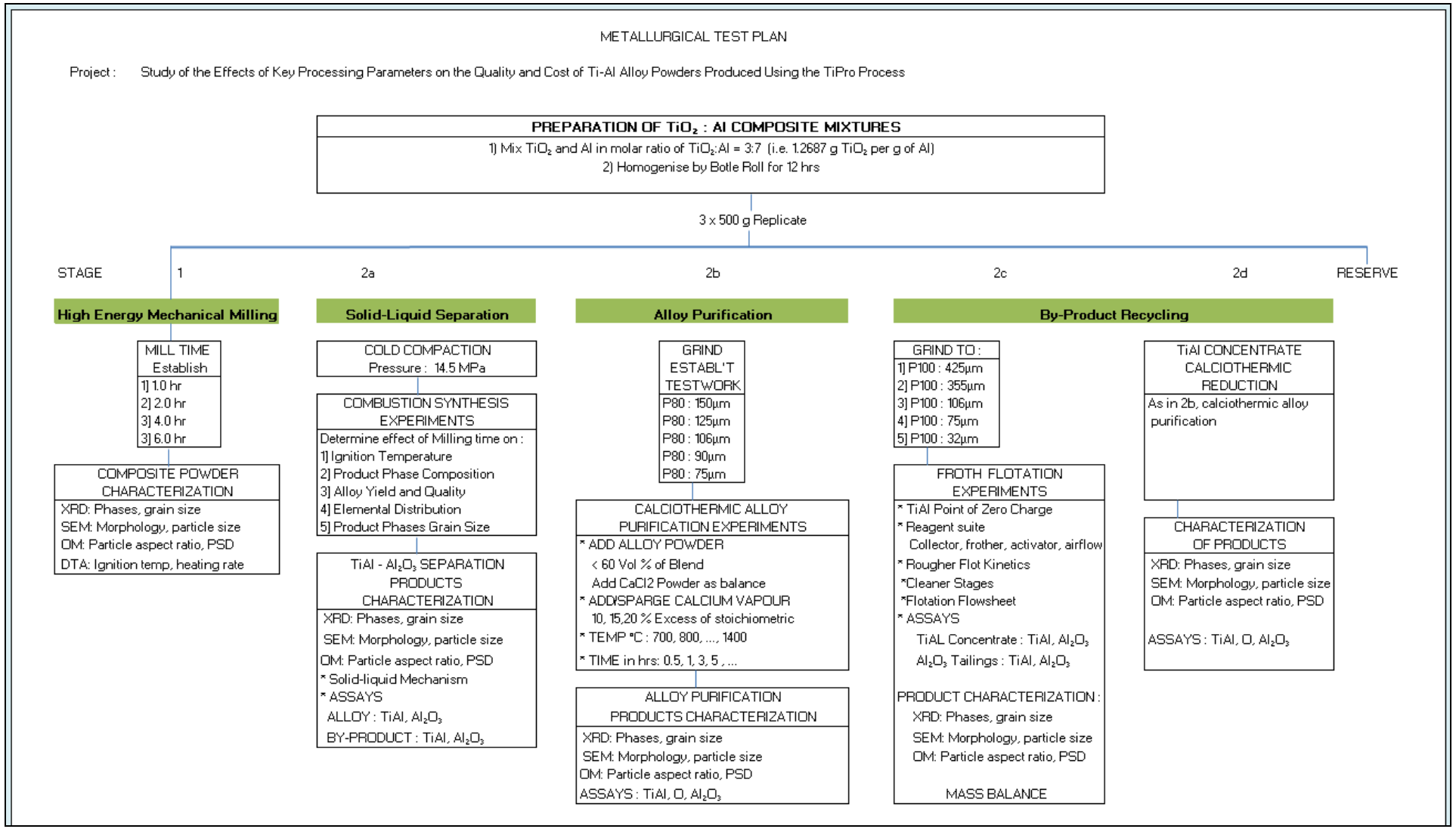

Figure 3.1: Metallurgical investigation plan

3.1 Preparing TiO_2/Al Composite Powders

The objective of making the reactant powders into TiO_2/Al composites before combustion synthesis was to enhance reaction kinetics. The TiO_2/Al composite powders were prepared by high energy mechanical milling using 98.5% pure, commercial grade TiO_2 0.2-µm particles (anatase supplied by Millennium Chemicals Ltd., Australia) and 99.5% pure commercial Al of less than 60-µm particle size (Ecka Granules Australia Pty Ltd). High energy mechanical milling was done in a Rocklabs Split Discus Mill (Rocklabs, New Zealand) (Figure 3.2).

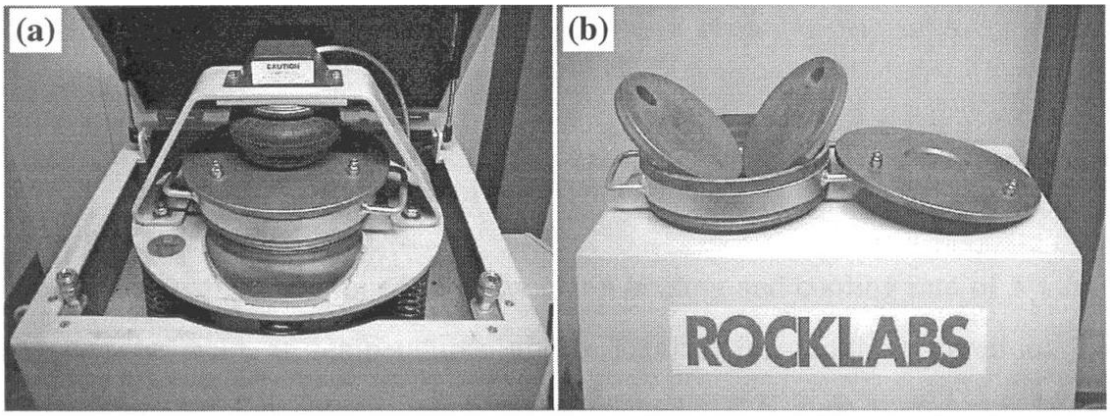

Figure 3.2: (a) Rocklabs Split Discus Mill (b) Discus and Vial

In the Rocklabs Split Discus Mill, the TiO_2-Al powder mixture was milled as it was repeatedly forged between two sliding discusses and also against the vial wall as each discus rotated and vibrated.

3.1.1 Discus Milling Procedure

Known amounts of Al and TiO_2 powders that met the stoichiometry of Equation (3-1) and gave a TiO_2:Al molar ratio of 3:7 were homogenized in a Bottle-roller mill for 12 h.

$$3\ TiO_2 + 7\ Al = 3\ TiAl + 2\ Al_2O_3 \qquad (3\text{-}1)$$

To process each batch, 500 g of the homogenized powder mixture was put in the Rocklabs Split Discus Mill vial along with 0.5 wt% of isopropyl alcohol as process control agent (PCA) to minimize excessive sticking of powders to the milling media. To avoid oxidation, the mill vial was evacuated and then filled with argon to about -5 kPa before milling.

3.1.2 Normalizing

After high energy mechanical milling, TiO_2/Al powders are extremely reactive therefore they need to be normalised before exposure to air. The following procedure was applied:

1. The discus mill bowl and milled TiO_2/Al powders were placed in a glove box.
2. A scope, thermometer and a thermocouple were placed in the glove box.
3. The glove box was closed and evacuated to -80kPa.
4. The glove box was then refilled to -5kPa with argon.
5. Steps 4 and 5 were repeated two times.
6. In the last refill with argon the pressure was left at 0kPa (ambient pressure) before opening the lid of the discus milling bowl.
7. The two discuses were carefully taken out of the bowl.
8. The powder was stirred and the temperature of the powders measured.
9. If the temperature was above 40°C, the powder was left to cool down below 40°C. Once the temperature was below 40°C, the glove box was evacuated to -20kPa.
10. Air was introduced into the glove box (by disconnecting the argon hose and opening the valve) until the pressure reached 0kPa and then closing the valve.
11. The powder was stirred and the temperature of the powder measured.
12. Steps 11 to 13 were repeated three times.
13. If the temperature was below 40°C, the glove box was evacuated to -50kPa and air introduced until ambient pressure.
14. The powder was stirred and the temperature of the powder measured.
15. If the temperature was below 40°C, the glove box was evacuated to -80kPa and air introduced until ambient pressure.
16. The powder was stirred and the temperature of the powder measured.
17. The powder was left to cool below 30°C before being removed from the glove box and being stored in a metal container.

3.1.3 Microstructure Optimization

To study the effect of microstructure on the downstream solid/liquid separation efficiency, milling was done for 1, 2, 4 and 6 h. The milling media (discus) to powder weight ratio was maintained at about 18:1. For each milling time, four 500-g batches prepared as detailed above were tested and characterized using OM SEM, XRD, XRF and DTA as detailed in 3.3 to establish the effect of milling time on:

- Microstructure development, compositional and particle size variation and
- Reaction rate, reaction temperature, temperature attained by products and phase separation during combustion synthesis at the solid/liquid separation stage

3.1.4 Composite Powder Compaction

To enhance heating efficiency and combustion synthesis kinetics during the solid/liquid experiments, reactant powders were compacted. Portions (400 g) of milled composite powder portions were cold pressed into 80-mm diameter x 37-mm thick compact discs (Figure 3.3) in a H13 tool steel die using an applied pressure of 14.5 MPa and 2-min dwell time in a 100-ton hydraulic press. This was replicated three times to get an average. Results are discussed in Chapter 4.

Figure 3.3: A 400-g milled TiO_2/Al composite powder green compact

3.2 Combustion Synthesis

The combustion synthesis and liquid/solid separation experiments were done under argon in equipment that consisted of an alternating current (ac) induction heating device, a stainless steel 316L grade shell as a conductive receptor, an O-Sialon extrusion die, thermocouples, and a USB TC-08 Picolog data logger for temperature monitoring (Figure 3.4). The 400-g green compacts of milled TiO_2/Al composite powders (Figure 3.3) were placed in the O-Sialon die and heated. The reaction temperature was monitored with a platinum-rhodium (B-type) thermocouple imbedded in the compact. Additional thermocouples (K-type) were used to monitor ambient and shell temperatures. The trials were done in triplicate. After ignition, which was marked by a "super-adiabatic peak" and fuming, the combustion synthesis products were extruded under light pressure (about 60 bars) to separate the liquid alloy-rich phase from the solid alumina-rich phase

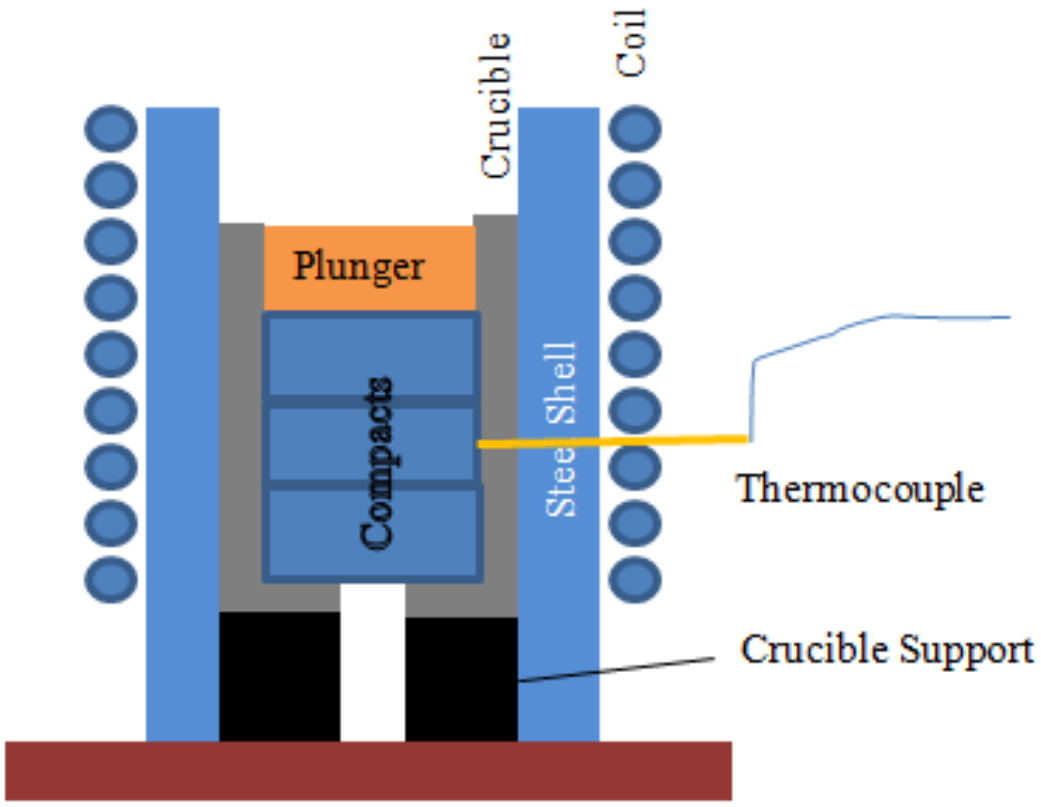

Figure 3.4: Schematic of the experimental set-up

3.2.1 Reactor Design Considerations

A previous study reported an alloy yield below 10% compared with the target of 50% required to ensure commercial success of the TiPro process (Raynova, 2007).

The low titanium alloy yield was attributed to poor molten alloy-solid separation because the alloy solidified before it could be extruded (Raynova, 2007). To overcome low alloy yields, this research is aimed at understanding the microstructure and flow patterns of liquid TiAl formed in combustion synthesis of TiO_2/Al powders milled for 1, 2, 4, and 6 h.

Titanium processing presents a significant challenge in reactor design due its immense reactivity. Therefore apart from designing for a reactor that maximizes heat transfer into the compacts while minimizing heat loss from the reactor, the design criteria should include inertness to titanium during processing. As the crucible is exposed to high temperatures and is in direct contact with molten reactive contents, O-Sialon was selected because it is thermally conductive, has a high bulk density, and is chemically and erosion resistant. O-Sialon is a ceramic with 65 wt% SiC and 35% Sialon (a Si_3N_4 base-ceramic in which some of the Si has been replaced with Al and some of the N has been replaced with O). Sialon has a compositional range of $Si_{6-x}Al_xO_xN_{8-x}$, where x is the number of oxygen atoms substituted for nitrogen and has a limiting value of 4.2 at 1700^{o}C and 2.0 at 1400^{o}C ([Davis, 1995). Given that Al readily reduces TiO_2 to produce Ti that in turn reacts with Si_3N_4 to produce TiN according to the Equation(3-2); it is inevitable that O-Sialon might introduce some contamination into the metal.

$$4\,Ti + Si_3N_4 = 3Si + 4TiN \qquad \Delta G_{1243K} = -125.740 \text{ kcal} \qquad (3\text{-}2)$$

To minimize conductive heat loss, an outer layer of insulation with low thermal conductivity and stable in the operating temperature range had to be used. A combination of kaowool and a fireclay-based refractory castable was considered. Kaowool has a very low thermal conductivity because of the large air space between the fibers. However; it cannot store heat because of its extremely low mass. To increase the heat-retaining capacity of the reactor assembly (and consequently extend the time the alloy phase was kept molten), a combination of the two insulation layers were applied (Richerson, 1992).

Unlike previous studies that used a tube furnace (Adam *et al.*, 2007), in this study thermal treatment was done using a reactor assembly incorporating a 26-mm thick, 230-mm long 316-Stainless steel shell as the secondary in the induction heating. The maximum operating temperature for 316-stainless steel is 900^{o}C (Peters *et al.*,

2003). A layer of alumina-based refractory cement, which acted as a radiation heat shield, was coated on the steel shell.

To enhance separation of molten TiAl from the solid alumina rich by-product, the O-Sialon crucible was mounted on a 100-mm high die, which also acted as the alloy collector. The volume of the alloy collector (receptor) was determined from the stoichiometric alloy fall estimated using Equation (3-1) as detailed in the calculation below:

Density of TiAl	3.9 – 4.1 g/cm^3
TiO_2 as weight fraction in reactant mixture	0.5592
Al as weight fraction in reactant mixture	0.4408
Total weight of reactant mixture	900 g
Weight of TiO_2 in mixture	503.28 g
Equivalent weight of TiAl expected	471.55 g
Volume of TiAl expected	120.91 cm^3
Volume of receptor (110% of TiAl expected)	133 cm^3

The criteria for selecting crucibles that were used for combustion synthesis experiments were based on inertness to chemical attack, cost effectiveness, adequate thermal shock resistance, compressive strength and the ability to facilitate molten alloy and solid alumina separation.

3.3 Sample Preparation and Characterization

Quantitative phase characteristics such as concentration, grain size of the product (alloy and corundum) phases, and oxygen associations are needed to achieve optimum alloy yields during solid/liquid separation and other downstream process stages. To characterise the samples using OM and SEM, powdered samples of reactants and products were mounted in resin for 24 h and then ground using silicon carbide (SiC) grinding papers in the sequence 320, 600 and 1000/1200 grit. To study the solid/liquid separation mechanism, longitudinal and transverse cross sections of the extrusion product (Figure 3.5) were cut using a wire-cutter. The cut samples were polished using 320, 600 and 1000/1200 grit SiC papers. Samples for XRD, LPSA and DTA analysis did not need to be mounted in resin.

Figure 3.5: Photographs of the extruded combustion synthesis product (a) before and (b) after sectioning with a wire-cutter

3.3.1 Optical Microscopy (OM)

Micrographs of polished samples were taken using an Olympus BX 60 optical microscope with a Nikon camera attachment. Phase microscopy analysis to determine the spatial distribution of TiAl, Al_2O_3 was done using Image-Pro Plus 6.3 (Media Cybernetics) and IQ Materials™ software (Media Cybernetics) was used for materials (grain size, percent area and particle size) analysis.

To study the flow mechanism during solid/liquid separation by extrusion, a longitudinal cross-section of the solid/liquid separation by-product from each experiment was delineated using X-Y coordinates (Figure 3.6). OM micrographs were taken at 5mm intervals using the Image-Pro Plus 6.3 software. The distribution of TiAl and Al_2O_3 within each delineated area of the entire longitudinal cross-section was then measured using the IQ Materials™ software. The micrographs and their corresponding TiAl content were presented as a montage depicting the spatial distribution TiAl and Al_2O_3. The TiAl spatial distribution obtained was used as the TiAl saturation in studying alloy flow mechanism of the extrusion by-product. The results are reported in Chapter 5.

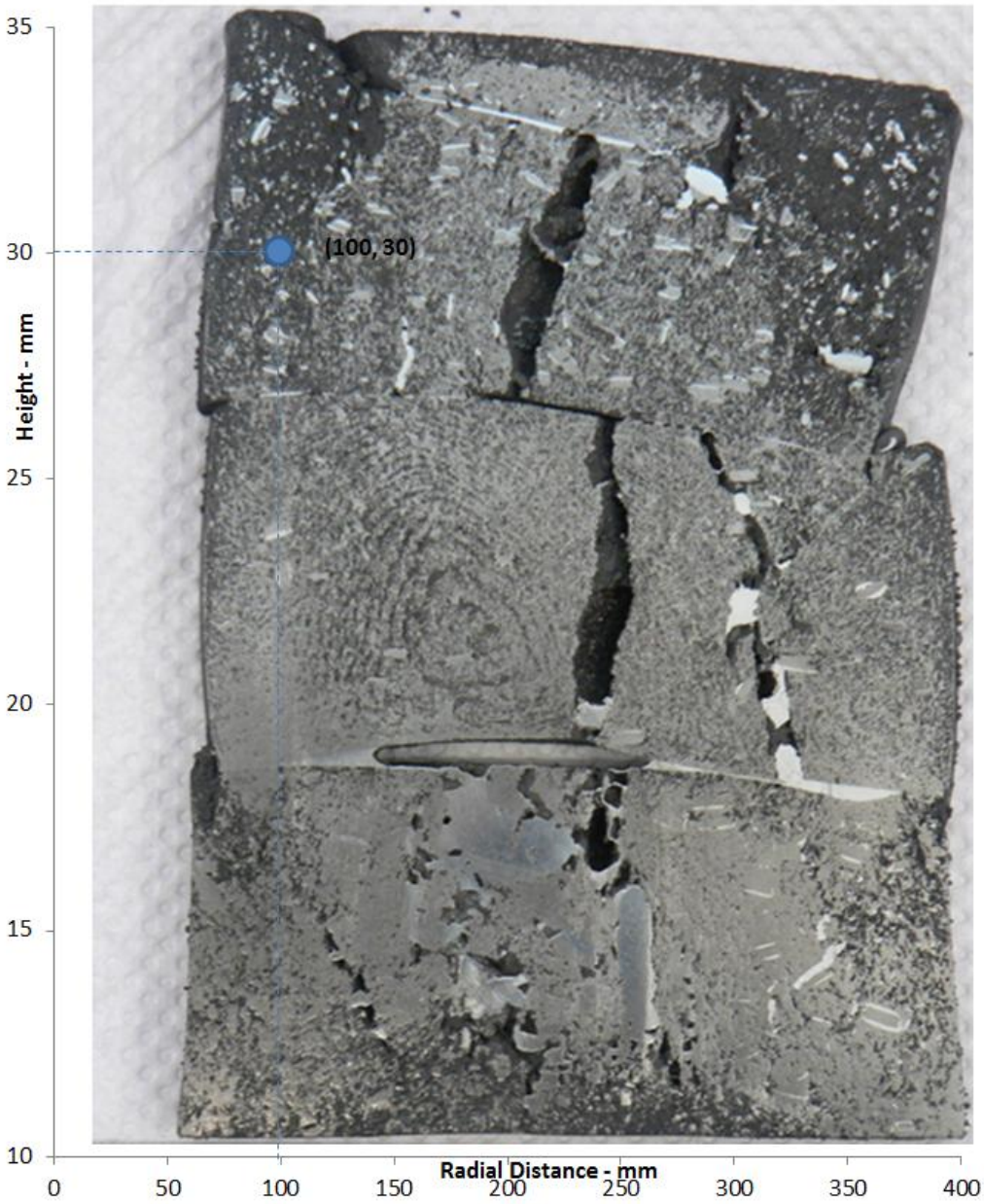

Figure 3.6: Co-ordinate grid for delineating TiAl relative abundance (saturation)

3.3.2 Scanning Electron Microscopy and EDS

Microstructural characterization of samples taken at every stage of the trials was done using a Hitachi S-4700 Scanning electron microscope equipped with energy dispersive spectroscopy (EDS). Alloy phase composition and element distribution within phases were determined using data from elemental maps and EDS analysis.

3.3.3 X-ray Diffractometry (XRD)

Phases in composite powders and products from various stages of the trials were characterized using a Phillips X-pert system diffractometer (XRD) with Cu Kα

radiation at 40 kV and 40 mA. The patterns were obtained using a 0.02^{o} step size averaging 5 seconds per increment. Samples were scanned whilst secured in either shallow stainless steel holders or as specimens mounted in epoxy resin. Indexing for phase composition was done using Phillips X-pert HighScore Software (PANalytical B.V.). The phase composition at various stages of the study was established using SEM and EDS, XRD.

3.3.4 Thermal Analysis

To establish thermal behavior of the composite powders, samples were analyzed by differential thermal analysis (DTA) in a TA Instruments SDT 2960 DTA under argon at a flow rate of 150 $mlsec^{-1}$. The data were used to optimize milling time and identifying ignition temperature. The DTA analyses were also done at a $10^{o}Cmin^{-1}$ scanning rate to attain a pre-determined temperature. After attaining the set temperature, the sample was held for 30 min. X-ray diffraction (XRD) analysis was used to identify phases formed during thermal analysis on samples which were removed from the DTA equipment at different temperatures during the thermal analysis experiment. DTA was supplemented with XRD analysis because DTA alone is not used for a complete interpretation of a system (Charsely & Warrington, 1992). DTA results were only indicative because they were done on loose reactant powders while combustion synthesis experiments were done using compacted reactant powders. However, DTA results can be used in establishing expected trends as the milling time is varied.

3.3.5 Particle Size Analysis (PSA)

An analysis of particle size distribution of homogenized powders and milled powders was done using a Mastersizer 2000 Laser particle sizer (Malvern Instruments Ltd., UK).

3.3.6 X-ray Fluorescence Analysis (XRF)

XRF analysis was used to check the elemental composition of reactant powders and extrusion by-product samples.

3.3.7 Determination of Corundum in Combustion Products

One (1) to two (2) grams of sample were treated with excess hydrofluoric acid (60gpl concentration) for 16 h. The solution was filtered and analysed by ICP as a second check on the composition of the products. The residue was thoroughly washed, dried and weighed. The weight obtained was calculated as corundum (Pratt, 1906). The residue was analysed by XRD to ascertain that Al_2O_3 was the only phase contained.

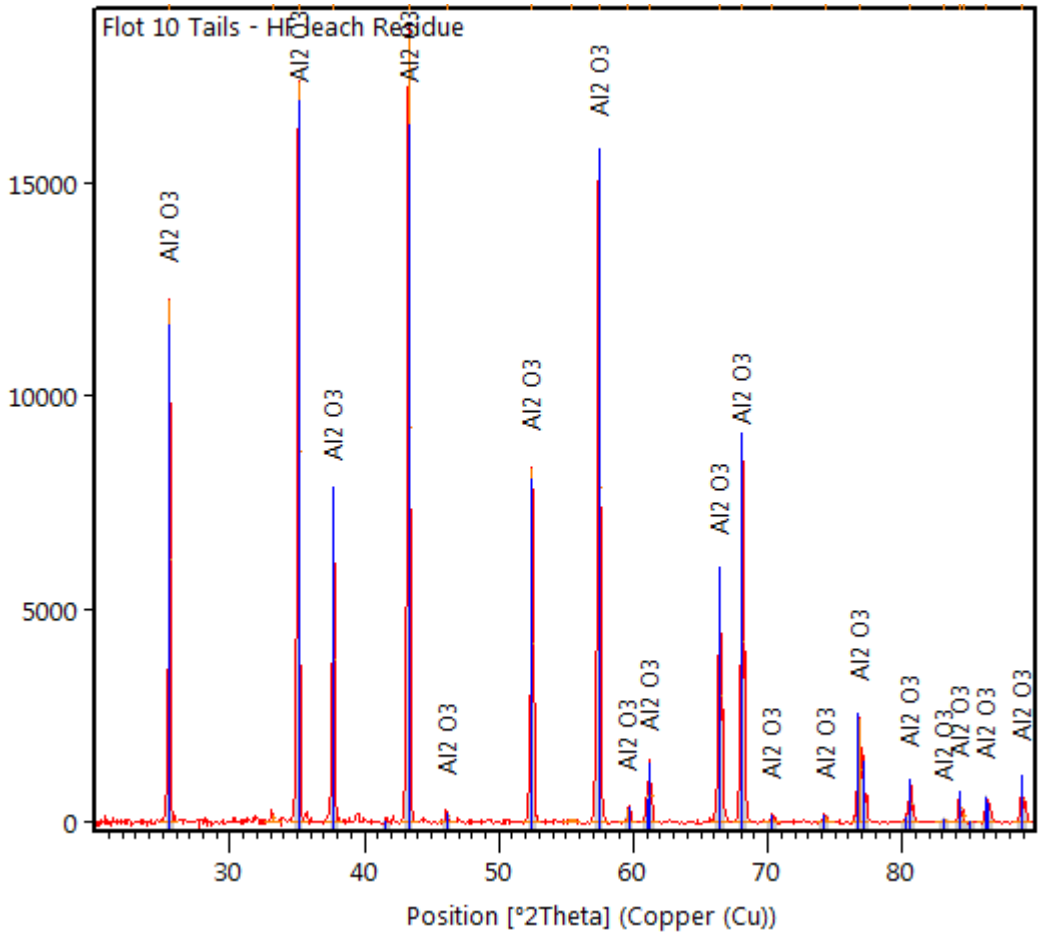

Figure 3.7: Phase composition of HF leach residue after gravimetric analysis of Al_2O_3

3.3.8 Phase Liberation Analysis (PLA)

To determine the liberation size of the TiAl phase in the extrusion by-product, samples were stage crushed to less than 6300 microns in a 500-mm x 245-mm TIDCO Swing Jaw Crusher with an 8500-micron gap-setting. The jaw crusher product was further milled in a UA 53 BICO Pulverizer; Model: 242-53 X3 (BICO-Braun Intern., US) using a gap setting of 0.280 mm. The two-stage

crushing procedure helped preserve the *in situ* texture of the extrusion by-product and also limited generating fines.

To minimize the coarse fractions being contaminated by fines (Burrows *et al.*, 2007), crushed samples were wet sieved into 6300, 1180, 425, 212, 106, 75 and 32-microns size fractions. OM micrographs, backscatter images, XRD and XRF analyses were done on the various fractions obtained to establish whether there was preferential breakage, which would be indicated by differences in deportment patterns of the TiAl and Al_2O_3 phases.

3.3.9 Determination of Porosity

The porosity in combustion reactants and products was determined using an Ultrapycnometer 1000 manufactured by Quantachrome Instruments. The pycnometer works on the Archimedes principle. Density is automatically calculated from the volume measured by the equipment. The porosity was then calculated from the difference between the material's specific gravity and the density determined using the pycnometer.

3.3.10 Ignition Temperature Measurement

Two thermocouples were used to monitor the temperature; one was drilled 1 cm into the green compact and the other on the surface of the green compact. The ignition temperature which was marked by evolution of fumes was measured with the thermocouple placed on the green compact surface. The one drilled 1 cm into the green compact was connected to a Picolog Datalogger that produced a temperature profile at a point 1 cm into the green compact. This was used to measure the combustion temperature only and not the ignition temperature because it lagged behind and understated the ignition temperature. (as indicated by thermographs in Figure 5.17, Figure 5.18 and Figure 5.26). The surface thermocouple gave the true ignition temperature reading during the experiment.

3.4 Froth Flotation

Less than 10% of the possible yield of primary TiAl alloy is obtained by extruding combustion synthesis product at the solid/liquid separation stage (Raynova, 2007). The extrusion by-product contains appreciable amounts of TiAl alloy, which must be recovered to increase process viability.

Gravity separation methods are ineffective because the density of TiAl and Al_2O_3 are similar. Froth flotation is often used to separate materials with similar physical properties. In froth flotation, minerals suspended in water are separated by attaching them to air bubbles to selectively levitate one mineral into the concentrate fraction, leaving the other mineral in the tailings. The froth laden with hydrophobic mineral particles overflows into a launder constituting a concentrate. The hydrophilic mineral particles collect at the bottom of the tank to form tailings. In forward flotation, the more valuable mineral reports to the concentrate stream whereas in reverse flotation it reports to the tailings stream (Figure 2.17). To enhance attachment of mineral particles to air bubbles, a surfactant (collector) is added to the slurry. A collector acts by coating and making surfaces of mineral particles hydrophobic (aerophilic). A frother is added to make stable bubbles that can support mineral particles without collapsing. Flotation is a proven, cost-effective mineral processing technology with minimal technology risk (Crozier, 1992; Wills, 2006). Flotation separation has the extra advantage that it does not alter alloy phase chemical composition.

3.4.1 Preliminary Sample Assessment

An initial sample assessment was made. This involved grinding the combustion synthesis product to various particle sizes and applying flotation parameters. These were established by measuring particle surface charge carried on contained minerals (TiAl and Al_2O_3). The surface charge carried by a mineral particle determines the efficiency of separation by froth flotation. To float a mineral particle, its surface charge is altered by selectively adsorbing molecules with surface active properties (surfactants) on it. Due to their amphiphilic structure (one containing a polar or hydrophilic head and a non-polar or hydrophobic tail), surfactants (collectors, frothers or activators) adsorb and generate a charge by acting like counter-ions in an electrical double layer formed between a particle surface and the suspending liquid (Figure 2.21). Surfactants are classified according to the head group type (ionic, non-ionic and amphoteric). Ionics can be either cationic or anionic. Cationic surfactants produce a positively charged surface and anionic surfactants produce a negatively charged surface.

In this study, the pH operating window for selectively floating corundum was determined by measuring the particle surface charge at various pH levels using a Mütek PCD-04 Travel particle charge detector (BTG Instruments) (Figure 3.8).

To measure the particle charge, an aqueous sample (0.1 g of powder in 150 ml sodium dodecyl sulphate solution) was placed in the measuring cell.

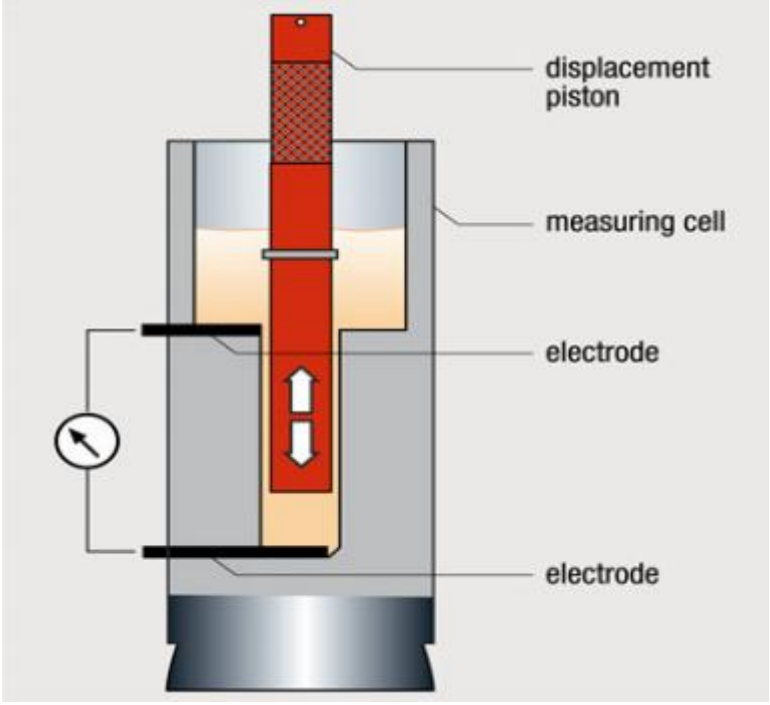

Figure 3.8: BTG Mütek PCD-04 Travel particle charge detector

Once turned on, the oscillating action of the cell piston induces a high flow rate that separates any charged material adsorbed to the cell wall from it counter-ions thereby creating a streaming potential. The current is picked-up by two electrodes and displayed on the touch screen while the pH was measured with the probe inserted in the cell. The pH of the aqueous sample was adjusted by adding drops of 100 gpl H_2SO_4 or 100 gpl Na_2CO_3 to the cell when and as necessary.

The point of zero charge (PZC) was obtained by plotting slurry pH against measured potential and used to determine whether a cationic or anionic surfactant was to be used.

3.4.2 Experiment Set-up

Flotation experiments were done using equipment manufactured in-house (Figure 3.9). The equipment had a sub-aeration assembly made from a 3500-ml Perspex cell and an agitator with a 70-mm diameter impeller. A rotameter installed in the air line between the compressor and the flotation cell was used for controlling and duplicating airflow from experiment to experiment (Dunne *et al.*, 2010).

Figure 3.9: Flotation experiment set-up

The flotation experiment procedure was as follows:

1. A 100-gram sample of extrusion by-product was gradually added to the flotation cell containing about 2500 ml of water with the impeller speed set at 1000 rpm and air inlet shut.
2. Over the following 3 min, 1000 ml more water was slowly added and impeller speed increased to 1500 rpm.
3. The mixture was then agitated for a further 3 min to thoroughly wet the sample.
4. Appropriate modifying reagents (activator or depressant) were then added and agitation continued for 5 min.
5. Additions of collector and frother were made and agitation continued for a further 5 min.
6. Air was then turned on to give 6 litres per min flow rate. At 15-sec intervals, a scraper was gradually moved through the concentrate to collect the froth. Froth produced over 1 min was collected as concentrate.
7. After 10 min, the impeller was stopped and any particles adhering to the sides of the cell and the impeller housing were transferred to the concentrate. The solids that collected at the bottom of the cell constituted the tailings.
8. Each concentrate and each tailing was dewatered and dried to constant mass and then reweighed.

3.4.3 Evaluation of Flotation Experiments

The criteria for evaluating flotation reagents and parameters are their collecting power (determined by recovery) and selectivity which is indicated by the grade of the concentrate produced. These two criteria are preferably evaluated using rougher kinetic tests and multiple-stage cleaning tests because they provide significant information (such as preliminary grade - recovery relationships, and flotation times) in a single test.

3.4.4 Rougher Flotation Kinetics

Rougher flotation tests were done by taking multiple concentrates over a measured time period. The grade of the individual concentrate samples taken every minute and the cumulative grade of the overall concentrate were plotted against time. The cumulative grade was also plotted on the secondary axis. Flotation is considered complete at the point where the incremental concentrate grade curve crosses the grade of the feed to the flotation test. The time at which this occurs determines the cumulative concentrate grade and the cumulative recovery of the test as no additional concentration can be achieved without regrinding the feed (Mular *et al.*, 2002).

3.4.5 Multiple Stage Cleaning Tests

To determine the potential for upgrading concentrates and to establish various factors, such as concentrate regrind, pulp dispersion and additional reagents (collector or activator) during cleaning, rougher concentrates from a test were combined and subjected to multiple cleaning stages. The results were plotted and evaluated by comparing the recovery at fixed concentrate grade for various flotation conditions or reagent schemes (Mular, *et al.*, 2002). After reviewing the initial rougher and cleaner flotation results alterations were made to grind size, reagent suite and flotation time to further enhance separation (Dunne, *et al.*, 2010).

3.5 Calcium Hydride (CaH_2) Reduction

Experiments to remove dissolved oxygen and alumina from the primary alloy were done using CaH_2 of 99.9% purity supplied by Aldrich, USA and 95% $CaCl_2$ (Sigma Aldrich, New Zealand). On an industrial scale, CaH_2 is preferred to other reductants (Al, Mg and Si) because reduction occurs at a lower temperature, it is less reactive (easily handled), and separation of the alloy from the by-product is

easily achieved by washing the product with acidified water. CaH_2 is capable of reducing oxygen levels to 0.07 wt% i.e. well below the stability of TiO, Ti_2O, Ti_3O the lower oxides of titanium (Kubaschewski et al, 1993) and unlike Al, CaH_2 has very little tendency to form alloys therefore the product yield is quantitative (Mackay, 1966). Also, unlike elemental Ca, CaH_2 forms a protective hydrogen atmosphere that is beneficial in reducing oxygen pick-up. However it more costly compared to Ca.

In a previous study the subject of US patent 2010/0015003 A1; reduction using CaH_2 was carried out between 1000^{o}C and 1300^{o}C in a tube furnace for a period of more than 2 h (Adam, 2010). In this study the reduction was carried out with a mixture of CaH_2 and $CaCl_2$ between 500^{o}C and 800^{o}C using an induction furnace (Figure 3.10). An induction furnace was preferred because of the relative ease in maintaining a reducing reaction atmosphere. The pressure in the glove box was maintained between -1 and 0 mbar while the oxygen level was 1 ppm.

The reduction experiments were conducted based on the stoichiometry of Equations (3-3) and (3-4).

$$Al_2O_3 + 3\,CaH_2 = 2\,Al + 3CaO + 3\,H_2 \qquad \Delta G_{1073K} = -29.969 \text{ kcal} \qquad (3\text{-}3)$$

$$\underline{O}_{Ti} + CaH_2 = CaO + H_2 \qquad \Delta G_{1073K} = -33.493 \text{ kcal} \qquad (3\text{-}4)$$

$\underline{O}_{Ti}$ is oxygen dissolved in titanium.

Figure 3.10: Reduction experiment in an induction furnace

3.5.1 Oxygen reduction (with Ca in $CaCl_2$) – Induction Furnace

The reduction was done using the following procedure:

1. An appropriate weight of Ca granules was loaded in the flask.
2. A mixture containing 5 g of TiAl(O) and 3.95 g $CaCl_2$ flux was added to the retort tube.
3. The retort tube was placed in the vessel case and the vessel case lid secured.
4. The whole assembly was inserted into the induction coil (in the glove box) Figure 3.10.

5. The glove box was continuously evacuated and purged with argon to maintain 1±1 mbar pressure and less than 100 ppm O_2.
6. The furnace was turned on.
7. Temperature was controlled by adjusting the power input and monitored using a B-type thermocouple connected to a TC-08 Data logger.
8. Upon attaining the set temperature value (e.g. 800^{o}C), the furnace was kept on for a predetermined number of minutes.
9. On completion and when the furnace had cooled to 60^{o}C, the pressure was adjusted to atmospheric pressure with argon or a vacuum pump before retrieving the reduction vessel and recovering the sample.
10. The sample was characterized using XRD, XRF, OM, SEM and gravimetric analysis.

3.5.2 Oxygen reduction (with Ca in $CaCl_2$) by reaction milling

Reaction milling was developed by Jangg to initiate reactions between Al, graphite (C), and O_2 by intensive milling (Lu & Lai, 1998). In this study, the following procedure was used

1. A mixture containing appropriate amounts of reactants (e.g. 22 g of TiAl(O), 1.35 g Ca and 3.95 g $CaCl_2$ flux) was added to the mill vial.
2. The sample was milled for 300 sec or longer for TiAl(O)/Al_2O_3.
3. About 5 g of the as-milled powder was leached with 400 ml acidified water (25^{o}C). The residue was filtered off and dried for 24 h in an oven set at 100^{o}C.
4. The sample was characterized using XRD, XRF, OM, SEM and gravimetric analysis.

The various trials were done in triplicate and the results averaged. Results are discussed separately in subsequent chapters.

3.6 References

Adam, G. (2010). Metal alloy powders production. US 2010/0015003 A1, Titanox Development Limited, USA.

Adam, G., Zhang, D. L., Liang, J., & Macrae, I. (2007). A novel process for lowering the cost of titanium. *Advanced Materials Research, 29-30*, 147-152, *Advanced Materials and Processing IV - Selected, peer reviewed papers presented at the 4th International Conference on Advanced Materials and Processing*.

Aldo Miners. (2012). *Flotation in Mining [Technology Industry Of Gold Mining Online Blog]*. Retrieved 20 December, 2012, from http://miningeducation.blogspot.com.au/2012/01/flotation-in-mining.html

Burrows, D., Fandrich, R., & Gu, Y. (2007). Automated mineralogy for ore characterisation and plant optimisation. In *Proceedings: Project Evaluation 2007: 19 - 20 June 2007 Melbourne, Australia* (pp. 179-187). Carlton, Vic., Australia: Australasian Institute of Mining and Metallurgy.

Charsely, E. L., & Warrington, S. B. (Eds.). (1992). *Thermal Analysis*. Leeds: The Royal Society of Chemistry.

Crozier, R. D. (1992). *Flotation* (1st ed.). Oxford, U.K.: Pergamon.

Dunne, R. C., Lane, G. S., Richmond, G. D., & Dioses, J. (2010). Flotation data for the design of process plants Part 1 - testing and design procedures. *Mineral Processing and Extractive Metallurgy, 119*(4), 199-204.

Fuerstenau, D. W., & Pradip. (2005). Zeta potentials in the flotation of oxide and silicate minerals. *Advances in Colloid and Interface Science, 114-115*, 9-26.

Kubaschewski, O., Alcock, C. B., & Spencer, P. J. (1993). *Materials Thermochemistry* (6th ed.). Oxford, U.K.: Pergamum Press.

Lu, L., & Lai, M. O. (1998). *Mechanical Alloying*. Norwell, Massachusetts, USA: Kluwer Academic Publishers.

Mackay, K. M. (1966). *Hydrogen compounds of metallic elements* General and industrial chemistry London: E & F N Spon.

Mular, A. L., Halbe, D. N., & Barret, D. J. (Eds.). (2002). *Mineral Processing Plant Design, Practice, and Control: Proceedings, Vol. 1* (Vol. 1). Littleton, Colorado, USA: Society for Mining, Metallurgy, and Exploration.

Peters, M. S., Timmerhaus, K. D., & West, R. E. (2003). *Plant Design and Economics for Chemical Engineers* (5th ed.). New York: McGraw-Hill.

Raynova, S. (2007). *Production of titanium and titanium based intermetallics and alloys*. [Unpublished report]. Hamilton, New Zealand: University of Waikato.

Richerson, D. W. (1992). *Modern ceramic engineering* (2nd ed.). New York: Marcel Dekker, Inc.

Wills, B. A. (2006). *Mineral Processing Technology: An Introduction to the Practical Aspects of Ore Treatment and Mineral Recovery* (7th ed.). Oxford, U.K.: Butterworth-Heinemann.

Chapter 4

High Energy Mechanical Milling

4.1 Introduction

High energy mechanical milling (HEMM) was developed at INCO's Paul D. Merica Research Laboratory for production of oxide dispersion strengthened (ODS) nickel-based super alloys but has since then been considered for application in the preparation of feedstock for metallurgical processes. In HEMM, the starting material is not homogeneous but usually a mixture of commercial powders. During high energy mechanical milling the powder mixture becomes more homogeneous as a result of material transfer (Blazquez *et al.*, 2013). Also as a result of new atomically clean reactive particle surfaces that are created and a reduction in inter-particle diffusion distances by intimate mixing, the kinetics of the chemical reactions are enhanced. Various studies (Fecht, 1995; Welham, 1998; Zhang, 2004) have demonstrated that mechanically milled TiO_2/Al powders react at a much lower temperature than unmilled reactants used in conventional thermochemical processing. This chapter presents and discusses results of the high energy mechanical milling of the TiO_2/Al powder mixtures that were later used as feed stock in the production of TiAl powders by combustion synthesis and solid/liquid separation by extrusion of the combustion synthesis product.

4.2 Results

4.2.1 Effect of Milling Time on Microstructure

The reaction between Al and TiO_2 is interfacial therefore the microstructure of the starting TiO_2/Al composite is critical to the reaction and the subsequent solid/liquid separation process (Ying *et al.*, 2004). During the initial 2 h of milling there was a noticeable increase in particle size due to forging and welding as the ductile Al particles were plastically deformed into elongated shapes and the brittle TiO_2 particles were fractured and imbedded into the Al. With further milling, fracturing superseded forging and welding. This resulted in a decrease in particle size, and more homogenous and fine microstructured powders whose composition approached the stoichiometry of the starting powder mixture (Blazquez, *et al.*, 2013). Short milling times produced coarse microstructured composite powders

with significant chemical composition variation within the particles and from particle to particle (Table 4.1 and Figure 5.20).

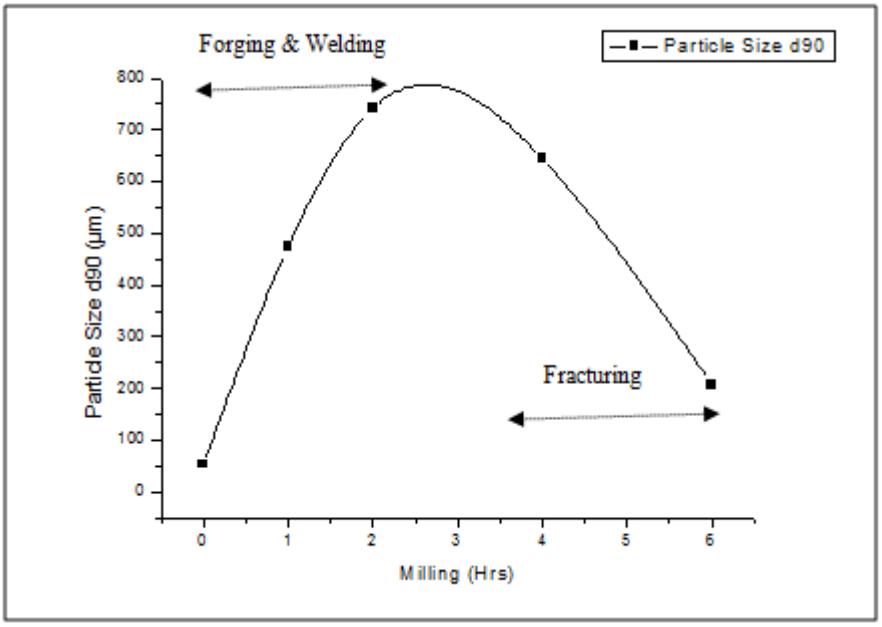

Figure 4.1: Evolution of the average particle size with milling time

The compositional variability of the TiO_2/Al composite powders produced by high energy mechanical milling decreased as the milling time was increased. The standard deviation of the Ti content of the particles in the powders milled for 1 h was 23.06 compared to 1.65 for powders milled for 6 h (Table 4.1)

The compositional and textural variability of the TiO_2/Al composite powders can adversely affect the subsequent solid/liquid separation process.

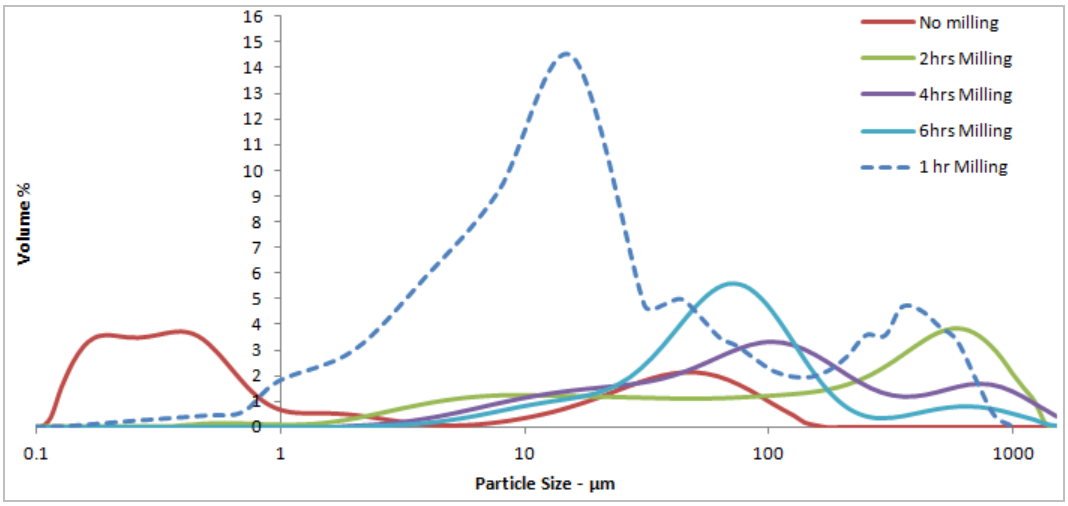

Figure 4.2: Effect of milling on particle size distribution

The unmilled powder mixture had a bi-modal particle size distribution (PSD) due to differences in particle size of the TiO_2 and Al component powders used

(Figure 4.2). The fine size fraction was predominantly TiO_2 (-0.2µm) while the coarser fraction was mainly Al (-60µm).

Table 4.1: Compositional variability of as-milled powders (EDS analyses)

Analyses in wt%					
1h Milling			6h Milling		
O	Al	Ti	O	Al	Ti
16.99	39.18	43.84	15.22	46.5	38.28
28.18	27.18	44.63	16.95	44.22	38.83
1.54	93.96	3.21	17.32	42.92	39.76
30.32	11.39	58.29	15.27	41.61	43.11
4.39	89.86	5.75	18.93	43.37	37.69
16.52	55.86	27.62	16.48	42.62	40.9
1.29	96.09	0.73	15.23	44.65	40.12
17.59	40.7	41.7	15.88	44.11	40.01
6.78	85.74	7.48	12.88	48.5	38.61
28.3	13.67	57.87	15.91	46.26	37.83
Std Dev.		23.06			1.65

During milling, the powder particle size and morphology changed with time. Because of forging and welding of powder particles, an initial increase in particle size was observed as the malleable was flattened. This was followed by a decrease in the powder particle size due to fracturing the hardened particles (Figure 4.2). As fracturing became more dominant there was a decrease in the proportion of the coarser size fraction. The net effect was an increase in mean size of fine fraction and a decreased mean size of coarse size fraction (Figure 4.1 and Figure 4.2).

The tap density of milled powders increased with the milling time (Table 4.2). However, when the milled composite powders were cold-pressed, the apparent density of the green compacts obtained, (determined from weights and dimensions) averaged 55%.

4.2.2 Effect of Milling Time on TiO_2/Al Powders Reactivity

The ignition temperatures of the combustion reaction that were extracted from the DTA traces of the powders milled for 1, 2, 4 and 6 h (Figure 4.3 and Table 4.2) indicate that the reaction ignition temperature decreases with an increase in the milling time. Milling creates new atomically clean reactive particle surfaces and also reduces inter-particle diffusion distances by intimate mixing. Therefore, sufficiently milled TiO_2/Al composite powders can react even below 660^{o}C, the

melting point of aluminium. This is in agreement with other studies (Kamali & Fahim, 2009; Liu *et al.*, 2006; Welham, 1998; Welham & Llewellyn, 1998; Zhang & Raynova, 2009; Zhang *et al.*, 2004). In the current study, the milling was aimed at obtaining a microstructure capable of igniting the TiO_2/Al combustion reaction at a temperature sufficient to produce molten TiAl with minimal external energy input.

Table 4.2: Relative tap densities and ignition temperatures of as-milled powders obtained from DTA traces

Milling Time (h)	Tap Density (g/cm^3)	Ignition Temperature (^oC)
0		900
1	1.14	849
2	1.20	829
4	1.53	541
6	1.72	532

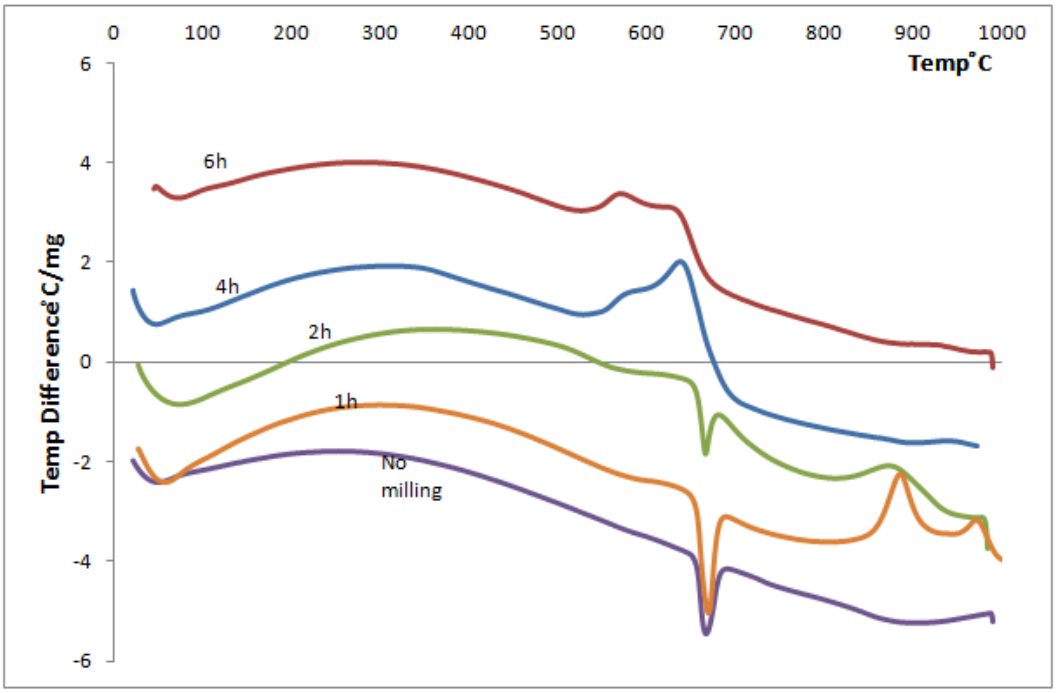

Figure 4.3: DTA for TiO_2/Al composite powders as a function of milling time

The criterion for selecting the milling time was based on optimising the downstream stage of solid/liquid separation. This required high porosity (characteristic of inhomogeneous reactant mixtures obtained by milling for 1 h). The higher porosity in powders milled for 1 h is probably due to evolution of volatiles contained in the green compacts and the fact that Al melts first and spreads on account of capillary forces leaving voids as illustrated in Figure 5.12(a)

and Figure 5.13. Coarse microstructured powders also allow the alloy phase has to be maintained liquid for long enough to facilitate extrusion of the alloy after combustion synthesis. Related research (Moore, 1995) has shown that high combustion temperatures cause gas channels, voids and surface to interior cracks. This is favourable for draining the alloy from the combustion product. In contrast, finer microstructured powders enable liquid Al is to spread more quickly between particles (because of shorter inter-particle distances) leading to enhanced reaction rates and a microstructure of lower porosity as observed in powders milled for 6 h. Taking into account thermodynamic and economic considerations that are elaborated in Chapter 5, powders milled for 1 h were preferred because of their potential to enhance alloy yields during solid/liquid separation.

4.2.3 Effect of Milling on Phase Composition

XRD patterns of the TiO_2/Al powders showed no evidence of a reaction between Al and TiO_2 even after 6 h of high energy mechanical milling (Figure 4.4); therefore the overall stoichiometric composition remained the same. However, powders milled for 1h exhibited a high variability in spatial distribution of constituents from particle to particle (Figure 5.20) giving an average Ti content of 29.11 wt%. This was lower than the chemical composition of the more homogenous 6h milled composite (39.31 wt% Ti). The Ti content of the starting powder mixture determined by XRF analysis was 35.69 wt% Ti; slightly lower than the average for the 6h milled powder because of Al loss (about 7 wt%) after 6h of milling. Short milling times produce composite material with significant chemical composition variation within the particles and from particle to particle (Lu *et al.*, 1995). Related research (Gheorghe & Rack, 2002) has reported that the reaction path and compounds formed depend on the TiO_2: Al ratio of the starting powder mixture (i.e. on the amount of Al available to react with the TiO_2). Intimately mixed powders provide much larger contact between reactants and bring each reactant within a composite particle to allow diffusion in all directions (Welham, 1998). Therefore the milling time was optimized to ensure formation of the desired titanium aluminide alloy composition and yield. As the milling time was increased, particles became more homogenous in composition (Figure 4.5).

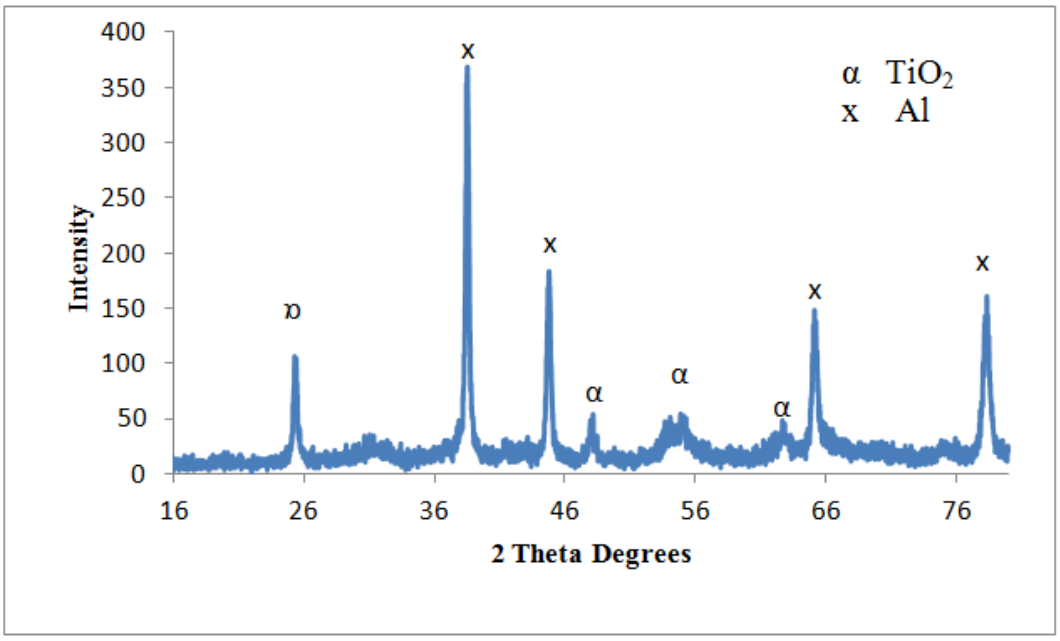

Figure 4.4: X-ray diffraction spectra of as milled TiO_2/Al powder mixture after milling for 6 h

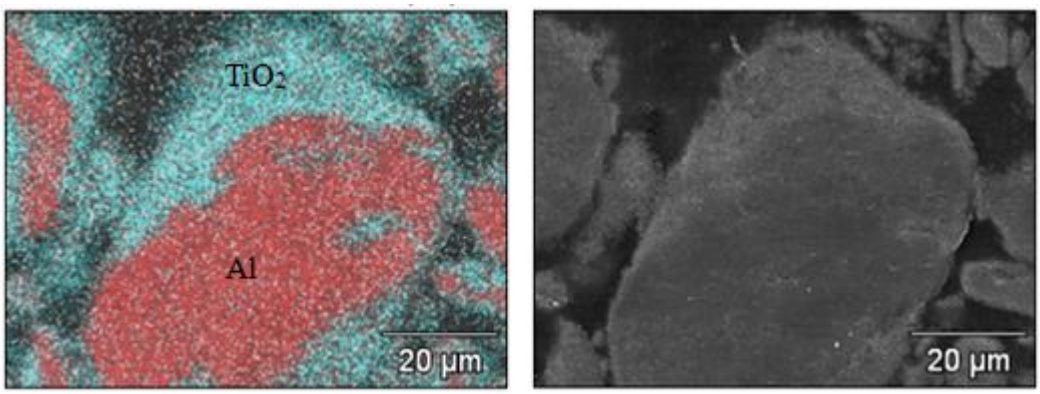

Figure 4.5: An inhomogenousTiO_2/Al mixture after 1h milling showing two distinct reactants

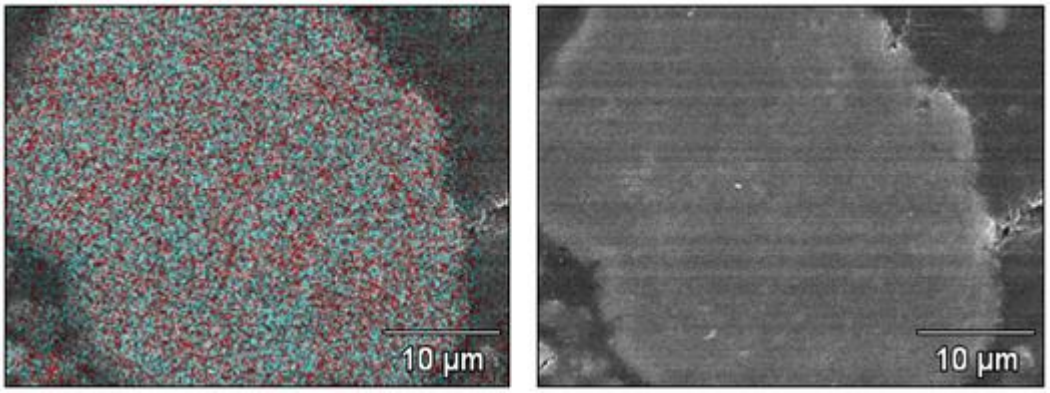

Figure 4.6: A still coarse but more homogenous powder after 2h milling

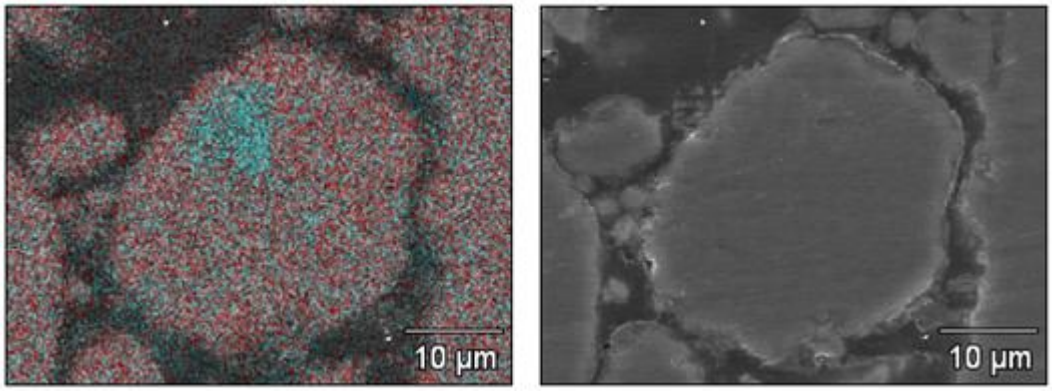

Figure 4.7: A more refined with blue Ti-enriched spots obtained after 4h milling

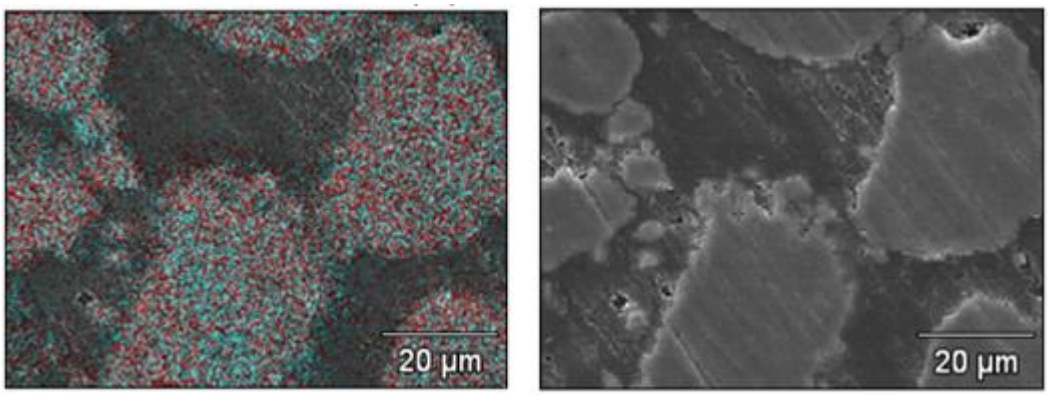

Figure 4.8 A fine microstructured and homogenous powder obtained after 6h

After milling for 2h, the TiO_2 particles were effectively incorporated into Al particles to form fairly homogenous composite powders (Figure 4.6). However, there were occasionally a few slightly titanium enriched areas (Figure 4.9).

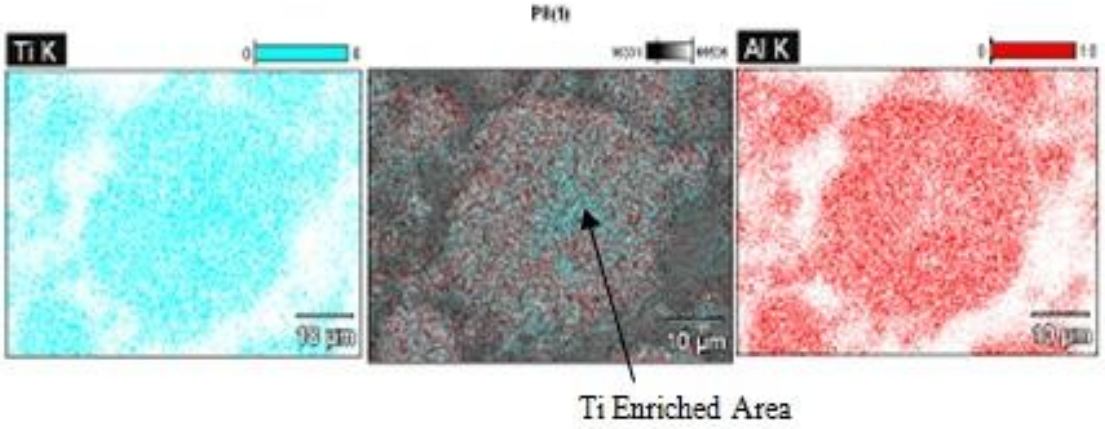

Figure 4.9: EDS element map of a powder produced after 4 h milling

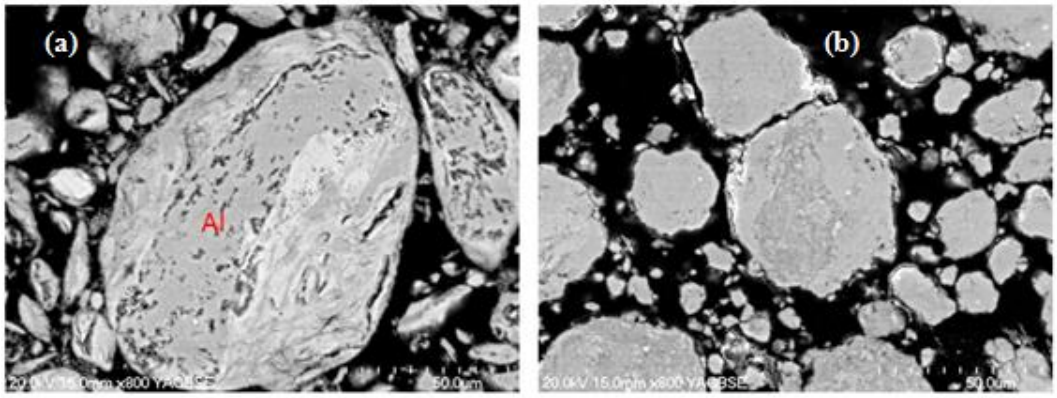

Figure 4.10: Back-scatter images of TiO_2/Al powders milled for (a) 1h, and (b) 6 h

4.2.4 Effect of Temperature on Phase Composition

When composite powders were reacted below 1000^oC (DTA combustion temperature), the product contained unreacted feed constituents (TiO_2 and Al) and intermediate phases ($TiAl_3$, $Ti_{0.72}O_2$, Ti_4O_7 and Al_2TiO_5). As the milling time was increased above 2h, the reaction went to completion at a lower temperature.

Table 4.3: Effect of reaction temperature on co-existing phases

Milling Time (h)	Combustion Temp (°C)	Phase Composition
2	270	TiO_2, Al, $TiAl_3$
	650	TiO_2, Al, $TiAl_3$, Ti_4O_7
	685	TiO_2, Al, $TiAl_3$, Al_2TiO_5
	1000	$TiAl_3$, Al_2O_3
4	278	Al, $Ti_{0.72}O_2$, TiAl
	575	$TiAl_2$, Al_2TiO_5
	1000	TiAl, Al_2O_3
6	571	TiAl, α-Al_2O_3
	928	TiAl, α-Al_2O_3

The kinetics of combustion synthesis are expected to be faster than observed in the above DTA results because of the shortened inter-particle distances and better heat transfer when reactants are compacted. The general trend observed in the DTA results is that combustion is incomplete at low temperatures and short milling times (Table **4.3**). To ensure the reaction goes to completion, the combustion reaction will be done above 930°C. From thermodynamic considerations elaborated in Chapter 2, this would also ensure sufficient heat to produce molten TiAl. Results of solid/liquid separation experiments (Chapter 5) showed that only powders milled for 1h fulfilled this criterion.

4.3 Summary

The results have demonstrated that high energy mechanical milling can be effectively used for preparing feed to the solid/liquid separation process. While there was no evidence of a chemical reaction between Al and TiO_2 during milling, it was observed that the milling intensity had a significant effect on the microstructure and reactivity of milled powders. Fine microstructured powders produced by prolonged milling ignited quicker and at lower temperatures. This resulted in low combustion temperatures and rapid solidification of the alloy that would cause low solid/liquid separating efficiencies.

Conversely, powders milled for shorter milling times had a coarse microstructure, higher compositional variability and a higher ignition temperature. A higher

ignition temperature is expected to be favourable for the solid/liquid separation because the TiAl phase in the combustion synthesis product would remain molten long enough to be extruded out. Therefore the powders milled for 1 h were deemed to be most suitable to be used in solid/liquid separation and consequently became the basis for testing unit process downstream the solid/liquid separation stage.

4.4 References

Blazquez, J. S., Ipus, J. J., Lozano-Perez, S., & Conde, A. (2013). Metastable soft magnetic materials produced by mechanical alloying: Analysis using an equivalent time approach. *JOM, 65*(7), 870-882.

Fecht, H. J. (1995). Nanostructure formation by mechanical attrition. *Nanostructured Materials, 6*(1-4), 33-42.

Gheorghe, I., & Rack, H. J. (2002). Influence of TiO_2/Al ratio on reaction path during reactive infiltration of TiO_2 by molten Al. *Materials Science and Technology, 18*(10), 1079-1084.

Kamali, A., & Fahim, J. (2009). Mechanically activated aluminothermic reduction of titanium dioxide. *International Journal of Self-propagating High-Temperature Synthesis, 18*(1), 7-10.

Liu, Z. G., Raynova, S., & Zhang, D. L. (2006). Investigation of a Discus-Milling Process Using a Powder Mixture of Al and TiO_2. *Metallurgical and Materials Transactions A, 37A*(1), 225-233.

Lu, Y. C., Agnew, S., Dieckmann, R., & Sass, S. L. (1995). Further characterization of the aluminium peroxide, AlO_2, formed by interfacial reaction between Pt and α-Al_2O_3. *Acta Metallurgica et Materialia, 43*(5), 1885-1893.

Welham, N. J. (1998). Mechanical activation of the solid-state reaction between Al and TiO_2. *Materials Science and Engineering A, 255*(1-2), 81-89.

Welham, N. J., & Llewellyn, D. J. (1998). Mechanical enhancement of the dissolution of ilmenite. *Minerals Engineering, 11*(9), 827-841.

Ying, D. Y., Zhang, D. L., & Newby, M. (2004). Solid-state reactions during heating mechanically milled TiO_2/Al composite powders. *Metallurgical and Materials Transactions A, 35*(7), 2115-2125.

Zhang, D., & Raynova, S. R. (2009). Patent No. US 2009/0311123 A1. Method for Producing Metal Alloy and Intermediate Products.

Zhang, D. L. (2004). Processing of advanced materials using high-energy mechanical milling. *Progress in Materials Science, 49*(3-4), 537-560.

Zhang, D. L., Cai, Z. H., & Adam, G. (2004). The mechanical milling of TiO_2/Al composite powders. *JOM - Journal of the Minerals Metals & Materials Society, 56*(2), 53-56.

Chapter 5

Liquid/Solid Separation

5.1 Introduction

When TiO_2/Al composite powders produced by high energy mechanical milling (HEMM), are preheated to the ignition temperature T_{ig}, a self-sustaining exothermic reaction, also referred to as a combustion synthesis reaction, occurs producing TiAl and Al_2O_3 at a temperature much lower than is possible with unmilled reactants (Welham, 1998; Ying *et al.*, 2004). The ignition temperature is determined by the milling intensity. Powders subjected to higher milling intensity ignite at lower temperatures. Depending on the milling intensity and ignition temperature, the combustion synthesis products may be solid, semi-solid or liquid. In the TiPro process, the combustion synthesis reaction produces solid corundum (Al_2O_3) and liquid TiAl. Liquid TiAl is subsequently separated from the solid corundum by extruding the combustion synthesis product during solid/liquid separation. Therefore, it is necessary to maintain the alloy phase in the liquid state long enough for it to be extruded and flow out of the solid corundum (Al_2O_3) inter-particle spaces. This chapter discusses the results of the solid/liquid separation experiments conducted to extract TiAl from the combustion synthesis $Ti_xAl_y(O)/Al_2O_3$ product.

5.2 Theory of Two Phase Flow in Porous Media

The products of combustion synthesis reactions are extremely porous; typically around 50% of theoretical density (Moore & Feng, 1995). Therefore, the extraction of liquid TiAl from the combustion synthesis product by extrusion can be considered to be a two-fluid phase flow system (consisting of liquid TiAl and a gas phase consisting of entrapped air and volatile combustion synthesis products) in a porous medium of corundum particles. Two phase flow in porous media is of significance, forming the basis for many important industrial applications, such as recovery of oil from reservoir rocks in petroleum production and in trickle-bed reactors for water purification processes and hydrogenation. In porous media, capillary pressure is a major factor as it affects liquid distribution, holdup and wetting efficiency (Lappalainen *et al.*, 2009). The capillary pressure can be described as the pressure gradient that arises due to the curvature of the interfacial

surface of two coexisting immiscible fluids. In the pore space of a porous material containing two fluids (liquid TiAl and gas phase), the interfacial boundary between the fluids is curved and the sharpness of the curvature is a function of the inter-granular spaces and the proportion of the coexisting fluids. The curvature results from the interfacial surface adopting a shape with the least interfacial-surface free energy compatible with the volumes of fluids present and the shapes of the retraining solid surfaces (Leverett, 1941). The capillary pressure, P_c, acting on the interface separating two phases is given by the Young-Laplace formula,

$$P_c = P_{nw} - P_w = \frac{2\gamma}{R} \tag{5-1}$$

$$\textit{where } R = \left(\frac{1}{R_1} + \frac{1}{R_2}\right),$$

P_{nw} and P_w are the pressures of the non-wetting and wetting phases, R_1 and R_2 denote the principal radii of curvature of the interface (Figure 5.1), and γ is the surface tension between the phases.

Since the interface is considered as a two-dimensional surface which spans a three-dimensional space therefore its shape cannot be sufficiently described by the curling seen in a single cross-section of the particle. There are two curvatures (referred to as principal curvatures C_1 and C_2) that characterise the shape at each point in space. The principle curvatures are the curvatures of the two lines of intercepts between the planes and the surface, which have almost circular shapes in close proximity to the point under consideration. The radii of these two circular fragments, R_1 and R_2, are called the principle radii of curvature, and their inverse values, $C_1 = \frac{1}{R_1}$ and $C_2 = \frac{1}{R_2}$, are referred to as the two principle curvatures (Zimmerberg, 2006).

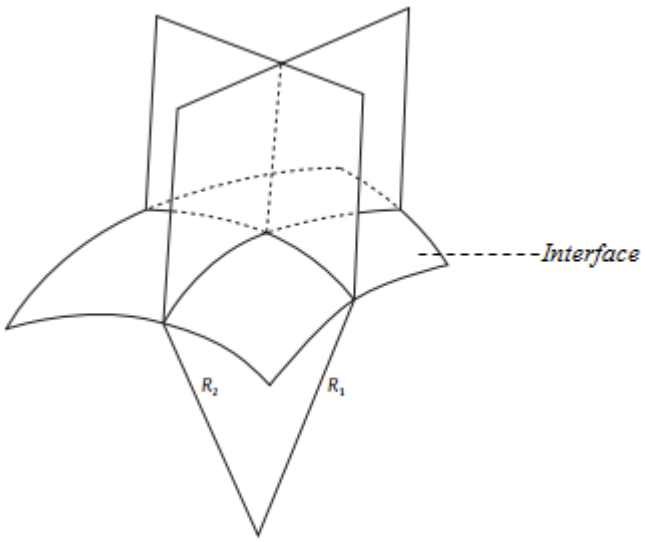

Figure 5.1: Concept of the principal radii of curvature of an interface (Zimmerberg, 2006)

The fluid having a fluid-solid contact angle between 0^o and 90^o is the wetting phase whereas the one with a contact angle between 90^o and 180^o is the non-wetting phase. The contact angle of liquid TiAl on Al_2O_3 is 38^o; therefore in the TiPro process TiAl is the wetting phase and gas is the non-wetting phase (Bear *et al.*, 2011).

Differing theories relating to capillary pressure (e.g. hysteresis) have been reported by various researchers; however there is general agreement that particle properties such as size, sphericity, and surface roughness influence capillary pressure (Bear, 1972). Capillary pressure increases with decreasing particle size and increasing surface roughness. As capillary pressure increases, imbibition increases at the expense of drainage and the flow of liquid out of the porous medium is impeded. It has been reported that the wetting phase gets imbibed much more in the grooves on the rough surface than in the pore spaces between the particles. Surface roughness also causes an increase in the film thickness on the particle surface (Lappalainen, *et al.*, 2009). This is unfavourable for solid/liquid separation as it increases liquid holdup.

The possible liquid configurations in porous media systems where gas and liquid coexist can be categorized into three saturation zones of the capillary pressure curve (Figure 5.2). At low content, the liquid phase occurs as pendular rings around inter-grain contacts (Figure 5.3(a)). The full liquid saturation, in which only the gas-liquid interface exists on the surface of the medium, corresponds to the capillary zone. In the zone of intermediate liquid saturation, or the funicular

region, the liquid forms various configurations referred to as funicular bridges. The funicular region results by coalescence of pendular rings (Smith, 1933) and its limits are not clear as they overlap with the pendular and the full saturation zones (Lappalainen, *et al.*, 2009). In the high liquid saturation zones the liquid is more loosely bound because of lower capillary pressure; therefore as the liquid saturation increases it gets easier to drain the liquid.

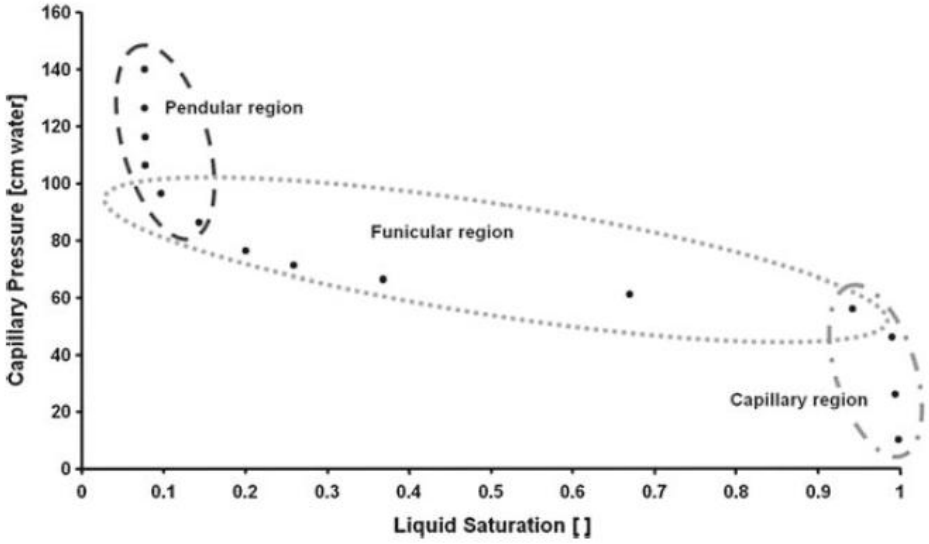

Figure 5.2: Capillary pressure – liquid saturation curve showing pendular, funicular and capillary regions (Lappalainen, et al., 2009)

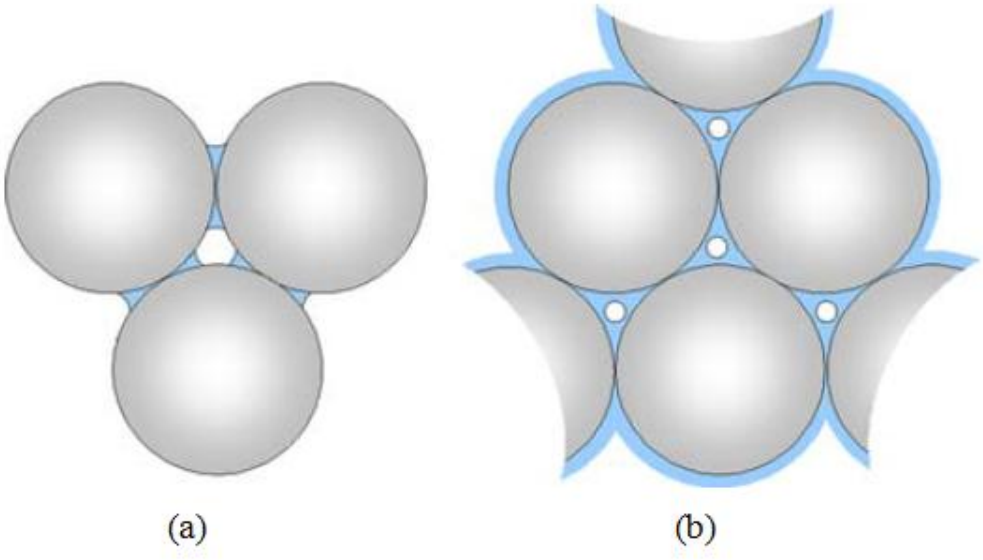

Figure 5.3: Liquid bridges in the (a) pendular and (b) funicular regions (Lappalainen, et al., 2009)

In the pendular region, capillary pressure is a function of the mean curvature which in turn is a function of the two principal radii, R_1 and R_2 (Figure 5.4). The capillary pressure-liquid saturation relationship is obtained by calculating the

capillary pressure and liquid saturation based on R_1 and R_2 using equation (5-1). The two radii depend on factors such as the pore size and geometry, wettability of the medium, saturations of the phases and whether the saturation state has been obtained by drainage or imbibition.

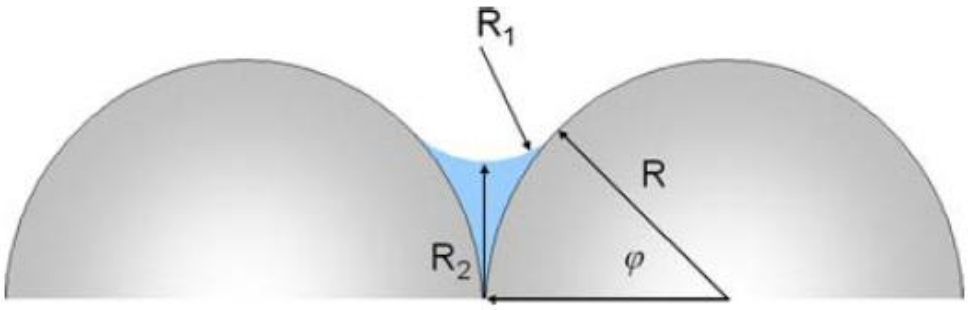

Figure 5.4: A schematic of the pendular ring at the inter-particle contact point showing the filling angle φ and the corresponding principal radii R1 and R2 (Lappalainen, et al., 2009)

The capillary pressure in the funicular region is determined by the particle interstices and is calculated using the hydraulic diameter D_H, ($R^* = 1/2D_H$) of the smallest pore in Equation (5-1).

> D_H = 4A/s, where A is the cross-sectional area and s is the wetted perimeter of the flow channel.

In the capillary region, the liquid starts flowing out and as the drainage force is exerted on the porous medium, the gas starts displacing first the liquid on the particle surface where the capillary force is zero. As the liquid surface lowers, the menisci of the inter-particle free surfaces gets smaller thereby increasing the capillary pressure. In non-homogenous porous media, the capillary pressure that holds the liquid in place varies spatially. Relatively less drainage force is required to displace liquid with gas in areas of higher porosity and larger particles. Capillary driven liquid flow can be radial in orientation as it is irrespective of pore orientation (Lappalainen, *et al.*, 2009).

5.2.1 Liquid-solid Interaction and Microstructure Evolution

The presence of the liquid phase creates conditions similar to liquid-phase sintering. Since there is no chemical reaction between the combustion products liquid TiAl and solid Al_2O_3, the interfacial energies have a dominant effect on microstructure evolution. If the liquid wets and spreads to cover the solid particles, the particles will be separated by a liquid bridge that significantly reduces inter-

particle friction so that they can easily rearrange under the compressive capillary stress of the liquid. A wetting liquid layer generates a compressive capillary force, which is equivalent to subjecting the system to a large external hydrostatic compression given by the Young and Laplace (Equation (5-1)). The large capillary pressures cause rapid particle rearrangement when the viscosity of the system is still low. Capillary pressure gradients will also cause liquid to flow from regions with large pores to regions with smaller pores thereby redistributing the liquid. This phenomenon accounts for why densification achieved with liquid-phase sintering that is significantly higher than in solid-state sintering. If the liquid wets and spreads over the solid particles, the solid-vapour interface of the particulate system is eliminated and pores form in the liquid. The reduction of the liquid-vapour interfacial area provides a driving force for shrinkage and consequently densification of the system. Following particle rearrangement, densification might occur by the solution-precipitation mechanism, and the liquid layer separating the grains progressively becomes thinner with time until the liquid capillary becomes too narrow for the liquid to flow.

5.2.2 Liquid-Phase Sintering Mechanisms

The basic mechanisms and processes occurring during liquid-phase sintering can be divided into three stages, each over-lapping with the successive stage.

5.2.2.1 Stage 1: Rearrangement and Liquid Redistribution

Investigations into sintering fine tungsten powders containing coarse nickel particles that melt into a liquid phase have established that the liquid redistributes sequentially in such a way that the small pores are filled first and the larger pores later (Park, 1986). This produces shrinkage and densification a feature that has been observed in the combustion synthesis products of the TiPro process. Once in small pores, the particle-wetting liquid phase is so tightly held by strong capillary forces that it cannot be drained out by extruding the combustion product.

Inhomogeneous powders that are characteristic of coarse microstructured powders milled for 1 h lead to inhomogeneous liquid distribution producing regions that are enriched with the liquid alloy.

The particle rearrangement process can be divided into the primary and the secondary rearrangement stages (Figure 5.5). The primary stage occurs rapidly soon after the formation of the liquid under the surface tension forces of liquid

bridges between particles. The secondary rearrangement occurs only if the liquid can penetrate the grain boundaries and fragment the polycrystalline particles. It is much more slowly than the primary rearrangement because it depends on the rate the grain boundaries dissolve away.

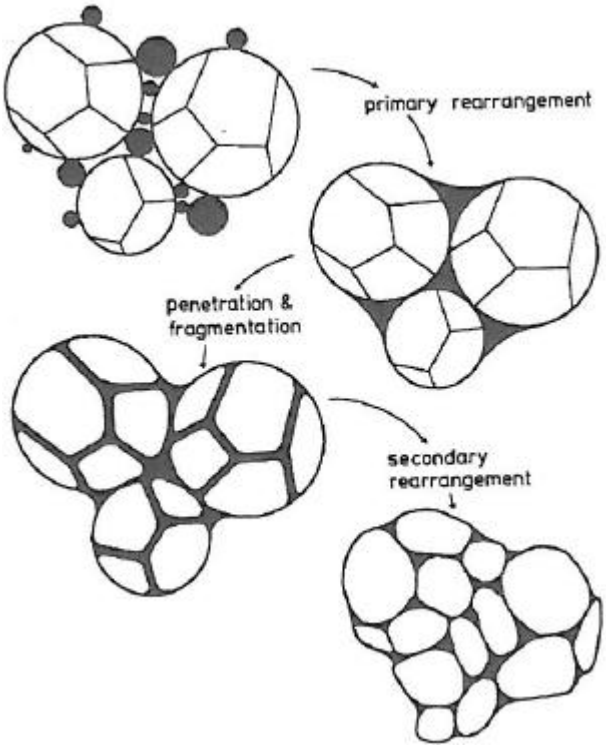

Figure 5.5: Schematic illustrating particle rearrangement of polycrystalline particles (Rahaman, 2003)

5.2.2.2 Stage 2: Solution-Precipitation

In stage 2, rearrangement decreases and solution-precipitation that leads to densification followed by coarsening dominates. In addition to solution-precipitation, coarsening also occurs by coalescence of small grains with contacting large grains. In coalescence, the grains are pulled into contact by a wetting liquid (Figure 5.6).

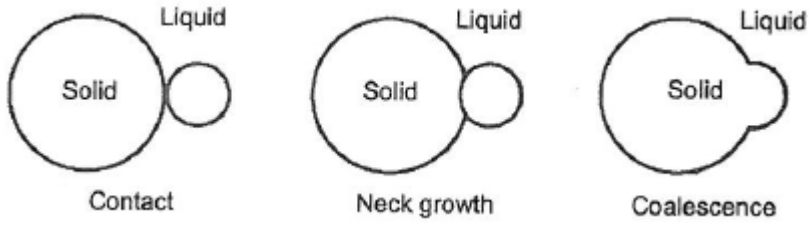

Figure 5.6: Schematic illustrating agglomeration by coalescence of small and large particles

In systems where no solid-solid contacts exist, coalescence may occur by migration of the liquid film separating the grains. This is referred to as directional grain growth.

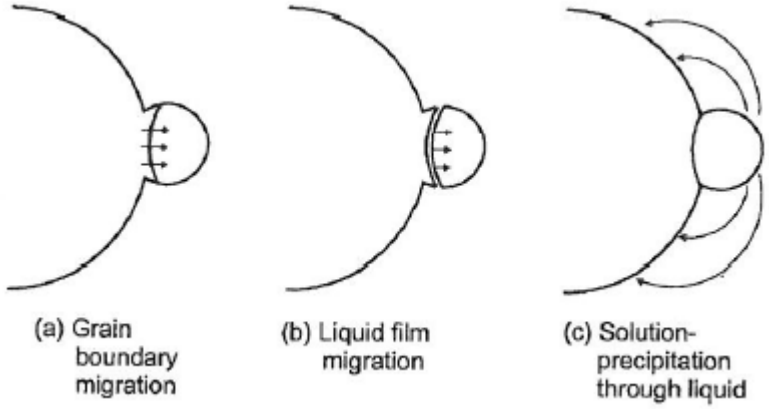

Figure 5.7: Three possible coalescence mechanisms between contacting grains. (a) Solid-state grain boundary migration; (b) liquid-film migration; (c) solution-precipitation through the liquid (Rahaman, 2003)

Tungsten crystal spheres sintered in the presence of liquid Ni showed one sphere grows at the expense of its neighbour (Figure 5.8). Electron probe analysis indicated that the shrinking grain consisted of pure W, while the precipitated material on the growing grain was a solid solution of tungsten containing 0.15 wt% Ni.

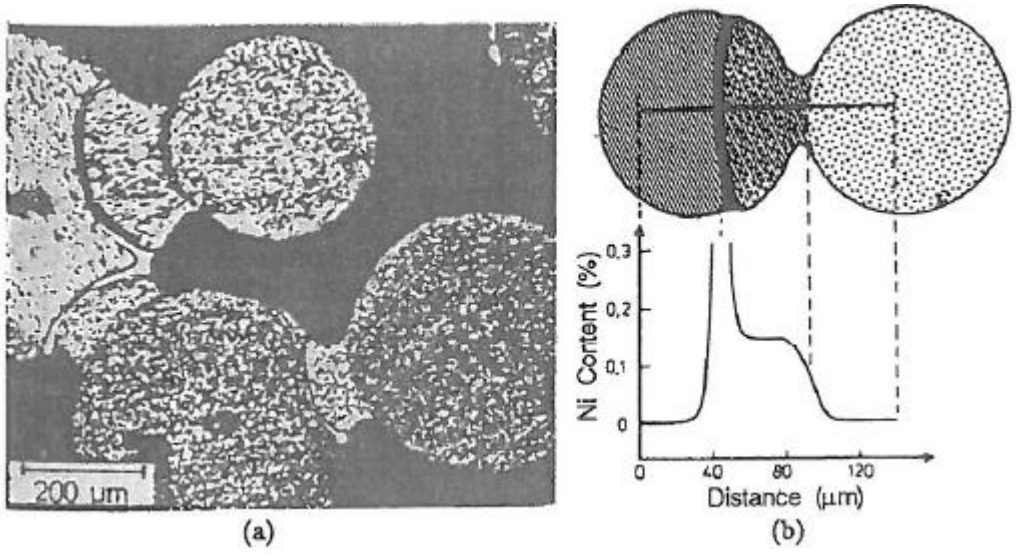

Figure 5.8: Directional grain growth during liquid-phase sintering of single-crystal W spheres with Ni at 1640ºC showing (a) the microstructure and (b) the microprobe analysis (Rahaman, 2003)

It is inferred that the compositional difference between the pure W and the solid solution provides a large decrease in chemical energy, which more than offsets the

increase in the interfacial energy and is therefore the driving force of the coalescence process (Rahaman, 2003).

5.2.2.3 Stage 3: Ostwald Ripening

In stage 3, densification slows down significantly giving way to microstructural coarsening by Ostwald ripening a process by which smaller particles are transported and deposited on to larger particles in order to reach a more thermodynamically stable state wherein the specific surface area is minimised. The bigger particles grow bigger at the expense of smaller ones (Figure 5.9). During grain growth, large pores remain stable until the liquid meniscus radius increases sufficiently to initiate capillary refilling of the pores thereby enhancing densification.

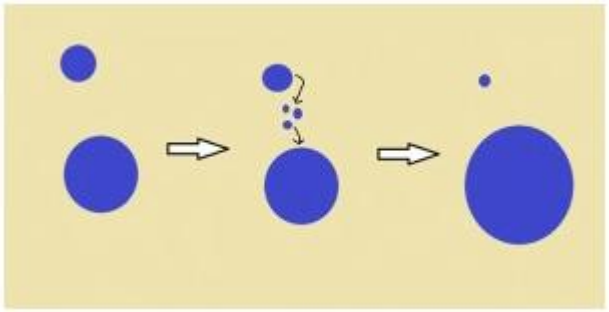

Figure 5.9: Schematic of Ostwald ripening showing growth of larger particles by deposition of smaller particles

5.3 Results

5.3.1 Composition of Products

XRD analysis results of the Ti-Al alloy and the co-existing Ti-Al / Al_2O_3 by-product obtained after extruding the liquid Ti-Al / solid Al_2O_3 mixture indicated that the alloy that was produced was predominantly TiAl with minor Al_2O_3 impurities. The by-product contained mainly Al_2O_3, TiAl (Figure 5.11(a) and (b)) and probably minor amounts of Ti_3Al, TiO and $TiAl_3$ (Figure 5.10). This was confirmed by EDS analyses (Table 5.1). The formation of titanium aluminide TiAl by preheating the reacting TiO_2/Al composite powders is therefore not hindered by kinetic and thermodynamic conditions used in the experiments. However, since the alloy phase has to be molten in order to facilitate its separation from solid alumina (Al_2O_3) the period that the alloy is maintained liquid is one of the critical parameters for increasing the alloy yields by extruding the combustion

synthesis product. Maintaining the alloy phase in a molten state is determined by a combination of interdependent factors such as the combustion temperature, heat losses and the rate of preheating the reactants.

Table 5.1: EDS analyses of the Ti-Al alloy and composite by-product

	Composition - Wt%		
Sample	Ti	Al	O
Alloy	64.43	34.30	1.77
Composite	30.12	44.95	24.95

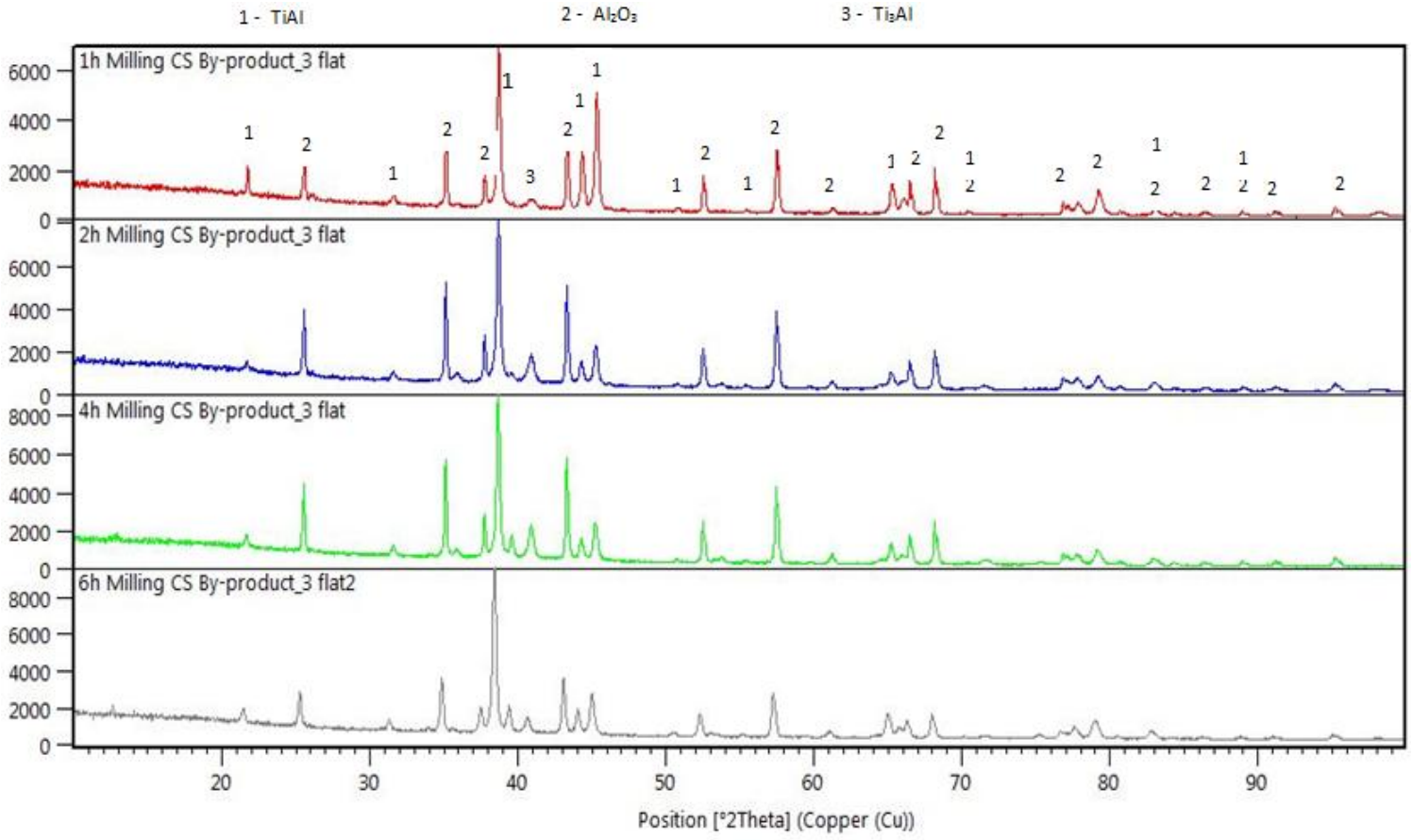

Figure 5.10: XRD patterns of solid/liquid separation by-products from combustion of TiO_2/Al powders milled for (a) 1h, (b) 2h, (c) 4h and (d) 6h, respectively

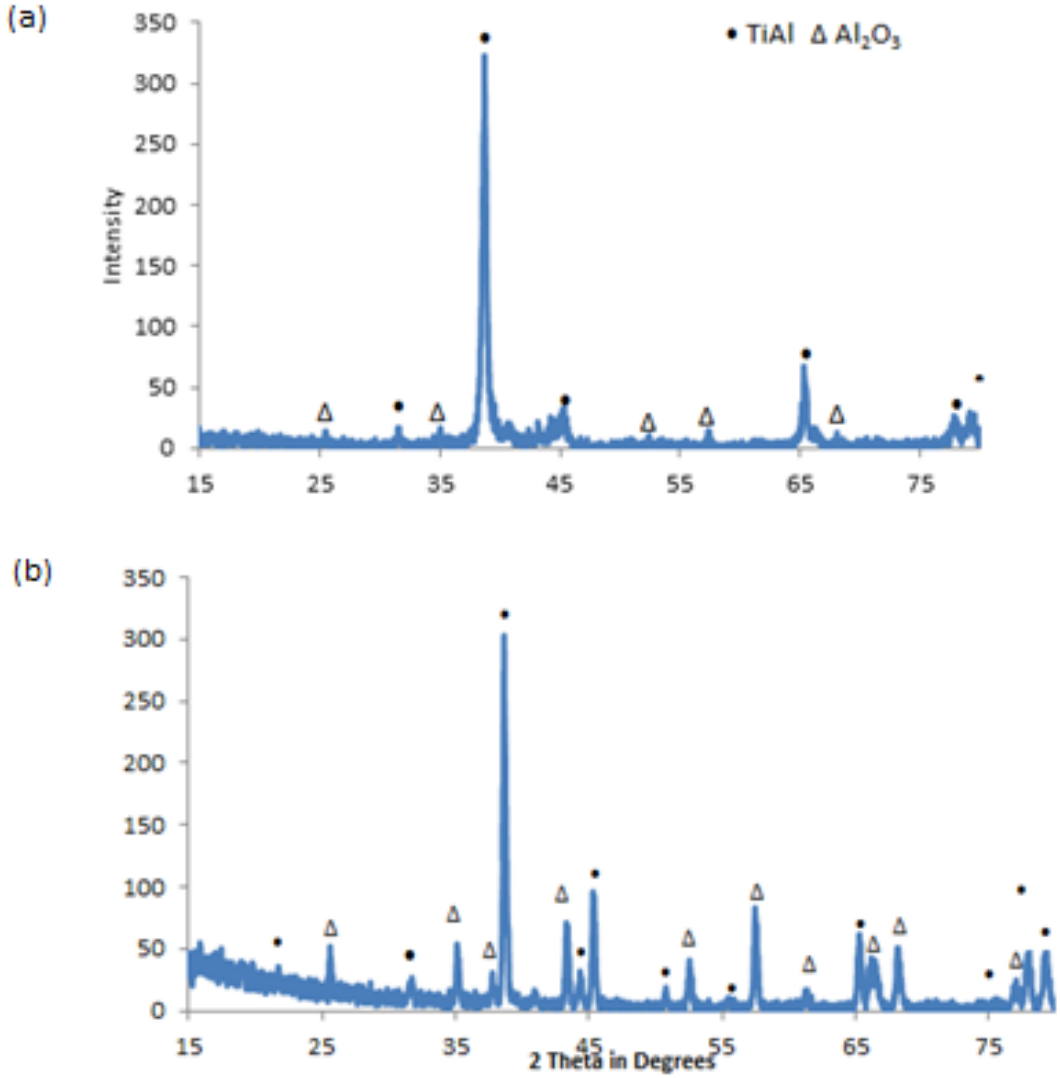

Figure 5.11: XRD patterns of (a) TiAl alloy and (b) extrusion by-product of the combustion synthesis product powders milled for 1h

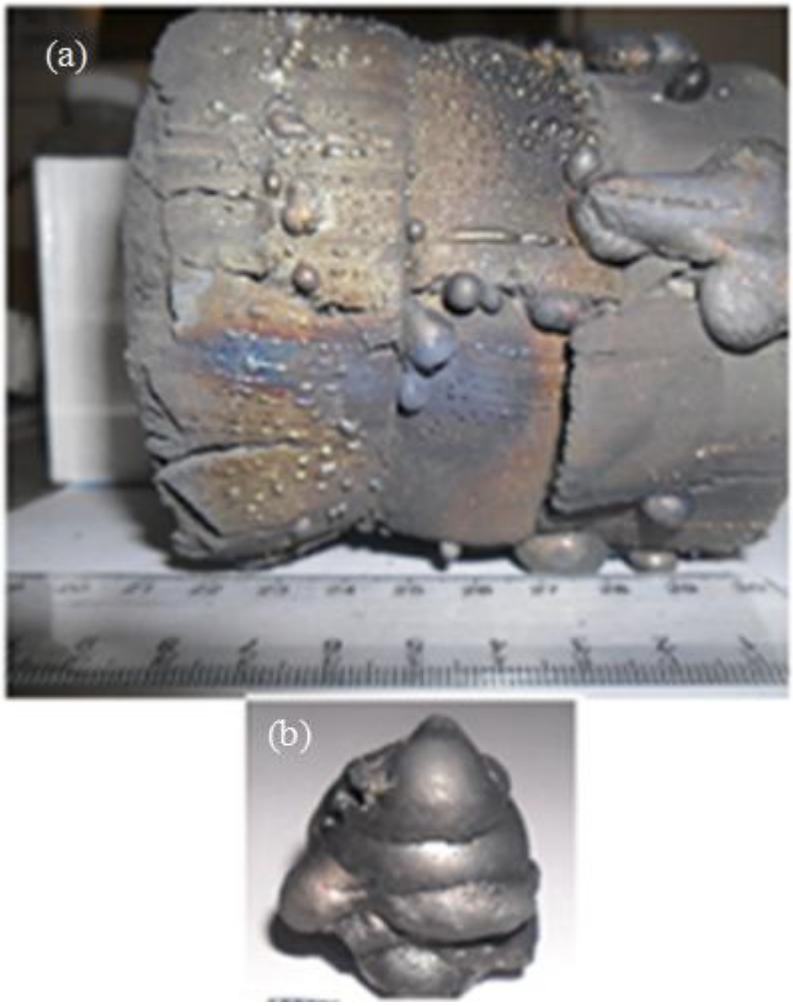

Figure 5.12: Extrusion products (a) By-product (b) TiAl alloy

5.3.2 Distribution of Co-existing Phases

The TiAl relative abundance (saturation level determined IQ Materials Software) of the extrusion by-product averaged about 15% TiAl (Figure 5.24). The spatial distribution, and association of co-existing phases on SEM element maps of a cross section of the combustion synthesis product, also confirm that the TiAl concentration was too low for much liquid TiAl to be extruded out (Figure 5.14). For liquid TiAl to be extruded out, the alloy phase has to be fully interconnected and the low capillary pressure conditions, prevalent at high TiAl concentration in the capillary zone, have to be attained (Figure 5.2).

The mechanism of TiAl grain growth through coalescence of pendular rings is illustrated by SEM elemental maps of a cross section of a combustion synthesis (CS) product (Figure 5.14). The spatial saturation of the CS product with liquid TiAl increases by rearrangement and agglomeration of Al_2O_3 particles (Figure 5.15). As the contact angle of TiAl on corundum (38^o) is low (Li *et al.*,

2008), molten TiAl has a tendency to wet and lubricate the corundum particle surfaces. This facilitates rearrangement of the corudum particles into denser agglomerates while leaving the TiAl to coalesce into bigger grains. Upon solidification, these big grains appear as isolated TiAl-enriched areas in pores and surounded by a TiAl(O)/Al_2O_3-composite intergrowth (Figure 5.13).

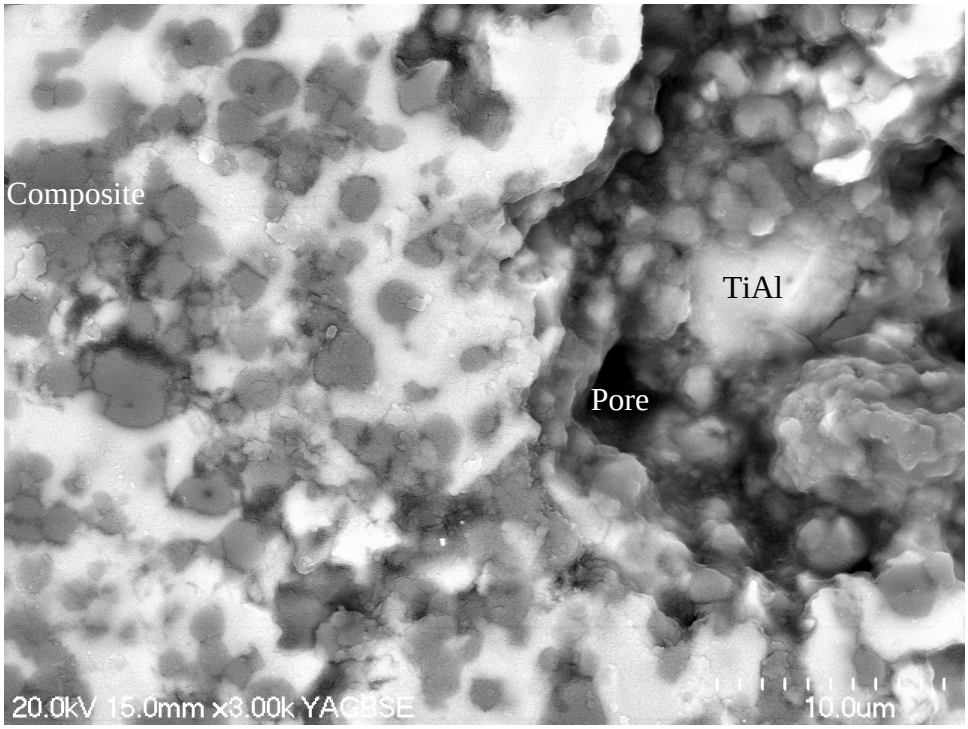

Figure 5.13: Coalesced TiAl in pores and surrounded by a TiAl(O)/Al_2O_3-composite

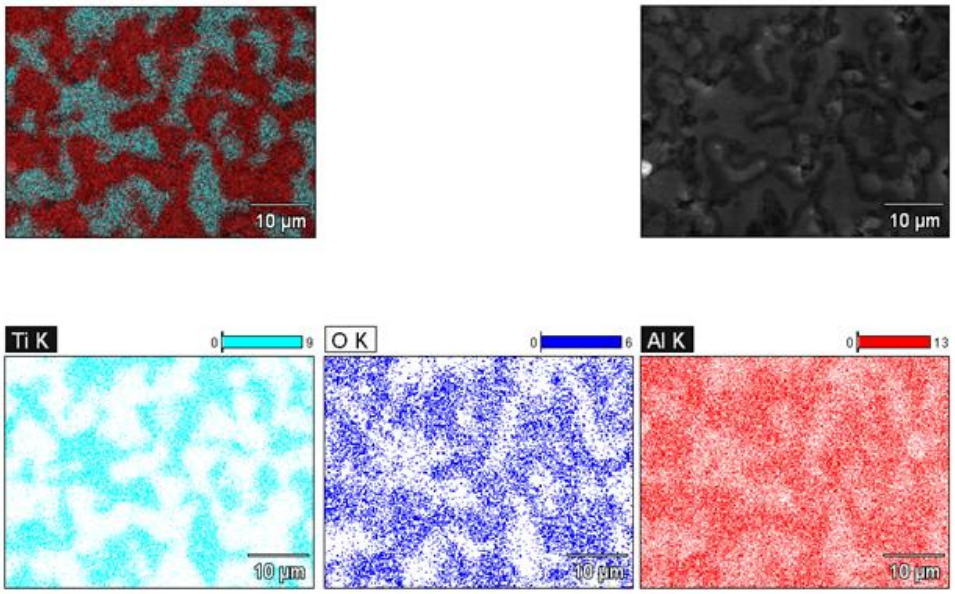

Figure 5.14: TiAl funicular bridges (light blue) of TiAl alloy in the combustion synthesis product of powders milled for 1h

According to Moore and Feng (1995), when particles are in contact with a wetting fluid an attractive force is generated that pulls particles together into denser agglomerates. The wetting fluid also lubricates the surfaces thereby facilitating particle rearrangement. Various research has reported this phenomen has been observed in liquid-phase sintering too (Anestiev, 2000; Moore, 1995; Rahaman, 2003). Particle rearangement of the initial or primary particle network is reported to occur rapidly in as little as a few minutes and has been associated with the enhanced densification that occurs during liquid-phase sintering in contrast with lower densification achieved in solid-state sintering (Rahaman, 2003; Moore, 1995; Anestiev, 2000). The micrograph of the combustion product (Figure 5.15) and that obtained by other researchers studying agglomeration during liquid-phase sintering (Figure 5.16) bear similar microstructural features of liquid distribution and particle rearrangement driven by capillary stress gradients that characterise liquid-phase sintering. The analysis of rearrangement in randomly packed packed array of particles is a challenging problem and understanding the process in real systems is limited (Rahaman, 2003).

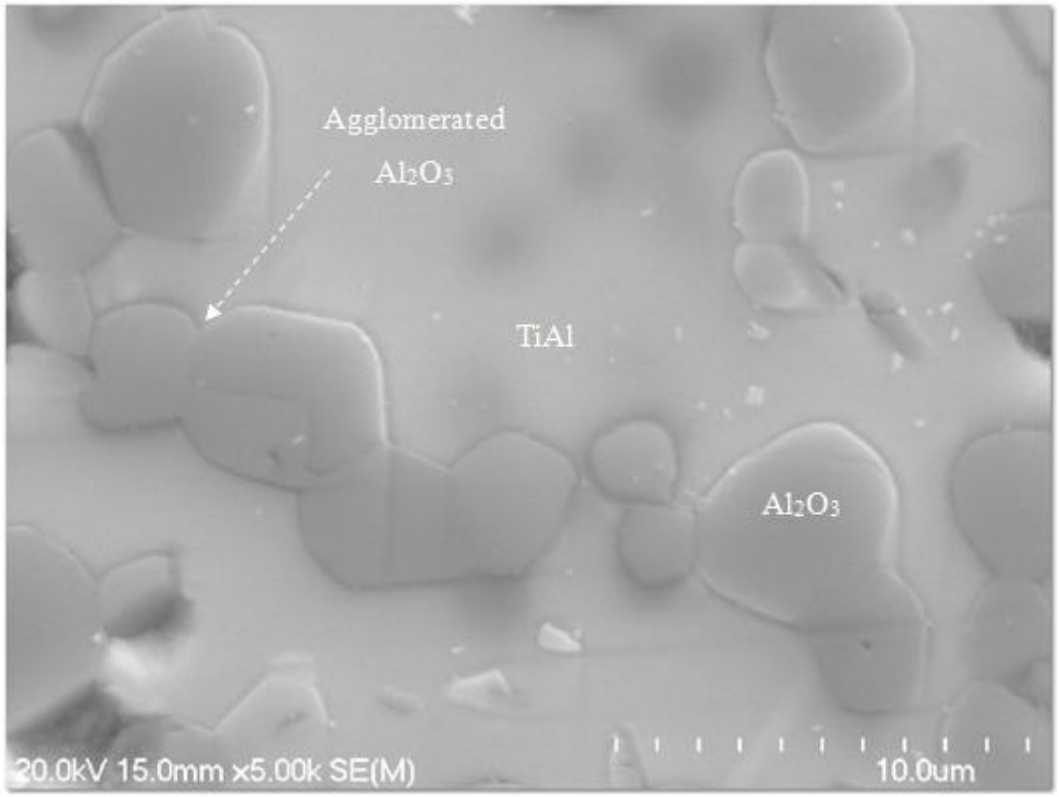

Figure 5.15: SEM image of Al_2O_3 agglomerates and coalesced TiAl in combustion synthesis product of powders milled for 1h

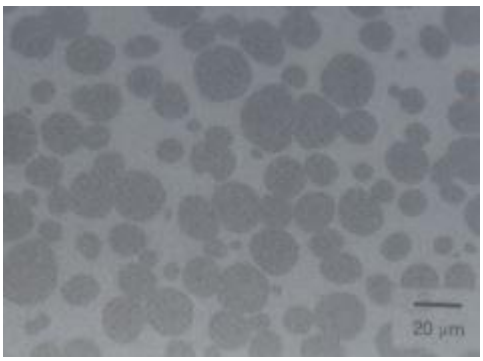

Figure 5.16: High magnification view of agglomeration in the W (15.4 wt% Ni + 6.6 wt% Fe) system after liquid-phase sintering for 1 min (Rahaman, 2003)

5.3.3 Effect of Milling Time

Powders produced after milling for different time durations exhibited different microstructural characteristics, thermodynamic and kinetic behaviour. Short milling times produced coarse microstructured composite powders with high ignition and combustion temperatures. The combustion temperature attained with powders milled for 1 h ignited at 970^{o}C and attained a combustion temperature above 1460^{o}C the melting point of TiAl (Figure 5.17).

However, the peak temperature could not be maintained long enough to facilitate solid/liquid separation. The temperature dropped to about 1200^{o}C (Figure 5.17). Significant amounts of TiAl still remained frozen in the extrusion by-product. Maintaining high temperatures and TiAl in liquid state is critical for high alloy yields.

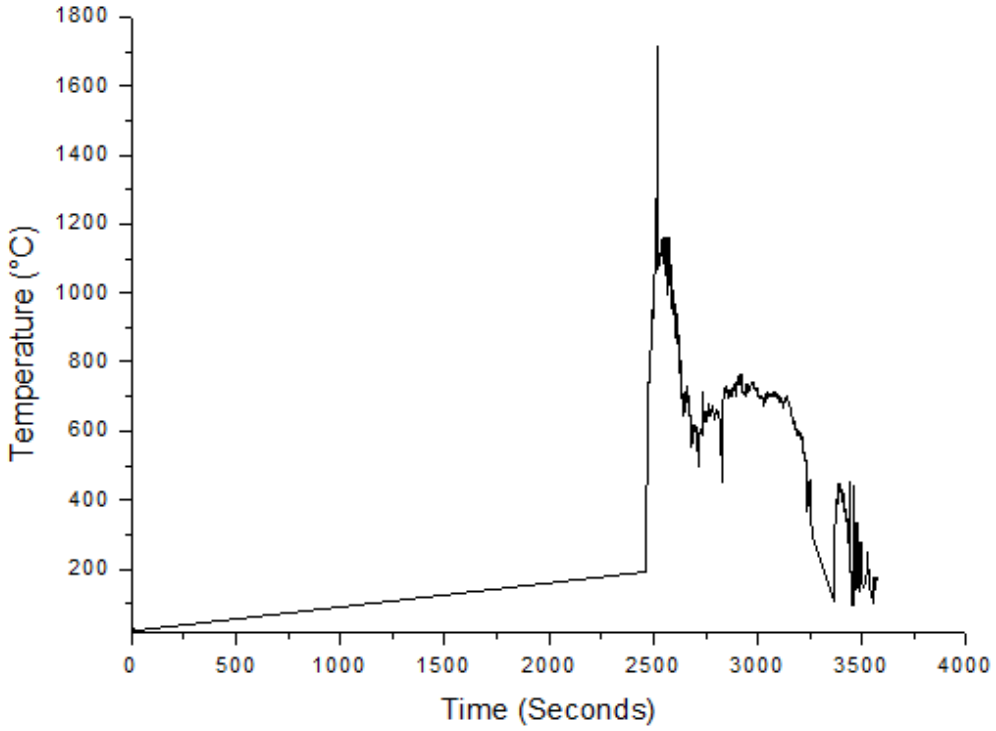

Figure 5.17: Thermograph of a compact of TiO_2/Al composite powder milled for 1h

As the milling time was increased the microstructure of the powders became finer; the ignition and combustion temperatures dropped. Powders milled for 4 h and 6 h ignited around 250°C and the combustion temperature was about 700°C (Figure 5.18 and Figure 5.19).

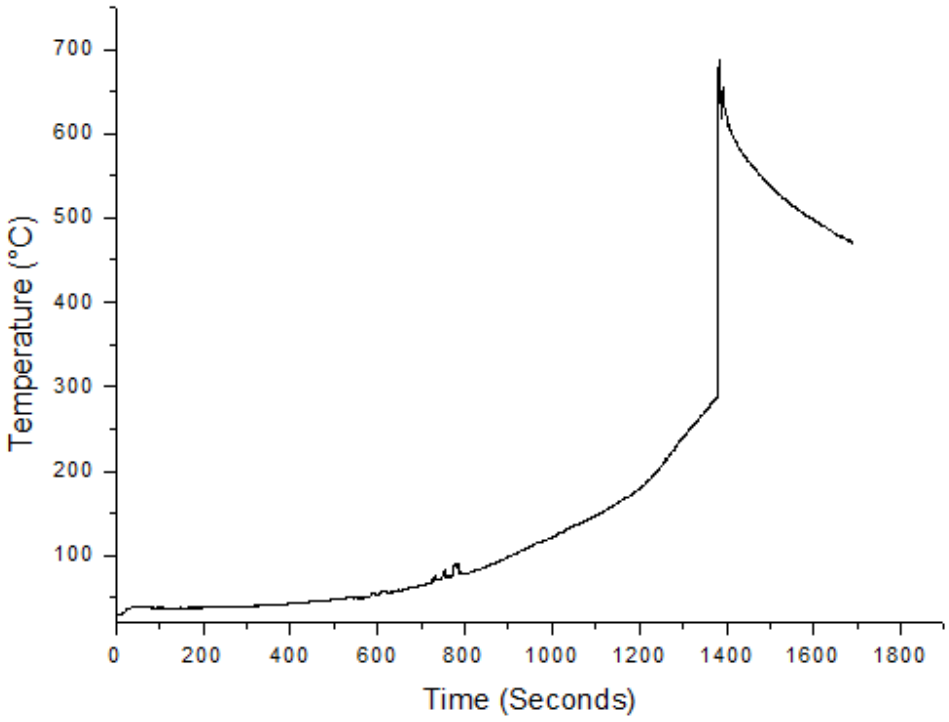

Figure 5.18: Thermograph of combustion synthesis of TiO_2/Al powders milled for 4h

Ignition time was 23 min and 20 min for powders milled for 4 h and 6 h respectively compared to 42 min for 1h-milled powder. Faster kinetics of 4 h and 6 h milled powders was due to the formation of more reactive fresh new surfaces (Fecht, 1995; Welham, 1998; Zhang, 2004).

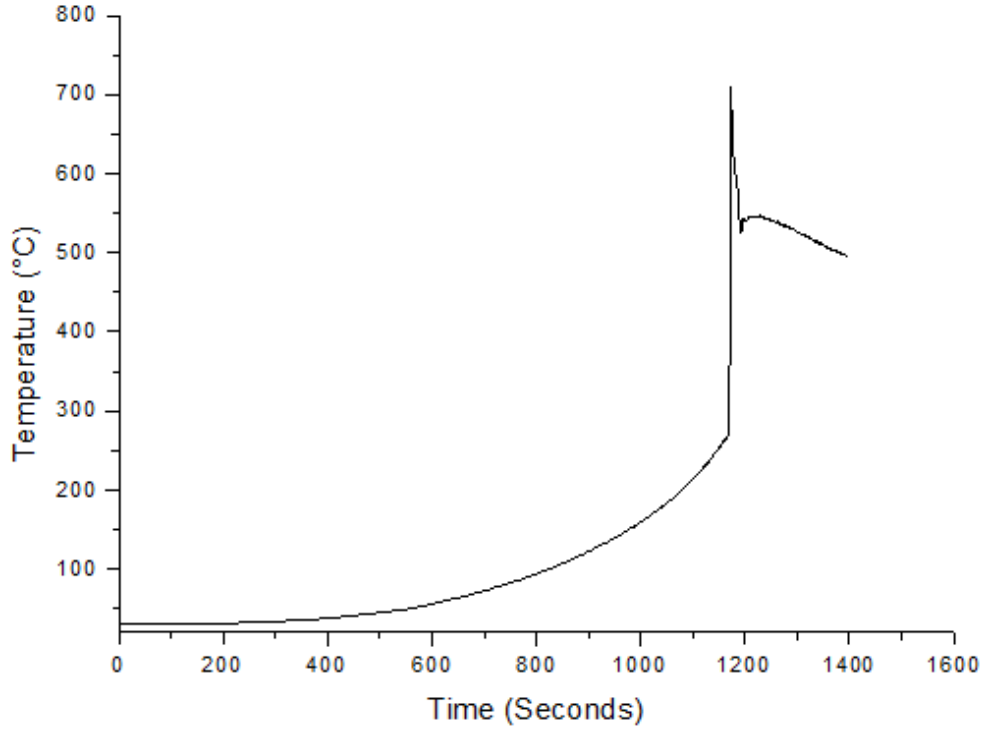

Figure 5.19: Thermograph of combustion synthesis of TiO_2/Al powders milled for 6h

XRD and EDS analyses of all the combustion product samples revealed the presence of significant quantities of residual TiAl. The Ti content of the composite particles in the powder milled for 1 h ranged between 0.73 and 58.29 wt% with a standard deviation of 23.06 wt%, compared to a range from 37.69 to 43.11 wt% Ti and 1.22 wt% standard deviation for the powder milled for 6 h. From the EDS element mapping and the optical micrographs (Figure 5.20) it was evident that as the milling time was increased, the composition of as-milled powder particles became more homogeneous and the thickness of reactants was reduced due to refinement of the composite structure. This caused a decrease of ignition temperature from above 970^{o}C for 1 h milled powder to about 250^{o}C for 6 h-milled powder. A higher ignition temperature is advantageous for solid/liquid separation because it allows the temperature of the products to be raised to above the melting temperature of TiAl. It was observed that the combustion temperature attained with powders milled for 4 h or 6 h was only 700^{o}C compared to 1714^{o}C

attained with powders milled for 1 h. When the combustion temperature was lower than 1460^{o}C the alloy solidified and could not be extruded out of the combustion synthesis TiAl(O)/Al_2O_3 product.

In contrast, when the powders milled for 1h were reacted, the product had a coarser microstructure of the two phases and when extruded; some liquid TiAl was recovered because TiAl remained molten for a longer period due to the higher ignition temperature and corresponding combustion temperatures attained. This is more favourable for the solid/liquid separation.

As illustrated by Table 5.3, Figure 5.20, Figure 5.21 and Figure 5.35, there was an apparent correlation between the microstructure of the as-milled TiO_2/Al composite powders and the grain intergrowth of TiAl and Al_2O_3 in the final combustion synthesis product.

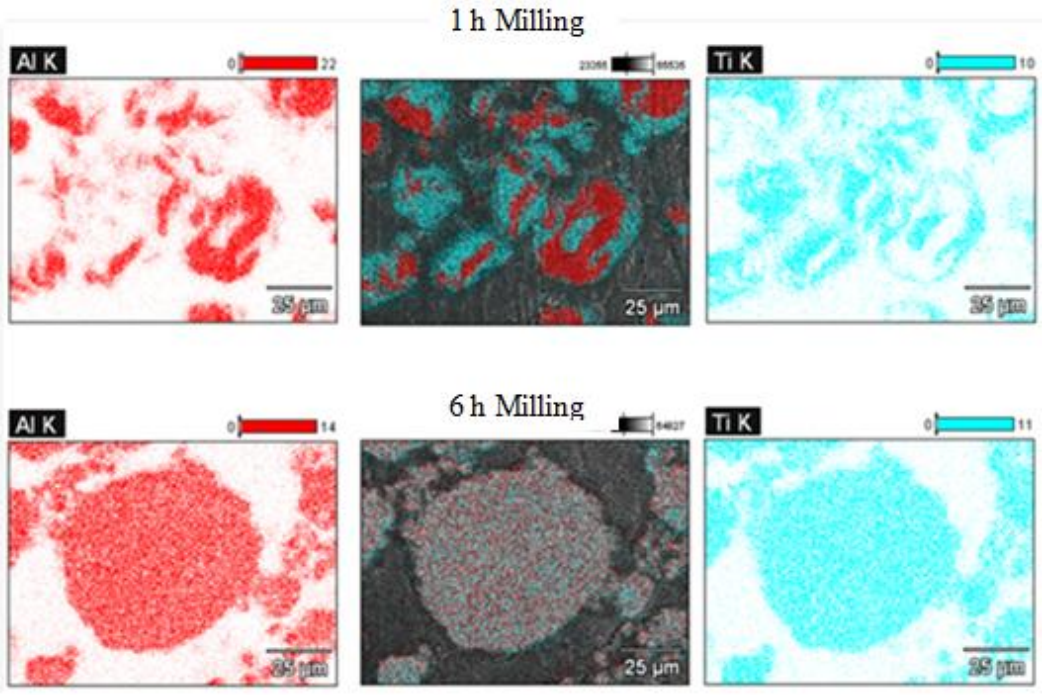

Figure 5.20: SEM element maps contrasting coarse and fine microstructures obtained after milling for 1h and 6 h respectively

It was also observed that, powders milled for 1 h were inhomogeneous with porosity varying in space; the resultant CS product exhibited more connectivity among pores and capillaries compared to fine microstructured powders milled for 6 h (Figure 5.21 (a) and (b)). Wider capillaries or pores are drained before narrower capillaries therefore powders milled for 1 h are more suitable for solid/liquid separation because interconnected pores facilitate flow of the alloy out of the combustion synthesis product during extrusion.

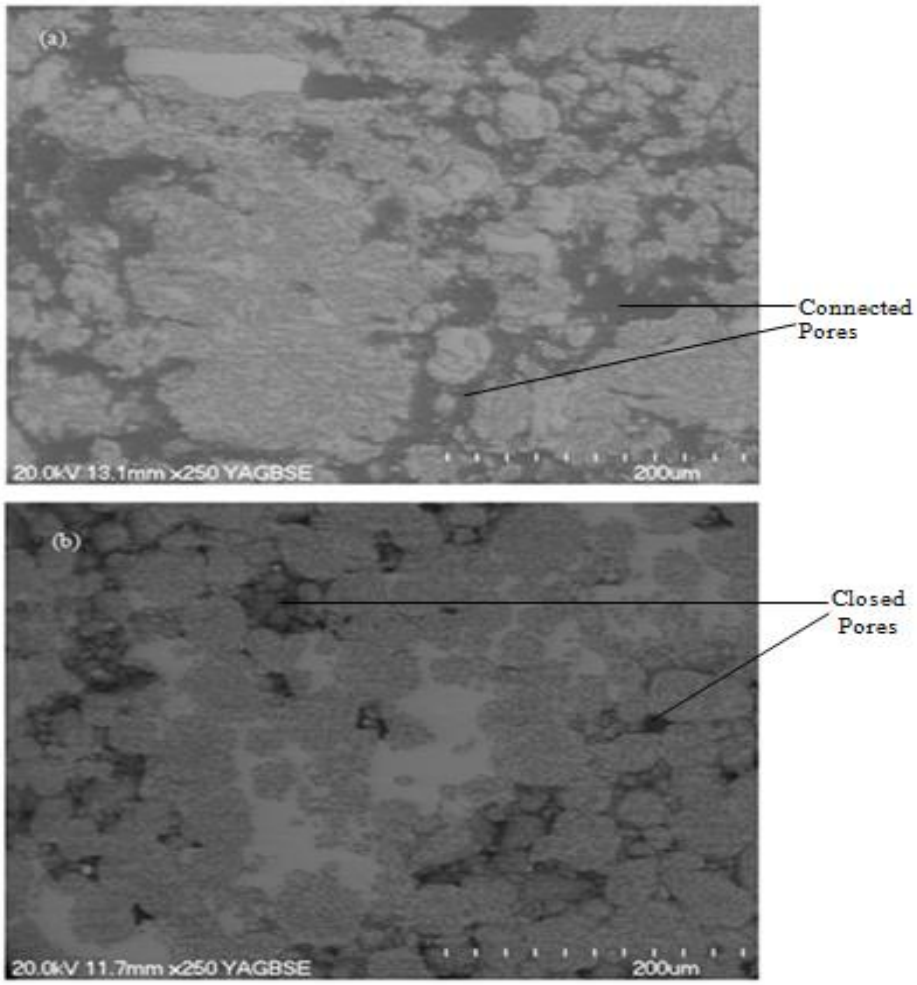

Figure 5.21: SEM Backscatter images of combustion synthesis products of TiO_2/Al composite powders milled for (a) 1h and (b) 6h, respectively

Figure 5.21 contrasts the microstructure obtained by shorter (1 h) and extended (6 h) milling. Drainage of the alloy from fine microstructured combustion products obtained by extended milling is more difficult because TiAl is held by capillary forces that are stronger in fine microstructured combustion products obtained by milling for 6 h. This is evident from the decreased porosity observed in combustion products milled for 6 h (6.8%) compared to 31.3% porosity in powders milled for 1 h.

5.3.4 Effect of Extrusion Pressure

The extrusion pressure was not varied in this study because results of the previous research (Raynova, 2007) showed that merely increasing the pressure did not increase alloy yields. This was due to the rapid solidification of TiAl. However, it is well known that in the extrusion die, the flow-motivating pressure varies depending on the position in the extruder. It is highest in the barrel and decreases along the axis of the extruder as illustrated in Figure 5.22.

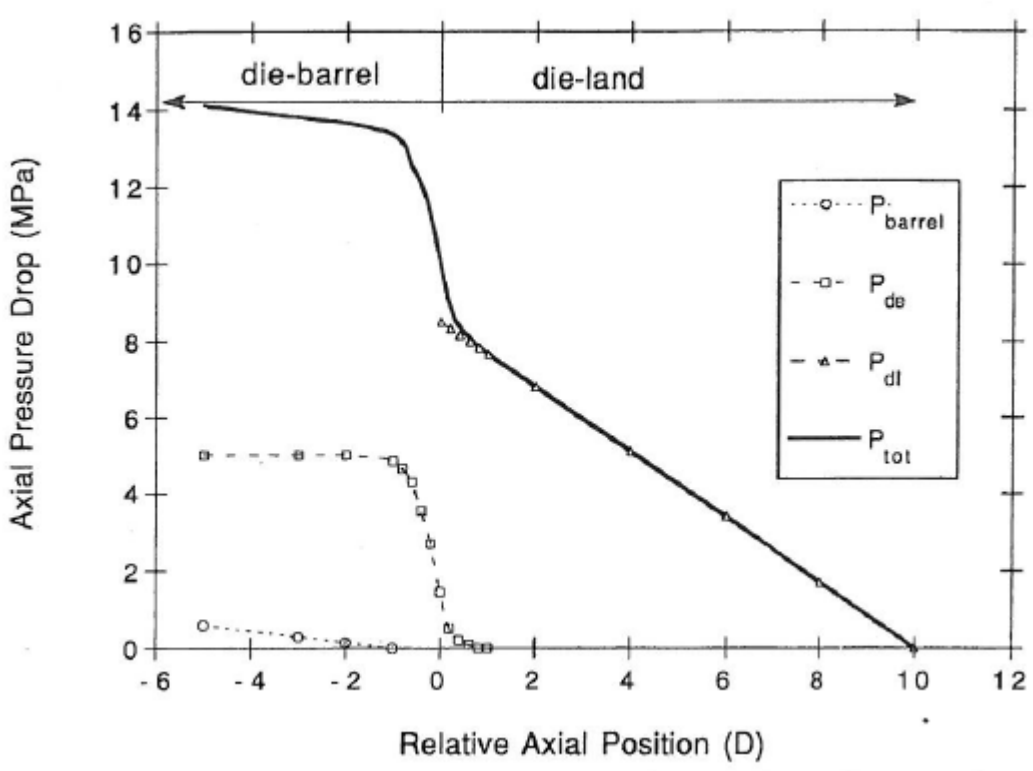

Figure 5.22: Mean axial pressure profile during extrusion and pressure drop in barrel, die entry and die-land (Reed, 1995)

The axisymmetric section of the combustion synthesis composite product (Figure 5.25) shows the effect of pressure on the spatial distribution of the TiAl and Al_2O_3 phases post extrusion. During extrusion the pressure inducing the flow of liquid TiAl is highest at the top (where the plunger makes contact with the compact) and decreases toward the bottom of the compacts. Migration of liquid TiAl under the action of the extrusion force is marked by an increase in intensity of the dark Al_2O_3 phase in the top region (Figure 5.25). This is also confirmed by an increase in TiAl and a decreasing Al_2O_3 concentration with an increase in axial distance from the top of the compact, the point of application of the extrusion pressure (Figure 5.24).

During extrusion, the spatial distribution of TiAl was changed (Figure 5.24 and Figure 5.25). The pressure inducing the flow of liquid TiAl was highest at the top (where the plunger makes contact with the compact) and decreased axially toward the bottom of the compact. This was marked by apparent depletion of the TiAl phase in the top region of Figure 5.25 that left the top enriched with the dark phase Al_2O_3 as the TiAl phase migrated away under the effect of the extrusion pressure.

Distribution of the residual TiAl in the extrusion by-product (Figure 5.24 and Figure 5.25) indicates that the flow of the liquid TiAl out of the combustion synthesis composite product during extrusion is pressure and temperature dependent. Therefore, the separation of liquid TiAl from corundum during the solid/liquid separation process can be described by Darcy's law. Darcy's law states that the volumetric flow rate, Q, of a liquid through a porous medium is proportional to the pressure gradient Δp, inversely proportional to the thickness of the combustion product L and proportional to the cross sectional area A. In Equation (5-2), L corresponds to the axial distance measured from the top of the combustion product, η the fluid viscosity while P_1 and P_2 are the upstream and downstream pressures, respectively

$$Q = kA\frac{P_1^2 - P_2^2}{2\eta L P_2} \qquad (5\text{-}2)$$

where k is the Darcy permeability of the material (German, 2005). It is well established that combustion synthesis products are characterised by high porosity (Moore & Feng, 1995). Permeability depends on both the material and the fluid properties and is inversely proportional to the fluid viscosity. The capillarity in the corundum particles tends to draw liquid TiAl into the corundum particles to form a viscous slurry (Figure 5.23) (Leverett, 1941). According to the Einstein-Roscoe equations, the viscosity of a liquid containing solid suspensions increases as the volume percent of solids contained increases (Wright *et al.*, 2001). Back scattered electron images of the extrusion by-product show Al_2O_3 existing as large agglomerates and as fine disseminations less than 2µm in a TiAl matrix (Figure 5.21). The fine Al_2O_3 disseminations in TiAl lead to an increase in the viscosity and adversely affect drainage of TiAl during extrusion. The increase in viscosity decreases the permeability, fluidity and flow rate of the TiAl through the corundum particles.

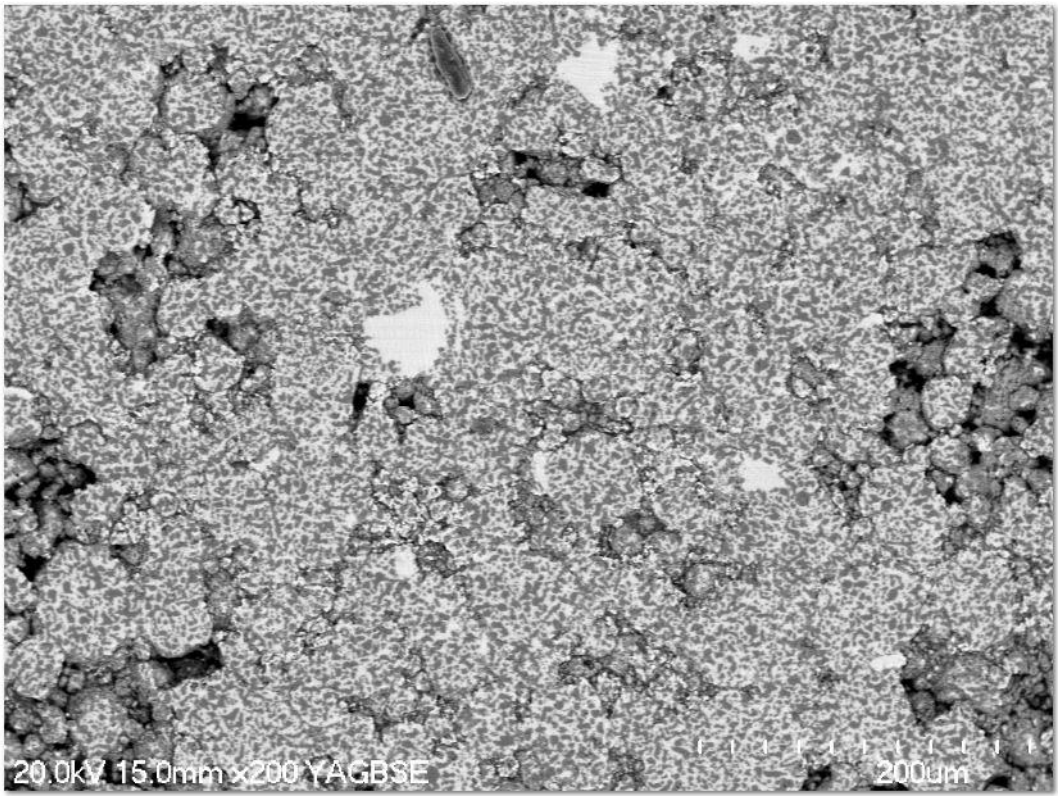

Figure 5.23: Formation of viscous slurry of fine Al_2O_3 particles (grey spots) in a white TiAl matrix of 1 h CS product (black spots are pores)

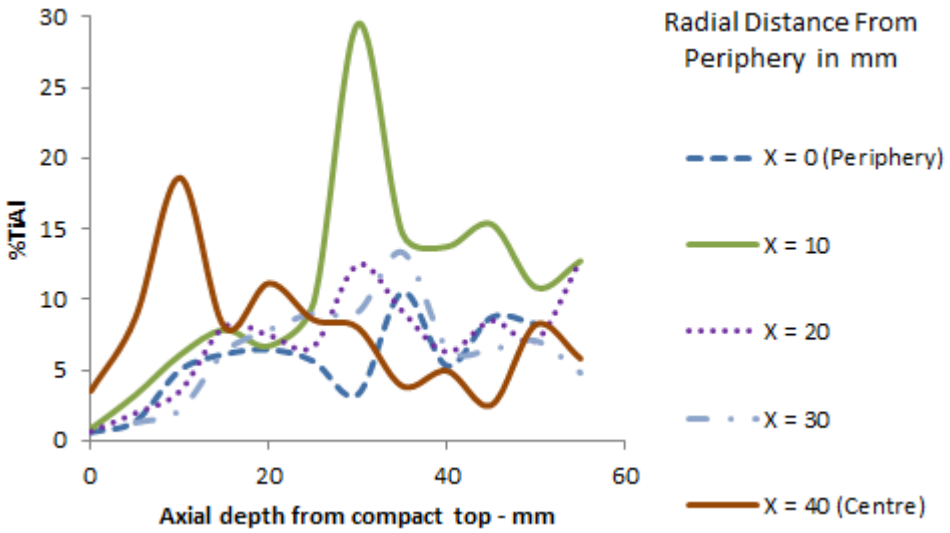

Figure 5.24: Spatial distribution (saturation level) of TiAl alloy phase with axial depth of the extrusion by-product (the axes are rotated 90º to the extrusion axis of Figure 5.25)

From Figure 5.24 it is apparent that except for the centre (x=40 mm), there is an increase in TiAl content from the top (the point of pressure application) to the

bottom of the compact. The liquid TiAl flow in the centre is more efficient due to less friction.

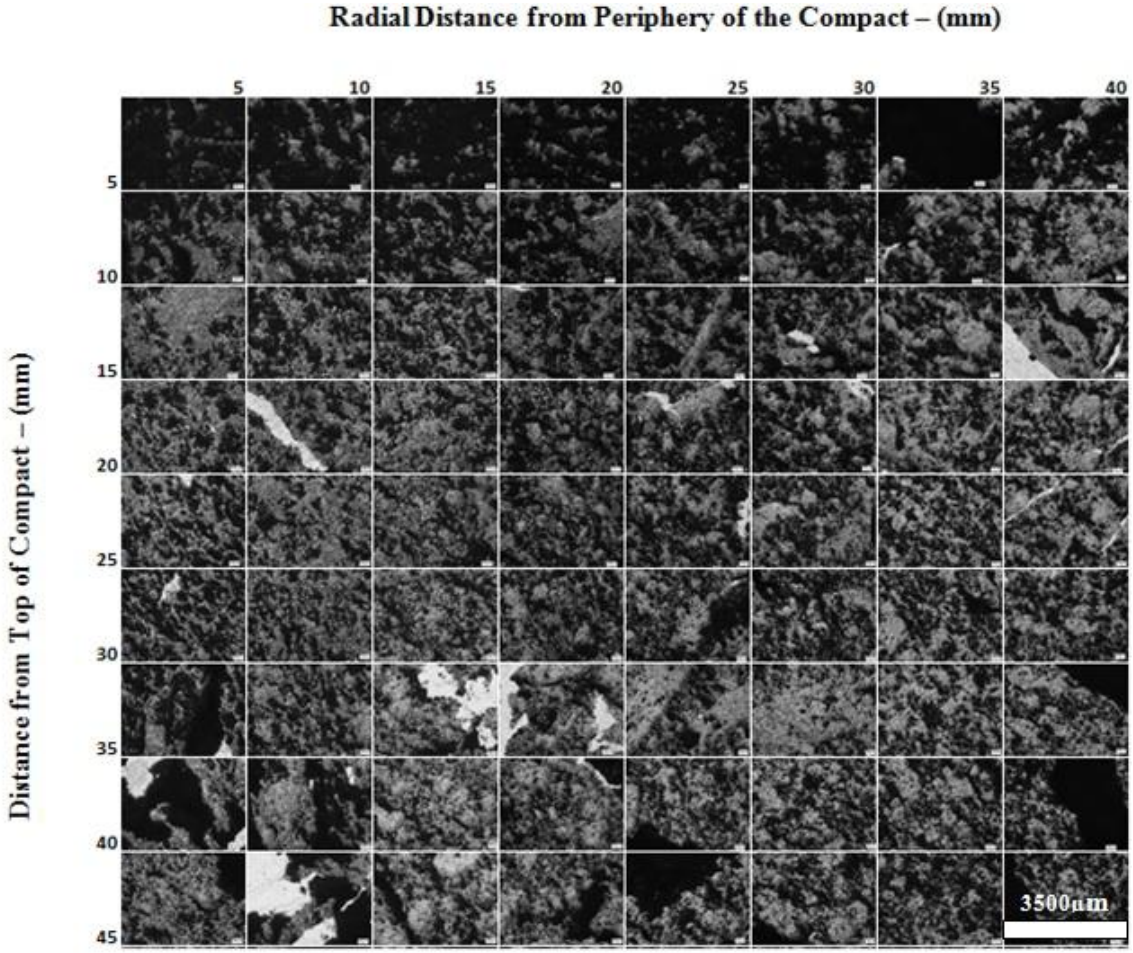

Figure 5.25: Spatial distribution of phases after extrusion. White = TiAl, Black = Al_2O_3 and Grey = TiAl (O)/Al_2O_3 composite

5.3.5 Effect of the Combustion Temperature

As stated earlier, the combustion temperatures attained with fine microstructured TiO_2/Al composite reactant powders (Figure 5.18 and Figure 5.19) were below 1460^{o}C, the melting point of TiAl, and therefore unfavourable for recovery of TiAl by extruding the combustion synthesis product. In contrast, when coarse microstructured reactant powders obtained by 1h high energy mechanical milling were reacted the combustion temperature was 1714^{o}C. However, due to the rapid cooling after combustion synthesis, there was still a significant quantity of residual TiAl in the extrusion by-product and the high combustion temperature attained rapidly fell from the peak temperature of 1714^{o}C to about 1200^{o}C (Figure 5.17). The peak temperature could not be maintained long enough to

facilitate solid/liquid separation. To study the effect of combustion temperature attained by the reaction products, extra heat was given from the induction coil to supplement the heat generated by the combustion reaction. This helped to heat the products and maintain the temperature of the products at 1788^{o}C for 43 min (Figure 5.26). However, despite holding the products above the melting point of TiAl, not much alloy was recovered as significant amounts of TiAl still remained solidified in the extrusion by-product. The flow of TiAl during extrusion is not solely determined by the combustion temperature but on other factors such as the liquid TiAl content attained before extruding the combustion synthesis product.

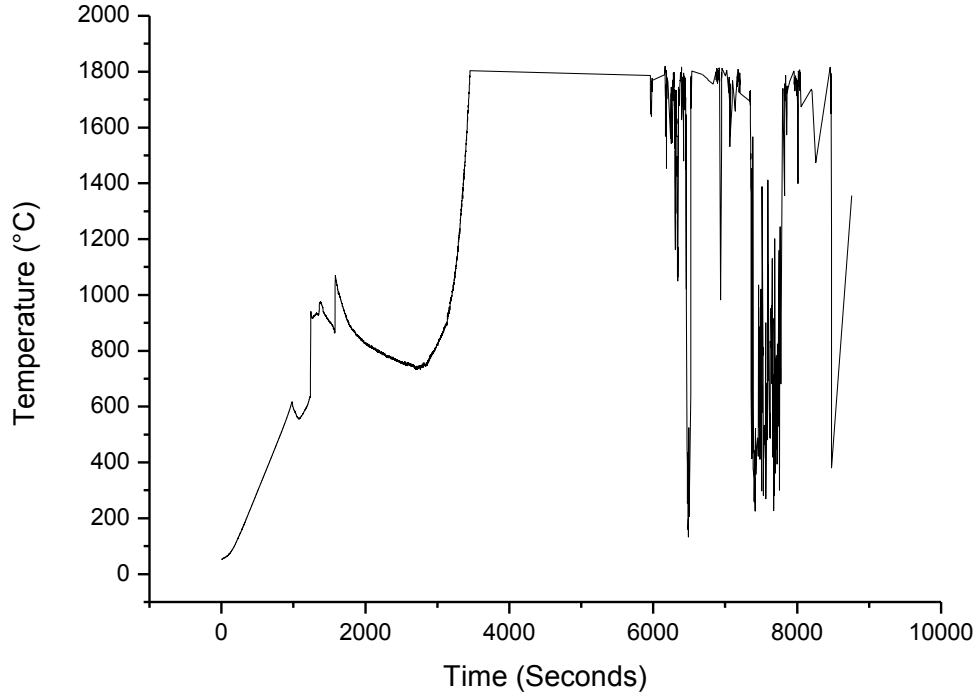

Figure 5.26: Combustion synthesis thermograph of TiO_2/Al powder mixture milled for 1 h (with 10% excess Al) and 41min holding at 1800^{o}C

5.3.6 Effect of the Reactants Preheating Rate

The results from the liquid/solid separation experiments, conducted with compacts made from the powders milled for 1 h, showed that the heating rate of the powder compact and holding the solid/liquid mixture at the maximum temperature for a period of time had a significant effect on the solid/liquid separation. It was observed that high heating rates led to the rapid vaporisation of volatiles, more cracking and porosity generation. The intrinsically generated porosity, in addition to the porosity carried over from the green compact porosity and volume changes

resulting from formation of products of higher molar density, compared to reactants, facilitated the outflow of the molten TiAl alloy phase (Long *et al.*, 1995; Moore & Feng, 1995; Rice & McDonough, 1985; Li, *et al.*, 2008). The generated porosity and cavities provided the network for melt flow during extrusion (Figure 5.29). The volume change resulting from the formation of TiAl and Al_2O_3 was about 17%. The formation of liquid TiAl contributed an additional source of porosity. When the heating rate was raised from 12.5^{o}C/min to 44.5^{o}C/min the combustion temperature attained rose from 1204^{o}C to 1788^{o}C and the alloy yield increased from zero to 9.7% (Table 5.2). At high preheating rates, the heat losses were offset without the temperature of the products rapidly plunging below the TiAl melting temperature. The residual porosity of the extrusion by-product of from the powders milled for 1 h was 31.3% compared to 6.8% for powders milled for 6 h.

Table 5.2: Effect of preheating rate on the yield of the alloy phase from TiO_2/Al powders milled for 1h

Sample No.	Preheating Rate (^{o}C/min)	Ignition Time (min)	Combustion Temperature (^{o}C)	TiAl Extrudate Yield (%)
1	44.5	40.8	1788	9.7
2	12.5	19.5	1704	0.0

The rate at which reactants are heated prior to combustion is critical to maintaining the alloy phase in liquid state and consequently affects alloy yields. According to Horvitz et al. (2002), at the low heating rate (Figure 5.28) no thermal explosion can take place, even if the reactants were heated above the ignition temperature, because of the partial transformation of the reactants into products during the slow heating, and the exposure of the sample to elevated temperatures (Horvitz, *et al.*, 2002). This reduces the exothermicity and the combustion temperature of the system.

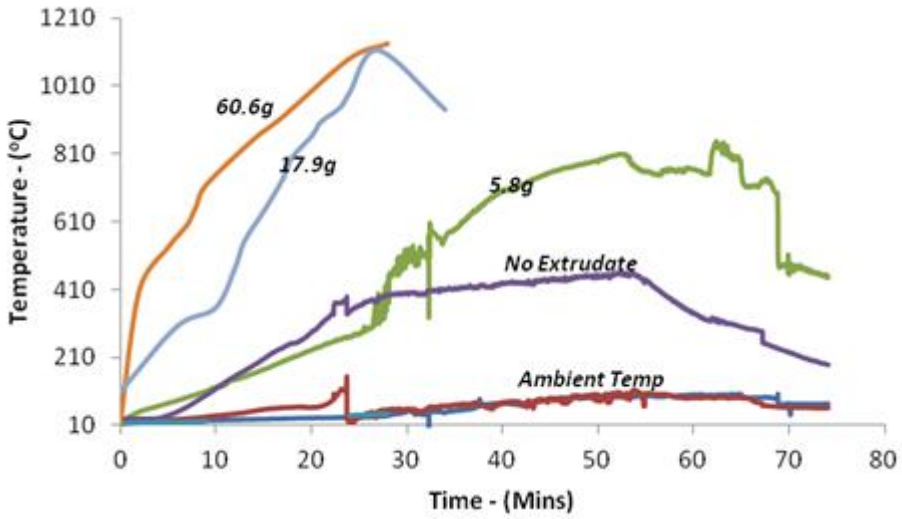

Figure 5.27: Effect of the rate of reactant preheating on the yield of TiAl alloy from powders milled for 1h

In this study there was complete transformation into TiAl and Al_2O_3 regardless of heating rate (Figure 5.11); however, the temperature attained by the alloy phase was lower causing it to solidify faster before extrusion (Figure 5.28).

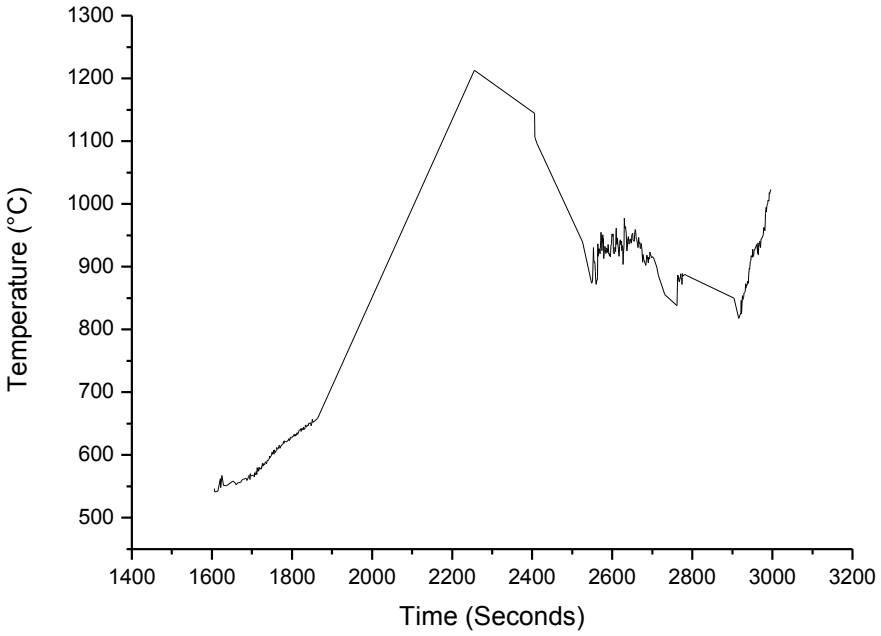

Figure 5.28: Combustion synthesis thermograph with a low (less than 10°C/min) preheating rate

Figure 5.29: Flow of the molten alloy phase (white phase) in the cracks in the combustion synthesis product during extrusion

For pressured liquid TiAl to migrate through and be separated from the solid Al_2O_3, the permeability of the combustion synthesis product has to be sufficiently high. The effect of gravity on separation is negligible because of the similarity in density of the two phases; therefore the liquid TiAl preferentially flows into cracks and pores regardless of spatial orientation (Long, *et al.*, 1995). This is evident from the orientation of the TiAl phase particles (Figure 5.29).

5.3.7 Solid/Liquid Separation Mechanism

Despite holding the products above the melting temperature of TiAl for 43 min, only a small fraction of the stoichiometric quantity of TiAl alloy expected was extracted by extruding the combustion product. This is due to the solid/liquid separation mechanism. The mechanism behind solid/liquid separation involves two capillary force driven processes; the growth of a continuous liquid TiAl phase by imbibition followed by drainage which is the flow of the alloy out of the combustion synthesis product. Products of combustion synthesis are characteristically porous. The porosity is passed on from reactants which are as-milled TiO_2/Al composites pressed into compacts with a green density of about 50

percent and not less than 70 percent in combustion products. Additionally, some porosity is generated by the vaporisation of volatiles during combustion. The pores are initially saturated with the gas phase. Therefore, after combustion, the gas phase in the pores forms an interface with the liquid TiAl and solid Al_2O_3. As the contact angle of liquid TiAl on Al_2O_3 (38^o), is less than 90^o, it tends to wet the solid Al_2O_3 and spontaneously flows in along the walls of the pores, displacing the non-wetting gas phase that initially saturates the pores by a capillary force driven process called imbibition (Bear, 1972; Bear, *et al.*, 2011; Li, *et al.*, 2008). The wetting process evolves through three stages of liquid TiAl saturation between 0 and 100%. At a very low liquid TiAl saturation (Figure 5.31), TiAl forms rings called pendular rings around Al_2O_3 particle contact points. At this low liquid TiAl saturation the rings are isolated and they do not form a continuous alloy phase, except for a thin molecular thickness film on the Al_2O_3 surfaces. No pressure can be transmitted from one ring to another within the liquid TiAl alloy phase. However, the intervening TiAl film on the alumina surfaces creates conditions similar to liquid-phase sintering, that reduce the inter-particle friction and facilitate the rearrangement of Al_2O_3 particles under the driving force of the compressive capillary stress of the liquid and the applied extrusion force. Rapid Al_2O_3 particle arrangement continues as long as the viscosity of the system remains low (Rahaman, 2003). The liquid TiAl saturation increases by imbibition and by the rearrangement of Al_2O_3 particles into agglomerates. According to Moore and Feng (1995), when particles are in contact with a wetting fluid an attractive force is generated that pulls particles together into denser agglomerates (Figure 5.30).

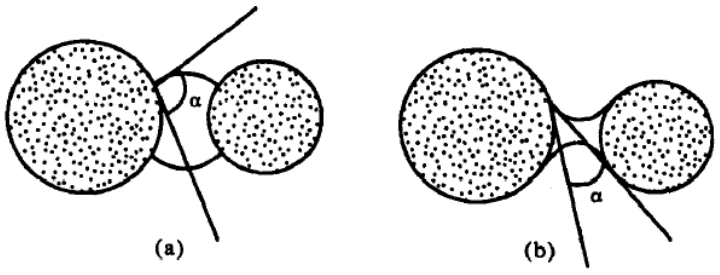

Figure 5.30: Effect of wettability on the force between particles (a) non-wetting, repulsive force; (b) wetting attractive, attractive repulsive force; α is the contact angle (Moore & Feng, 1995)

As the TiAl phase saturation increases, the pendular rings expand until a continuous TiAl alloy phase is formed at a critical saturation referred to as

equilibrium saturation to the liquid TiAl phase. It is only above the critical saturation, called funicular, that the liquid TiAl is able to flow. With a further increase in the saturation of liquid TiAl, the non-wetting fluid (i.e. gas phase) is no longer a continuous phase; it breaks into individual bubbles lodged in the larger pores that can only move by exerting sufficient pressure on the liquid TiAl. The resulting state, referred to as the insular state of the non-wetting (gas) phase, may probably be the source of high dissolved oxygen content in TiAl alloy phase (Bear, 1972).

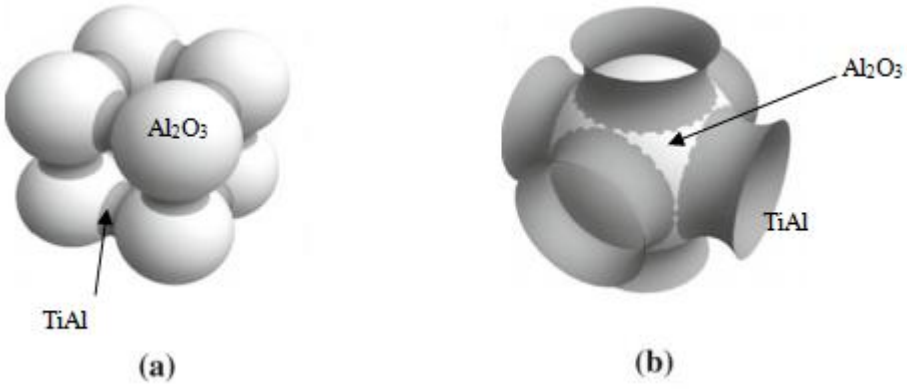

Figure 5.31: Al_2O_3 particles with TiAl pendular rings (a) isolated from each other (b) touching each other (Bear, et al., 2011)

According to Bang-sheng et al. (Li, *et al.*, 2008) the oxygen from the wetted Al_2O_3 combines with Ti from molten TiAl to form TiO on the surface of Al_2O_{3-x}.

Once liquid TiAl saturation is attained, a certain pressure must be achieved in the gas phase before the gas can begin to penetrate the combustion synthesis product, displacing the liquid TiAl contained in it and consequently allowing drainage of the alloy phase. The capillary pressure that must be built up at the TiAl-gas phase interface before drainage of the liquid TiAl starts is referred to as threshold pressure or bubbling pressure (Bear, 1972). As the liquid TiAl saturation is reduced, the channels of the liquid TiAl break down and become discontinuous throughout the CS product. Therefore the liquid TiAl is unable to flow and extraction of TiAl is limited by this mechanism. This threshold is attained faster in combustion products of powders milled for 6 h than in their 1 h counterparts and is illustrated by the absence of discrete TiAl grains in Figure 5.34.

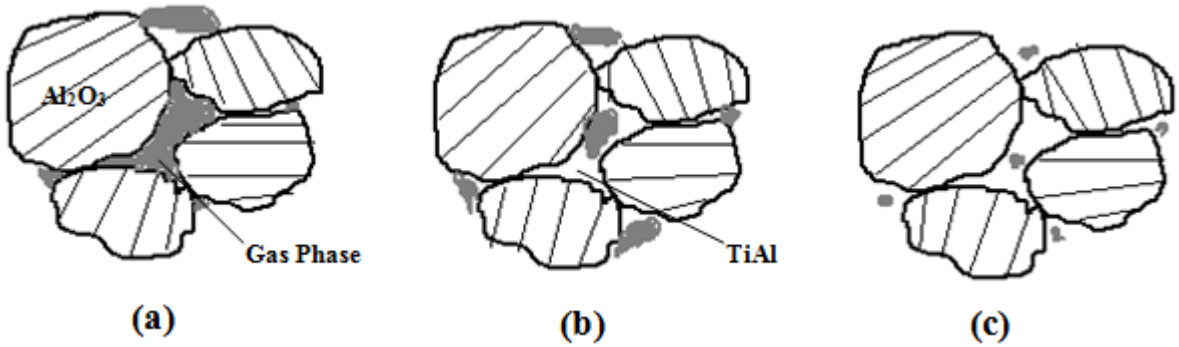

Figure 5.32: Fluid content states of TiAl wetted Al_2O_3 particles (a) at very low TiAl saturation, (b) at increased TiAl content and (c) above equilibrium content of TiAl where TiAl flow starts and some gas is entrapped

In contrast, combustion products of powders milled for 1 h (Figure 5.33) exhibit discrete TiAl grains, an indication of better liquid TiAl flow conditions resulting from the higher combustion temperature and porosity attained (Table 4.2 and Table 5.3).

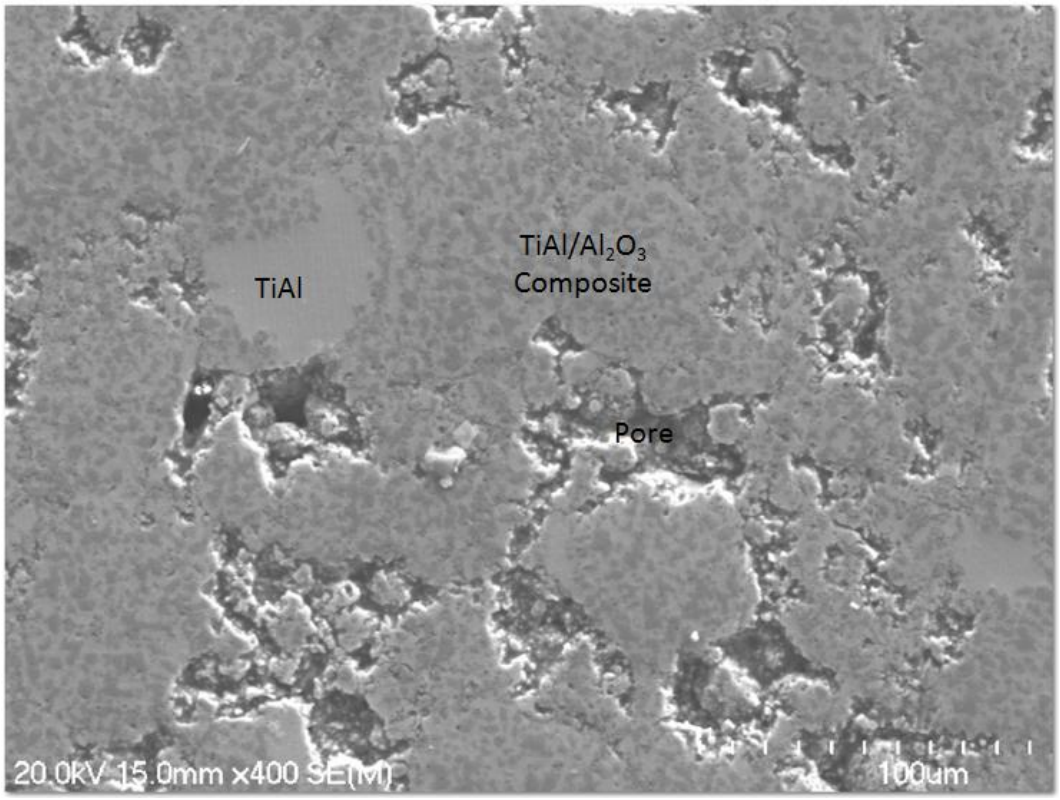

Figure 5.33: Combustion product of powders milled for 1 h showing alloy discreet alloy particles, $TiAl/Al_2O_3$ composite areas and pores

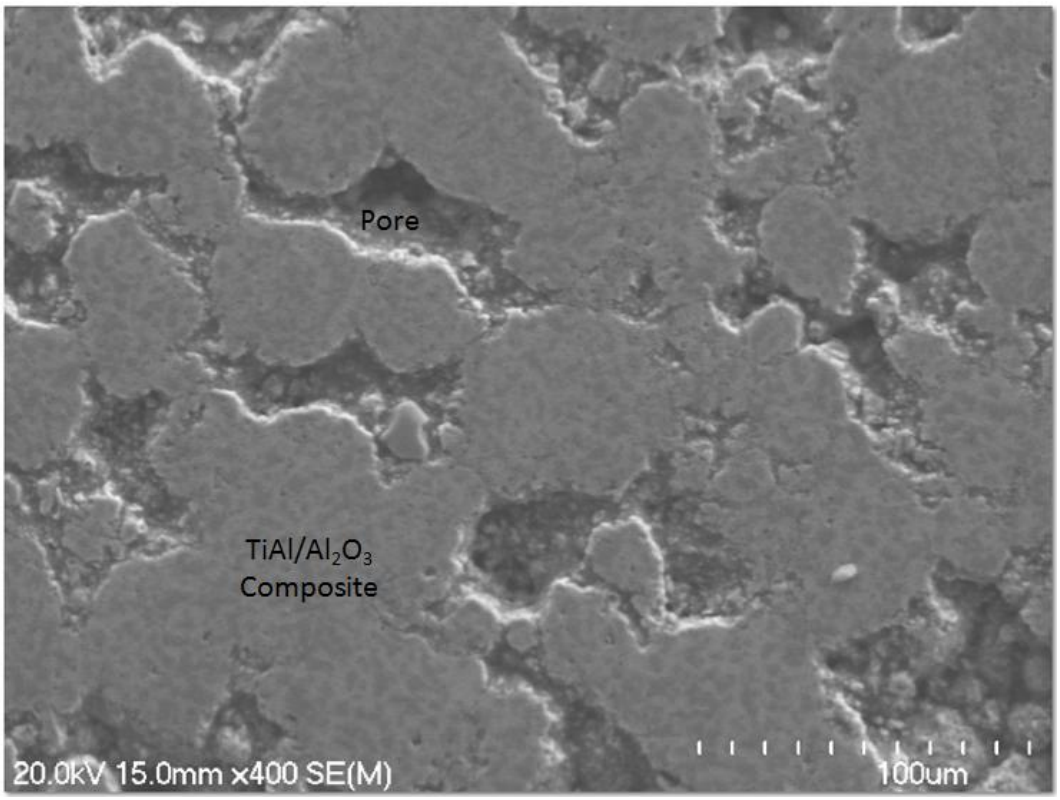

Figure 5.34: Combustion product of powders milled for 6 h showing $TiAl/Al_2O_3$ composite areas and pores but no discreet alloy particles

Table 5.3: Effect of milling time on the (a) particle size distribution and porosity of reactants (b) porosity of products

Milling Time (h)	As-Milled Powder PSD - d_{90} (µm)	Porosity (%)	
		Green Compact	CS Product
0	53	-	-
1	474	42.1	31.3
2	742	39.7	19.0
4	644	35.7	5.3
6	207	37.6	6.8

Figure 5.15 shows that the solid/liquid separation involves a liquid-phase sintering type mechanism in which Al_2O_3 particles rapidly agglomerate. Figure 5.35 shows that the agglomeration increases with milling intensity. As indicated by the connectivity of Al_2O_3 particles, the intensity of agglomeration in products of reactants milled for 6 h was evidently higher than those produced from powders milled for 1 h. This was probably due to more intimate mixing and shorter inter-particle distances in 6 h products.

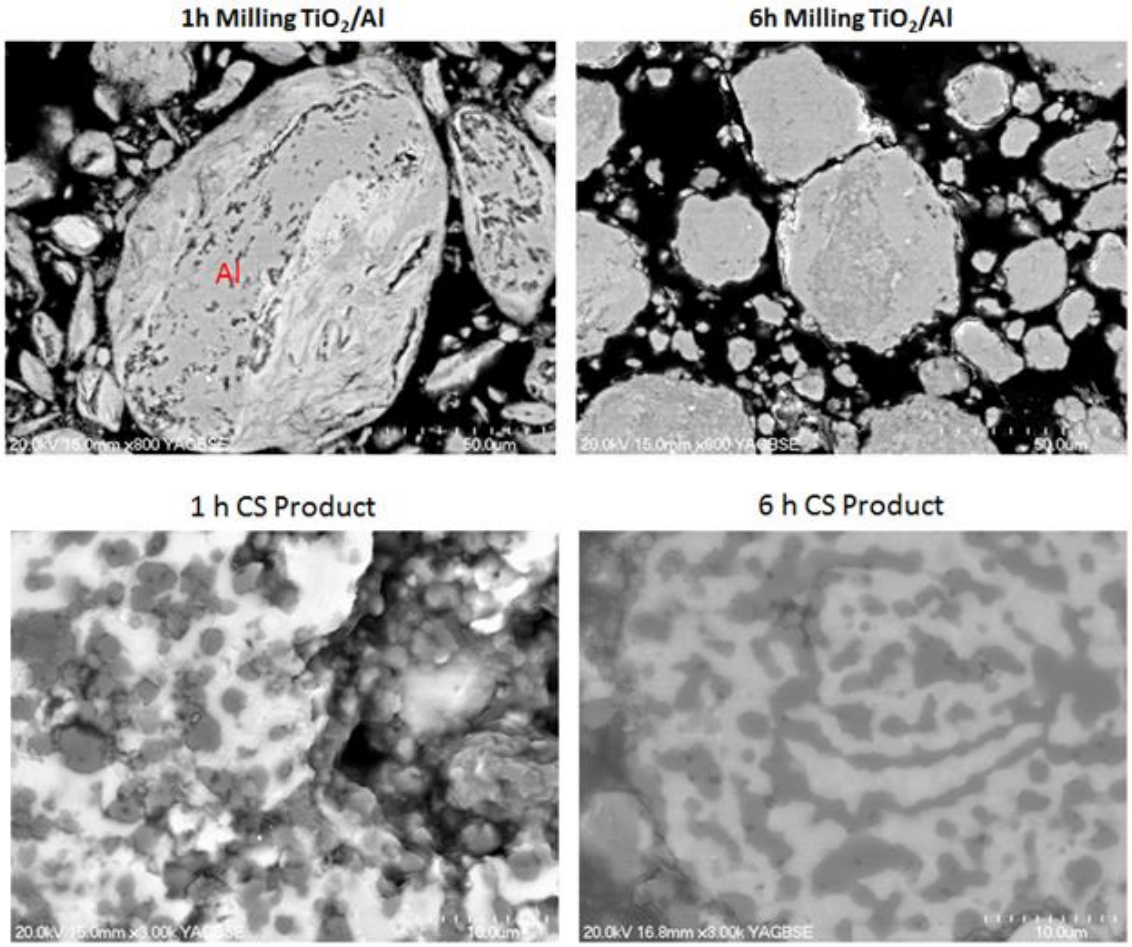

Figure 5.35: Correlation between microstructures of as-milled TiO_2/Al powders with the TiAl-Al_2O_3 particles intergrowth in the combustion product. More intense agglomeration in the 6 h product

5.4 Conclusion

X-ray diffraction (XRD) analysis (Figure 5.11) revealed that irrespective of the microstructure of reactants, the final combustion products were TiAl and α-Al_2O_3 (corundum) a high temperature polymorph of alumina; indicating that the combustion synthesis reaction went to completion. This was also confirmed by EDS (Table 5.1) and thermodynamic considerations. The combustion temperature of about 700^oC, attained with powders milled for 4 h (Figure 5.18) and 6 h (Figure 5.19), is significantly lower when compared with 1700^oC and above for powders milled for 1 h (Figure 5.17). This had an adverse effect on solid/liquid separation and alloy yields. The alloy phase could not be extruded out of the combustion synthesis TiAl(O)/Al_2O_3 product.

In contrast, powders milled for 1h produced a coarser microstructure of the two phases and upon extruding the combustion synthesis product, some liquid TiAl was recovered. However, the TiAl yield was low. Characterising the extrusion by-product by optical and scanning electron microscopy, and also confirming the characterisation with EDS and XRD analyses, indicated that significant quantities of residual TiAl were still present in the extrusion by-product (Figure 5.29).

The flow of the alloy during solid/liquid separation is governed by Darcy's law. Therefore the permeability, weight and thickness of the compacts formed from the reactants have a significant effect on the pressure driven molten TiAl flow during solid/liquid separation by extrusion. Table 5.3 shows that powders milled for 1h produced a combustion product with higher permeability (31.3% porosity), and these were therefore the most suitable for solid/liquid separation, compared to more intensely milled powders (6.8% porosity). The temperature attained by the combustion synthesis products and the level of extrusion pressure applied have a significant effect on solid/liquid separation and the yield of Ti-Al alloys produced by the TiPro process. The combustion temperature is a function of interdependent factors, such as the rate of preheating the reactants and the milling time. It was possible to attain temperatures above 1700^oC with the microstructure developed by milling TiO_2/Al powder mixtures for 1 h. However, it is apparent that in addition to maintaining the TiAl phase temperature above the melting point of TiAl (1460^oC) and exerting adequate extrusion pressure during extrusion, the level of TiAl saturation and the wetting properties of TiAl on Al_2O_3 particles are critical to increasing the alloy yields during solid/liquid separation. The

combustion synthesis product had some isolated TiAl-saturated (almost pure TiAl) particles of various sizes; however the average TiAl content was only 15% TiAl. At such a low TiAl saturation, the liquid TiAl is held by extremely high capillary forces in the combustion synthesis product, resulting in poor liquid TiAl outflow or drainage during extrusion. Therefore to increase TiAl yields other supplementary separation techniques, such as froth flotation and leaching must be used, together with extrusion to recover the residual TiAl contained in the extrusion by-product.

Oxide Dispersion Strengthened Materials (ODS) Application

The stable viscous slurry illustrated by Figure 5.23 can be used to produce oxide dispersion strengthened (ODS) titanium-based materials. Oxide dispersion strengthened materials contain a matrix in which an oxide is finely dispersed. By incorporating hard phases (Al_2O_3, TiC, TiN and NbC) into the matrix which might be for example titanium, iron or any other structural material, desirable properties such as high-wear-resistance can be imparted to the material. In mechanically alloyed dispersion-strengthened aluminium alloys it has been observed that since an aluminium oxide layer is always present either on the surface of the powder particles before processing or after milling, its incorporation into the alloy during solidification enhances the mechanical properties of the alloy significantly. Also, like in the TiPro process to minimise cold welding when milling aluminium (a ductile metal), process control agents (PCAs) which are usually hydrocarbons are added. During milling, Al_2O_3 and Al_4C_3 are formed due to the reaction of Al with PCA decomposition products oxygen and carbon. The oxide- or carbide–type dispersions about 30 to 50 nm in size stabilise the ultrafine grain size. This results in a 50% increase in strength, higher fracture toughness, and improved resistance to stress corrosion cracking and fatigue crack growth in mechanically alloyed materials (Suryanarayana, 2004). In this study, combustion products of TiO_2/Al powders milled for extended periods (2 h, 4 h and 6 h) might be more suited as starting feedstock for oxide dispersion strengthened materials because of their increased homogeneity (Table 4.1, Figure 5.20 and Figure 4.5 to Figure 4.8).

5.5 Summary

The solid/liquid separation stage in the TiPro process is critical because it determines the primary TiAl yield, purity and cost. Therefore the TiPro process

design criteria are based on optimizing the solid/liquid separation. In preparing reactant powders, by high energy mechanical milling, the high kinetics have to be balanced with the objective of achieving a high combustion temperature to extrude liquid TiAl out of the combustion synthesis product.

The combustion temperature attained with compacts of powders milled for 6 h was too low (700^{o}C) to facilitate the solid/liquid separation mechanism. The microstructure of the product consisted of a dispersion of submicron solid Al_2O_3 particles in a TiAl matrix, (Figure 5.21(b)). It also exhibited a closed porosity as indicated by low porosity (about 6.8%) determined with a pycnometer. In contrast, the combustion of powders milled for 1h (31.3% pycnometric porosity) resulted in a product with a coarse microstructure and high permeability or interconneted porosity that facilitated alloy out-flow during extrusion. However, despite high combustion temperatures and permeability, the TiAl yield by extrusion was only slightly above 10%. The low yield has been attributed to the wetting properties of liquid TiAl on Al_2O_3 particles and the low TiAl saturation of the combustion synthesis product during extrusion. Other researchers that have studied similar systems in which a liquid co-exists with solid particles while heating have come up with the Classic Liquid-phase sintering model and the Pore filling model both of which demonstrate that the conditions prevalent during solid/liquid separation only lead to densification and not separation of the phases (Kang, 2005). This is borne out by previuos workers on this project that reported a yield of only 4% (Raynova, 2007).

The flow of liquid TiAl during solid/liquid separation can be treated on the basis of a two-fluid flow involving liquid TiAl and a gas phase (air and combustion volatiles) in a porous medium of Al_2O_3 particles. In such a system, the level of liquid TiAl saturation attained in the combustion product has to exceed a critical value. Once the combustion product is sufficiently saturated with liquid-TiAl, the pressure of the gas phase increases to what is referred to as threshold pressure or bubbling pressure (Bear, 1972). At that pressure, the gas begins to penetrate the combustion synthesis product displacing the liquid TiAl contained in it and consequently allowing drainage of the alloy phase. As the liquid TiAl content is reduced, the channels of the liquid TiAl break down and become discontinuous throughout the CS product. Therefore the liquid TiAl is unable to flow and extraction of TiAl is limited by this mechanism.

When the TiAl content level is low, liquid TiAl is held by extremely high capillary forces in the combustion synthesis product. Also according to Darcy's law, an increase in viscosity of liquid TiAl due to the presence of submicron Al_2O_3 particles could cause poor outflow or drainage of liquid TiAl during extrusion. Therefore to increase TiAl yields, other supplementary separation techniques, such as froth flotation and leaching, must be used together extrusion to recover the residual TiAl contained in the extrusion by-product. Extracting TiAl by solid/liquid separation by extrusion on its own is not viable however; the process might find application to produce oxide dispersion strengthened (ODS) materials.

A more effective alternative of extracting TiAl from the combustion product than solid/liquid separation by extrusion would probably be using cryolite to dissolve away Al_2O_3. The cryolite – alumina system is well-established in aluminium smelting practice due to the high solubility of Al_2O_3 in cryolite. Cryolite ionises into hexafluoroaluminate (AlF_6^{3-}) which dissociates further into tetrafluoroaluminate (AlF_4^-), sodium (Na^+) and fluoride (F^-) ions as follows:

$$Na_3AlF_6 - 3Na^+ + AlF_6^{3-}$$

$$AlF_6^{3-} \leftarrow\rightarrow AlF_4^- + 2F^{2-}$$

At low concentrations, Al_2O_3 dissolves by forming oxyfluoride ions ($Al_2OF_{2n}^{4-2n}$) with an Al: O ratio of 2:1.

At higher concentrations, Al_2O_3 dissolves by forming oxyfluoride ions ($AlOF_n^{1-n}$) with an Al: O ratio of 1:1.

$$Al_2O_3 + 4AlF_6^{3-} - 3Al_2OF_6^{2-} + 6F^-$$

$$Al_2O_3 + AlF_6^{3-} - 3AlOF_2^-$$

In aluminium smelting cell practice the Al_2O_3 concentration is maintained between 2 and 6 wt%. The saturation varies between 7 and 12 wt% depending on composition and temperature. By adding 5-7% CaF_2, 5-7% AlF_3 and 0-7% LiF the smelting temperature is reduced to 940-980^{o}C (Staley, 1991-1998). It is evident from Figure 5.36 that the liquidus temperatures in the system are much lower than in the solid/liquid separation of the TiPro process.

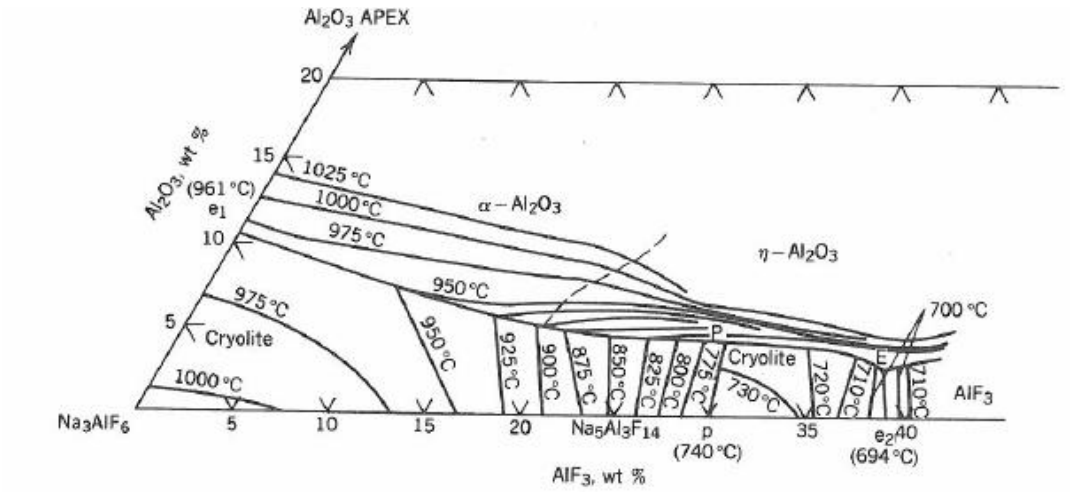

Figure 5.36: Ternary diagram of the Na_3AlF_6-AlF_3-Al_2O_3 system (Staley, 1991-1998, p. 193)

5.6 References

Bear, J. (1972). *Dynamics of Fluids in Porous Media* Environmental science series (New York, 1972-). New York: Elsevier.

Bear, J., Rubinstein, B., & Fel, L. (2011). Capillary pressure curve for liquid menisci in a cubic assembly of spherical particles below irreducible saturation. *Transport in Porous Media, 89*(1), 63-73.

Fecht, H. J. (1995). Nanostructure formation by mechanical attrition. *Nanostructured Materials, 6*(1-4), 33-42.

German, R. M. (2005). *Powder metallurgy & particulate materials processing*. Princeton, New Jersey: Metal Powder Industries Federation.

Horvitz, D., Gotman, I., Gutmanas, E. Y., & Claussen, N. (2002). In situ processing of dense Al_2O_3-Ti aluminide interpenetrating phase composites. *Journal of the European Ceramic Society, 22*(6), 947-954.

Lappalainen, K., Manninen, M., Alopaeus, V., Aittamaa, J., & Dodds, J. (2009). An analytical model for capillary pressure - Saturation relation for gas-liquid system in a packed-bed of spherical particles. *Transport in Porous Media, 77*(1), 17-40.

Leverett, M. C. (1941). Capillary behavior in porous solids. *Transactions of the AIME, 142*(1), 152-169.

Li, B. S., Liu, A. H., Nan, H., Bi, W. S., Guo, J. J., & Fu, H. Z. (2008). Wettability of TiAl alloy melt on ceramic moulds in electromagnetic field. *Transactions of Nonferrous Metals Society of China, 18*(3), 518-522.

Long, S., Zhang, Z., & Flower, H. M. (1995). Characterization of liquid metal infiltration of a chopped fibre preform aided by external pressure—II. Modelling of liquid metal infiltration process. *Acta Metallurgica et Materialia, 43*(9), 3499-3509.

Kang, S.-J. L. (2005). Sintering: Densification, Grain Growth & Microstructure Amsterdam ;Boston ;London: Elsevier Butterworth-Heinemann,.

Moore, J. J., & Feng, H. J. (1995). Combustion synthesis of advanced materials: Part I. Reaction parameters. *Progress in Materials Science, 39*(4–5), 243-273.

Rahaman, M. N. (2003). *Ceramic Processing and Sintering* (2nd ed.). New York: Marcel Dekker.

Rice, R. W., & McDonough, W. J. (1985). Intrinsic volume changes of self-propagating synthesis. *Journal of the American Ceramic Society, 68*(5), C122-C123.

Smith, W. O. (1933). The final distribution of retained liquid in an ideal uniform soil. *Journal of Applied Physics, 4*(12), 425-438.

Welham, N. J. (1998). Mechanical activation of the solid-state reaction between Al and TiO_2. *Materials Science and Engineering A, 255*(1-2), 81-89.

Wright, S., Zhang, L., Sun, S., & Jahanshahi, S. (2001). Viscosities of calcium ferrite slags and calcium alumino-silicate slags containing spinel particles. *Journal of Non-Crystalline Solids, 282*(1), 15-23.

Ying, D. Y., Zhang, D. L., & Newby, M. (2004). Solid-state reactions during heating mechanically milled TiO_2/Al composite powders. *Metallurgical and Materials Transactions A, 35*(7), 2115-2125.

Zhang, D. L. (2004). Processing of advanced materials using high-energy mechanical milling. *Progress in Materials Science, 49*(3-4), 537-560.

Chapter 6

Froth Flotation

6.1 Introduction

The results in the previous chapter demonstrated that the TiAl yields obtained by solid/liquid separation were low and uneconomical. For that reason froth flotation was considered and evaluated as an alternative method for recovering the alloy. Froth flotation is a separation process that utilises differences in wettability of mineral particles suspended in water. The differences in wettability of minerals can be inherent or imparted by use of surface active reagents which are usually hydrocarbon compounds (Yarar, 2000). Separation is achieved by selectively attaching the desired mineral to gas bubbles to provide levitation. Flotation is the cheapest and most versatile mineral processing technique applied in the separation of minerals with similar physical and chemical properties (Crozier, 1992; Wills, 2006). The objective of this study was to evaluate the efficacy of flotation in concentrating the TiAl content by separating corundum from the residual alloy contained in the extrusion by-product. The desired product would be a TiAl-rich fraction that could be processed to recover TiAl with less reductant at the alloy purification or oxygen removal stage. The option of separating corundum from the alloy phase by flotation is attractive because flotation is a proven cost effective mineral processing technology with minimal associated technology risk. Also, the alloy phase does not undergo a chemical change during flotation. A detailed description of froth flotation is given in Section 2.4.4 of Chapter 2 (Literature Review).

6.2 Experimental

6.2.1 Sample Preparation

To study the phase size and association, the texture of the extrusion by-product was preserved by crushing in stages. The first crushing stage was done to a relatively coarse size of about 80 per cent passing 1.18 mm using a 500 mm x 250 mm TIDCO Swing Jaw crusher. The jaw crusher product was subsequently crushed to less than 280 microns to achieve good liberation of TiAl and corundum rich phases using a BICO Pulveriser (BICO, Burbank, California). The various

size fractions that were produced were studied by optical microscopy to establish the liberation size of the TiAl and corundum phase particles.

6.2.2 Flotation Testing

Froth flotation testing was done to recover the residual alloy from the extrusion by-product. The option of separating the corundum from the alloy phase by flotation is attractive because of the associated lower technology risk given that flotation is a proven mineral processing technology and also the alloy phase does not undergo a chemical change (Yarar, 2000). In this study the flotation scheme used is referred to as reverse flotation because corundum, the less valuable mineral, was transferred to the float fraction while the desired product, TiAl, was left in the tailing.

The flotation tests were carried out using in-house apparatus consisting of a sub-aeration assembly, a 3500 ml Perspex cell and an agitator with a 70 mm diameter impeller. The flotation testing was done in two stages comprising the initial stage referred to as rougher stage and the cleaner stage. The objective at the rougher stage was to maximise the removal of Al_2O_3 into the float section. The resultant tails were subsequently floated to remove as more residual Al_2O_3 at the cleaner flotation stage. A 100 gram sample of the extrusion by-product was gradually transferred to the flotation cell containing about 2500 ml of water, with the impeller rotating at 1000 rpm and the air inlet shut. Mixing was continued for 3 min while slowly adding more water and increasing the impeller speed to 1500 rpm. Agitation was continued for a further 3 min in order to ensure thorough wetting of the sample. The appropriate modifying reagents (activator or depressant) were added and agitation continued for 5 min without air. Additions of collector and frother were made and agitation continued for a further 5 min. Air was turned on and adjusted to a predetermined flow rate using a rotameter. Every 15 sec, the scraper was gradually moved through the concentrate to collect a froth increment. The total froth produced over a 3-min period was collected as concentrate. At the end of 3 min, the impeller was stopped and all the particles adhering to the sides of the cell and the impeller housing were restored to the concentrate. The concentrate and tailings were de-watered and dried separately to constant mass and weighed.

Table 6.1: Flotation reagents suite and conditions

Reagent	Name	Dosage	g/MT
Reverse Flotation Acid pH 2.5-3.0 Media			
Corundum Collector	Sodium Dodecyl Sulphate	10^{-4}M	405
		10^{-5}M	40.5
Corundum Activator	Hydrofluoric Acid (HF)		500.0
Frother	Pine Oil		50.0

Conditions:

Pulp Density	8%
Conditioning Time	5 Min
Flotation Time	5 Min (Rougher)
	1.5 Min (Cleaner)
Impeller speed	1500 rpm
Air flow rate	3.0 – 6.0 litres/min
Air: Solids Ratio	41 (g/g basis)

Figure 6.1: Flotation experiment set-up

6.3 Results

6.3.1 Phase liberation analysis of flotation feed

Characterization of the extrusion by-product was done using optical microscopy (OM), XRD, SEM and EDS. These techniques indicated the presence of significant amounts of the TiAl alloy phase containing entrapped and finely disseminated primary and agglomerated corundum particles of about 1.5 microns and above in diameter (Figure 6.2). To selectively adsorb the collector at the corundum particle surface the two constituent phases have to be adequately liberated by controlled milling.

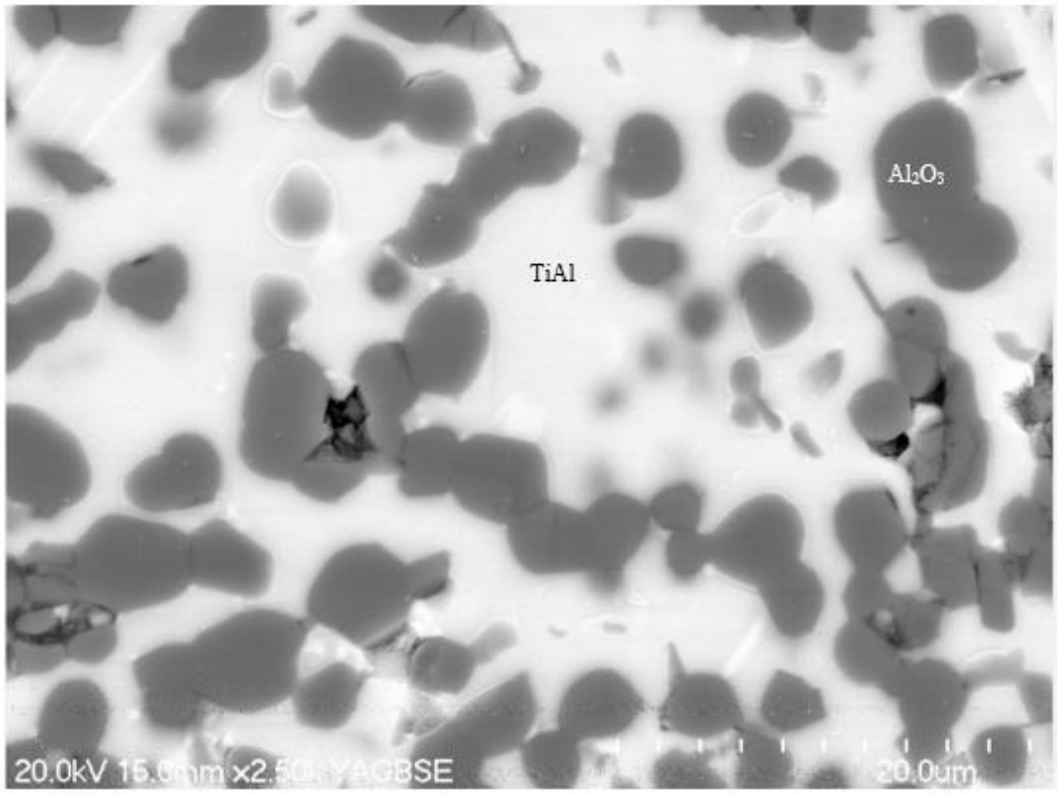

Figure 6.2: SEM Backscattered image of a cross-section of feed to flotation showing Al_2O_3 inclusions in TiAl

Liberation of the alloy phase particles was achieved by grinding the extrusion by-product to 106 – 75 μm (Figure 6.3). This particle size range is also favourable for the froth flotation process.

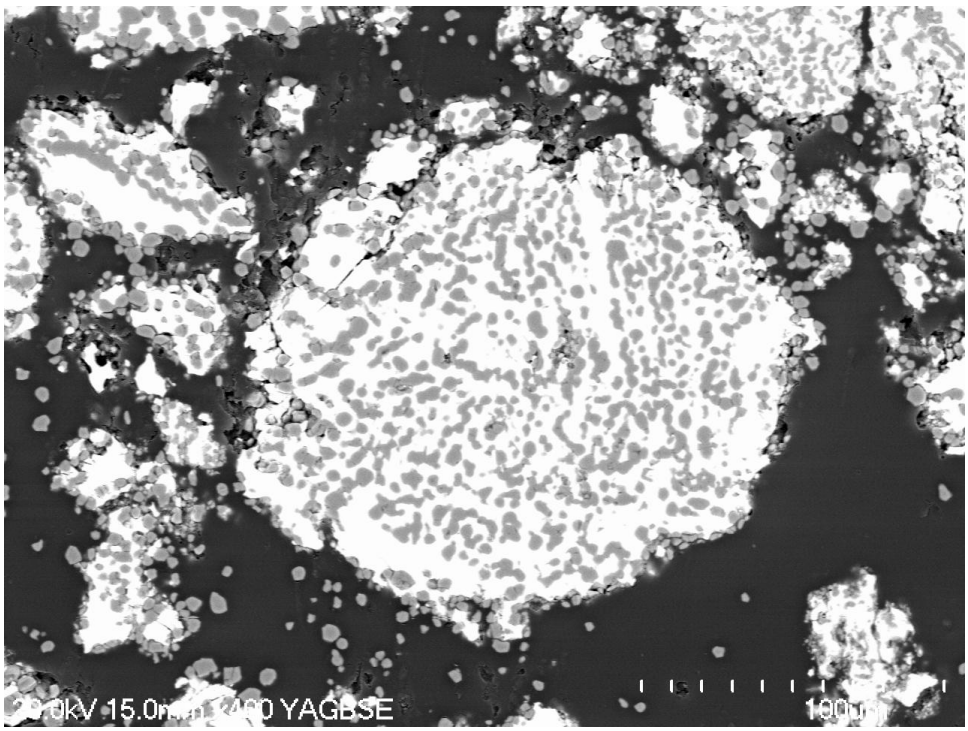

Figure 6.3: Back-scatter image illustrating the alloy phase liberation

The TiAl content of the milled extrusion by-product increased with decreasing particle size. This was caused by the preferential breakage of the softer TiAl alloy phase (Figure 6.4). The Bond work index (a parameter for expressing the resistance of a material to crushing) of corundum is 56.70kWh/ton (Wills, 2006) indicating that corundum is more resistant to crushing compared to TiAl. The TiAl enriched fines, generated by the differential grindability, were the first to report to the froth fraction (Figure 6.5). This trend may be used as a pre-flotation sorting stage to enhance the overall TiPro process efficiency.

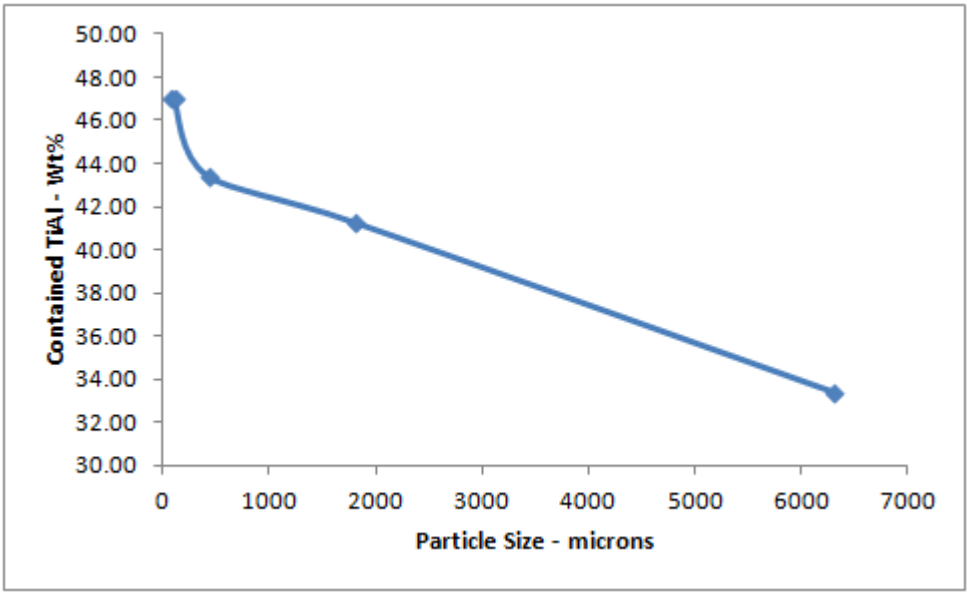

Figure 6.4: Effect of preferential breakage on TiAl content of size fractions

The TiAl content of slimes collected during the first 2 min. of desliming rose up to 59.5 wt% compared to 46.7 wt% for the feed head grade (Figure 6.5).

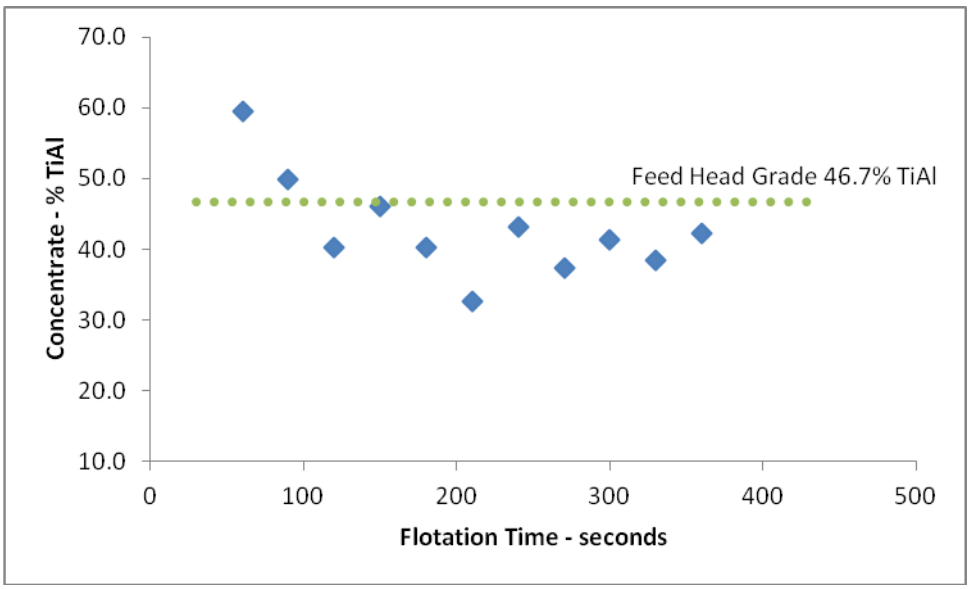

Figure 6.5: Pre-flotation desliming showing high grade slimes in the first 100 min

6.3.2 Effect of pH on Selectivity of Flotation

Based on the point of zero charge (PZC) for TiAl that was determined from zeta potential measurements and the PZC of Al_2O_3 obtained from literature (Modi & Fuerstenau, 1960), the optimum window for selectively floating Al_2O_3 using an anionic collector such as sodium dodecyl sulphate, is around pH 4; between the point of zero charge (PZC) for TiAl and Al_2O_3 (Figure 6.6).

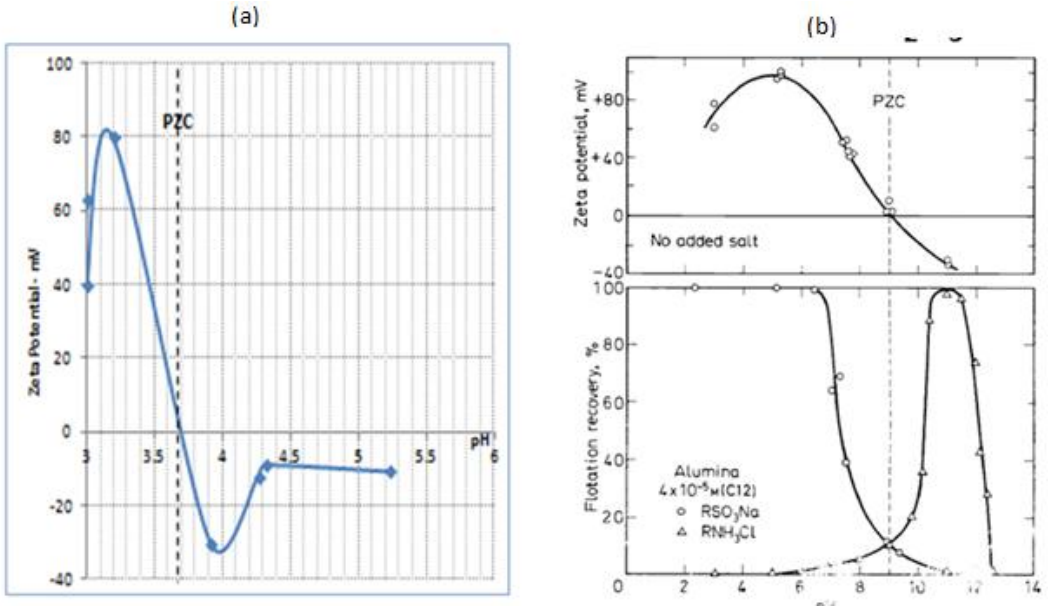

Figure 6.6: Point of zero charge (PZC) of (a) TiAl at pH 3.7 determined in this study and (b) Al_2O_3, pH 9.1 derived from literature (Fuerstenau & Pradip, 2005)

At pH 4, the Al_2O_3 particles are positively charged therefore they attract the polar side of collector molecules. The collector molecules end up forming a thin film on the particles thereby making them hydrophobic hence floatable.

The separating efficiency of froth flotation is expressed by the enrichment ratio which is the ratio of the grade of the TiAl concentrate to the grade of the feed (Wills, 2006). It is evident from (Table 6.2) that the low enrichment ratio, at pH 10, was because above pH 3.7, (the PZC of TiAl), the collector molecules do not attach on to TiAl particles because the TiAl surface is negatively charged. Low enrichment ratios at pH 3.2 occurred because of poor selectivity as both Al_2O_3 and TiAl were floatable below pH 4.

Table 6.2: Effect of pulp pH and sodium dodecyl sulphate (Al_2O_3 collector) on separation during rougher flotation

pH = 10	Reagents - g/t				Enrichment
At Grind -212 to +106µm	SDS	H_2SO_4	Pine Oil	HF	Ratio
Head Grade					
Rougher Concentrate	405	-			1.4
Rougher Tail					1.4
pH = 4.2					
Head Grade					
Rougher Concentrate	40		50	40	0.6
Rougher Tail					1.8
pH = 3.2					
Rougher Concentrate	405				1.2
Rougher Tail					1.5
pH = 3.2					
Rougher Concentrate	40		50	40	1.5
Rougher Tail					1.5

6.3.3 Rougher Flotation Kinetics

During the first 2 min of rougher flotation, the TiAl content of the concentrate is high due to the high TiAl containing slimes generated by milling (Figure 6.7). Thereafter, there was a drop in TiAl content (or alternatively an increase in the Al_2O_3 concentrate grade) until the limiting Al_2O_3 recovery was attained. This occurred after 7 min.

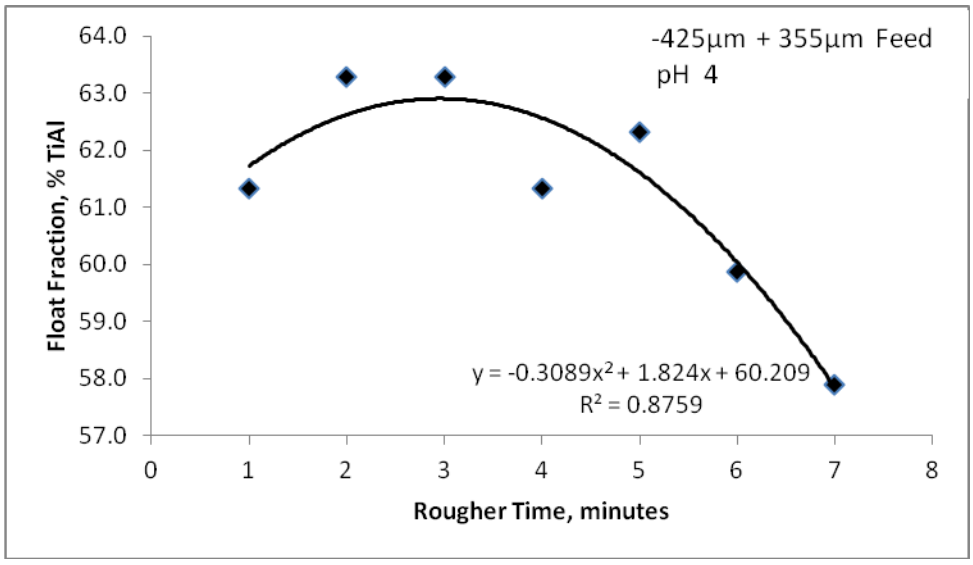

Figure 6.7: Rougher flotation kinetics

In Figure 6.7, this corresponds to the point where the incremental grade curve crossed the feed grade (44.7% Al_2O_3). Beyond this point no more Al_2O_3 can be recovered without regrinding the sample.

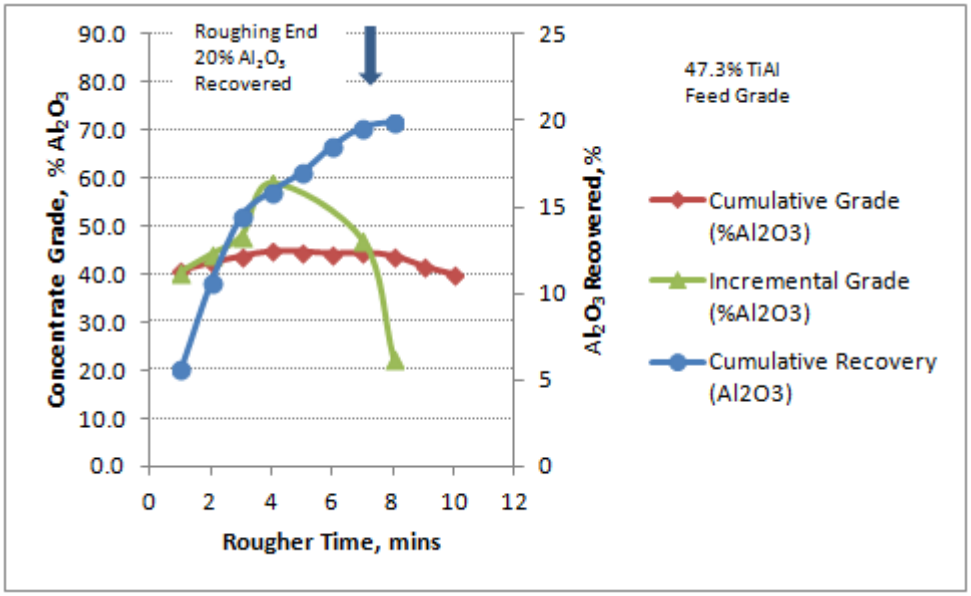

Figure 6.8: Rougher flotation kinetics for Al_2O_3 using incremental grade evaluation

The optimum rougher flotation residence time (when the recovery curve stops its steep increase and flattens) occurred after 7 min. At this point, 65.7% of the TiAl was recovered into a TiAl-rich fraction (tailings) containing 71.0 wt% TiAl. This represented a 20% removal of the total Al_2O_3 fed to the process (Figure 6.8).

Table 6.3: Rougher flotation mass balance

Input	Weight (g)	TiAl wt%	Fine TiAl (g)	Mass %Dist	TiAl %Dist
Feed	100	55.3	55.3	100	100
Products					
Concentrate	48.2	40.5	19.5	48.2	35.3
Tails	51.2	71.0	36.3	51.2	65.7
Unaccountable Gain/(Loss)	0.6		-0.6	0.6	-1.1
Total	100		55.3	100	100

6.3.4 Effect of Air to Solids Ratio

The mass distribution to the concentrate and tails fractions varied and there was a noticeable loss in separating efficiency and mass distribution to the Ti-rich (Tails)

fraction as the mass of Air: Solids Ratio was increased above 41 (Table 6.4). This was probably due to froth collapse caused by non-quiescent pulp-froth interface (Dunne *et al.*, 2002).The grade of the TiAl-rich fraction obtained with the -425 +355 μm particle size range was highest at the Air to Solids Ratios of 41.

Table 6.4: Effect of Air to Solids Ratio on mass distribution

Air: Solid Ratio (g/g)	Feed Particle Size (μm)	Material Distribution – (Wt %)			TiAl in Tails (Wt %)
		Concentrate	Tails	Accretions	
41.1	-425 +355	31.0	60.4	8.6	71.0
60.8	-425 +355	14.9	76.5	8.5	61.4
91.2	-425 +355	83.8	2.4	2.6	59.8
61.3	-355	88.8	3.4	7.8	64.2
45.6	-32	86.2	8.7	5.1	57.6

6.3.5 Cleaner Flotation

The mass balance of the cleaner flotation indicated significant unaccountable alloy losses (Table 6.5). The TiAl content of both cleaner flotation products was much lower than the 71.8 wt% TiAl, the grade of the cleaner flotation feed.

Table 6.5: Cleaner flotation mass balance

Input	Weight (g)	TiAl wt%	Fine TiAl (g)	Mass %Dist	TiAl %Dist
Feed	25.3	71.8	18.2	100.0	100.0
Products					
Concentrate	16.4	55.2	9.1	64.8	49.8
Tails	6.9	59.6	4.1	27.3	22.6
Unaccountable Gain/(Loss)	(2.0)		(5.0)	(7.9)	(27.5)
Total	23.3	56.5	13.2	100.0	100.0

The losses can be attributed to the dissolution of TiAl by HF acid which was used as the Al_2O_3 activator. This was confirmed by the XRD analysis of the solids obtained by boiling the filtered flotation liquor to dryness (Figure 6.9). The major constituents of the solids were TiO_2 and Al_2O_3.

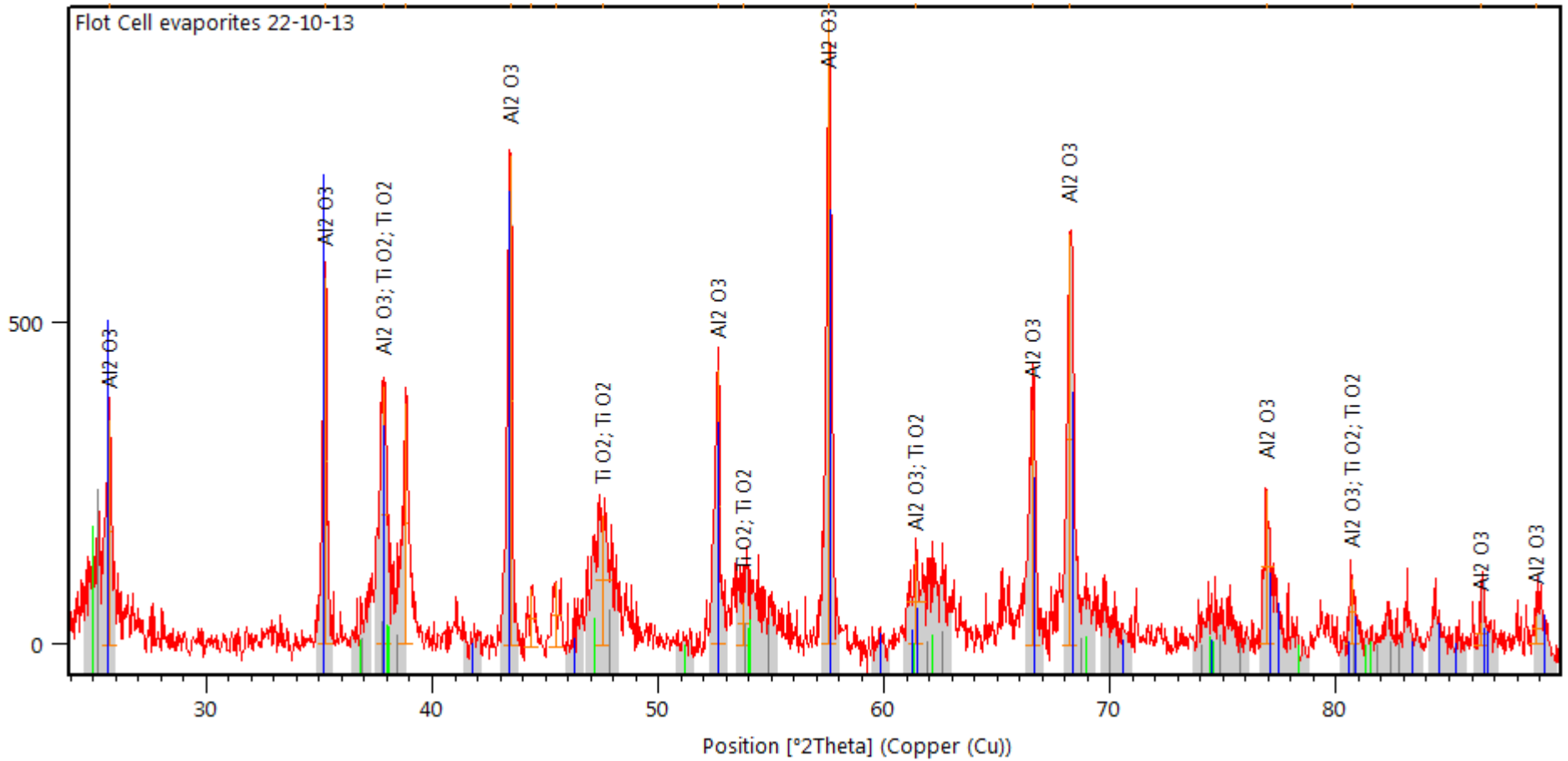

Figure 6.9: XRD analysis of solutes dissolved during flotation

6.3.6 Characterisation of Flotation Losses

Besides acid-soluble losses, TiAl losses were due to incomplete liberation and TiAl and Al_2O_3 remained intimately associated. Using SEM in BSE mode, images of the flotation products (Figure 6.10, Figure 6.11 and Figure 6.12) show fine dispersions of Al_2O_3 in a TiAl matrix, as described in the solid-liquid separation mechanism (Chapter 5). This is because the contact angle of TiAl (38^o) is low; TiAl is imbibed into Al_2O_3 particles.

The intimate association of the phases imposes a huge limitation on how efficiently the alloy phase can be recovered by physical methods only. To evaluate the separation efficiency at each set of flotation parameters, an index was calculated using the equation proposed by Schulz (Wills, 2006):

$$\text{Separation efficiency} = R_{TiAl}\text{-}R_{Al_2O_3} = 100C\, m_{Ti}\,(c_{Ti} - f_{Ti})/(m_{Ti} - f_{Ti})\, f_{Ti} \qquad (6\text{-}1)$$

where R_{TiAl} and $R_{Al_2O_3}$ are the recovery of TiAl and Al_2O_3 respectively, to the tails (i.e. theTiAl-rich concentrate), C is the total feed weight that reports to the TiAl-rich concentrate, f_{Ti} is the Ti content of the feed, c_{Ti} is the Ti assay of the TiAl-rich concentrate (i.e. the sample left in the cell at the end of the test) and m_{Ti} is the percentage Ti in this sample.

Table 6.6: Effect of flotation air and grind size of feed on the separation of TiAl from Al_2O_3 using sodium dodecyl sulphate as Al_2O_3 collector at pH 4.2

Feed Grind (µm)	Superficial Air Velocity (cm sec^{-1})	Separation Efficiency (%)
-425 to + 355	0.5	44.3
-425 to + 355	0.9	0.5
-355	0.5	5.9
-32	0.5	2.6

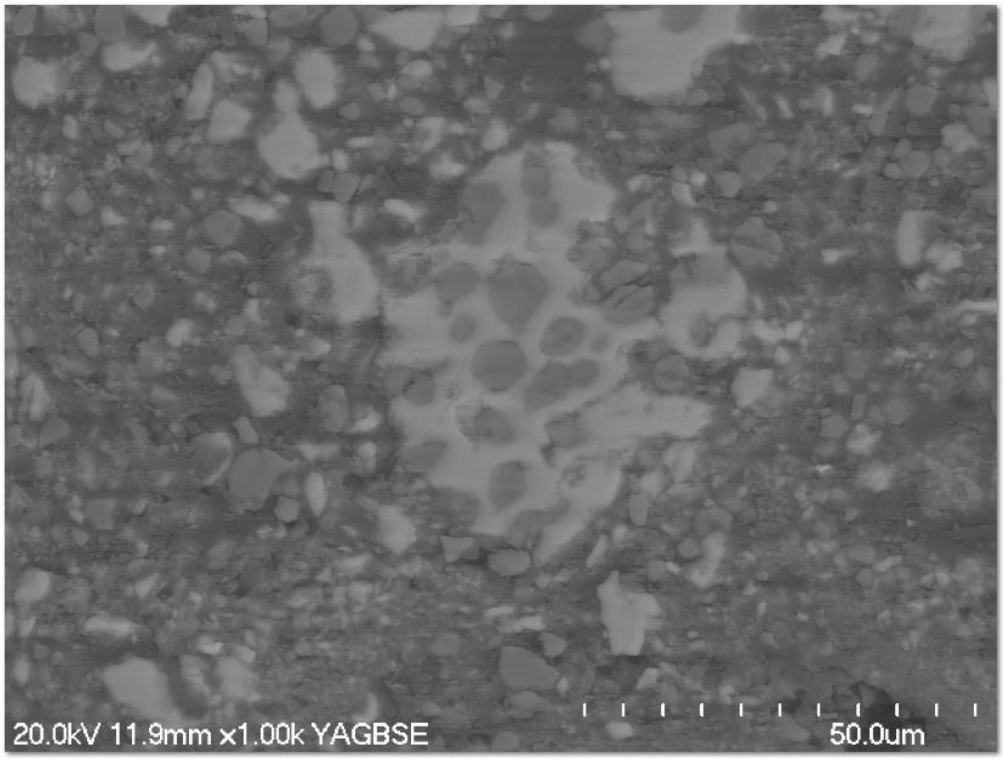

Figure 6.10: SEM backscattered image of flotation slimes with TiAl (light phase) and TiAl(O)/Al_2O_3 (grey phase)

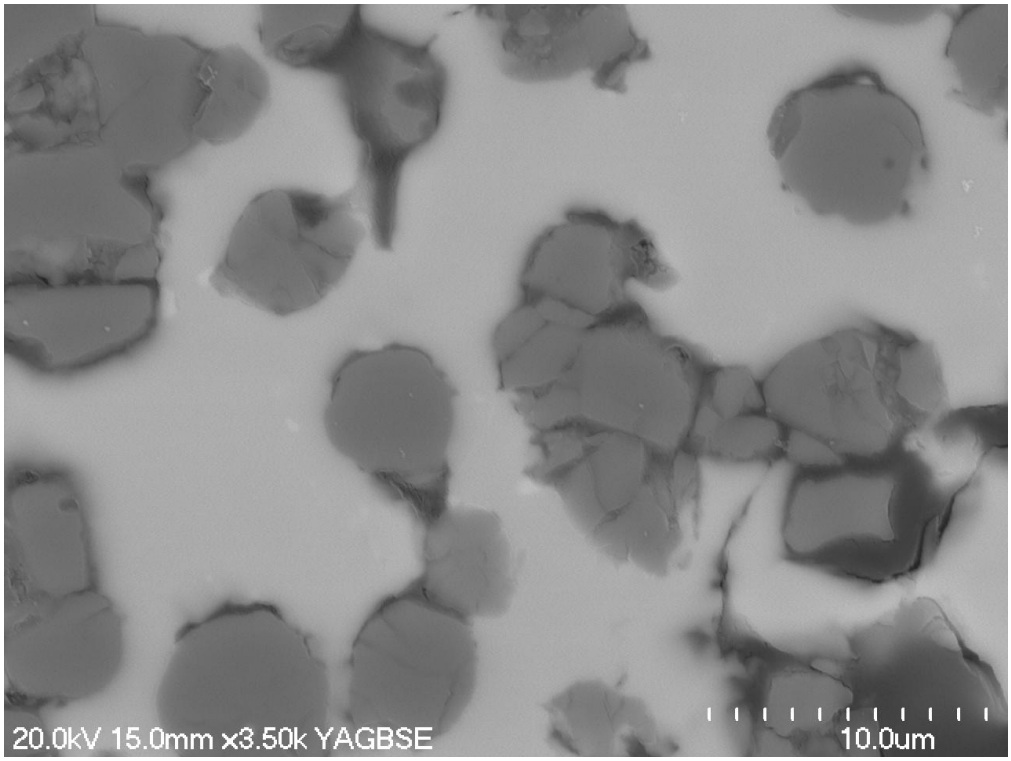

Figure 6.11: SEM backscattered image of the flotation concentrate

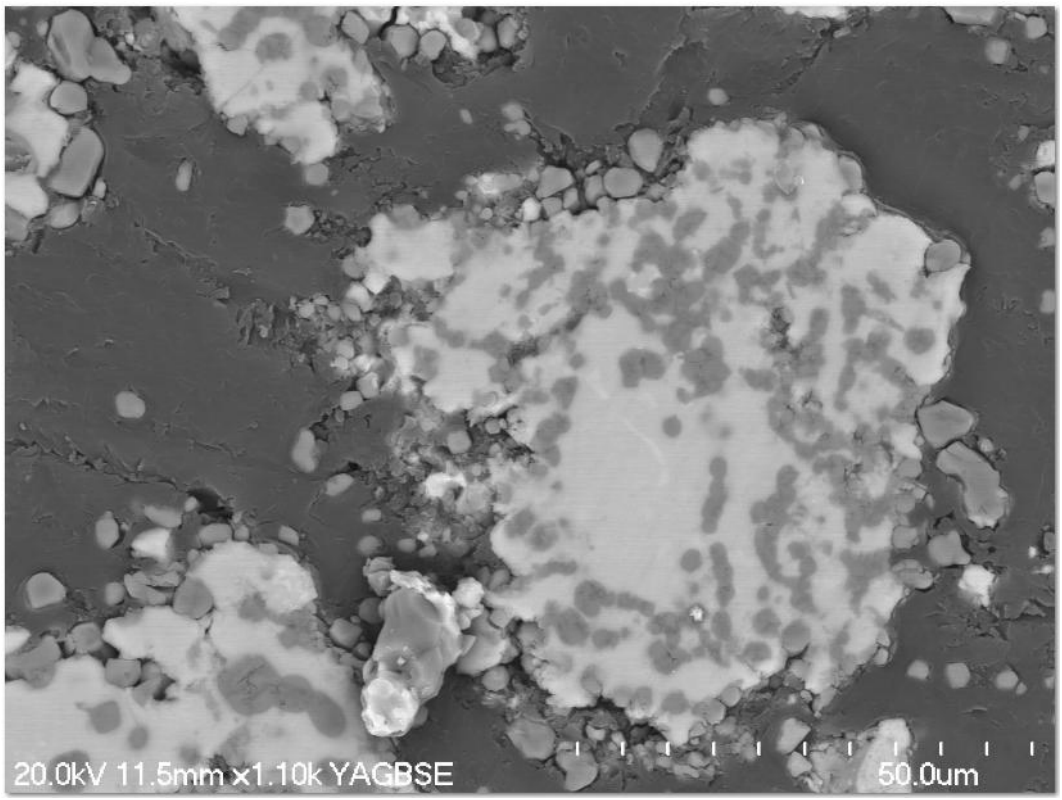

Figure 6.12: SEM backscattered image of +32 -56 microns regrind size fraction

The selectivity of froth flotation toward Al_2O_3 was influenced by pH, feed particle size, collector dosage and flotation air flow rate. The separation efficiency reached its maximum in the region slightly above pH 3.7; the point of zero charge of TiAl and declined away from it. For instance, at pH 3.2, the separation efficiency was only 17.3% in comparison to 44.3% at pH 4.2. Since pH 3.2 is below the point of zero charge of TiAl, both TiAl and Al_2O_3 were positively charged. Since the negatively charged sodium dodecyl sulphate collector attached to and floated both TiAl and Al_2O_3 no separation could be effected. However, between pH 4 and pH 9.1 (the point of zero charge of Al_2O_3), the surface of TiAl particles became negatively charged while the Al_2O_3 particles remained positively charged. This made Al_2O_3 selectively floatable (Fuerstenau, 2005). The results demonstrated that selective flotation of Al_2O_3 with sodium dodecyl sulphate was possible at around pH 4.

The separation efficiency dropped significantly as the superficial air velocity was increased from 0.5 cm sec^{-1} to 0.9 cm sec^{-1}. This could be attributed partly to froth collapse caused by non-quiescent pulp-froth interface (Dunne, 2002). Decreasing the flotation feed particle size from -425 +355 µm to less than 32 µm, while

maintaining the superficial air velocity at 0.5 cm sec^{-1} and the pH at 4.2, resulted in a corresponding decrease in the separation efficiency from 44.3% to 2.6% (Table 6.6). This was probably due to TiAl losses to slimes. Increasing the collector dosage from 40 g/t to 405 g/t of feed had a similar adverse effect on the separation efficiency.

6.3.7 Conceptual Flowsheet

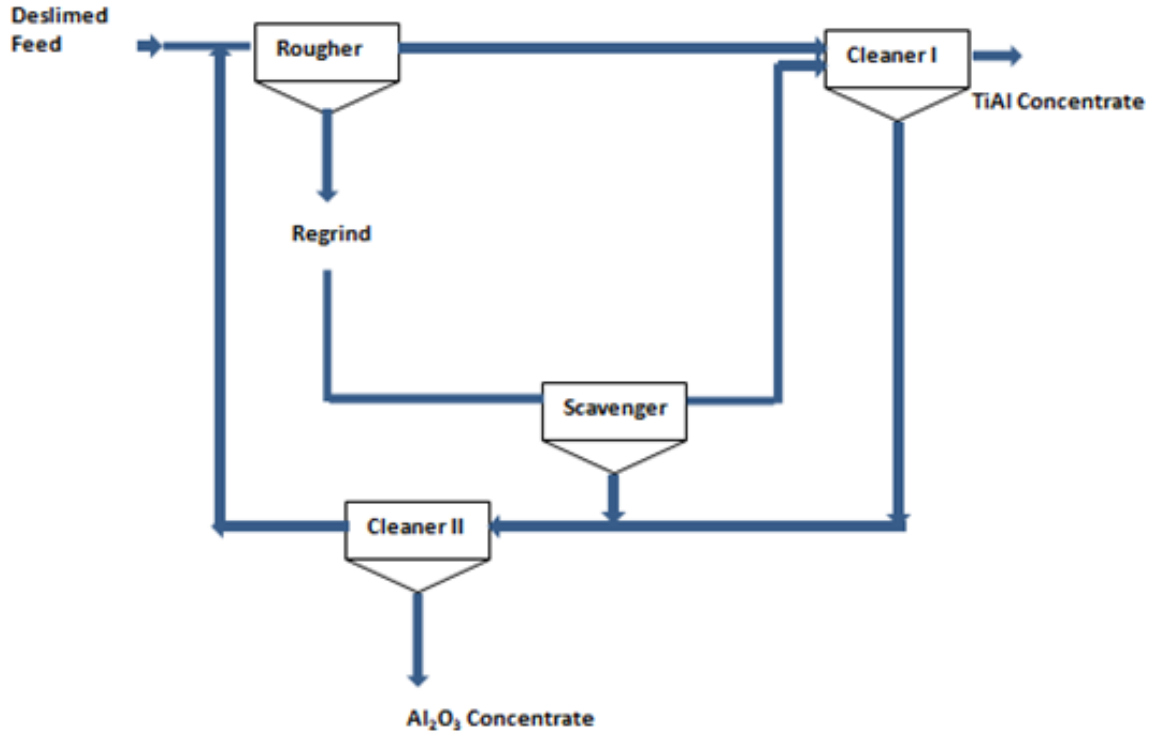

Figure 6.13: Conceptual flowsheet for the separation of TiAl from Al_2O_3 by froth flotation

6.4 Conclusion

- Froth flotation has a potential application in recovering some TiAl into a TiAl-rich fraction of the CS by-product by using anionic surfactants at slurry of pH 4 and feed particle size of -425 µm. The TiAl recovery at the rougher flotation stage was 65.7 wt% at 71.0 wt% TiAl grade. This corresponded to removing 20 wt% of the total Al_2O_3 in the flotation feed. Further rejection of Al_2O_3 to increase the grade and recovery of TiAl requires multiple cleaning stages using an Al_2O_3 activator that is less aggressive to TiAl.

- Flotation is more selective between PZC of Al_2O_3 (pH 9.1) and PZC of TiAl (≈pH 3.7).
- Excessive collector dosages adversely affect the separating efficiency. A dosage of 10^{-5}M sodium dodecyl sulphate is more effective.
- The separating efficiency is also sensitive to the specific air flow. An Air: Solids ratio of 41.1 gave more efficient separation when floating feed with a particle size from -32 to -425 μm.
- TiAl losses are mainly due to TiAl wetting and being imbibed on to Al_2O_3 particles surfaces and incomplete liberation of the TiAl phase.
- Pre-flotation de-sliming recovers high TiAl slimes that can be fed downstream. Therefore, there is potential to increase throughput by de-sliming the flotation feed and routing slimes downstream in the flotation circuit (Figure 6.13).

6.5 References

Crozier, R. D. (1992). *Flotation* (1st ed.). Oxford, U.K.: Pergamon.

Fuerstenau, D. W., & Pradip. (2005). Zeta potentials in the flotation of oxide and silicate minerals. *Advances in Colloid and Interface Science, 114-115*, 9-26.

Modi, H. J., & Fuerstenau, D. W. (1960). Flotation of corundum. *Transactions of the American Institute of Mining, Metallurgical, and Petroleum Engineers, 217*, 381-387.

Wills, B. A. (2006). *Mineral Processing Technology : An Introduction to the Practical Aspects of Ore Treatment and Mineral Recovery* (7th ed.). Oxford, U.K.: Butterworth-Heinemann.

Yarar, B. (2000). Flotation. In *Kirk-Othmer Encyclopedia of Chemical Technology*: John Wiley & Sons, Inc.

Chapter 7

Alloy Purification and Costing

7.1 Introduction

The previous chapter sought to increase the grade of the TiAl-rich product, by removing as much Al_2O_3 as possible, because it is a major contributor of oxygen in titanium produced by the TiPro process. The presence of oxygen for which titanium has an immense affinity is detrimental in both the processing and application of titanium and its alloys. To overcome oxygen contamination, conventional titanium extraction is often carried out in an oxygen free chloride environment. In the TiPro process however, oxygen contamination is unavoidable because TiAl is produced from TiO_2. Oxygen that occurs as dissolved species and Al_2O_3 inclusions requires subsequent removal. The price of titanium in 2012 varied from about US$15/kg to about US$1000/kg depending on impurity level and particle size (Qian *et al.*, 2012). Since oxygen is one of the major impurities determining the quality and cost of titanium powders, purification is incorporated to satisfy the increasingly demanding quality specifications in application (Table 7.1). This chapter is divided into two parts. Part I discusses the results obtained in experiments conducted to reduce the oxygen content, while Part II determines the cost and quality of TiAl produced by the TiPro process. Capital and operating costs have also been estimated.

Table 7.1: Common titanium metal grades

Grade	Impurities in ppm				
	O	C	Fe	Ca	Cl
ASTM Gr 1	1800	1000	2000		
ASTM Gr 2	2500	1000	3000		
ASTM Gr 3	3500	1000	3000		
ASTM Gr 4	4000	800	5000	1000	

For a metal to be used to remove oxygen from the alloy and the by-product of the TiPro process, its oxide has to be more stable than oxides of titanium and aluminium. It also has to easily separate from the alloy. These criteria limit the

choice to Ca, Mg, Li and Sr. Calcium is usually preferred because, in addition to its low melting point and viscosity of the reaction product, calcium is capable of reducing Al_2O_3 and removing the oxygen dissolved in titanium also (Kubaschewski *et al.*, 1993). In the purification of titanium, Ca can be used in form of Ca metal or CaH_2 according to the reactions shown below (Belyanchikov, 2010)

$$3\ CaH_2 + Al_2O_3 = 2Al + 3CaO + 3H_2 \quad \Delta G_{1073K} = -29.969\ \text{kcal} \tag{7-1}$$

$$CaH_2 + \underline{O} = CaO + H_2 \quad \Delta G_{1073K} = -33.493\ \text{kcal} \tag{7-2}$$

$$3\ Ca + Al_2O_3 = 2Al + 3CaO \quad \Delta G_{1073K} = -64.062\ \text{kcal} \tag{7-3}$$

$$Ca + \underline{O} = CaO \quad \Delta G_{1073K} = -44.874\ \text{kcal} \tag{7-4}$$

$\underline{O}$ = oxygen dissolved in TiAl alloy
CaO = calcium oxide dissolves in the carrier $CaCl_2$ subsequently

Previous attempts to replicate the use of the calcium vapour process have failed. Another study (Adam, 2010), purified $Ti(Al,O)/Al_2O_3$ with CaH_2 at 1100°C. The product contained 8000 ppm O and 4300 ppm Ca. CaH_2 is preferred to Ca because it is easier to control (Wiberg, 1971). The objective of the current reduction experiments is to investigate the feasibility of using lower temperatures. All the experiments were conducted on a scale of a few grams. This has potential economic benefits for the plant scale process.

PART I: Alloy Purification Results

7.2 Reduction Using Ca

To remove oxygen using calcium, the reductant (Ca) can be used in granular or in vapour form. The main advantage of Ca vapour is that unlike Ca granules its purity is less critical. However, equipment requirements are more complex.

7.2.1 Ca Granules

When Ca granules were mixed and reacted with the alloy the reduction product picked up some contamination from the reductant and the reactor material.

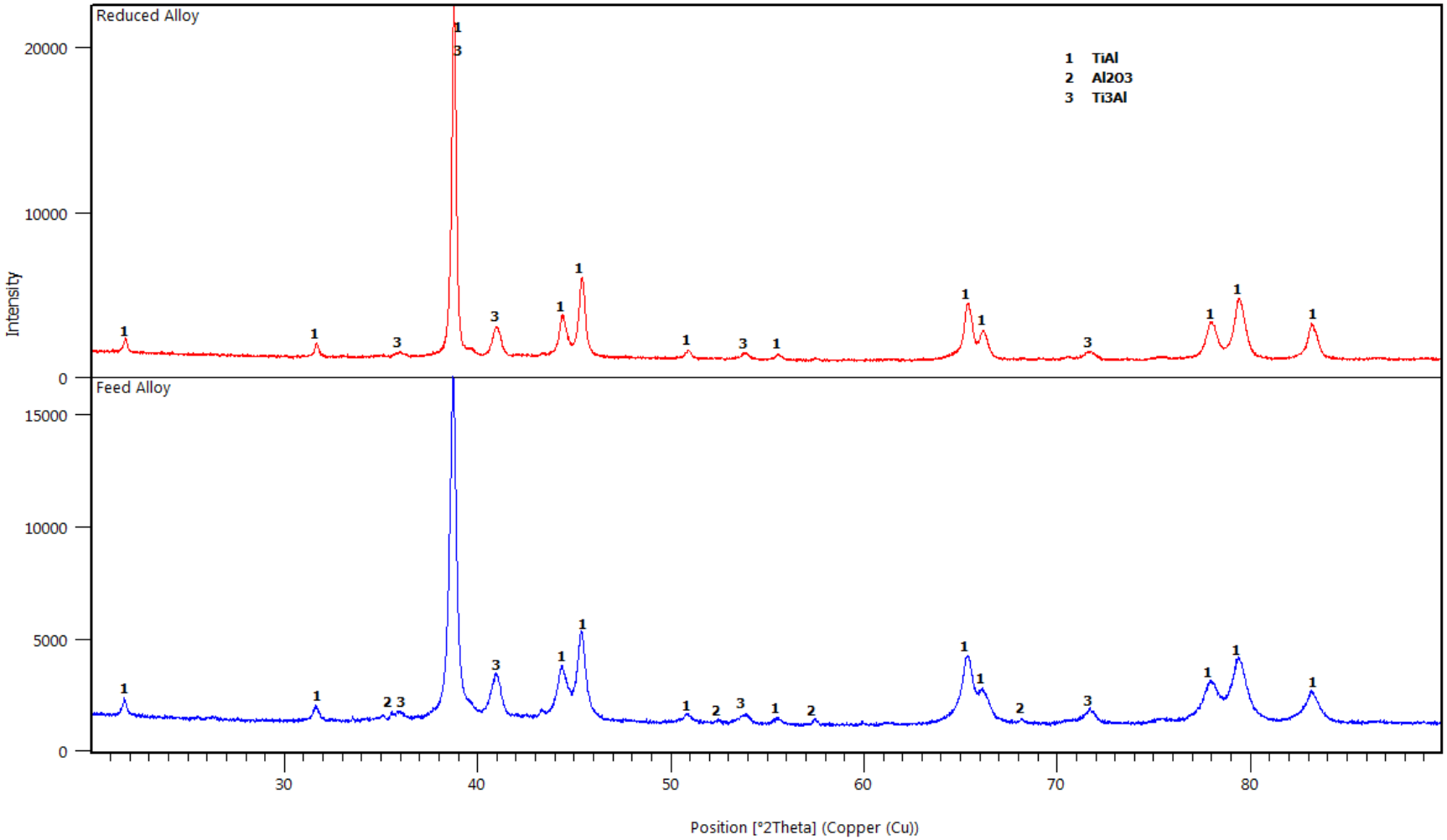

Figure 7.1: Comparison of XRD analyses of the alloy before reduction (feed alloy) and purification (reduced alloy)

Figure 7.1 compares the phase composition before and after reduction with calcium granules. The Al_2O_3 in the reduced product was below the detection limit of XRD analysis. This is in agreement with Equations (7-3) and (7-4) that are thermodynamically feasible as indicated by the Gibbs free energy of reaction.

7.2.2 Ca Vapour

The use of Ca vapour overcame contamination resulting from the reductant, however, reactor sourced contamination was still significant. Whether the Ca was mixed with other reactants or introduced as a vapour the attack on the retort was evident. The process has also been reported to be difficult to scale up because of problems in ensuring a homogeneous reaction when reducing large tonnages of feed in a single reactor (Okabe *et al.*, 2004).

XRD analysis (Figure 7.2) indicates that Ti was completely oxidised to $CaTiO_3$ and TiO_2 while the Al_2O_3 intact. This was confirmed by SEM – EDS, which only showed Ti existing in association with Ca and O_2 but not with Al (Figure 7.3).
The Al_2O_3 could not be reduced and instead the titanium became oxidised. This might be attributed to reactions (7-5) and (7-6).

$$4AlTi + 4CaCl_2 + 7O_2 + 4H_2O = 4CaTiO_3 + 2Al_2O_3 + 8HCl$$
$$\Delta G_{1073K} = -1280.860 \text{ kcal} \quad (7\text{-}5)$$

$$4AlTi + 4CaCl_2 + 9O_2 = 4CaTiO_3 + 2Al_2O_3 + Cl_2$$
$$\Delta G_{1073K} = -1267.517 \text{ kcal} \quad (7\text{-}6)$$

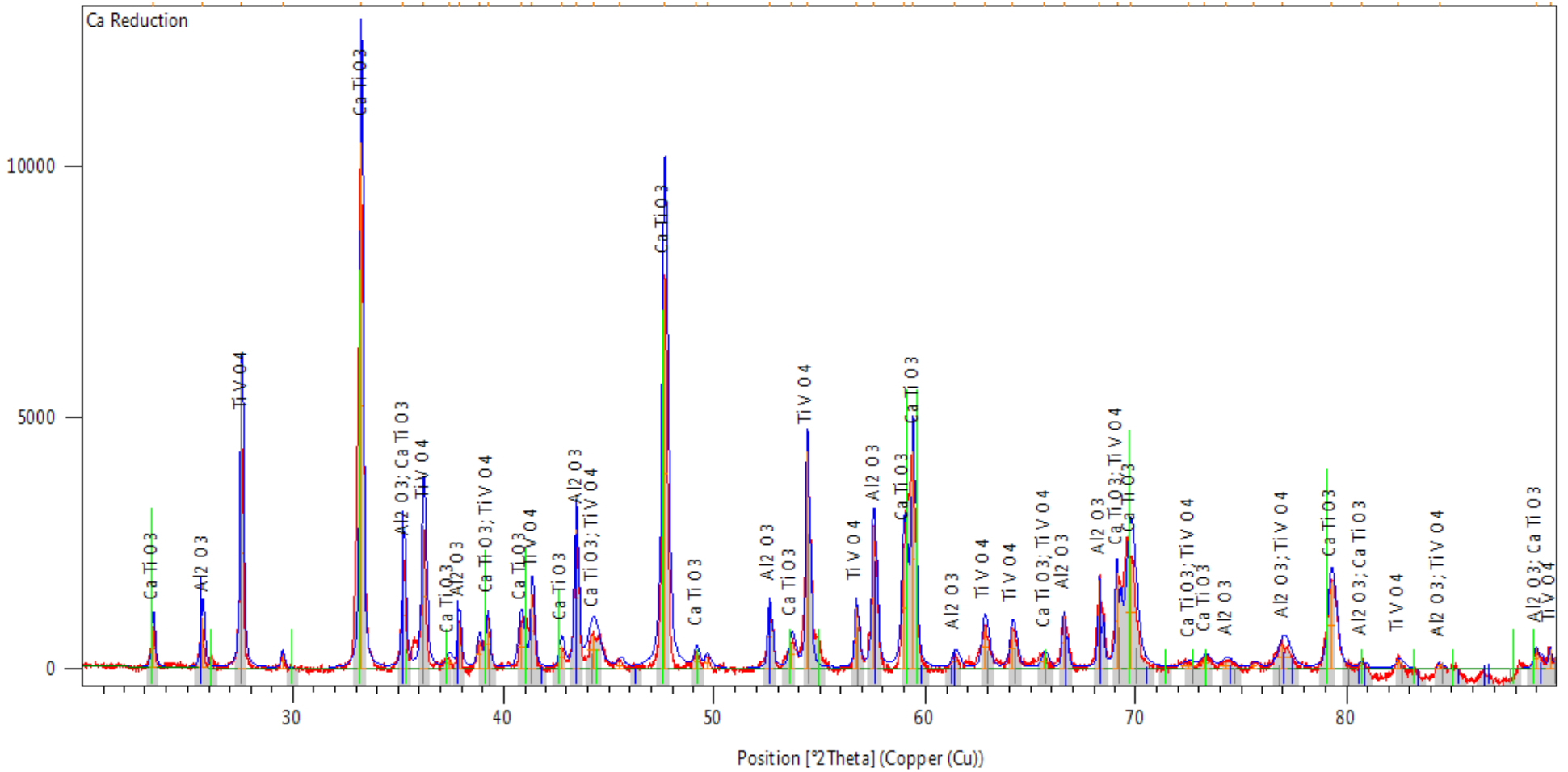

Figure 7.2: XRD pattern for the Ca reduction product showing $CaTiO_3$, unreduced Al_2O_3 and V contamination

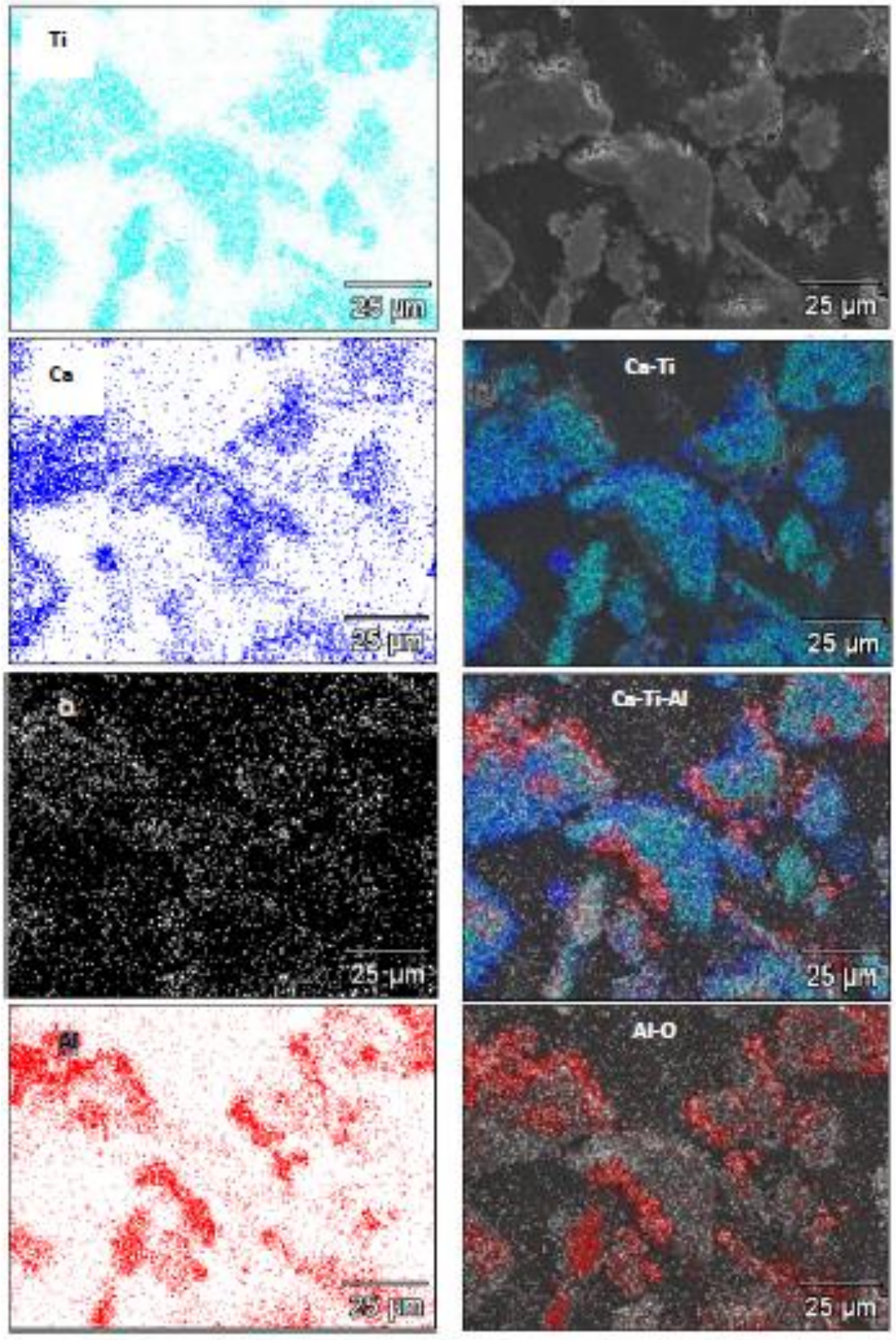

Figure 7.3: SEM -EDS element maps of the Ca reduction product

7.3 Reduction Using CaH_2

When the reduction was carried out with a mixture of CaH_2 and $CaCl_2$, it was possible to maintain the O_2 level in the chamber at 1ppm and the pressure between 0 and -1 mbar. The reduction was carried out for 1 h and below 800^oC (Figure 7.4). This is in agreement with Wiberg and Amberger (1971) who have stated that reduction of Al_2O_3 with CaH_2 starts at about 500^oC and is complete at 750^oC. Low O_2 levels in the chamber could be maintained because the H_2, produced when CaH_2 reduces Al_2O_3, forms a protective reducing atmosphere (Wiberg & Amberger, 1971).

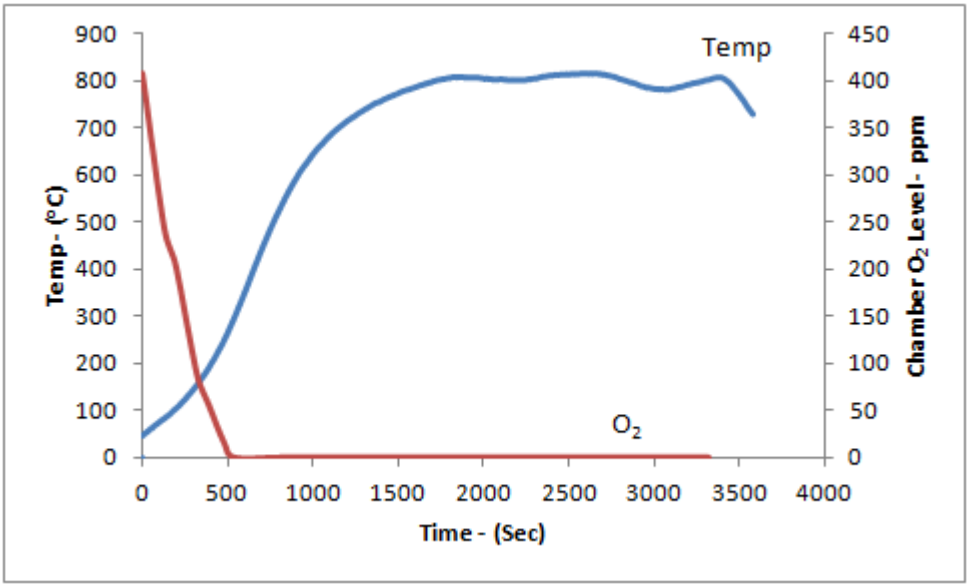

Figure 7.4: Temperature profile and chamber O_2 level during CaH_2 reduction

After 1h, the XRD pattern of the reduction product showed the presence of TiAl, Ti_3Al, Ti_2Al, CaClOH, and CaO; but Al_2O_3 was below the detection limit (Figure 7.5). Gravimetric analysis of the reduction product showed that the Al_2O_3 had dropped from 5.18 wt% Al_2O_3 (equivalent to 2.44% O_2) to 1.61% O_2. Upon washing the product with water at 60^oC, CaClOH and CaO were completely leached out (Figure 7.6).

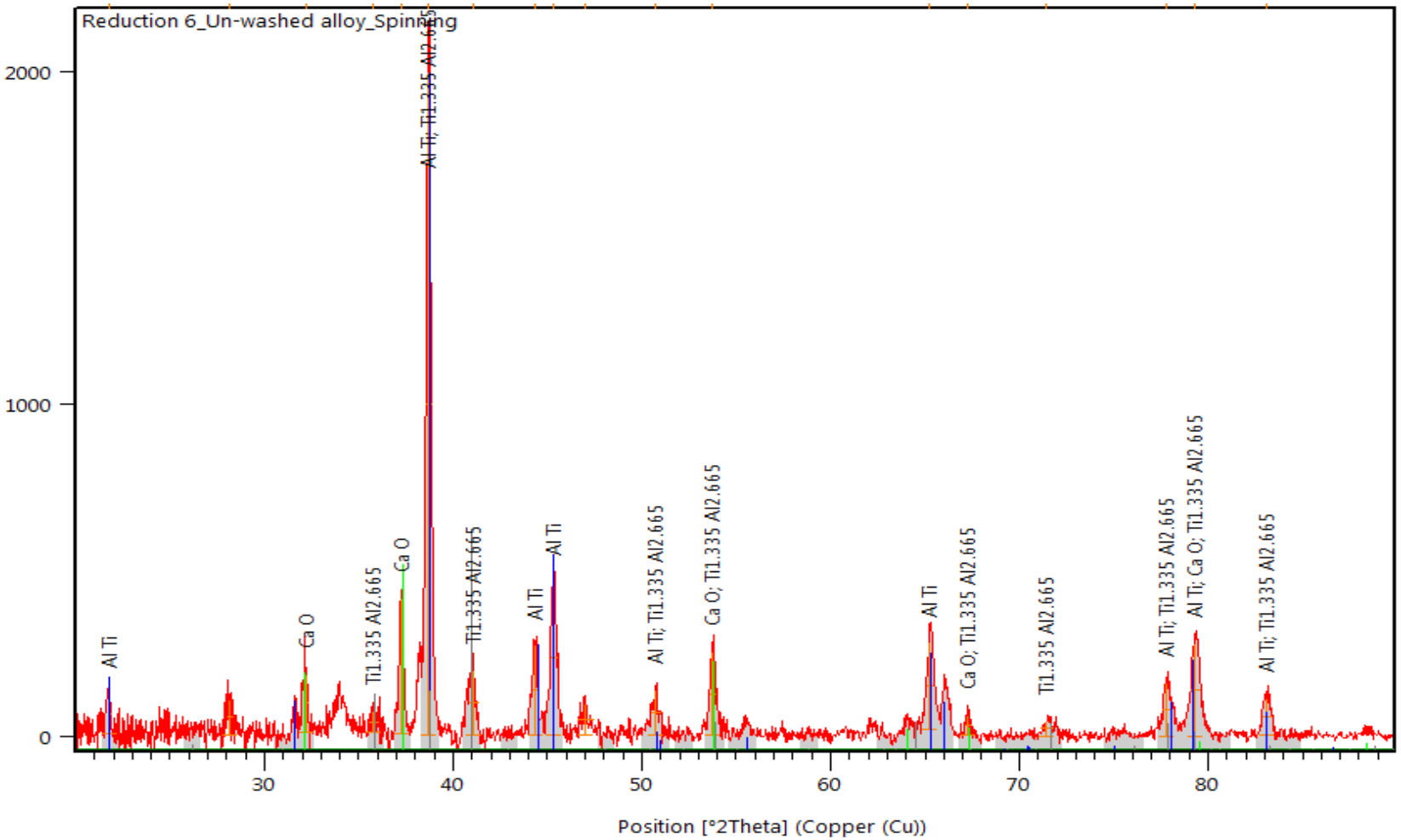

Figure 7.5: XRD pattern of reduction product before washing

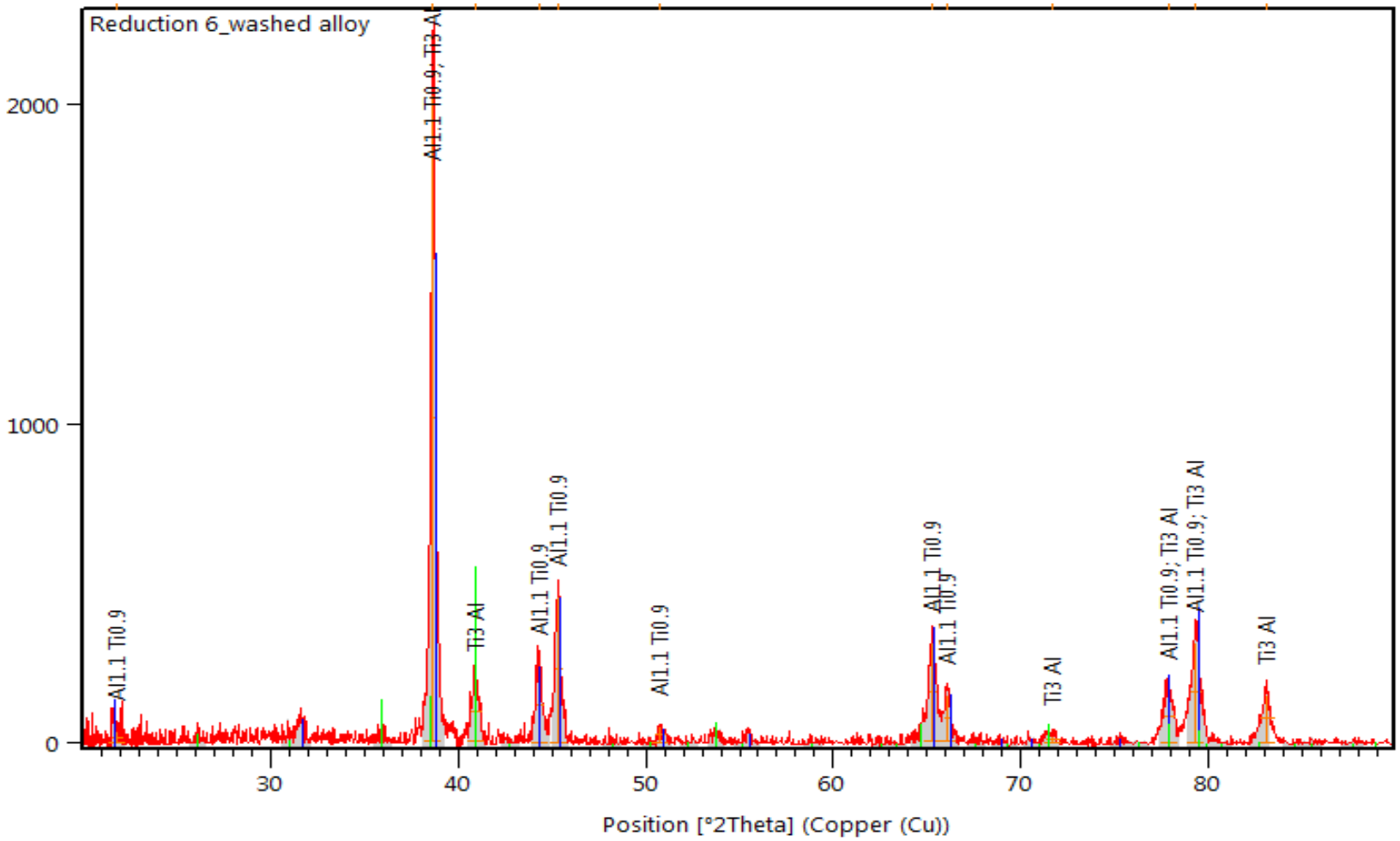

Figure 7.6: XRD pattern of reduction product after washing with acidified water at 25ºC

The calcium hydroxychloride (CaClOH) might have been formed by the reaction between Ca, $CaCl_2$ and H_2O (Equation(7-7)).

7.4 Alloy Purification by Reaction Milling

When a mixture of $CaCl_2$, Ca and TiAl(O) was subjected to high energy mechanical milling for 300 seconds, the Al_2O_3 was reduced (Figure 7.7) and the as-milled product contained CaClOH ; probably formed by the reaction Equation (7-7).

$$CaCl_2 + Ca + 3H_2O = 2CaClOH + H_2 \quad \Delta G^{\circ}_{298K} = -12.706 \text{ kcal} \tag{7-7}$$

Equation (7-7) can be broken into the following steps

1. Reduction of Al_2O_3

$$3Ca + Al_2O_3 + 3H_2O = 3Ca(OH)_2 + Al \quad \Delta G^{\circ}_{298K} = -95.300 \text{ kcal} \tag{7-8}$$

2. Reduction of Al_2O_3

$$3Ca + Al_2O_3 = 3CaO + 2Al \quad \Delta G^{\circ}_{298K} = -55.050 \text{ kcal} \tag{7-9}$$

3. Calcium hydroxide formation

$$CaO + H_2O = Ca(OH)_2 \quad \Delta G^{\circ}_{298K} = -13.420 \text{ kcal} \tag{7-10}$$

4. Calcium hydrochloride formation

$$CaCl_2 + Ca + 2H_2O = 2CaClOH + H_2 \quad \Delta G^{\circ}_{298K} = -12.706 \text{ kcal} \tag{7-11}$$

The formation of CaClOH is accompanied by the partial replacement of TiAl with $Ti_{0.9}Al_{1.1}$, which contains a higher proportion of Al (Figure 7.7). The formation of additional Al probably results from Equation (7-8). After the as-milled powder was leached with acidified water at 25°C, the residual Al oxides in the residue were below the detection limit of XRD analysis (Figure 7.8). However; oxygen analysis by inert gas fusion-ASTME 1409-13 method indicated a drop in oxygen content from 2.69% O_2 to 1.01% O_2 after processing for 5 min.

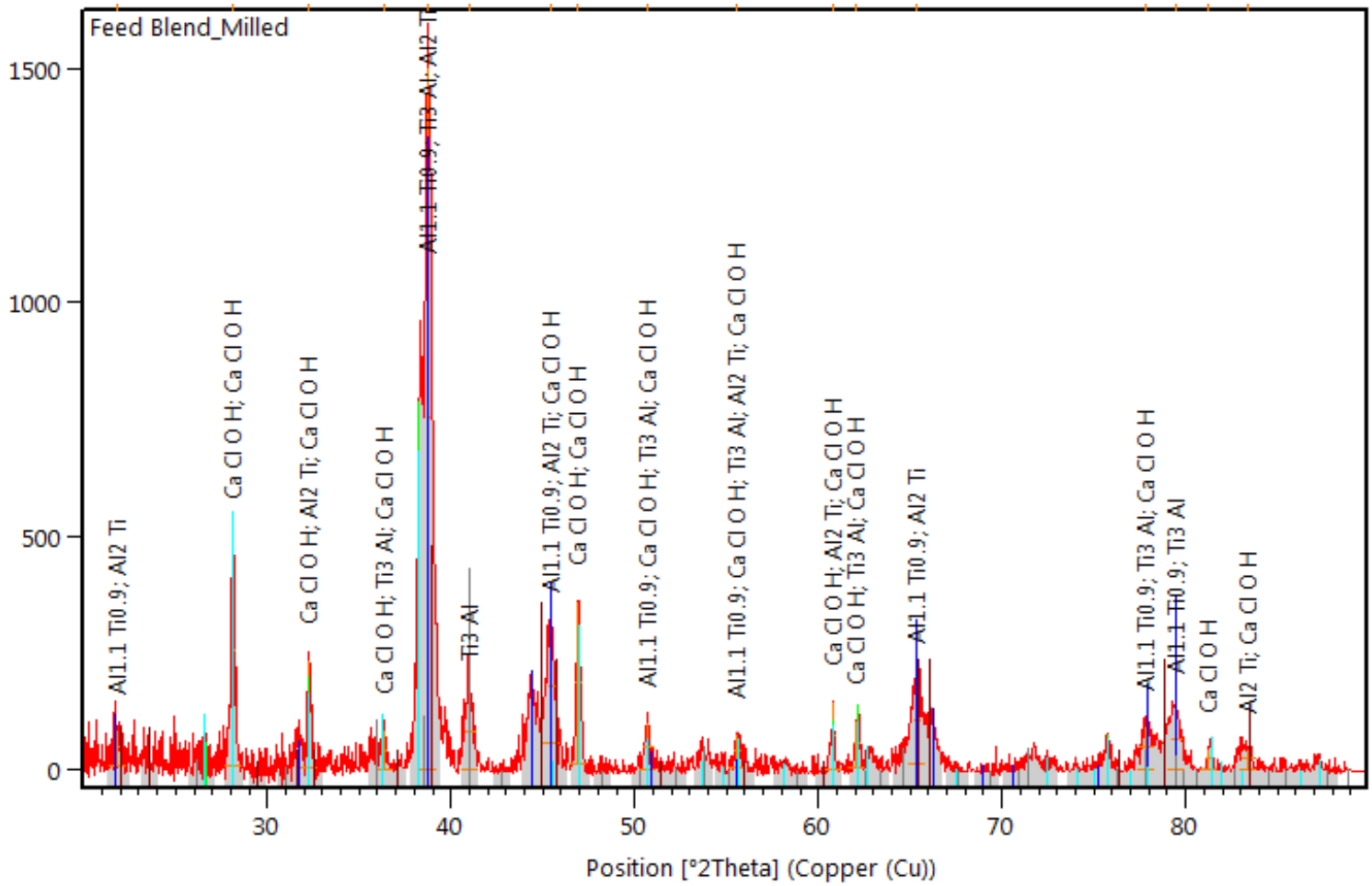

Figure 7.7: XRD analysis of the Alloy-Ca-$CaCl_2$ after high energy mechanical milling

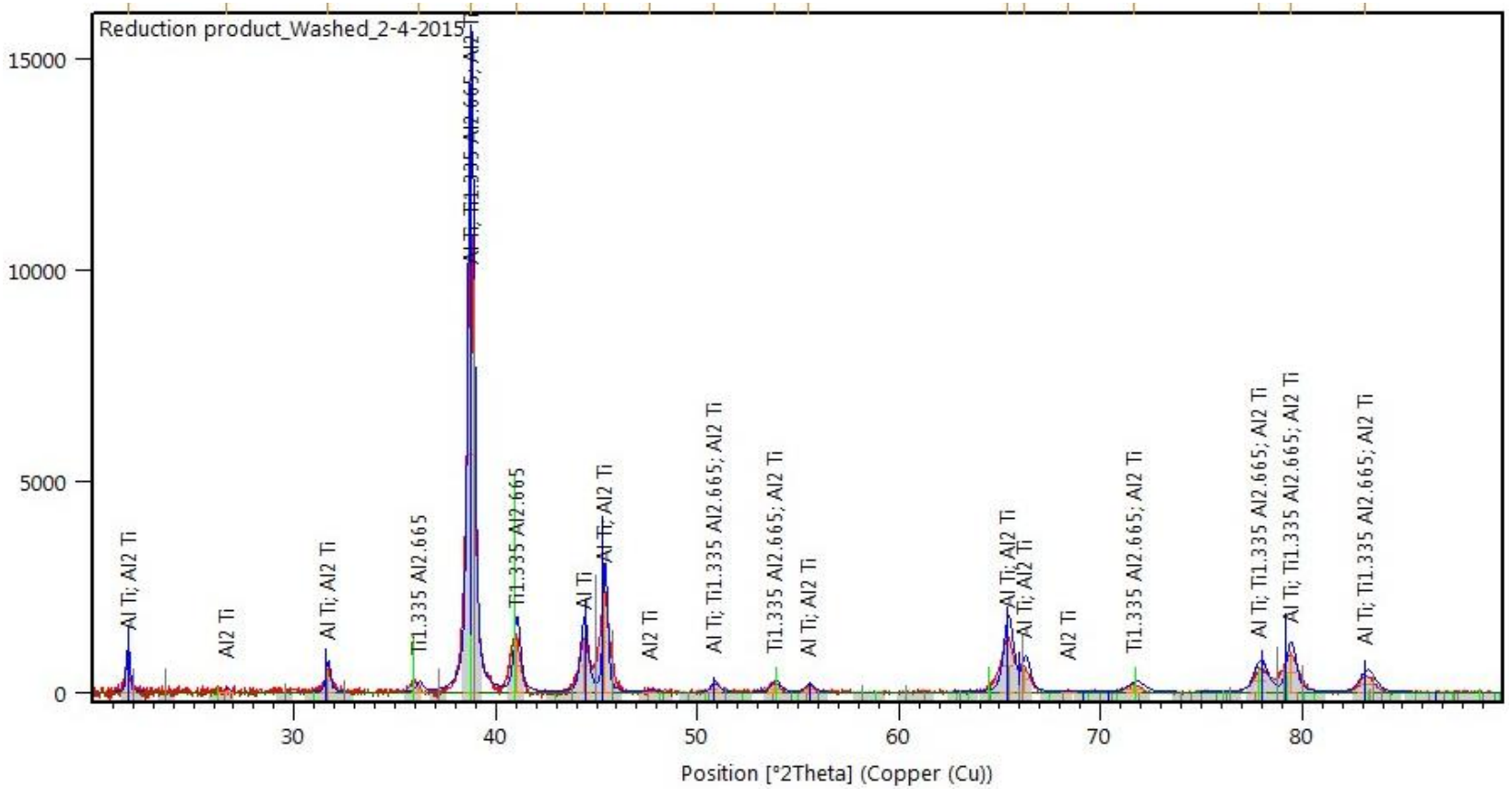

Figure 7.8: Composition of powder purified by reaction milling

The powder purified by reaction milling is irregular in shape (Figure 7.9). The median size (d_{50}) of the powder was 75 µm and the d_{90} was 142 µm (Figure 7.10).

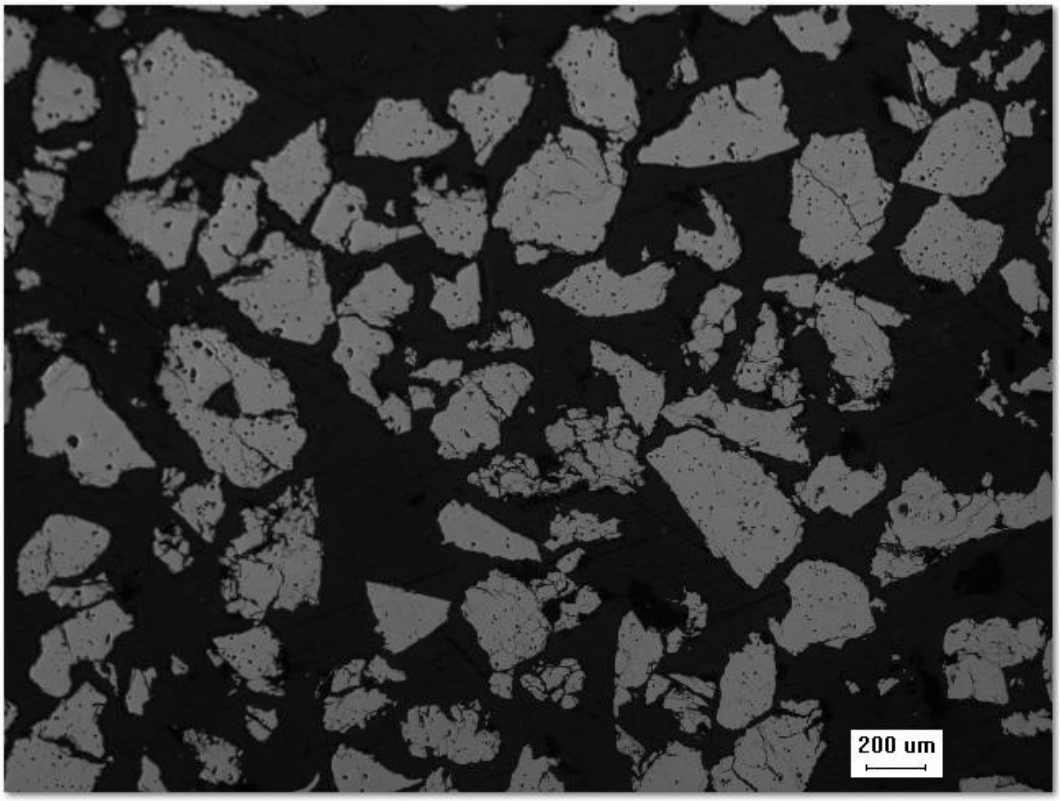

Figure 7.9: OM micrograph of a cross section of TiAl powder purified by reaction milling (x100 magnification)

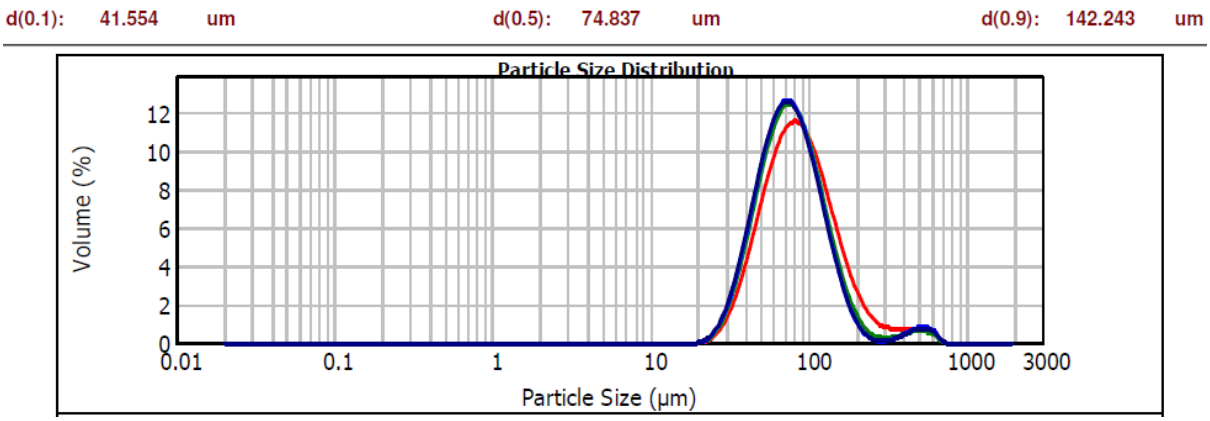

Figure 7.10: Particle size distribution of washed alloy powder

PART II: Process Costing

The objective of this part is to determine operating and capital costs based on conceptual design and estimated prices derived from the metallurgical testing results. Therefore the estimate is of a preliminary type with a level of accuracy of ±20% (Noakes, 1993). The incremental effects of each process step on the cost of producing TiAl alloy by the proposed flow sheet have been estimated. The cost indices obtained from government agencies have been used to estimate equipment prices where quotations from manufacturers were not available (Bouman *et al.*, 2005). The spreadsheets are included in the appendices.

The process flowsheet was evaluated under the following unit operations:-

- high energy mechanical milling
- liquid/solid separation
- froth flotation
- alloy purification

Three downstream alternatives for processing the extrusion by-product comprising calciothermic reduction/ direct leach, TiO_2 recycle and flotation/ leach/ TiO_2 recycle were evaluated.

7.5 Calciothermic Reduction and Direct Leach

In this scenario, the milled extrusion product was reacted with calcium (in a $CaCl_2$ flux) to remove oxygen that exists as Al_2O_3 inclusions and dissolved species in titanium in the alloy (Equations (7-3) and (7-4)). The reduction reaction was initiated either thermally or by milling as described in Chapter 3. The reduction product was leached with water to extract the alloy.

7.6 TiO_2 Recycle

In a related proof of concept study (Jennings, 2013) it was demonstrated that the TiAl contained in the extrusion by-product could be converted to recyclable TiO_2 at 92.3% yield. In addition, about 75% Al_2O_3 that could be sold to smelters was recovered. However, the process conditions were not optimised. Based on the mass balance and cost of direct materials, conversion to TiO_2 appears uneconomical when considered on its own. The projections made from the empirical results of the study indicate that the cost of inputs is higher than the value of products (Table 7.2).

The conceptual study does not state the chemical reaction equations involved in conversion to TiO_2. However, to calculate the stoichiometric input requirements and products this study has assumed the following chemical equations

$$6H_2SO_4 + 2TiAl = Ti_2(SO_4)_3 + Al_2(SO_4)_3 + 6H_2 \quad (7\text{-}12)$$

$$Ti_2(SO_4)_3 + 6NaOH = 2Ti(OH)_2O + Na_2SO_4 \quad (7\text{-}13)$$

$$Al_2(SO_4)_3 + 6NaOH = 2Al(OH)_3 + Na_2SO_4 \quad (7\text{-}14)$$

$$Al_2(SO_4)_3 + 6NH_4OH = 2Al(OH)_3 + 3(NH_4)_2SO_4 \quad (7\text{-}15)$$

7.7 Flotation/ Calciothermic Reduction /Leach/ TiO_2 Recycle

By upgrading the extrusion by-product from 47.4% to 71% TiAl using froth flotation the calcium reductant requirement is reduced from 0.56 to 0.34 tonnes/tonne TiAl. This corresponds to a saving of about US$1600/tonne TiAl produced. Therefore, to make the TiPro process more economical, only the TiAl-lean product of flotation should be converted to TiO_2. Conversion of the entire extrusion by-product stream to TiO_2 can result into a high circulating load and poor process economics given the low yield (10%) at the solid/liquid separation stage.

Table 7.2: Cost of raw materials and expected revenue

Material	Price US$/T	Empirical		Stoichiometric	
		T/T Composite	US$/T Composite	T/T Composite	US$/T Composite
Input					
Composite		1			
H_2SO_4	200	2	400	1.744	349
NaOH	320	5.25	1680	1.423	456
NH_4OH (28 wt %)	300	17.857	5357	2.227	668
NaF	750	0.025	19	0.025	19
Total Direct Materials Cost - US$			**7456**		**1491**
Product					
TiO_2	3000	0.601	1803	0.601	1803
Al_2O_3	600	0.291	175	0.291	174.6
Total Revenue		0.892	1978	0.892	1978
Gross Profit			**-5478**		**487**

7.8 Economic analysis for a 500 tonnes per annum (tpa) TiAl plant

OSBL Capital Cost	40% of ISBL cost
Engineering Cost	30% of ISBL + OSBL cost
Contingency	20% of ISBL + OSBL cost
Working Capital	7 weeks' cost of production less 2 weeks' feedstock costs

The economic assumptions such as the tax rate, depreciation method and period are detailed in Appendix 1.

Table 7.3 gives a summary of the economic analysis of a 500-tpa capacity plant operating at 65% yield of TiAl. The calculations are detailed in Appendix 1. Appendices 2 to 7 all feed into Appendix 1. The 500 tpa design criteria is based on metallurgical results of the study, economic considerations and current industry practice and facilities under development (Froes).

- The total investment cost is calculated in Appendix 1 by adding the total fixed capital cost and the working capital.

- The total fixed capital cost is calculated in Appendix 1 and includes the total installed cost which is the cost of the plant itself (inside battery limits, ISBL), the cost of modifications to the site infrastructure (offsite battery limits, OSBL), contingency costs, engineering and construction costs.
- The total installed cost is calculated in Appendix 3.
- Simple pay-back period = Total Investment cost ÷ Average annual cash flow

The following costs were calculated using industry practice factors (Towler & Sinnott, 2012).

OSBL Capital Cost	40% of ISBL cost
Engineering Cost	30% of ISBL + OSBL cost
Contingency	20% of ISBL + OSBL cost
Working Capital	7 weeks' cost of production less 2 weeks' feedstock costs

The economic assumptions such as the tax rate, depreciation method and period are detailed in Appendix 1.

Table 7.3: Economic analysis of TiPro process operating at 65% yield

Total Investment Cost	US$5,914,692		
Total Plant Installed Cost	US$2,858,202		
Fixed Capital Cost	US$4,716,033		
Average annual cash flow	$5,678,666	Simple pay-back period	1.04 years
	10 years	15 years	20 years
Return on investment	91.17%	97.52%	
NPV	$10,915,626	$15,941,831	$18,436,734
IRR	62.0%	63.3%	63.4%
NPV to year 1		-$5,114,303	

7.9 Conclusion

- The study has demonstrated the efficacy of reducing the oxygen content of TiAl produced by the TiPro process by using either Ca or CaH_2. CaH_2 does not form lower oxides and has very little tendency to form alloys therefore the product yield is reported to be quantitative (Wiberg & Amberger, 1971).

- Ca is more attractive because it is cheaper than CaH_2. Reactive milling of a mixture of TiAl(O) or TiAl(O)/Al_2O_3 with Ca and $CaCl_2$ is easier to scale up compared to Ca vapour reduction.
- About 62% removal of oxygen (i.e. from 2.69 to 1.01% O_2) was achieved by reaction milling in fewer than 300 sec.
- The preliminary production cost estimate, at US$23.92 per kg TiAl alloy powder, compares favourably with most emerging cost reduction titanium production technologies that are targeting costing reductions of 30 or 50% and more of the Kroll process (EHK Technologies, 2004).
- The total investment cost of a 500-tonne per annum TiPro process plant operating at 65% efficiency was estimated at US$5,914,692. With an average annual cash flow of US$5,678,666 pay-back period would be 1.04 years. This corresponds to 91.19% return on investment, NPV of US$10,915,626 and an IRR of 62% over 10 years.

7.10 References

Adam, G. (2010). Metal alloy powders production. US Patent 2010/0015003 A1, Titanox Development Limited, USA.

EHK Technologies. (2004). *Summary of Emerging Titanium Cost Reduction Technologies*. Retrieved 15 August, 2011, from http://www.ornl.gov/sci/propulsionmaterials/pdfs/Emerging_Titanium.pdf

Froes, F. H. (n.d.). *Developments in Titanium P/M*. Retrieved October, 2013, from http://www.uobabylon.edu.iq/eprints/publication_10_14475_394.pdf

Jennings, P. A. C. (2013). *Recovery and Purification of Titanium Dioxide and Aluminium Compounds from Corundum By-product of the TiPro Process.* thesis, University of Waikato, Hamilton.

Kubaschewski, O., Alcock, C. B., & Spencer, P. J. (1993). *Materials Thermochemistry* (6th ed.). Oxford, U.K.: Pergamum Press.

Okabe, T. H., Oda, T., & Mitsuda, Y. (2004). Titanium powder production by preform reduction process (PRP). *Journal of Alloys and Compounds, 364*(1-2), 156-163.

Qian, M., Yang, Y. F., Yan, M., & Luo, S. D. (2012). Design of low cost high performance powder metallurgy titanium alloys: Some basic considerations. *Key Engineering Materials, 520*, 24-29.

Towler, G., & Sinnott, R. K. (2012). *Chemical Engineering Design : Principles, Practice and Economics of Plant and Process Design (2nd ed.)*. London, GBR: Butterworth-Heinemann.

Wiberg, E., & Amberger, E. (1971). *Hydrides of the elements of main groups I - IV*. New York: Elsevier.

Chapter 8

Conclusions and Recommendations

8.1 Introduction

In this study, the key factors affecting the cost and quality of TiAl powders produced by the TiPro process have been systematically investigated, by analysing three main unit operations of this process (milling, combustion and oxygen removal). This chapter presents the conclusions and recommendations for further work.

8.2 Conclusions

In the current state of the invention, where alloy separation is extracted by extruding the combustion product, the TiPro process is not viable due to poor yields. The throughput, alloy product purity and yield of the TiPro process are constrained by the solid/ liquid separation unit operation. When extrusion is the sole separation technique, the alloy yields are limited to only 10% of total input, as against a minimum yield of 60% required to make the process economically viable. Therefore, unless the solid/ liquid separation is supplemented by other separation techniques, such as froth flotation and leaching, the cost of producing titanium alloy powders by the TiPro process will be high and the quality of the alloy poor, consequently making the process uneconomical. This study has demonstrated that froth flotation can recover 65.7 wt% of TiAl content of the extrusion by-product into a 71.0 wt% TiAl grade product. Al_2O_3 is the main impurity (accounting for the balance of 29 wt%). This corresponds to removing 20 wt% of the total Al_2O_3 contained in the extrusion by-product (flotation feed). The potential exists to increase the TiAl grade further by multiple flotation stages. However, further work is required to investigate more suitable reagents than the HF acid that was used to activate Al_2O_3 in this study.

The TiAl-lean flotation by-product stream can be leached in sulphuric acid (H_2SO_4) to recover TiO_2 and Al_2O_3 separately (Jennings, 2013).

8.2.1 Solid/ Liquid Separation Mechanism

- The solid/ liquid separation process can be described as the flow of liquid TiAl through a porous media of Al_2O_3 particles. Parameters such as the porous media permeability, wetting properties and viscosity of TiAl, that influence the flow and subsequent separation of TiAl during extrusion can be represented by three main governing equations :

    1. The Washburn Equation: $\mathbf{P = -4\,\gamma \cos\theta\,(d_p)^{-1}}$
    2. Darcy's Law: $\mathbf{Q = K_p\,A\,\Delta P(\eta L)^{-1}}$
    3. An Einstein-Roscoe type equation: $\mathbf{\eta = \eta o\,(1- af)^{-n}}$

- The average TiAl saturation of the combustion product at about 0.15 is inadequate to sustain flow during extrusion because at such a low saturation level, the capillary pressure (the force holding TiAl in the pores) is high.
- Increasing the TiAl saturation reduces the capillary pressure.
- TiAl saturation increases by Al_2O_3 agglomeration and TiAl coalescence. This phenomenon requires TiAl to be a liquid.
- The finely suspended Al_2O_3 particles increase the viscosity and consequently inhibit separation of TiAl.
- Also due to a low contact angle (38^o) of liquid TiAl, wetting properties on Al_2O_3 inhibit separation. Liquid TiAl merely wets the solid Al_2O_3 particles creating liquid-phase sintering like conditions that redistribute the liquid TiAl and agglomerate Al_2O_3 particles thereby densifying the extrusion by-product. Therefore, extrusion is not an efficient way of recovering TiAl from the combustion product.
- To economically extract TiAl, other techniques should be used to supplement extrusion.
- Froth flotation can be used to increase the grade of the TiAl-rich phase from about 47% to 71% TiAl, before the alloy purification stage, in order to minimise reductant costs at the calciothermic reduction stage.
- Alloy purification consists of calciothermic reduction followed by leaching with water at 60^oC.

- Apart from poor alloy yields, scaling the solid/liquid separation up might pose heat balance and mass flow related challenges because of the observed rapid cooling of the combustion synthesis product.

8.2.2 Effect of Milling Intensity on Solid/ Liquid Separation

Reactant powders milled for 1 h are more suitable for solid/ liquid separation compared to powders milled for a longer duration. The combustion of powders subjected to more intense milling are characterised by closed porosity and the temperature attained by products is too low to facilitate separation. Powders milled for 1 h have a coarse microstructured combustion product with open porosity. The temperature attained by products is above the TiAl melting point 1460^{o}C. This is favourable for separating TiAl from solid Al_2O_3 by extrusion.

8.2.3 Alloy Purification

Purification of the alloy using Ca in the presence of $CaCl_2$ is preferred to CaH_2 on account of cost. The reaction is initiated by reactive milling of a mixture of TiAl(O) or TiAl(O)/Al_2O_3 with Ca and $CaCl_2$. XRD analysis showed that the alloy containing 5.1 wt% Al_2O_3 (equivalent to about 2.44 wt% O_2) upon being subjected to reaction milling was free of Al_2O_3.

The production cost using Ca is estimated to be US$23.29 per kg TiAl alloy powder at 65% recovery of TiAl. Plant yield increases to US$151.40 per kg TiAl at the current TiPro process yield of 10%. To compare favourably against most emerging cost reduction titanium production technologies, the TiPro process should achieve cost reductions 30, 50% and more of the Kroll process (EHK Technologies, 2004). This criterion cannot be satisfied given the low TiAl yields in the current state of the art in TiPro process. Also, when Ca is replaced by CaH_2 as reductant the production cost of TiAl alloy increases to US$38.53 per kg TiAl at 65% plant yield and to US$250.44 per kg TiAl at the current achievable TiPro process plant yield of 10%.

8.3 Recommendations for Further Work

Since the yield at the solid/liquid separation stage is low (10% of input), the following should be studied to enhance the viability of TiPro process:

- Feasibility of increasing the TiAl grade further by multiple flotation stages or by other separation techniques to obtain a product with a higher content of TiAl.
- Other techniques of separating Al_2O_3 from TiAl such as conventionally fluxing it into a molten slag by adding suitable chemical compounds such as cryolite that can combine with Al_2O_3 to form a low-melting point slag that could be skimmed off the surface of the molten alloy bath.

This study has demonstrated the efficacy of various alloy purification alternatives, however, the alloy yield of each process need to be studied and optimised.

8.4 References

EHK Technologies. (2004). *Summary of Emerging Titanium Cost Reduction Technologies*. Retrieved 15 August, 2011, from http://www.ornl.gov/sci/propulsionmaterials/pdfs/Emerging_Titanium.pdf

Jennings, P. A. C. (2013). *Recovery and Purification of Titanium Dioxide and Aluminium Compounds from Corundum By-product of the TiPro Process.* thesis, University of Waikato, Hamilton.